Universiteit Utrecht

Origin and emplacement of ultramafic bodies in the Köli nappe and the lower- and upper belt of the Seve Nappe Complex, Central Scandinavian Caledonides

Benders, P.G.P.
Master thesis, department of earth sciences, University of Utrecht
Utrecht, the Netherlands, April 2015

Supervisor: Dr. Herman van Roermund

Abstract

The Scandinavian Caledonides is composed out of a westward dipping and north-south running nappe stack with multiple outcrops of orogenic peridotite bodies. Earlier research has revealed different mechanisms by which the ultramafic mantle material is incorporated into the country rock, either as obducted ophiolites or as mantle wedge peridotites (MWP). The Seve Nappe Complex (SNC) which is build out of the high grade middle belt (granulite facies), bounded by the medium grade upper- and lower belt (amphibolite facies), contains abundant ultramafic bodies. Recently the ultramafic bodies in the middle belt have been classified as MWP, however the mechanism of peridotite emplacement in the upper- and lower belt remains unknown. This thesis investigates the deformational, mineralogical and chemical evidence of the country rocks and the peridotites of the upper- and lower belt plus the overlying Köli belt in order to determine their provenance and mechanism of emplacement. This research has found that peak metamorphism of the country rocks and peridotite of the same unit are in correspondence. However prior to their mutual metamorphic history the peridotites have experienced (intense) serpentinization and exhumation. The provenance of the upper and lower Seve belt peridotites have been interpreted as sub-cratonic. We propose that the peridotites of the upper- and lower belt are of the Ocean-Continent transition zone (OCT) type exposed and serpentinized during hyper extension of the western margin of Baltica. Subsequently they have become metamorphosed under amphibolite facies during the Finnmarkian metamorphic overprint (500Ma). The Köli peridotite is also of ophiolitic type (type undetermined) that has progressively metamorphosed, but during a later event, the Scandian metamorphic overprint (425 Ma). Geodynamical models of the development of the Caledonides have to be reconsidered by including the crustal emplacement of various types of peridotites from the hyperextended margins of Baltica.

Graded by: Dr. Herman van Roermund & prof. Dr. Martyn Drury

Table of content

1) Introduction

Orogenic peridotites are ultramafic rocks coming from the mantle. Most of the entire mantle in composed of these rocks (Bucher & Grapes, 2011), but only seldomly are they exposed at the surface, where they are accessible for research. The Scandinavian Caledonides are one of the best suited places for research into the origin of such orogenic peridotites. The Scandinavian Caledonides are an old and deeply eroded mountain belt and therefore give a special insight in the processes that occur at deep crustal levels during orogenesis. The rocks which are formed at the base of the orogeny are currently exposed at the surface after having been exposed to hundreds of million years of erosion and isostatic adjustment.

The Caledonian orogeny began with the conversion of the continents Laurentia and Baltica and the closure of the Iapetus and Aegir Oceans which separated both continents. The Caledonian orogeny in Scandinavia consists of multiple stages of collision namely the Finnmarkian orogeny (~500 Ma) (Andréasson & Albrecht, 1995), the Trondheim orogeny (~480) (Gee, 1987), the Taconian orogeny (~460Ma) (Roberts, 1980), the Jämtlandian (454 Ma) (Brueckner & van Roermund, 2004) and the Scandian orogeny (~430-390 Ma) (Gee, 1975). The Scandinavian Caledonides were heavily affected by the Cenozoic opening of the Atlantic Ocean, which effectively reversed the previous continental movement, and separated Laurentia (now North-America) from Baltica (now Eurasia) again. The Caledonian orogeny, however, still has a profound effect on the geology found in Scandinavia today. The Scandinavian Caledonides consist of a series of north-south striking nappes which have been thrusted eastward onto the Baltic plate (Törnebohm 1872; Strand & Kulling 1972; Gee & Sturt, 1985). These nappes are westward dipping and westward thinning (Zachrisson, 1969, 1973; Nicholson and Rutland, 1969; Gee, 1975) and can be subdivided into five major units. From bottom to top (i.e. east to west): the Autochthon, the Lower Allochthon, the Middle Allochthon, the Upper Allochthon and the Uppermost Allochthon (Roberts & Gee, 1985). The nappes represent different pre-Caledonian depositional environments. The Autochthon, consist of pre-Caledonian continental sediments of the Baltic shield and underlying basement. The Lower and Middle Allochthon represent respectively the continental margin and continental/ocean transition zone of Baltica (Gee et al., 2008), whereas the Upper Allochthon represents the domain of the former Iapetus Ocean including associated ophiolites (Gale & Roberts, 1974; Gee, 1975; Stephens & Gee, 1985). The Uppermost Allochthon is believed to be the domain of the continental margin of Laurentia (Stephens & Gee, 1985; Roberts et al, 1985; Roberts 2003). The focal point of this master thesis is the Seve Nappe Complex (SNC), which represents the upper part of the Middle Allochthon. Figure 1.1 outlines the extension of the allochthons in the Scandinavian Caledonides. In the central Swedish Caledonides of N. Jämtland and southern Västernbotten the SNC has been further subdivided into three belts, from top to bottom (i.e. west to east), the western belt, the central belt and the eastern belt (Trouw, 1973; Zwart, 1974; Williams & Zwart 1977). In more recent literature these belts are now referred to as the upper-, middle- and lower belt respectively (Zachrisson, 1993; Zachrisson & Greiling, 1993). A distinct feature of the Scandinavian Caledonides is the occurrence of Alpine-type peridotites in many different levels of the tectono-stratigraphy (Qvale & Stigh, 1985; Bucher-Nurminen, 1991) and this also holds for the SNC. Traditionally the peridotites were interpreted as remnants of sub-oceanic mantle material; more

particularly the deeper sections of ophiolites that were tectonically obducted on the adjacent continent (Coleman, 1972) and subsequently incorporated as orogenic peridotites in the various nappes during the Caledonian orogeny (Andréasson, 1994; Bucher-Nurminen, 1991; Qvale & Stigh, 1985; Zwart 1974). More recently, following similar discoveries in the Alps and Pyrenees (Boillot et al., 1987; Manatschal, 2004; Péron-Pinvidic & Manatschal, 2009), orogenic peridotite massifs of the SNC in southern parts of the Caledonides are interpreted to represent remnants of a hyper-extensional Baltic continental margin (Andersen et al., 2012). However, the discovery of ultra-high pressure minerals, found in metamorphosed crustal rocks (Chopin, 1984; Smith 1984) and in eclogite and garnet peridotite of UHP terranes (Sobolev & Shatsky, 1990; Yang et al., 1993, 1994; Dobrzhinetskaya et al., 1995; van Roermund & Drury, 1998; Song et al., 2004) required an alternative tectonic model which could explain their tectonic emplacement into the surrounding continental crust (Brueckner, 1998). Brueckner & van Roermund (2004) and Brueckner et al. (2004) first described relict garnet peridotites, which were incorporated during orogenesis from the mantle into the continental crust during initially subduction of continental crust to deep levels (eclogite facies ~ +50 km) and subsequent rebound to the surface (Brueckner 1998). Recently such relict orogenic garnet peridotites were rephrased by Van Roermund (2009) as mantle wedge garnet peridotites (MWGP). In addition two large orogenic peridotite bodies in the middle belt of the SNC in Västerbotten, called the Kittelfjäll Spinel Peridotite (KSP) and the Frinningen Garnet Peridotite (FGP), has also been interpreted as mantle wedge peridotites (Clos et al. 2014; Mattia et al. 2015). In contrast the orogenic peridotites found in the Köli nappe, such as the large Aunere body, is still interpreted as an obducted ophiolite (Trouw, 1971; Zacharisson, 1973; Bucher-Nurminnen, 1991; Eide & Lardeaux, 2002). This entails that the Scandinavian Caledonides in central Sweden has two distinct types of orogenic peridotites incorporated in their country rocks during its development. The upper belt which is positioned in between the Köli nappe and the Middle belt, and the Lower belt which is positioned east and stratigraphically below the Middle belt, have orogenic peridotite bodies which origin is currently unknown. Both the upper- and lower belt of the SNC have been metamorphosed into amphibolite facies (Trouw 1973, Bierman 1979, Calon 1979, Zwart 1974, Williams & Zwart 1977, van Roermund & Bakker 1983), an intermediate grade compared to the greenschist facies metamorphic grade of the Köli nappes (Zachrisson, 1969; Trouw, 1973; Zwart, 1974; Gee et al., 2010) and the granulite to eclogite facies of the Middle belt of the SNC (Zachrisson 1974, Zwart 1974, Trouw 1973, Williams & Zwart 1979, van Roermund & Bakker, 1984; Van Roermund 1985, 1989; Brueckner & van Roermund, 2004).

The aim of this project is to determine the origin of the orogenic peridotite bodies found in country rock gneisses of the upper- and lower belt of the Seve Nappe Complex in southern Västerbotten, central Sweden and to formulate a tectonic model which can explain their tectonic emplacement into their present environment. This will be done by determining the type of mineral assemblages, including their relative timing of growth versus deformation events (recognized in both the surrounding country rocks and the orogenic peridotite lenses), their overgrowth relations of multiphase metamorphism, and its relation to deformational structures. All these characteristics will provide constraints on the PT trajectory and emplacement of these orogenic lenses into the continental crust during formation of the Scandinavian Caledonides. The obtained results will be

compared to existing tectonic models about the formation of the SNC and the Scandinavian Caledonides as a whole. These models should provide a satisfying explanation for the similarities and dissimilarities of the orogenic peridotites found in the upper- and lower belt of the SNC with the ophiolitic peridotites found in the overlying Köli Nappe (Trouw, 1971; Zacharisson, 1973; Bucher-Nurminnen, 1991; Eide & Lardeaux, 2002) and the mantle wedge peridotites found in the Middle belt of the SNC (Clos et al., 2014; Mattia et al., 2015). The peridotites of the upper- and lower belt have, before onset of this research, not been investigated on their origin and trajectory. This research will therefore contribute by either strengthening existing views or providing new insight on the formation of the Caledonides and the transport of the nappes.

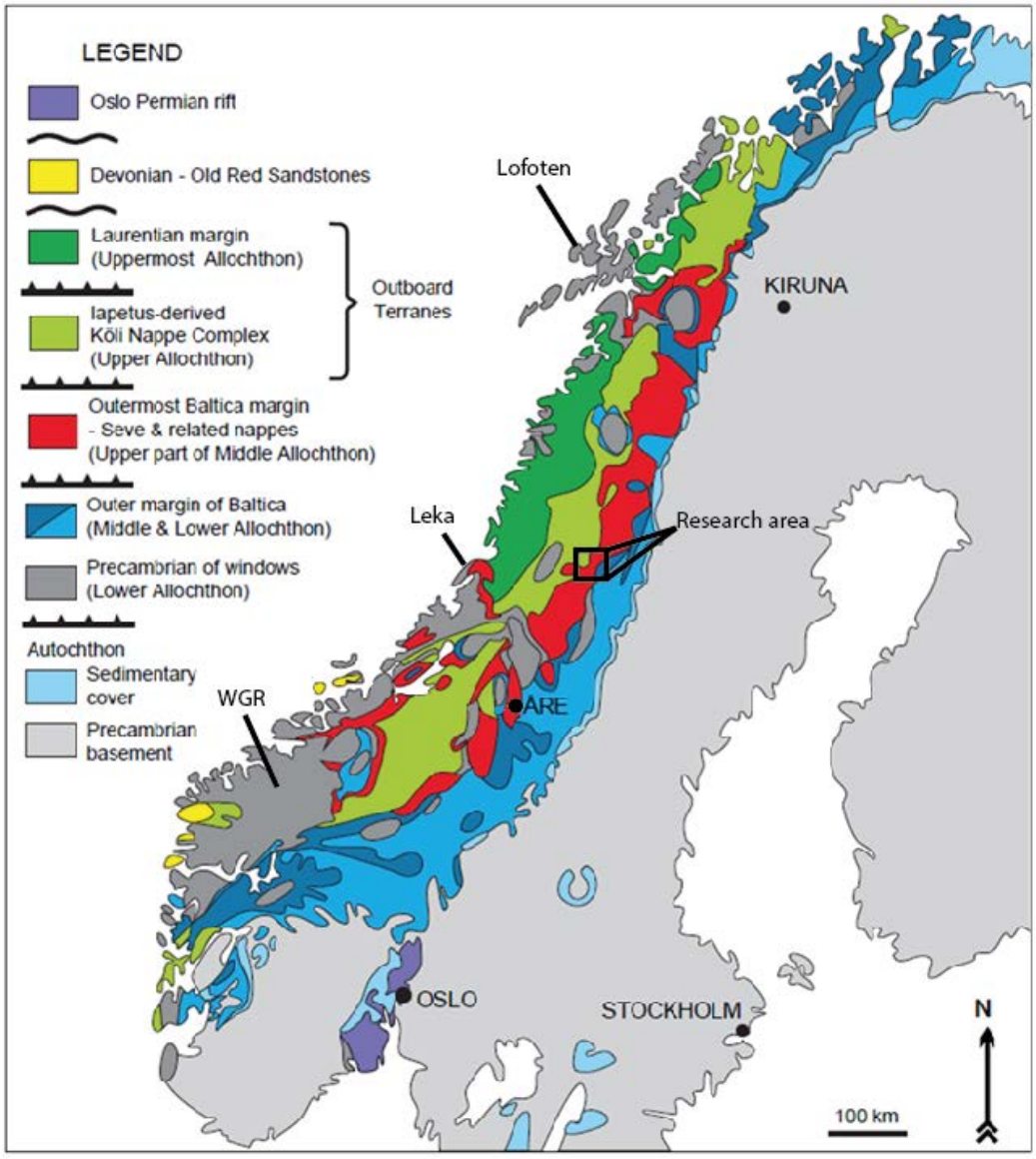

Figure 1.1 Tectonostratigrafic map of the Scandinavian Caledonides, illustrating the position of the Allochthons and Autochthon. Modified after Gee et al. (2010). A Geological map of the research area is illustrated in figure 2.2 and 3.1.

2) Geological background

2.1 Basic components of the Caledonides

The Caledonides form a complex orogeny which includes multiple former continents. It is agreed upon that the continents Laurentia, Avalonia and Baltica are involved in the collision. It was an immense tectonic event involving three of the six independent plates recognized in the Early Paleozoic. Some time prior to the Caledonian orogeny there was one supercontinent positioned on the southern hemisphere on Earth, called Rhodinia, which started to break up approximately 750Ma (Torsvik & Cocks, 2005). At 650 Ma the continent Laurentia, which consisted of the present North-American, Greenland and Scotland, and the continent Baltica, which consisted of the current East-Europe and Scandinavia, broke away from the remainder of Rhodinia, Gondwana (fig 2.1). This plate movement resulted in the development of the Iapetus Ocean, separating Laurentia from Gondwana and Baltica. In the mid-Ordovician, Avalonia, which consisted of o.a. current England and parts of NW-Europe, started to drift away from Gondwana towards Baltica, thereby narrowing the Tornquist Sea which separated the continents. The tectonic regime inside the Iapetus Ocean switched from an extensional to a convergent mode at approximately 560Ma (Cocks & Torsvik, 2005) and resulted in the closure/ subduction of the Iapetus and Tornquist Ocean eventually leading to the collision of Laurentia, Baltica and Avalonia.

The movement of the plates is illustrated in figure 2.1. The illustration by Robert (2003) is based on paleomagnetic reconstructions by Torsvik et al. (1996), Torsvik (1998) and Cocks & Torsvik (2002). Highlighted are the continents which are involved in final continent-continent collision of the Scandian orogeny, Laurentia, Baltica and Avalonia plus Siberia, which is believed to have played an indirect role in the earlier Finnmarkian orogeny (Torsvik & Rehnström, 2001).

The convergence of Laurentia and Baltica has led to four orogenic events, wherein the continent-continent collision between Laurentia and Baltica was the final event, called the Scandian orogeny (~430-390 Ma) (Gee, 1975). This event was pre-dated by a series of other orogenic events involving the oceanic crust and multiple micro-continents assumed to have been present in the Iapetus Ocean. These orogenic events are the Finnmarkian (~500 Ma) (Andréasson & Albrecht, 1995), the Trondheim (~480) (Gee, 1987), the Taconian (~460Ma) (Roberts, 1980) and the Jämtlandian (454 Ma) (Brueckner & van Roermund, 2004), and will be covered in more detail below in chapter 2.5 where the various models which describe the development of the Scandinavian Caledonides are discussed.

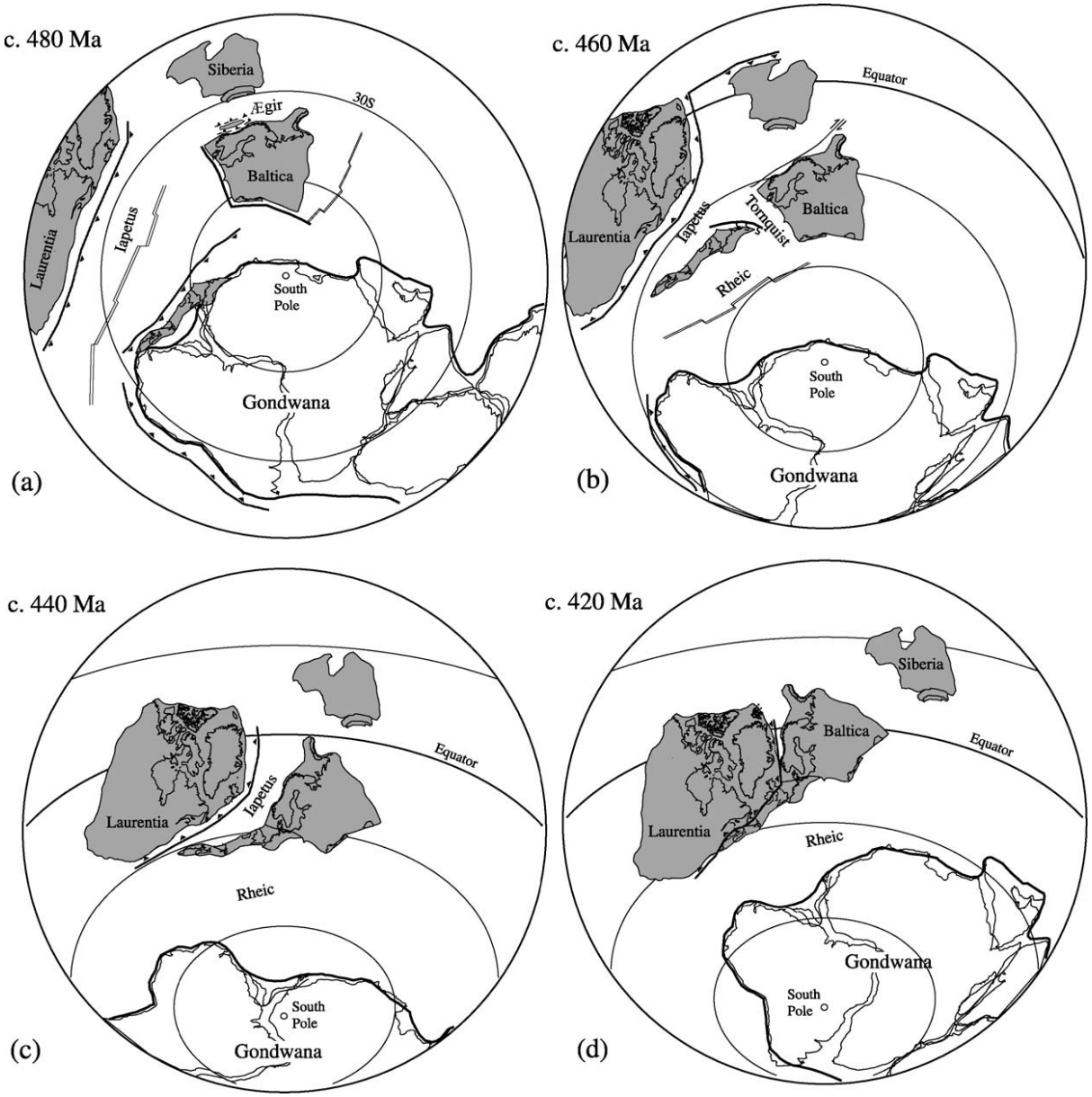

Figure 2.1 Paleogeographic reconstructions of the positions of the continents from Early Ordovician (480Ma) to late Silurian (420Ma). Gondwana is unmarked due to the lack of relevance for the Caledonian orogeny. The reconstruction is done by Roberts (2003) based on the work of Torsvik et al. (1996), Torsvik (1998) and Cocks & Torsvik (2002). **a** Late Tremadoc to Floian time, approximately coeval with the Trondheim event. **b** Late Darriwilian to Sandbian time, approximately coeval with the Taconian event. Avalonia has disconnected from Gondwana and shifted northward towards Baltica. **c** Early Silurian time, the Iapetus is closing rapidly and the continent Laurentia and Baltica are moving towards each other. Avalonia has connected to Baltica by this time. **d** Late Silurian time, Baltica and Laurentia collide during the Scandian orogeny.

2.2 Scandinavian Caledonides

The Caledonides is an old orogeny that has taken place in the Early Paleozoic. When it seized to be an active orogeny, around 390 Ma (Gee, 1975), the global tectonics have of course continued. Ever since, the continents have converged into the super continent Pangea and subsequently diverged again resulting in the current plate configuration. This has also affected the Caledonides. In between North America and Greenland on one side and Europe on the other, the Atlantic Ocean arose, leaving vestiges of the Caledonides spread out around its periphery. The part of the Caledonides which is located on Scandinavia is referred to as the Scandinavian Caledonides. The Scandinavian Caledonides are positioned in the far west of Scandinavia and is a roughly North-South running belt which is exposed over a length of 2000 km and is 300 km at its widest. The Scandinavian Caledonides are not only built up out of nappes which are transported eastward and thrusted onto the Baltic shield (Törnebohm 1872; Strand & Kulling 1972), but also involved parts of the underlying crystalline basement, hereafter called the caledonized basement.

These thrust nappes are grouped on the basis of their origin into five major tectonic units (Robert & Gee, 1985). These units will be discussed in order of their tectono-stratigraphic position from bottom to top (i.e. east to west) and grouped based on their paleogeographical positions predating the Caledonian orogeny.

The Autochthon is the lowest unit of the Scandinavian Caledonides. It represents the continental environment of the Baltic shield. The Autochthon in the east forms the crystalline base over which the nappes are thrusted and is not heavily affected (i.e. deformed and metamorphosed) during the orogeny. The Autochthon consists of a pre-Cambrian basement and an un-metamorphosed Vendian to Silurian sediment cover (Hacker & Gans, 2005). The overlying tectonostratigraphic units are denoted as Allochthons, referring to their transport from distal areas onto the Baltic shield.

The Lower Allochthon represents the most proximal unit. The rocks found here are deposited on the pre-Caledonian continental margin of Baltica. The deformation that occurred here is shallow, with little involvement of basement rocks. The Lower Allochthon is generally metamorphosed in the low to middle greenschist facies (Robert & Gee, 1985). At several locations, in the west such as Lofoten and the Western Gneiss Region (WGR) (fig 1.1), the basement of Baltica crops out between the higher stratigraphic units of the Allochthons. Here the pre-Cambrian crystalline windows are high grade, e.g. the WGR has experienced UHP metamorphism which depths >185 km (van Roermund & Drury, 1998).

The Middle Allochthon represents the pre-Caledonian transition between the continental margin of Baltica and the domain of the Iapetus Ocean. It consists of multiple nappes and nappe complexes, in tectono-stratigraphical order from bottom to top: the Tännes Augen-, Granite Mylonite-, and Offerdal nappe, the Särv nappes and the Seve Nappe Complex (SNC). This unit has a complex deformational history which leads to diverse metamorphic grades ranging between eclogite facies to middle greenschist facies (Gee et al., 2010). The upper SNC contains abundant ultramafic lenses. In this research the focus will be on the SNC which will be discussed in more detail below.

The overlying Upper Allochthon represents the pre-Caledonian domain of the Iapetus Ocean. It consists of the Köli Nappe Complex (KNC). Also the KNC includes large numbers of ultramafic

bodies. These bodies are believed to represent the deep sections of an ophiolite (Trouw, 1971; Zacharisson, 1973; Bucher-Nurminnen, 1991; Eide & Lardeaux, 2002). The transition from the SNC to the KNC is marked by a decrease in metamorphic grade. At most places a marked tectonic contact is present. The metamorphic grade of the KNC ranges between low and high greenschist facies (Gee et al., 2010).

The Uppermost Allochthon is the most distal unit. It is believed to represent the continental margins of Laurentia (Stephens & Gee, 1985; Roberts et al, 1985) and also contains ultramafites. This unit is metamorphosed to upper amphibolite facies conditions. The nappe structure of the Scandinavian Caledonides shows a simple distribution regarding their origin. Tectono-stratigraphic high units represent the distal parts, whereas the lower units represent the proximal continental parts. Metamorphically the distribution is not that straightforward, with large jumps between the different tectono-stratigraphic units and even nappes belonging to the same unit. Additionally, the ages of metamorphism is diverse and does not show a simple trend, tectonostratigraphically from top to bottom: the Köli 425 ±5 Ma (Reymer, 1979), the upper belt 491.2 Ma ± 22 Ma (Gademan, 2011), the middle belt 502.3 ± 20 Ma (Gademan, 2011) and 445 Ma (Brueckner & van Roermund, 2004; Brueckner et al., 2004; Root & Curfu, 2011) and the WGR 415-397 Ma (Terry et al. 2000), indicating the complexity of the Caledonian tectonic evolution. This will have to be addressed in the tectonic models describing the development of the Scandinavian Caledonides.

2.3 Seve Nappe Complex (SNC)

The SNC consists of various imbricated thrust sheets which are very diverse in metamorphic grade and lithology. Traditionally the SNC was considered to be part of the Upper Allochthon and formed the lower part of the Köli Seve Nappe Complex (Robert & Gee, 1985). More recently the SNC was reclassified as the top of the Middle Allochthon (Gee et al., 2008). The SNC is believed to represent the ocean-continent transition and not, such as the Upper Allochthon, the oceanic domain of the Iapetus Ocean (Gee et al. 2008). The SNC is overlain by the Köli Nappe to the west via a tectonic contact (Zachrisson, 1973) and overlies the Särv Nappe and other nappes belonging to the Middle and Lower tectono-stratigraphic units to the east (Zwart, 1974). The SNC is subdivided into three N-S running belts. From west to east, the upper/western belt, the middle/central belt and the lower/eastern belt. Tectono-stratigraphically this is also the order from top to bottom and in recent literature these belts are referred to as the upper belt, the middle belt and the lower belt, respectively.

The upper belt is predominantly composed of garnet-micaschist and quartzitic garnet-micaschist, named the Svartsjobäcken schists, plus meta-basic amphibolites and ultramafic bodies (Trouw, 1973; Zwart, 1974). The upper belt is metamorphosed to lower amphibolite facies. Due to truncation by the overlying Köli Nappe in the central part of the upper belt is not exposed over the entire length of the SNC, as is illustrated in figure 2.2. The upper belt contact with the Middle belt is poorly exposed. It therefore remains unclear if the contact between the belts is gradual or tectonic. The middle belt is high grade compared to its bordering nappes. It consists of migmatic gneisses and metabasic rocks (Zwart, 1974). There are variations in metamorphic grade from north to south (figure 2.2). The Marsfjället gneisses in the north are metamorphosed to upper

amphibolite to granulite facies (Zwart, 1974; Williams & Zwart, 1977), the Avardo gneiss in the central part to eclogite facies (van Roermund & Bakker, 1983; van Roermund 1985) and the Lillfjället gneiss in the south to low pressure granulite facies (van Roermund, 1985). Recent studies have shown that the middle Seve nappe near Friningen has undergone UHP metamorphism based on kyanite bearing eclogites (Janak et al., 2013) and the occurrence of microdiamonds in the Avardo gneiss (Majka et al., 2015). All middle belt rocks, independent of metamorphic grade, contain lenses of ultramafic material. The contact separating the Middle belt and the underlying lower belt is tectonic (Zwart, 1974). The lower belts lithology consist of garnet-micaschist, marble, meta-arkose, quartzite, amphibolite and ultramafic bodies (Zwart, 1974; van Roermund & Bakker, 1983) metamorphosed to lower amphibolite and upper greenschist facies (Zwart, 1974; Williams & Zwart, 1977; van Roermund & Bakker, 1983). Exception to this metamorphic field range is the (U)HP Tjeliken lens south of Friningen (fig 2.2). The lower belt borders the underlying nappes of the Middle- and, at some areas, the Lower Allochthon, this contact is also tectonic (Zwart, 1974).
Note that there is no linear trend in the metamorphic grade of the belts of the SNC. The metamorphic grade increases from the upper belt into the middle belt, but this trend is inversed from the middle belt going into the lower belt. Also, as mentioned above, the middle belt has a range of metamorphic facies from north to south. This illustrates the complexity of the Seve Nappe Complex.

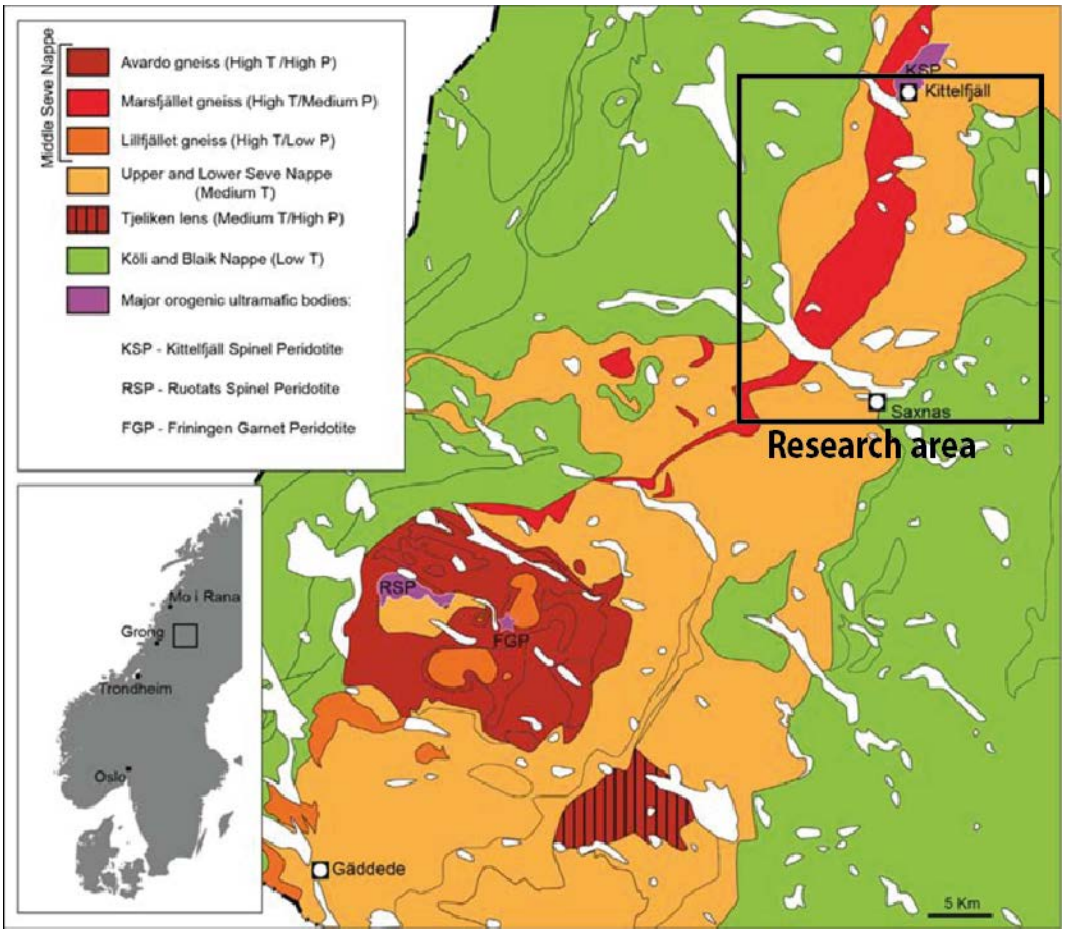

Figure 2.2 Metamorphic map of the SNC and juxtaposed nappes in North-Jämtland/ South-Västerbotten, Central Sweden (Clos et al., 2014). Note that a detailed geological map of the research area is illustrated in figure 3.1.

2.4 Peridotites

2.4.1 Orogenic peridotites

Peridotites are of ultra-mafic composition ($SiO_2 \leq 50$ Wt%) and are believed to compose Earths entire mantle (Jagoutz et al., 1979). The chemical composition of these rocks is based on studies performed on mantle xenoliths and tectonically emplaced orogenic peridotites. Primary or undepleted mantle is of lherzolitic composition (figure 2.3). Chemical differentiation occurs as adiabatic decompression by upwelling asthenospheric mantle leads to partial melting and subsequent crustal lithosphere formation. Volatile elements such as Si, K, Na, Al Ca and Fe partition into the melt and are thus depleted in the residual mantle. Subsequent melting would result in depletion of the mantle peridotites with a change in composition to more enriched refractory elements such as Cr and Mg. The mineral assemblages found in primary mantle lherzolite is dominated in order of relative abundance by the three minerals olivine (Ol), orthopyroxene (OPX) and clinopyroxene (CPX) together with an Al-bearing phase, garnet, spinel or plagioclase. The latter depending on pressure, respectively indicated in the order of decreasing pressure. During partial melting CPX Al-silicates are the first minerals to be removed from the mineral assemblage as Ca an Al easily partition into the melt. Subsequently OPX is removed by partitioning of Si, which leaves Ol as the only major mineral. Continuous extraction would therefore lead to the evolution of the bulk rock composition from lherzolite to harzburgite to, in most depleted stages, dunite. The process of depletion described above has occurred continuously throughout Earth's history and has led to the formation of both sub-continental and sub-oceanic lithospheric crust. However, their genesis is not identical and this is reflected in the peridotites of the lithospheric mantle below the ocean, the sub-oceanic lithospheric mantle (SOLM), and below the continent, sub-continental lithospheric mantle (SCLM). Oceanic crust is a relatively young lived geological feature typically not exceeding 250Ma before being reincorporated into the mantle along a destructive margin. In contrast, continental crust is not reincorporated into the mantle (i.e. apart from during dunk-tectonics (Brueckner & van Roermund, 2004); see chapter 2.5.2) and can be of Archean age. Here the lithospheric mantle below the continents will reflect these ages. Therefore, orogenic peridotites of SOLM origin have an age restriction of 250 Ma prior to their crustal emplacement, whereas in the case of orogenic peridotites of SCLM origin this restriction is up to 2-3 Ga. In addition, the age of the lithospheric mantle is reflected in its composition. During the Archean mantle temperatures were higher than they are at present. This resulted in the extraction of komatiitic melts at high temperatures and great depths (T>1800C°; P=3-7 GPa). Partial melting under these conditions was higher than today, up to 40% (Herzberg, 2004), compared to current standards extreme. Therefore, the SCLM of Archean age is highly depleted and more buoyant. Progressive cooling of the Earth and decrease of heat flow resulted in a reduction of partial melting, 30% during Proterozoic and 20-10% during Phanerozoic (Walter, 1998; Griffin et al., 2009), resulting in a less extreme depletion trend for such lithospheric mantle fragments making them less buoyant.

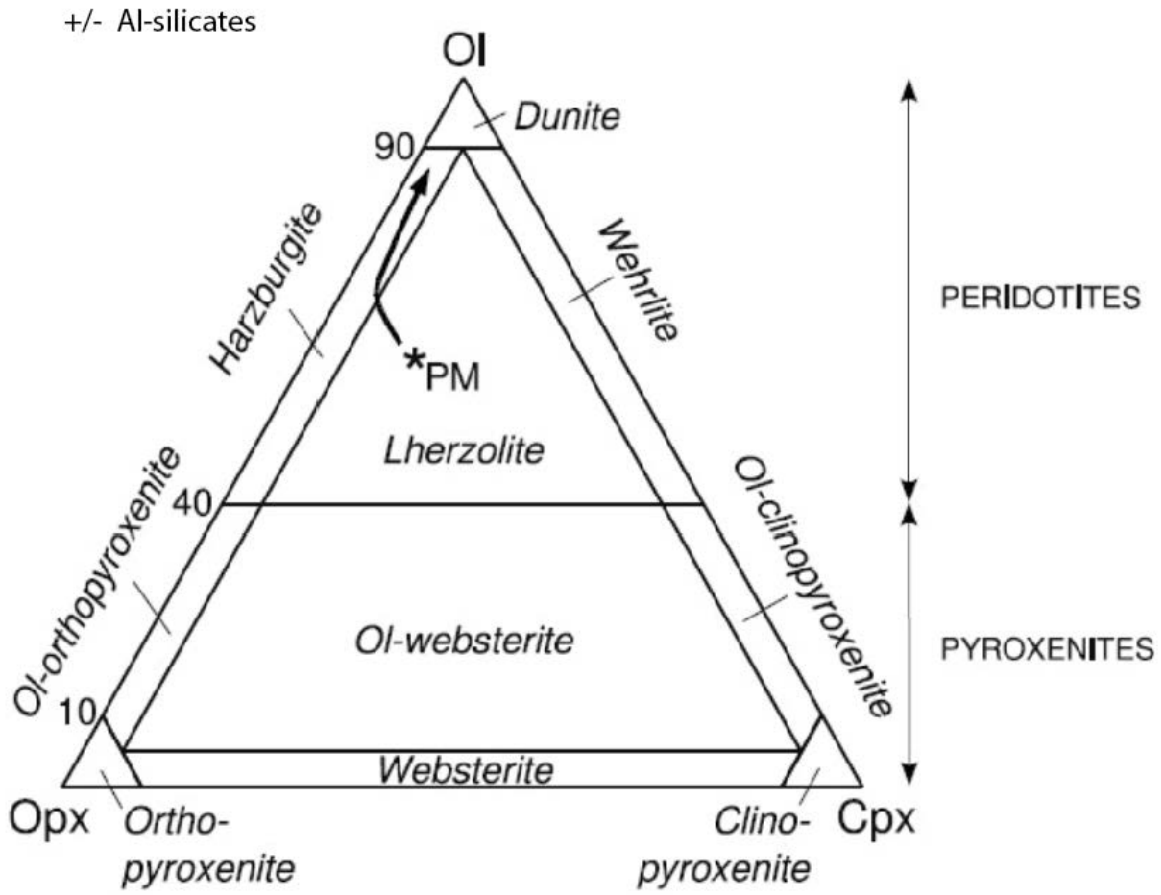

Figure 2.3 Triangular classification diagram of ultramafic rocks based on the mineral constituents (Ol-OPX-CPX). *PM indicates the composition of unaffected fertile mantle rocks or primary unmolten mantle. The black arrow indicates the depletion trend. As mantle peridotites get progressively more depleted their composition moves from lherzolite to harzburgite and finally to dunite. After Spengler (2006).

2.4.2 Classification of peridotites

Peridotites comprise the bulk of the upper mantle and with it a large part of the solid Earth. However despite being extremely abundant, these terrains are unfortunately not accessible and scientists have to work with peridotites that are transported in some way to the surface and/or incorporated in the crust. These peridotites are subdivided into two groups 1) the Xenolithic peridotites and 2) the Orogenic or Alpine type peridotites (Wyllie, 1969). Xenolithic peridotites are rock fragments which have been incorporated in magmatic material as the igneous material solidifies and subsequently transported to the surface. Alpine type peridotites are incorporated in the crust by tectonics (de Roever, 1957; Den Tex 1969; Coleman, 1971, 1977). Most of the peridotite bodies found in the Scandinavian Caledonides are of the Alpine type, which is evident due to its emplacement in meta-pelites (Qvale & Stigh, 1985). Alpine type peridotites were further subdivided in (a) the Ophiolite sub-type (i.e. obduction of oceanic crust) and (b) the Rootzone sub-type (den Tex, 1969) (i.e. high grade/deep mantle material). Later authors have expended on this a proposed mechanism by which incorporation can occur. Cuthbert & Carswell (1990) and

Froitzheim & Manatschal (1996) described the incorporation of peridotites in the base of the crust by deep level ductile imbrication of the crust. This mechanism can explain the emplacement of spinel peridotite, but occurs at depths to shallow to explain the emplacement of garnet peridotite. Garnet is the stabile Al-bearing mineral in peridotite from depths in excess of 60-80 km depending on temperature. Brueckner and Medaris (2000) proposed subduction as the mechanism to achieve these depths and garnet peridotites incorporation via two routes. Peridotites which are incorporated into the subducting plate from the overlying mantle wedge, further subdivided into four groups (see chap. 2.4.4) and now called mantle wedge garnet peridotites (MWGP) (van Roermund, 2009). Alternatively, garnet peridotite can be formed by the prograde metamorphism of peridotites which have been incorporated into the crust prior to subduction, now called subduction zone garnet peridotite (SZGP). The peridotites at that stage would include low grade spinel or plagioclase as Al-bearing phase. If subduction proceeds to depths within the stability field of garnet prograde metamorphism can occur. Both MWP and SZP when occurring at shallow depths can lead to spinel peridotites. However, the age of both types of peridotite will be different. In fact, the age of SZGP will correspond to the age of the collisional orogeny, whereas the MWGP pre-dates it.

2.4.3 Obducted Ophiolitic peridotites

Ophiolitic peridotite

Continent-continent collisions are Earths great mountain range builders. It is however pre-dated by a phase of oceanic crust consumption. Remnants of oceanic crust have been found throughout the world in most mountain ranges as it is wedged in between the two converging plates. These remnants are marked by a distinct sequence of rock composition and structures called the ophiolite sequence, which relates to the genesis of obducted ocean/sea floor. There are two types of ophiolites: the classic Penrose-type ophiolite, which relates to the formation of oceanic crust, and the OCT-type, which is related to magma poor hyper-extension. Both types are generally associated with heavy serpentinization as water is introduced from the overlying water column along the associated normal faults.

Penrose-type ophiolite

The Penrose-type peridotite is the typical ophiolite sequence as defined during the Penrose field conference on ophiolites (1972). The sequence is formed during an extensive period of oceanic crust and SOLM formation. The base of the sequence is formed by ultramafic peridotite from the upper mantle, which is often depleted by the melt extraction which led to the formation of the overlying oceanic crust. Towards the top the peridotites are overlain by gabbros, sheeted dikes and pillow basalts covered by marine sediments. These mafic rocks are derived from the underlying asthenosphere as mantle material is decompressed at high temperature during extension resulting in partial melting. The top of the sequence is marked by oceanic sediments as the area gradually moves away from the oceanic spreading ridge and volcanic activity resides. The ultramafic basal segment of the Penrose-type involves slightly depleted mantle material since the amount of extracted melt, which formed the oceanic crust, is only in the order of 20-10% (Walter,

1998; Griffin et al., 2009). In the Scandinavian Caledonides there are several assumed Penrose-type ophiolites. The Leka ophiolite, located on the west coast of Norway (fig 1.1), contains the entire sequence as determined at the Penrose conference (1972) (Austrheim & Prestvik, 2008). Other peridotite bodies such as the Aunere peridotite located in the Köli nappe of Marsfjällen area are equally classified as the Penrose-type peridotite (Trouw, 1971; Zacharisson, 1973; Bucher-Nurminnen, 1991; Eide & Lardeaux, 2002) although they do not contain the entire ophiolite sequence, hereafter called dismembered ophiolite, in which the ultramafic base was interpreted to be detached from the overlying gabbro's, dykes and marine sediments. The latter peridotite has been explained as being the dismembered part of an ophiolite sequence. Dismembered ophiolites are not uncommon since their emplacement is accompanied by heavy thrust faulting.

OCT-ophiolite

The OCT-type ophiolite (Foucher et al., 1982; Brun & Baslier, 1996) differs from the classical Penrose-type by a change in tectonic setting. Although both ophiolite types originate by a phase of crustal extension, the OCT-type is not associated with the development of new oceanic crust (Whitmarsh et al., 2001; Manatschal, 2004; Péron-Pinvidic & Manatschal, 2009; Chew & van Staal, 2014). The ocean-continent transition zone is extremely thinned magma-poor continental margin developed by hyperextension of the continental crust and underlying lithospheric mantle. Normal shear zones extensively thin the continent and sub-continental lithosphere and ultramafic mantle. In this process the SCLM is exhumed and can form windows at the surface. The OCT-ophiolitic sequences therefore does not, or to a minor extent, include the basic middle segments of the Penrose-type (i.e. gabbros, sheeted dikes and pillow basalts) and is solely marked by the ultramafic basal segment followed by a marine sedimentary cover. The ultramafic base of the OCT-type ophiolite represents exhumed sub-continental lithospheric mantle. Their composition ranges from fertile lherzolite to depleted dunite, however sub-cratonic mantle lithosphere is generally strongly depleted due to the high melting ratio of 40% (Walter, 1998; Griffin et al., 2009) during the time of their development (i.e. Archean). However, the sub-continental lithosphere could have experienced events of refertilization due to the introduction of basic dykes.

Ophiolite emplacement

Emplacement of ophiolites occurs in two stages. The first stage may begin with the inception of inter-oceanic subduction. This will result in an overriding and a subducting oceanic plate. The subducting plate is gradually consumed into the mantle, whereas the overriding plate is obducted upon the growing accretionary complex above the subduction zone. This first stage of obduction is illustrated in figure 2.4. The second stage begins when ocean closure has progressed to the stage that the subducting plate is fully consumed and the adjacent continental crust has reached the subduction zone. This remnant geometry of the intra-oceanic subduction (i.e. a fully subducted and an obducted oceanic plate) and continuing convergent forces will force the thin oceanic plate to be thrust upon the continental crust (i.e. obduction) and thereby emplacing the ophiolite sequence on continental crust. This system is inherently unstable since the relatively buoyant continental crust is overlain by less buoyant oceanic crust (Dewey, 1976). According to this mechanism the peridotite becomes incorporated into the overriding plate.

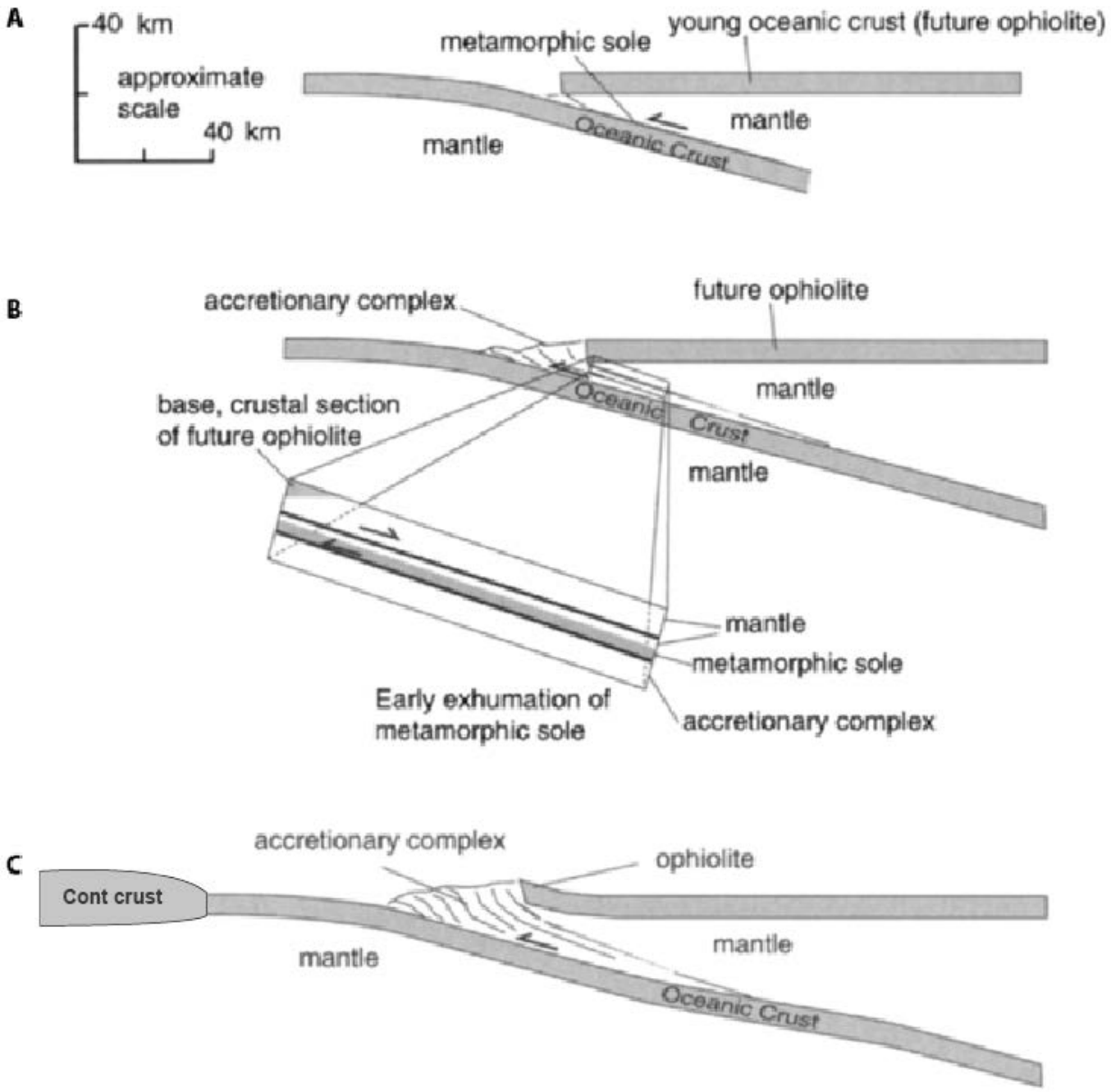

Figure 2.4 Intra-oceanic ophiolite emplacement. **a** Inception of thrusting beneath oceanic lithosphere, results in the formation of a metamorphic sole running beneath the SOLM of the overriding plate. **b** Ongoing subduction, material scrapped of subducting slab forming an accretionary complex. **c** Continued subduction leads to the growth of the accretionary wedge and the obduction of the ophiolite sequence on top of it. The peridotites at the surface are derived from the overriding plate. Continued subduction leads to the obduction of the ophiolite onto the continental crust. Modified after Wakabayashi & Dilek (2003).

2.4.4 Mantle wedge peridotites

Mantle wedge (garnet) peridotites (MW(G)P) are incorporated from the hanging wall into a subducting continental plate. They can, however, have a very distinct chemical signature. Zhang et al. (2010) treats four subtypes of mantle wedge garnet peridotites, their emplacement and chemical features (A, B, C and D in figure 2.5). These subtypes are endmembers based on the type of continent involved in the collision (i.e. normal continent= thin SCLM vs. cratonic continent= thick SCLM) and activity of the mantle wedge (i.e. degree of asthenospheric upwelling). Considering a mantle wedge which is static and cold, the MWGP will reflect the age of the lithospheric mantle and will therefore always predate the age of the collision event. If cratonic crust is involved (type A) the age of MWGP's can be much older and PT-conditions related to the formation of the olivine-garnet assemblage can be much higher in the SCLM than compared to normal continental crust (type C). In a system of a dynamic mantle wedge MWGP will no longer yield similar ages to the lithospheric mantle. In fact, hot and dynamic asthenosphere will be incorporated in the hanging wall and ages of the garnet-olivine assemblage will correspond to the age of the collision event. Asthenospheric upwelling will occur at shallower levels below a normal continent (Type D) compared to a cratonic continent (Type B) and this is reflected in the PT-conditions during mineral formation. Figure 2.5 displays the tectonic settings in which incorporation of the various types of MWGP can occur. This emplacement is closely related to the geodynamical model of the Scandinavian Caledonides as presented by Brueckner & van Roermund (2004) (see chapter 2.5.2). This process can equally incorporate spinel peridotite, then called mantle wedge spinel peridotite (MWSP), if it occurs at depths <70km. Contrarily, ophiolitic peridotites cannot include garnet since they originate from much shallower depths. By this mechanism the peridotite becomes incorporated into the subducting plate.

Figure 2.5 Simplified illustrations showing the geodynamical incorporation of the four mantle wedge garnet peridotite subtypes (position marked by symbol). The diagrams on the left (A_1, B_1, C_1, D_1) correspond to the geodynamical setting prior to incorporation. The diagrams on the right (A_2, B_2, C_2 and D_2) correspond to the geodynamical setting during incorporation. **A** Old and thick SCLM (cratonic) collides with "normal" continental crust. Since the mantle wedge is cold and static, the age of the incorporated garnet peridotites correspond to the formation of the (cratonic) SCLM (i.e. up to Archean age). **B** Old and thick SCLM (cratonic) collides with "normal" continental crust. However, as a consequence of asthenospheric upwelling in the mantle wedge and corresponding high temperatures, the age of the incorporated garnet peridotites corresponds to the collision event opposed to the SCLM. **C** "Normal" continent collides with thin SCLM of other "normal" continent. Since the mantle wedge is cold and static, the age of the incorporated garnet peridotites correspond to the formation of SCLM, which always pre-dates the collision event. **D** "Normal" continental crust collides with thin SCLM of other "normal" continent. However, as a consequence of asthenospheric upwelling in the mantle wedge and corresponding high temperatures, the age of the incorporated garnet peridotites may correspond to the collision event. After Zhang et al. (2010).

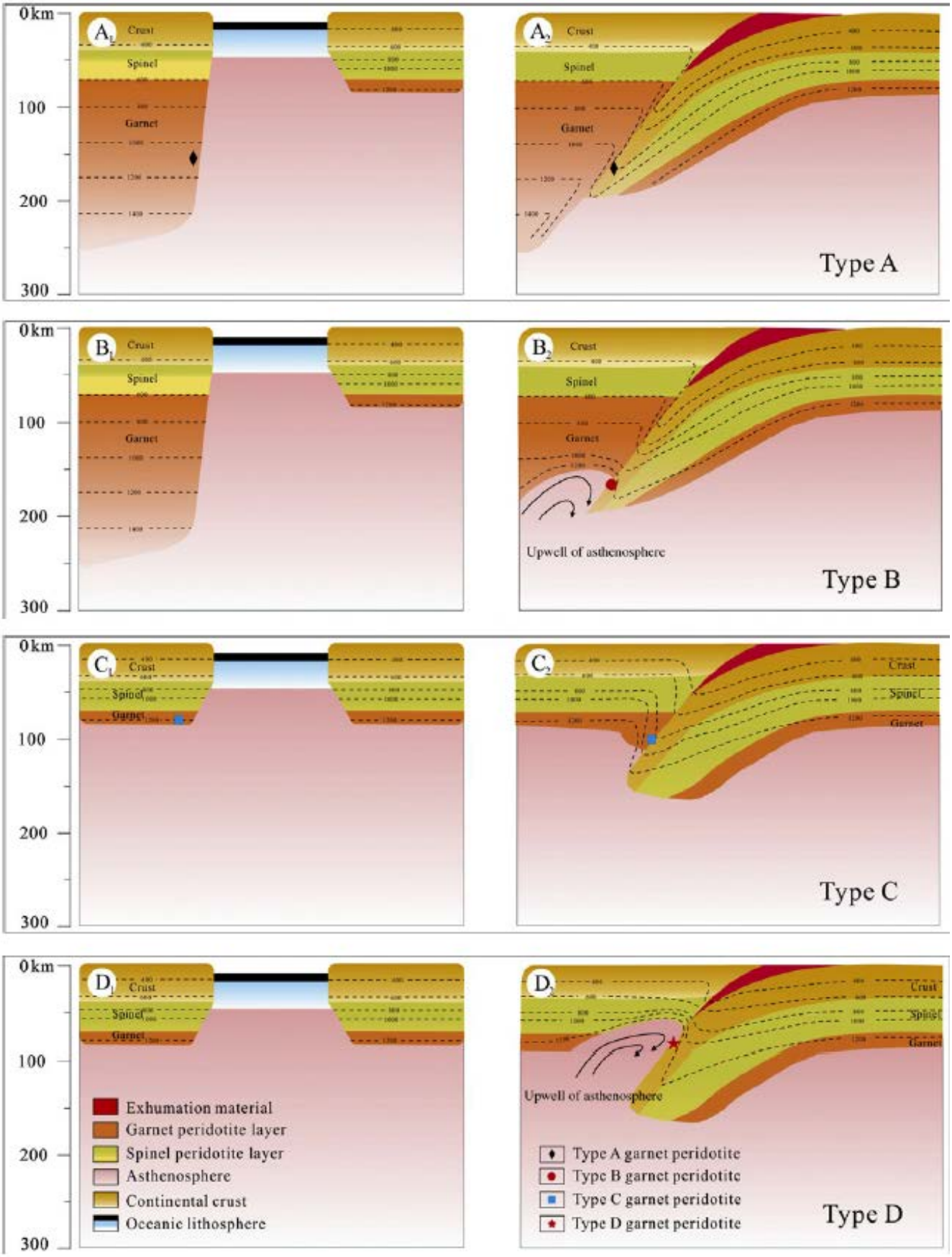
0km
100
200
300
A1
Crust
Spinel
Garnet
A2
Crust
Spinel
Garnet
Type A
B1
Crust
Spinel
Garnet
B2
Crust
Spinel
Garnet
Upwell of asthenosphere
Type B
C1
Crust
Spinel
Garnet
C2
Crust
Spinel
Garnet
Type C
D1
Crust
Spinel
Garnet
Exhumation material
Garnet peridotite layer
Spinel peridotite layer
Asthenosphere
Continental crust
Oceanic lithosphere
D2
Crust
Spinel
Garnet
Upwell of asthenosphere
Type A garnet peridotite
Type B garnet peridotite
Type C garnet peridotite
Type D garnet peridotite
Type D

2.5 Geological models of the Scandinavian Caledonides

The Scandinavian Caledonides are an old and deeply eroded mountain belt. Some evidence of its development has been long lost in the hundreds of million years since the orogeny was active. The nappe structure of the Caledonides was recognized as far back as in the 19th century by Törnebohm (1872). Gee (1975) proposed a geodynamical model, based on the work done by Zachrisson (1969) and Zwart (1974) on the nappe structures and their metamorphic grade. Gee's 1975 model did not involve subduction, but assumed the nappes were transported over a décollement surface, separating the nappes from the rigid basement below. Gee's 1975 geodynamical model pre-dates the concept of plate-tectonics, and in light of current knowledge seems outdated. It, however, formed the basis of the geodynamical models to follow. Three recent models will be further discussed in this chapter, namely Roberts (2003), Brueckner & van Roermund (2004) and Hacker & Gans (2005). These models describe various orogenic phases with ages that can differ. It is important to realize that the tectonic processes are diachronous and can occur at slightly different times depending on location. Taking into account the length of the Baltic continent involved in the Caledonian orogeny and the many assumed island arcs and/or micro-continents spread across the Iapetus Ocean, deformation/metamorphism may have occurred at any given time during the Caledonian orogeny resulting in different ages of metamorphic assemblages formed in the nappes.

2.5.1 Roberts (2003)

Roberts (2003) recognizes and describes four (or five) major orogenic events in his geodynamical model of the Caledonides (fig 2.6/2.7/2.8/2.9). The late stage orogenic collapse is debatable whether or not it is part of the continent-continent collision of the Scandian orogeny. Other models do not deal with the orogenic collapse as a separate phase. For reasons of convenience both events are discussed below as one phase, the Scandian orogeny. Roberts (2003) recognizes the following four orogenic phases which are according to their age, the Finnmarkian orogeny (542-510 Ma), the Trondheim orogeny (479-468 Ma), the Taconian orogeny (472-444 Ma) and finally the Scandian orogeny (428-398 Ma).

The Finnmarkian orogeny

The first orogenic phase, the Finnmarkian, heralded the onset of the Caledonides. According to Roberts (2003) this did not involve Laurentia and/or the Iapetus, such as in later stages of the Caledonian orogeny, but rather Siberia and the Ægir Sea. This concept is controversial for several reasons. Siberia would only have partitioned in this first phase and eluded further involvement in the Caledonides. Furthermore, according to Torsvik & Rehnström (2001) this would require an inter- or post-Finnmarkian anti-clockwise rotation of Baltica to occur before later stages of the orogeny. The Finnmarkian is interpreted to be the result of the collision between Baltica and a magmatic arc in the Ægir Sea. The margin of Baltica was subducted beneath the magmatic arc reaching eclogite facies metamorphism. Rapid exhumation led to the emplacement of the nappes onto the Baltic plate. Figure 2.6 illustrates the Finnmarkian orogeny according to Roberts (2003). Peridotite incorporation in this phase could have occurred as MWP or as OCT-type ophiolites.

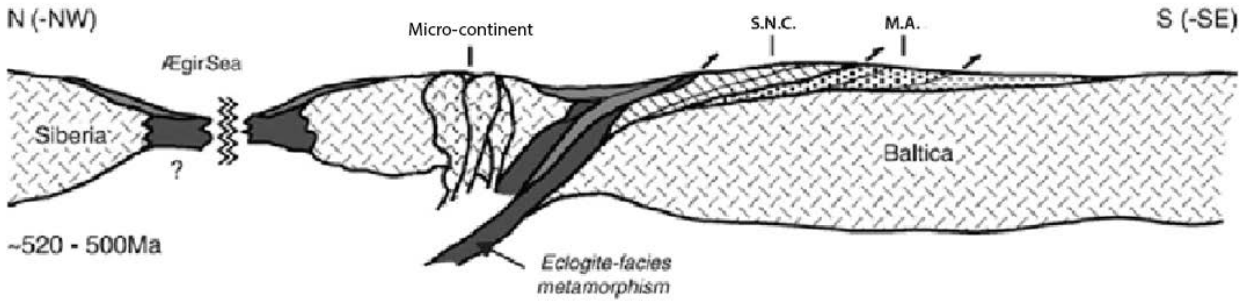

Figure 2.6 Schematic illustration of the Finnmarkian accretionary event (520-500 Ma) according to Roberts (2003). The subduction of the ocean/continental margin transition down to eclogite facies was followed by exhumation and subsequent emplacement on to the Baltica continent. Index: S.N.C. (Seve Nappe Complex), M.A. (other Middle Allochthon). Minor adjustments after Roberts (2003).

The Trondheim orogeny

Further south, in the vicinity of Trondheim, Holtendahl (1920) was the first to recognize an orogenic phase, then named the Trondheim disturbance. It was at that time regarded as being part of the early Caledonian orogeny. However, subsequent research revealed the timing and paleogeographic position are very different (Gee, 1987). The Trondheim phase (figure 2.7), which occurred 480 to 475 Ma, involves a micro-continent rifted off Baltica in pre-Caledonian time and the subduction by oceanic crust (Köli) in the direction of the Iapetus (i.e. northwest-ward). Metamorphic conditions reached blueschist facies, ergo the ophiolites were obducted and emplaced on to the Baltic plate (Eide & Lardeaux, 2002). Peridotites belonging to this phase must be of the Penrose-type or OCT-type ophiolites.

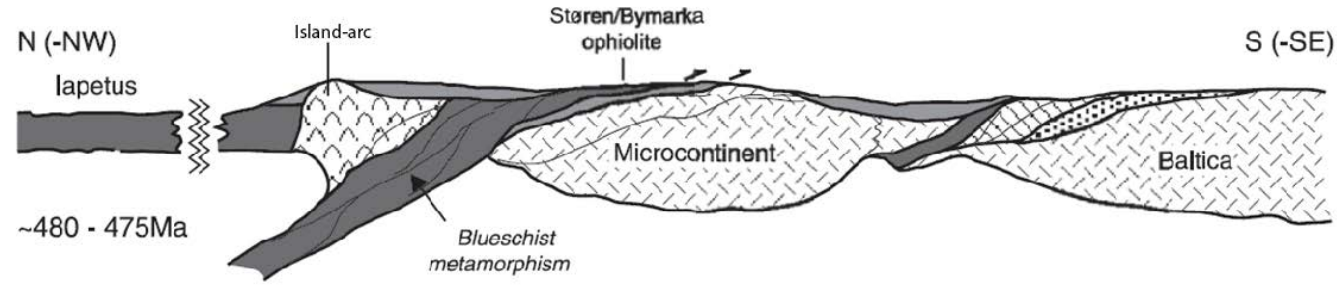

Figure 2.7 Schematic illustration of the Trondheim phase (480-475 Ma) according to Roberts (2003). Oceanic crust (ophiolite) is subducted beneath the island arc and reaches blueschist facies. Shortly after the easternly positioned ophiolites are obducted eastward onto the micro continent plate. After Roberts (2003).

The Taconian orogeny

The Taconian, unlike the previously discussed phases occurs on the opposite side of the Iapetus and involves the eastern side of Laurentia. Laurentia collided with a magmatic island arc. The ocean/eastern margin of Laurentia subsides beneath and partly accretes to the magmatic island arc (figure 2.8). This resulted in metamorphism and ophiolite obduction (470-450 Ma), corresponding with the Jämtlandian on the eastern side of the Iapetus Ocean (Breuckner & van Roermund, 2004). The rocks involved in this event have later detached and have been emplaced on to the Baltic plate high in the tectonostratigraphy during the Scandian orogeny forming the Uppermost Allochthon, as is discussed below. The Uppermost Allochthon is where the Laurentia affiliated meta-sediments and basement units are currently positioned in the Scandinavian nappe pile (fig 1.1). Metamorphism may reach eclogite facies during the Taconian (up to 2.8 GPa) (Corfu et al., 2003). This was followed by rapid exhumation, similar as is described above for the Finnmarkian orogeny on the other side of the Iapetus Ocean some 50 Ma earlier. Orogenic peridotites which could have been incorporated in this phase are of the ophiolite type.

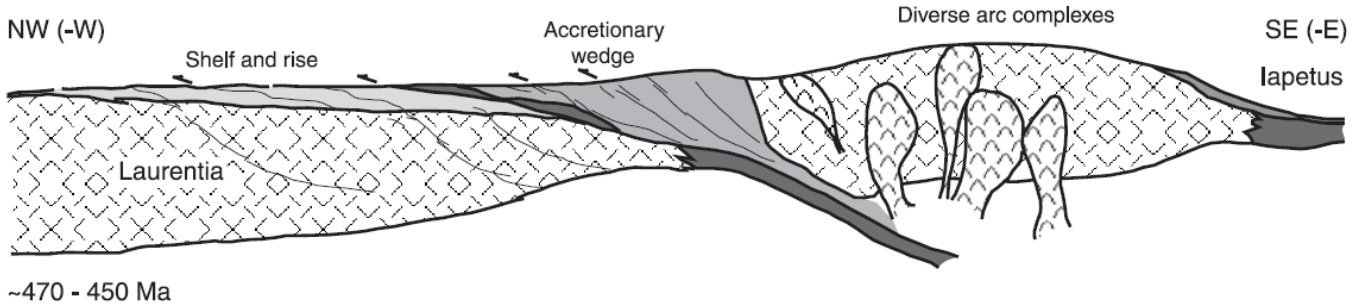

Figure 2.8 Schematic illustration of the Taconian phase (470-450 Ma) according to Roberts (2003). Laurentia collides with a magmatic island arc. Subduction of the ocean-continent transition (OCT) of Laurentia beneath the arc. The collision results in accretion and ophiolite obduction onto Laurentia. After Roberts (2003).

Scandian orogeny

The main and final phase of the Caledonian orogeny is the Scandian (figure 2.9). It is the continent-continent collision between Laurentia and Baltica which led to intense crustal thickening/under thrusting further east. The Baltic margin subducts beneath Laurentia and during this phase the nappes were positioned on top of one and other, resulting in the basic geometry of westward dipping Allochthons on top of the sedimentary cover of Baltica, the Autochthon. Also the Laurentia associated meta-sediments of the Uppermost Allochthon are amongst those. Parts of the down going subducting slab are currently exposed at the surface. The most important and biggest are the Western Gneiss Region (WGR) and Lofoten (fig 1.1). Geochronologic analysis, performed on zircons and monazites in UHP rocks of the WGR, has shown both subduction (to ~125 km) and subsequent exhumation have been rapid processes (Terry et al., 2000; Spengler et al., 2009) possibly taking under 10-15 Ma. During this process MWP could have been incorporated in the subducting Baltic slab.

During later stages of the Scandian orogeny compression started to wane. Diminishing convergent forces left the Caledonides overthickened, which in turn led to orogenic collapse (figure 2.10). Roberts (2003) recognizes three stages. The first stage is compression at all levels of the crust. The second stage is of initial orogenic collapse confined to the orogenic wedge with coeval compression at depth. The last stage is extension at all levels. In this model the extension of the Caledonides has led to the first exhumation of the (U)HP rocks in the WGR.

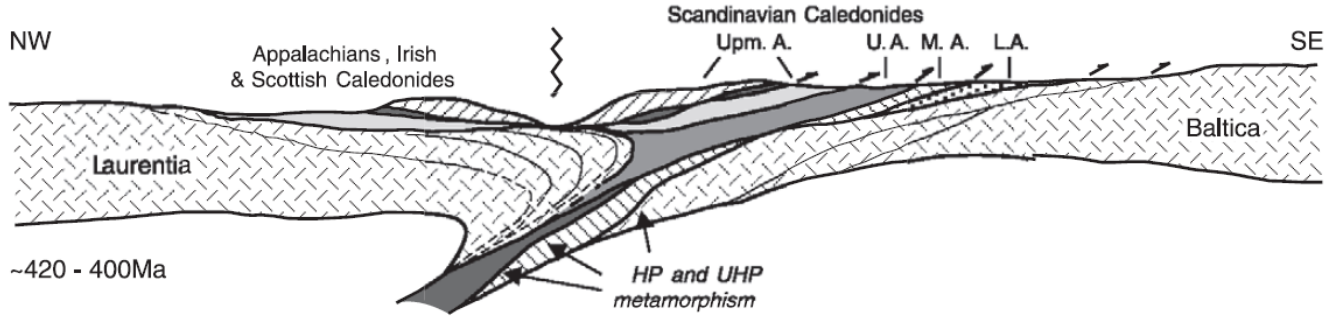

Figure 2.9 Schematic illustration of the Scandian phase (420-400 Ma) according to Roberts (2003). Continent-continent collision between Laurentia and Baltica, with the Baltic margin subducting beneath Laurentia. Index: Upm.A (Uppermost Allochthon), U.A. (Upper Allochthon), M.A. (Middle Allochthon) and L.A. (Lower Allochthon).

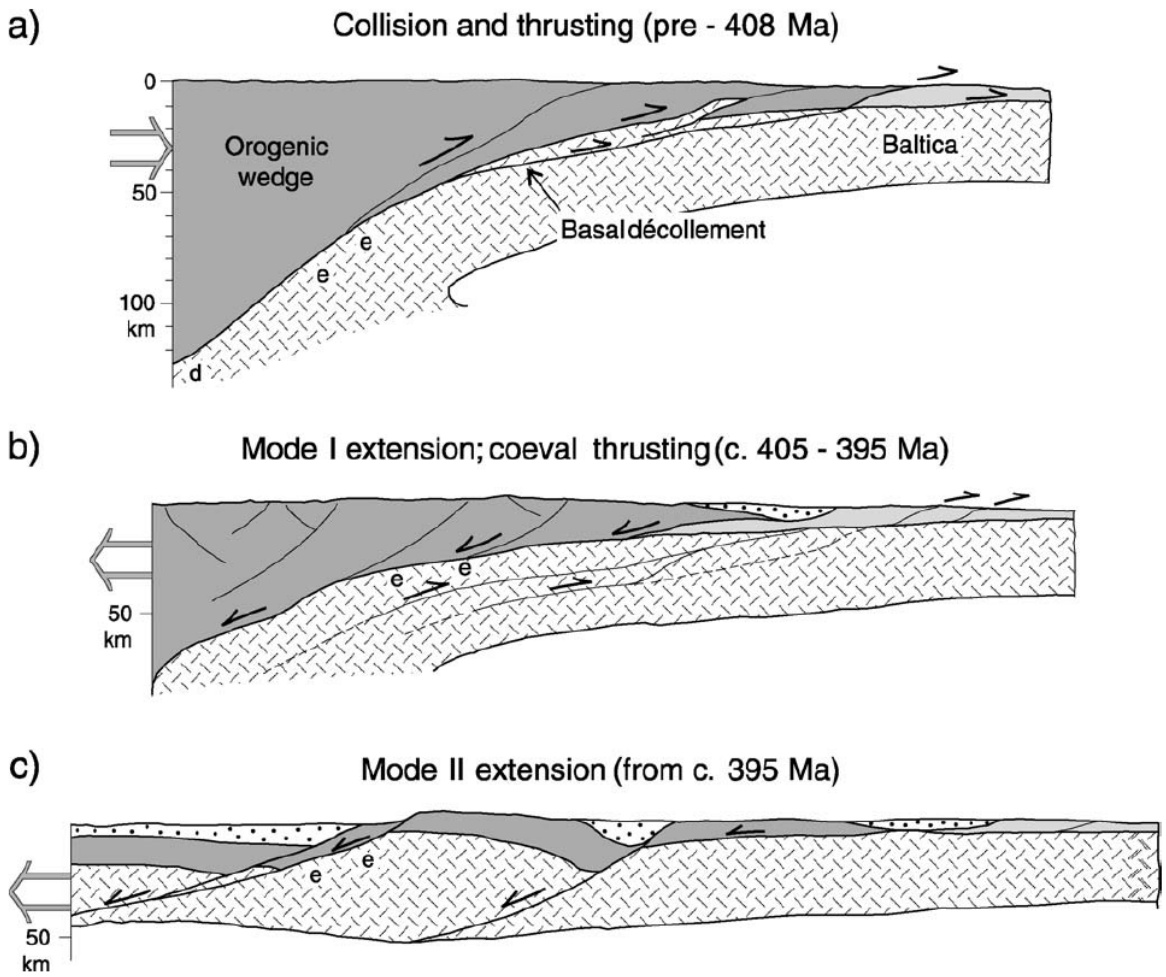

Fig 2.10 Schematic illustrations of the continent-continent collision and subsequent orogenic collapse according to Roberts (2003). **a** The first stage: collision/subduction throughout all levels of the crust. **b** Second stage: initial orogenic collapse at shallow levels of the crust and coeval compressional movement at deeper levels of the crust. **c** Last stage: orogenic collapse throughout all levels of the crust, leading to exhumation of the (U)HP rocks.

2.5.2 Brueckner & van Roermund (2004)

Throughout the Scandinavian Caledonides various ultra-high pressure minerals such as coesite and micro diamonds are discovered within eclogite bearing terranes (Smith, 1984: Dobrzhinetskaya et al., 1995). In order to form these terranes continental crust or parts of continental crust must have subducted to large depths, metamorphosed and resurfaced. This realization has led to the development of the geological concepts of slab pull (Brueckner, 1998) and later dunk-tectonics (Brueckner & van Roermund, 2004). For comprehensibility reasons these concepts will be explained prior to discussing the geodynamical model of the Scandinavian Caledonides.

Slab-pull & dunk-tectonics

The Wilson-cycle describes the various stages of continental divergence and convergence in 2D (Wilson, 1968). The Caledonian orogeny occurs during the closure stage of the cycle. The oceanic crust of the Iapetus which originated in the rifting Rhodinia forming Laurentia and Baltica is subducted along one or a series of destructive margins that ultimately leads to a final continent-continent collision. The process of subduction is driven by the density difference between gabbroic oceanic crust and the more felsic composition of continents and island arcs. As the oceanic crust is completely subducted, the destructive margin meets an island arc or (micro-)continent. It is the latter that now will be subducted below the destructive margin by the principle of slab-pull due to the relative high combined density of the oceanic crust metamorphosed to eclogite and the island arc/(micro-)continent compared to normal island arcs/(micro)continents. In this way the subducting continental slab can reach depths greater than what can be achieved by crustal thickening in conventional continent-continent collision models. The combined down going slab will internally experience different buoyancy forces which could lead to rupture between the heavy oceanic and the light continental lithosphere, called slab breakoff (von Blanckenburg & Davies, 1995). The disconnection of the oceanic lithosphere stops further subduction of the continental crust, but this will not necessarily result in its return to the surface. The crustal terranes need to delaminate from the underlying mantle before eduction occurs (Ernst et al., 1997). Buoyancy effects can lead to the continental terranes exiting the mantle and reach lower crustal levels (Andersen et al., 1991), but this effect is limited due to the density increase caused by the recent (U)HP metamorphism. Eduction to sub-surface levels can be acquired via multiple suggested mechanisms (Warren, 2013). Such as incorporation by continued convergence or exhumation by orogenic collapse to name a few. The sequence of slab-pull, slab-breakoff and eduction defines dunk-tectonics (figure 2.11). This model has also been used to explain the incorporation of mantle wedge garnet peridotites within crustal terranes (Brueckner, 1998; van Roermund, 2009; Clos et al., 2014).

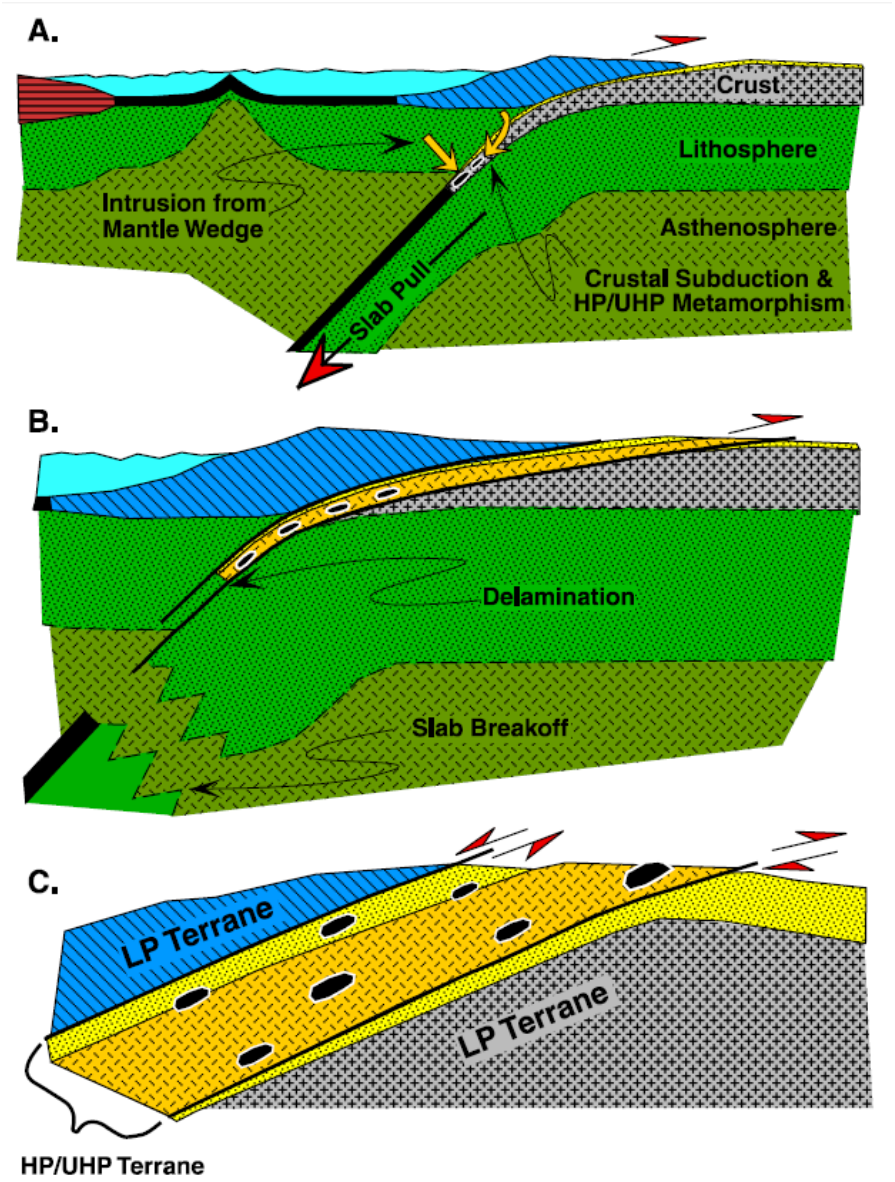

Figure 2.11 Simplified illustration of the dunk-tectonics model. **a** Subduction of continental lithosphere by slab-pull of foregoing oceanic lithosphere. Mantle wedge intrusions can occur. **b** Slab breakoff, negatively buoyant oceanic lithosphere continues to subside, positively buoyant continental lithosphere moves upward. Note: the occurrence of delamination of crustal terranes from mantle and the subsequent eduction of (U)HP rocks. **c** Geometry at the surface of educted (U)HP terranes. Note: the two type of faults. After Brueckner & van Roermund (2004).

Tectonic model

Brueckner & van Roermund (2004) describe three major orogenic events in their geodynamical model of the Caledonides. These distinct phases with corresponding ages are the Finnmarkian (500 Ma), the Jämtlandian (454 Ma) and the Scandian (430-400 Ma). On the other side of the Iapetus a fourth phase is recognized approximately simultaneously with the Jämtlandian, the Taconian (~450 Ma), but it is not incorporated in their model.

Finnmarkian

The Finnmarkian orogeny is the result of the collision between a micro-continent (C) and the Virisen Island Arc (fig 2.12). The micro-continent is believed to be an outboard terrane which previously rifted from Baltica (Gayer et al., 1987). Whereas the Virisen Island Arc originated by intra-oceanic subduction. During the collision the micro-continent subducted deep beneath the Virisen Island Arc due to slab-pull of the foregoing eastern Iapetus oceanic plate. The micro continent reached depths of circa 60 km (Andréasson & Albrecht, 1995). Slab break off and delamination of the crustal terrane enables its eduction creating the Virisen Norrbotten Composite Terrane (VNCT). The VNCT was at this point still separated from Laurentia by the western Iapetus and from Baltica by a rifted basin (fig 2.12b). The Finnmarkian was a collision not directly involving either of the large continents, Laurentia or Baltica, but was rather an intra-oceanic event. This phase is illustrated in figure 2.12. Ophiolite types could have been incorporated in the overriding plate and MWP in the subducting plate, however not of the garnet type because the lithosphere below the island arc would have been too thin.

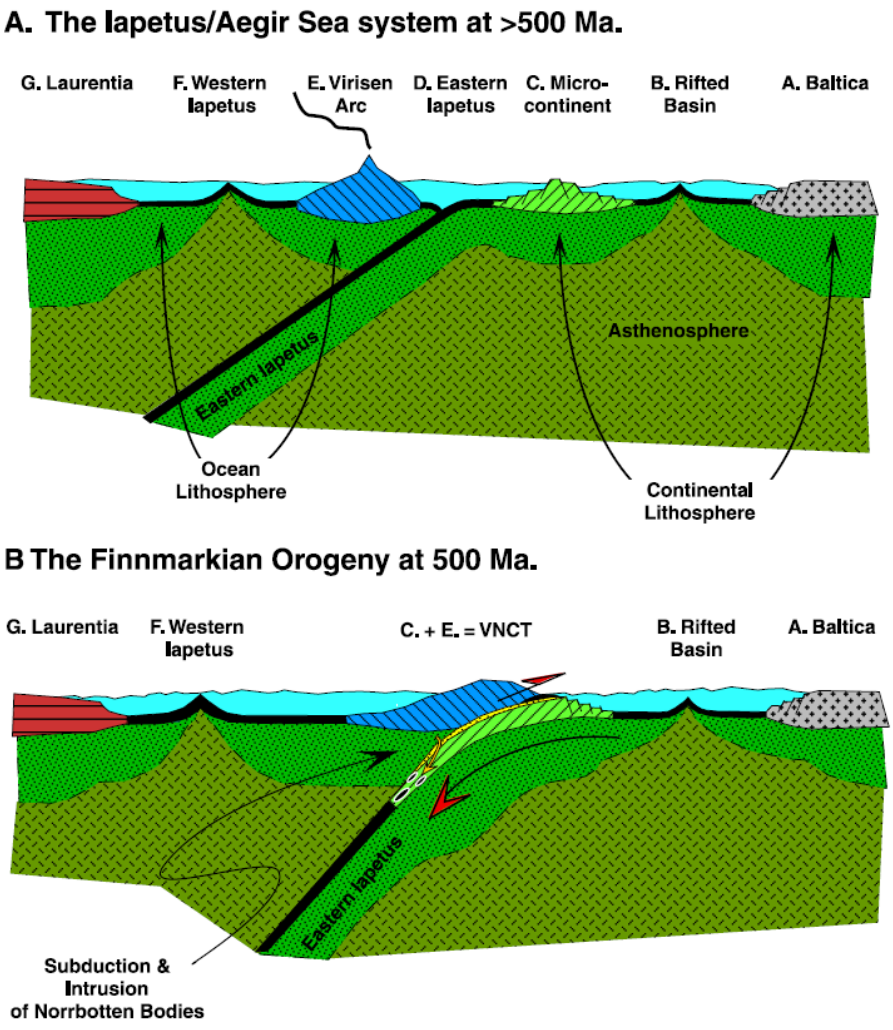

Figure 2.12

a Schematic illustration of the pre-Finnmarkian intra-Oceanic configuration of the Iapetus Ocean and its basic components.

b The Finnmarkian orogeny, the subduction of the micro continent beneath the Virisen arc. Mantle wedge spinel peridotites incorporation, metamorphism followed by slab breakoff and delamination occurs. Eduction leads to the formation of the Virisen/Norrbotten composite terrane (VNCT). After Brueckner & van Roermund (2004).

Jämtlandian

Post-Finnmarkian the convergence continued through subduction of the western Iapetus and the rifted basin. The latter closed between 500 Ma and 454 Ma by subduction along its western border beneath VNCT. The subduction of the rifted basin led to melting and igneous intrusions into the VNCT. Intrusive and extrusive complexes within the Köli Nappe yield ages between 483 and 456 Ma (Roberts & Stevens, 2000). The progressive closure of the Eastern Iapetus led to the convergence of VNCT and Baltica and resulted in the eventual collision between the two during the Jämtlandian orogeny, wherein the margin of Baltica was pulled beneath VNCT by the foregoing oceanic plate (Eastern Iapetus). The eclogite metamorphic facies was reached before subsequent slab breakoff, delamination and exhumation to amphibolite facies conditions. Around 440 Ma eduction of the continental terranes was completed. During subduction or eduction mantle wedge peridotites are incorporated into the SNC (e.g. the Friningen garnet peridotite (Gilio et al. 2015) and the Kittelfjäll spinel peridotites (Clos et al. 2014)). This orogenic event is illustrated in figure 2.13a-b.

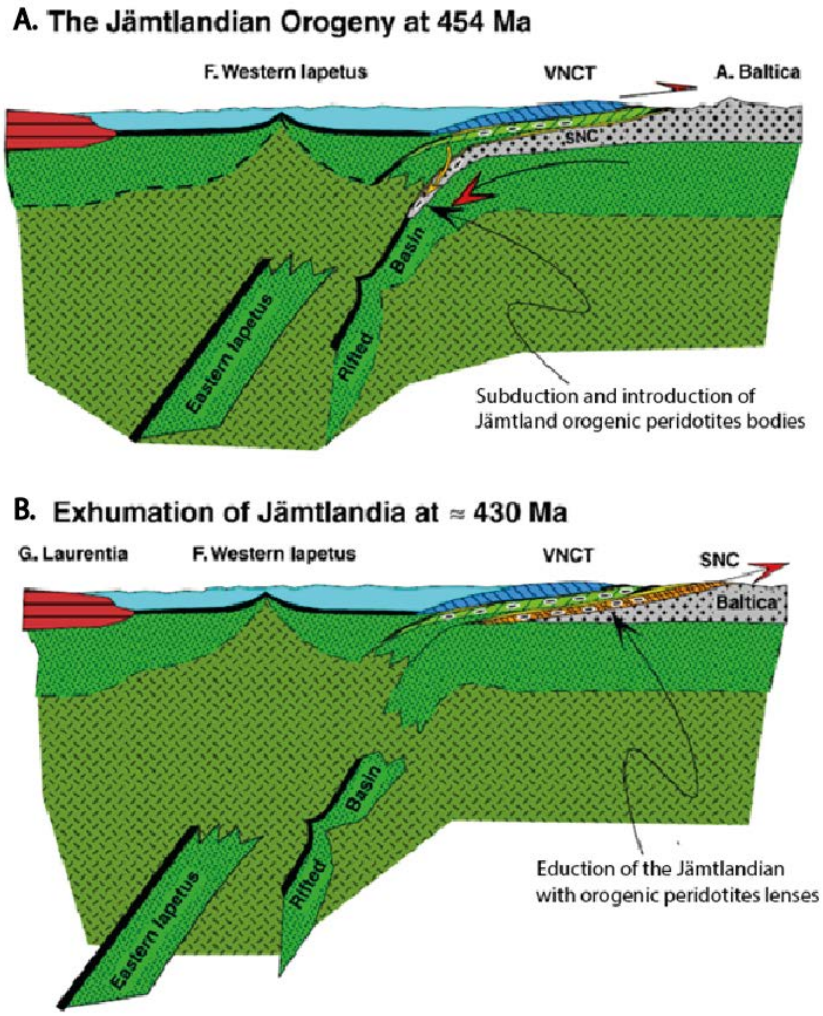

Figure 2.13

a The Jämtlandian orogeny, Baltica subducts beneath the VNCT. Mantle wedge peridotite incorporation, deformation and metamorphism up to coesite eclogite facies conditions occurred.

b Slab breakoff of the oceanic plate (Eastern Iapetus) and delamination results in the eduction and emplacement of (U)HP terranes eastward over the Baltic plate. Index: Seve Nappe Complex (SNC). After Brueckner & van Roermund (2004).

Scandian

On the other side of the Iapetus subduction along the destructive margin of Laurentia continued to progress. The western Iapetus, at that time the only remaining part of Iapetus, closed. i.e. the Köli nappe was emplaced on top of Baltica related nappes, thereby obducting a Penrose type ophiolite sequence. The convergent movement of Laurentia and Baltica reached its apex with the continent-continent collision at 425 Ma, the Scandian orogeny. In the Scandian event Laurentia overthrusted the western edge of Baltica. This event caused the eastward transport of Laurentia affiliated rocks, such as the uppermost Allochthon, and reactivates the previously accreted underlying oceanic and Baltica-affiliated Allochthons including the Köli further east over the Baltic plate. The Scandian orogeny began at approximately 430 Ma (Gee, 1975; Spengler et al, 2009), but the peak metamorphism of the eclogite facies in the Western Gneiss Region occurred sometime after, between 418 and 400 Ma (Tucker et al., 1987; Williams et al., 1999; Terry et al., 2000; Spengler et al., 2009). Part of the subducting Baltic crust is currently exposed in the Western Gneiss Region. Initially, eduction occurred via buoyancy forces similar to what is seen in the previously discussed Finnmarkian and Jämtlandian orogenic events. Eventually transport to the surface is acquired by uplift due to post-Scandian extensional collapse. During subduction and eduction MWP were incorporated in the subducting country rock. This orogenic event is illustrated in figure 2.14.

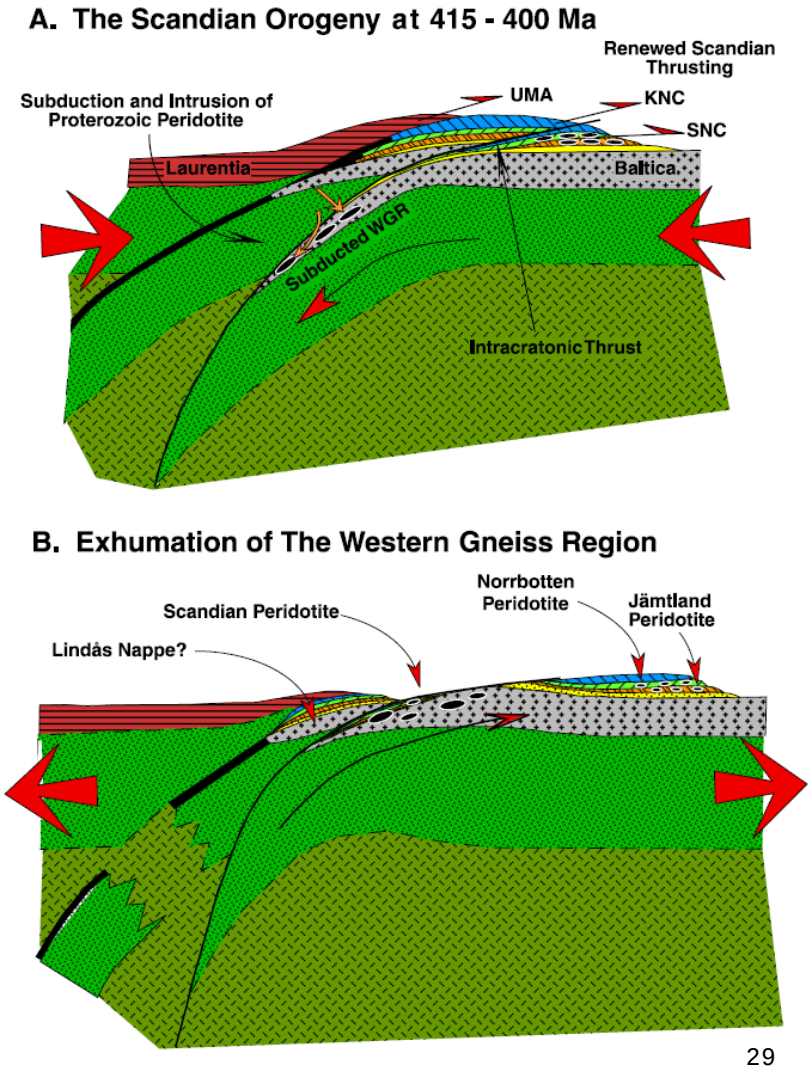

Figure 2.14

a The Scandian orogeny, the continent-continent collision and subsidence of Baltica westward beneath Laurentia. Reactivation along earlier contacts resulting in the stacking of the Allochthons.

b Final eduction of the (U)HP Baltic basement rocks found in the Western Gneiss Region, followed by extension/orogenic collapse of the Caledonides. After Brueckner & van Roermund (2004).

2.5.3 Hacker & Gans (2005)

Hacker & Gans (2005) base their tectonic model on thermobarometry and thermochronology of the (U)HP terrane in the WGR and structurally overlying oceanic and continental (Köli and Seve) nappes. Their research concludes UHP metamorphism occurred in the late stages of the Caledonian orogeny (fig 2.15e), post-dating ophiolite obduction and subduction. Unlike the above mentioned authors Hacker & Gans (2005) do not postulate island-arcs or micro-continents to support their model. They focus on the path the nappes underwent (i.e. subduction/exhumation), rather than speculating on the causes of this path. In their model they recognized four major events and corresponding ages, called the Trondheim (480-470Ma), the Jämtlandian (450-445Ma), an extensive extensional period (454-432Ma) and the Scandian (437-415Ma). The Finnmarkian, which was discussed in the foregoing geodynamical models, is according to Hacker & Gans (2005) a period of tectonism related peripherally to the Scandian UHP event and was not discussed further. The Trondheim and the Jämtlandian are events which have resulted in nappe stacking, but have not contributed to UHP metamorphism. During the Trondheim orogeny ophiolites of the Köli nappes are trusted eastward upon the Gula nappe. During the Jämtlandian the Seve Nappes subducts westward beneath the Köli-Gula nappes, which led to its thickening, heating and subsequent exhumation.

The Jämtlandian was followed by an extensive magmatic period, during which significant amounts of new oceanic crust was formed. This was accompanied by intrusions of plutons and dikes in the Uppermost Allochthon and Köli nappes. Absence of plutons of the same age in the underlying stratigraphy suggests the emplacement of the Uppermost Allochthon and Köli nappes postdates this event. This phase of rifting, within the overall compressional regime, marks an important interregnum. This would hold that the late stage Scandian orogeny is unrelated to the foregoing contractional events. The Scandian, the fourth tectonic event is according to Hacker & Gans (2005) the first that relates directly to the UHP metamorphism. This diachronous event caused the eastward transport of nappes. Nappe emplacement occurred in the west at approximately 437 Ma and ended at 415 Ma in the east. The Scandian event began with the thrusting of the Köli Nappes onto the Seve Nappes and the Upper Allochthon onto the Köli Nappes, creating the basic geometry of tectonostratigraphic units (i.e. Uppermost Allochthon to Autochthon) we recognize in the field today. At 420 Ma this stack has reached its furthest point east, although peak UHP metamorphism still occurred some 10Ma later. The Western Gneiss Region which forms part of the basement of the subducting Baltic plate must have progressively subsided. Four mechanisms that could have contributed to this subsidence are proposed (for additional reading we refer to Hacker & Gans (2005)), however no sequential exhumation processes are proposed. According to this model MWGP can only be incorporated in the WGR during the last stage. It does not explain the UHP-metamorphism in the SNC at 465-445 Ma (Brueckner et al., 2004; Brueckner & van Roermund, 2007; Root & Corfu, 2012) nor the incorporation of mantle wedge peridotites into the SNC (Clos et al., 2014; Gilio et al., 2015). All orogenic peridotites in the Köli and Seve nappe are, according to this model, of the ophiolite type, with the sole example of the WGR which are MWGP.

leaving this model severely limited. The complete model of Hacker & Gans (2005) is illustrated in figure 2.15.

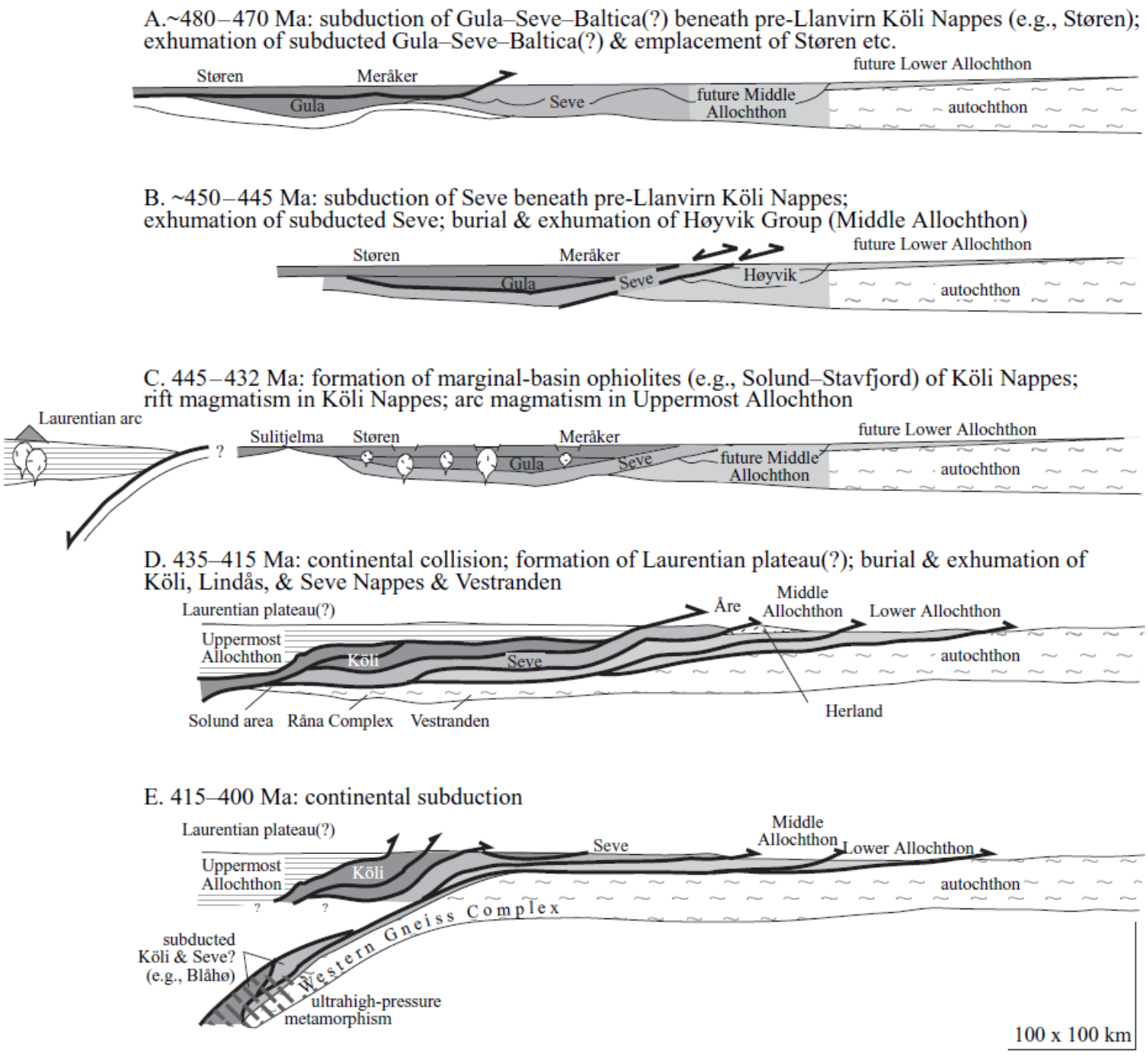

Figure 2.15 A schematic illustration showing the development of the Scandinavian Caledonides as described by Hacker & Gans (2005) **a** Westward underplating of the Gula- and Seve nappes. Furthermore, the emplacement of the lower parts of the Köli nappes onto the Baltic continent **b** Shallow subduction of the Seve nappe is followed by its exhumation and emplacement between the lower Köli nappes and the lower allochthon. **c** The formation of the marginal-basin ophiolites during rift magmatism. **d** Collision of Laurentia and positioning of the marginal basins including basement on top of the Seve nappe. **e** Subduction of Baltica to large depths leading to ultra-high pressure metamorphism and possible MWGP introduction. After Hacker & Gans (2005).

3) Methods

3.1 Sample collection

Based on geological maps by Trouw (1973) and the Swedish geological survey (Zachrisson, 1993; Zachrisson & Greiling, 1993) the latter being to a large degree based on fieldwork performed by students of the University of Leiden in the seventies and eighties, a preliminary selection of peridotite- and country rock sample locations were determined and subsequently visited by the author. These locations where selected such to represent an adequate distribution between the lower- and upper belt and take into account accessibility. In total twenty-five hand samples were collected in the Marsfjällen area in southern Västerbotten, Sweden. Seventeen samples in the vicinity of Kittelfjäll and eight samples in the vicinity of Marsliden, as is indicated in figure 3.1. Sample numbers 1-5 are collected from the Aunere ultramafic body positioned in the Köli nappe. Sample numbers 6-11 and 18+20-25 are gathered from or near a northern and a southern ultramafic body positioned in the lower belt and the sample numbers 12-17 are collected from or near two ultramafic bodies that outcrop in the upper belt. Corresponding coordinates are indicated in table 3.1. The samples are predominately ultramafic of composition, however a smaller portion is pelitic country rock (samples: 1, 8, 12, 13 and 18) in order to provide reference PT-conditions in the matrix-rocks. All hand samples are orientated during collection with marker pen and GPS-locations are recorded so that the original orientation and position can be reconstructed.

3.2 Sample preparation

From all collected hand samples orientated uncovered thin sections were prepared. Each hand sample was cut into 2 cm wide blocks to facilitate the cutting process. These blocks are marked with marker pen to preserve the original position in the sample. The thin sections are subsequently marked in correspondence with the block it is made of. By doing so information of the position is retained and the thin sections can be placed in regional perspective. The thin sections are all uncovered and well-polished into 30 µm thick films. After this the thin sections are coated with a carbon coating so it conduct electrons and the thin sections can be used for Scanning Electron Microscope (SEM) and Electron Microprobe (EMP) analyses. All thin section numbers correspond to the sample number given in table 3.1 and figure 3.1.

3.3 Optical microscopy

The primary analyses of the thin sections are done by optical microscopy. It confirms or rejects the rock classifications made in the field. Mineral identification based on mineralogical properties under plain polarized light and cross polarized light provides a reliable first order assessment of the minerals present and their relation to one and other. Later analyses (SEM or EMP) yield conclusive assessments by chemical analyses. All thin sections are scanned to provide a numbered digital overview system on which enlargements, structures, overgrow relations and chemical analyses have been indicated. All illustrated in the appendices.

3.4 Scanning Electron Microscope (SEM)

SEM analyses are done on the Table-Top SEM of the Utrecht University in the joint environmental laboratory in Utrecht. Backscatter electron imaging was used to provide an overview of the location for chemical analyses and to display mineral relations. Complementary to optical microscopy, Electron-dispersive X-ray spectroscopy (EDX) was used to determine mineral type by means of a semiquantative method producing normalized chemical composition data. Chemical analyses are performed under high-vacuum conditions using a 15 Kv electron beam. Chemical analyses run for a total of 50 seconds per location.

3.5 Electron Microprobe (EMP)

Electron microprobe analyses are performed on the FEG-JEOL of the Utrecht University in the joint environmental laboratory in Utrecht. Using an acceleration voltage of 15 kV and a beam current of 20 nA. The EMP has all the functions of the SEM, however the analyses output is not normalized, which makes it better suitable for the recognition of hydrous minerals. In addition, the precision is better (±1.5% S.Ω) providing more precise major and minor element oxides weight measurement in minerals. Furthermore, the EMP yields un-normalized data which can be used for analyses on hydrous minerals. For Fe^{2+}/Fe^{3+} calculations on microprobe data the procedure of Zane and Weiss (1988) has been adopted.

3.6 Numbering system

All chemical analyses retrieved by the EMP and SEM are listed in table 1-4 of appendix I. The third column in table 1 and 2 and the second column in table 3 and 4 refer to EMP/SEM spot the number ascribed to a specific analysis. The fourth column in table 1 and 2 and the third column in table 3 and 4 lists the number of the appendix of the BSE image enlargement on which the location of the analysis are indicated with the corresponding point. The middle section in the appendix corresponds to the thin section number it is located on (e.g. Appendix III-9-2, is the second enlargement corresponding to thin section 9). Appendix II includes the scans of the thin sections used in this thesis. Each scan contains a maximum of two different types of rectangular enlargements boxes, one corresponding to the optical microscopy photographs as depicted in chapter 4 and 5 of this thesis and the other corresponding to enlargements as listed in Appendix III. The optical images are indicated by a rectangular black frame. The connected number corresponds to the figure it refers to in the thesis (e.g. 4.5c corresponds to figure 4.5c on page 46). The references to the enlargements are marked by a transparent blue frame. The connected number is the corresponding thin section number followed by the number indicating a specific enlargement (e.g. 14-3 corresponds to the third BSE image of thin section 14).

Table 3.1

Tectono-metamorphic unit	Sample #	Rock type	Coordinates
Köli	1	Meta-pelite	N 65°13'11.6 / E 15°14'11.9
	2	Peridotite	N 65°13'10.6 / E 15°13'27.8
	3	Peridotite	N 65°13'10.6 / E 15°13'27.8
	4	Peridotite	N 65°13'10.6 / E 15°13'27.8
	5	Peridotite	N 65°13'10.6 / E 15°13'27.8
Lower Seve belt	6	Peridotite	N 65°15'24.9 / E 15°40'00.6
	7	Peridotite	N 65°15'24.9 / E 15°40'00.6
	8	Meta-pelite	N 65°14'59.7 / E 15°43'57.8
	9	Peridotite	N 65°15'24.9 / E 15°40'00.6
	10	Peridotite	N 65°15'24.9 / E 15°40'00.6
	11	Peridotite	N 65°15'24.9 / E 15°40'00.6
Upper Seve belt	12	Meta-pelite	N 65°14'45.4 / E 15°21'26.3
	13	Meta-pelite	N 65°14'45.4 / E 15°21'26.3
	14	Peridotite	N 65°14'23.0 / E 15°20'35.5
	15	Peridotite	N 65°14'23.0 / E 15°20'35.5
	16	Peridotite	N 65°14'06.0 / E 15°21'45.4
	17	Peridotite	N 65°14'06.0 / E 15°21'45.4
Lower Seve belt	18	Meta-pelite	N 65°03'55.7 / E 15°31'21.2
	19	Amphibolite	N 65°03'55.7 / E 15°31'21.2
	20	Peridotite	N 65°04'13.4 / E 15°30'37.4
	21	Peridotite	N 65°04'13.4 / E 15°30'37.4
	22	Peridotite	N 65°04'13.4 / E 15°30'37.4
	23	Peridotite	N 65°04'13.4 / E 15°30'37.4
	24	Peridotite	N 65°04'13.4 / E 15°30'37.4
	25	Peridotite	N 65°04'13.4 / E 15°30'37.4

Table 3.1 Overview table listing the samples used in this thesis, the coordinates of the outcrop, the rock type and corresponding nappe. Locations of samples indicated on figure 3.1.

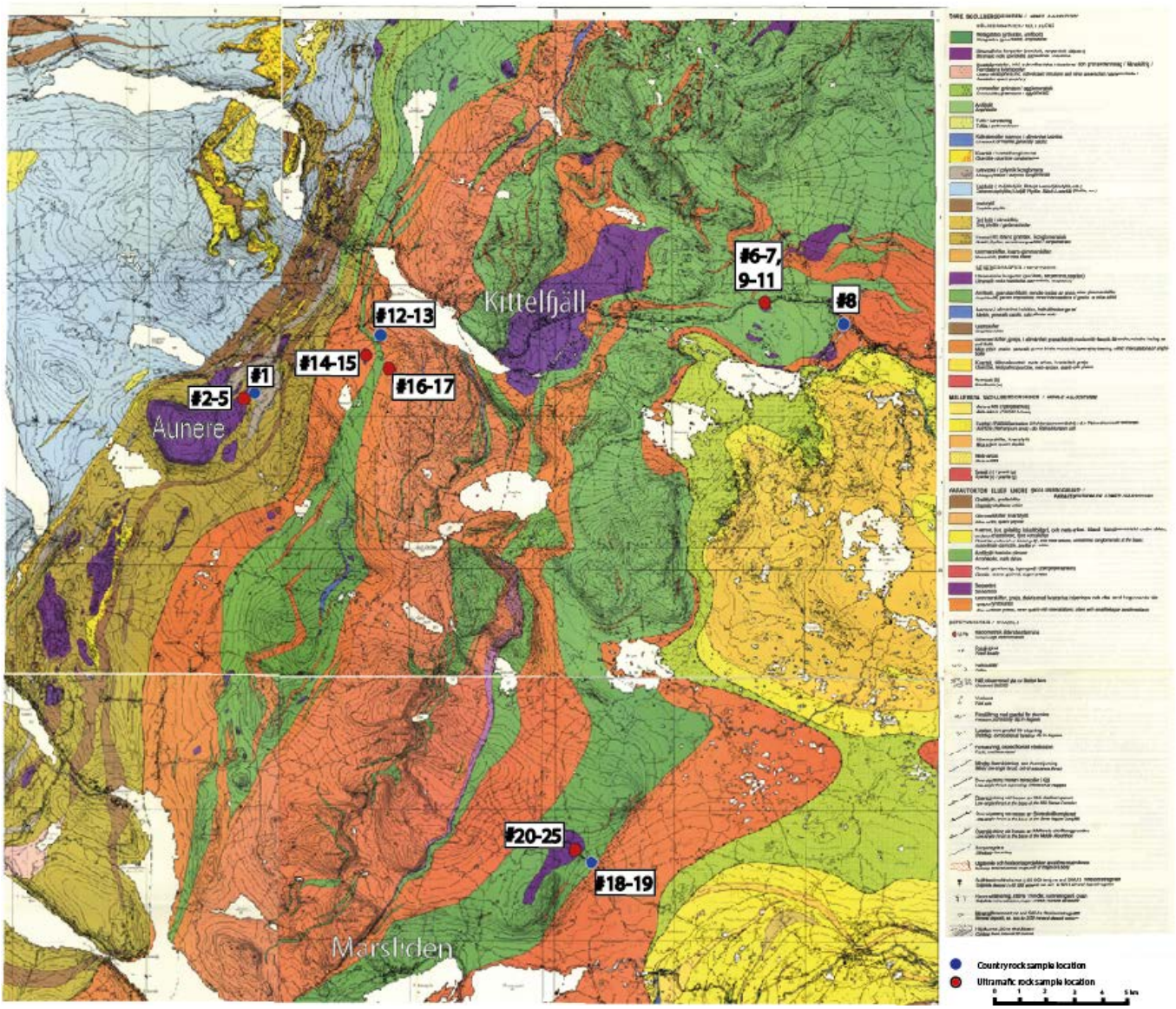

Figure 3.1 Geological map of the Marsfjället area, Västerbotten, Central Sweden. The numbers refer to the sample locations. Red dots indicate locations of peridotite samples. Blue dots indicate locations of country rock samples. Modified after Zachrisson & Greiling (1993) and Zachrisson (1993).

4) Orogenic Peridotites

4.1 Location

Samples have been taken from various peridotite bodies in the Marsfjäll area, Västerbotten, Sweden (fig 3.1). These peridotite lenses are selected such, as to cover the entire tectonostratigraphy of the Seve nappe. Clos et al. (2014) performed in-depth research on the Kittelfjäll Spinel Peridotite, Gilio et al. (2015) on the Friningen Garnet Peridotite, both locations come from the middle belt of the Seve Nappe, locations indicated in figure 2.2. Therefore, this research's additional samples have been taken from the upper- and lower belt of the Seve Nappe (figure 3.1) in order to extend on their work. In the upper belt two small bodies are sampled which outcrop south-west of Kittelfjäll (#14-17). In the lower belt one peridotite body is sampled east of Kittelfjäll beside the road to Dikanäs (#6-7, 9-11) and a second peridotite body further to the south, west of Saxnäs and just north of the hamlet of Marsliden (#20-25). In addition the large Aunere peridotite body in the Köli nappes located west of Kittelfjäll is sampled (#2-5). All locations of these peridotites are indicated in figure 3.1 and their coordinates are listed in table 3.1. Calon (1979) has described the Alpine type peridotites of the Seve/Köli nappe, at that time still part of a single nappe complex, the Seve-Köli Nappes Complex. His work provides the framework of this research. The following chapter will give a brief summary of the lithological and structural features of the orogenic peridotites within the upper- and lower belt of the Seve nappe and the Köli nappe.

4.2 Lithologies

The orogenic peridotite bodies in the SNC are found throughout all three belts and have varying sizes ranging from several square meters to several square kilometers. They are predominantly of the dunite and harzburgite subtype, with the exception of several garnet peridotites found in the middle belt and lower belt near Friningen, Northern Jämtland, Sweden, which are partly of the lherzolite subtype (du Rietz, 1935). The ultramafic bodies found in the Köli are chiefly of the harzburgite subtype and are usually strongly serpentinized. In a few bodies subordinate, clinopyroxene-rich lithologies have been found (du Rietz, 1935). In contrast to the SNC, the peridotites found in Köli nappe are restricted to the older lower parts of the tectono-stratigraphic sequence (Zacharisson, 1969). Within the Köli nappe conglomerates of ultramafic composition are found (Trouw, 1973), of which the Ro conglomerate is the best known. This conglomerate is comprised of serpentinized conglomerate/breccia and interpreted to be of sedimentary origin (Strand & Kulling, 1972).

None of the peridotites found in the Seve or Köli nappe show a clear genetic association with igneous rocks, as is seen in a typical Penrose-ophiolite sequence (Calon, 1979; Penrose, 1972). Most peridotites occur as lenticular shaped bodies outcropping amidst meta-pelites along interpreted tectonic contacts. The longest dimension of the bodies is generally aligned (sub) parallel to the regional foliation, which strike trends NNE-SSW.

4.3 Structures

4.3.1 Köli

S0 – Compositional layering

In several locations, mainly the center of the Aunere body, compositional layering can be observed. Less resistant layers are often pure and un-altered dunite, whereas the more resistant layers are the altered serpentinites. The layering resembles that of consolidation and is referred to as S_0 (Trouw, 1973).

Pre-D1/Protolith

No evidence of the protolith assemblage that predates serpentine formation was found in the Köli samples and no evidence of a deformation pre-dating the foliation cleavage, D2.

D1

Not expressed in the Aunere peridotite of the Köli nappe.

D2 - Foliation

The peridotite bodies appear to have behaved as massive units. The foliation cleavage of the adjacent rocks only protrudes into the outer parts of the body, and does so in the form of an anastomosing fracture cleavage (Trouw, 1973). This fracture cleavage consists of relative small grained parallel running serpentine (S2).

D3- Crenulation

The Köli peridotites have experienced an additional stage of deformation (D3). The S2 foliation in the serpentinite is folded into a crenulation that has become overgrown by olivine. Within the large, second generation olivine, serpentine inclusions with two distinct orientations are preserved. These orientations represent the flanks of the D3 crenulation (fig 4.2d). The crenulation is found only at several locations in the samples suggesting the crenulation was not pervasive.

4.3.2 Upper Seve belt

Pre-D1

The protolith assemblage shows signs of minor deformation. The shape of the olivine minerals is elongated, with the aspect ratio approximately 1:3. In addition, several olivine crystals show signs of undulatory extinction and their grain boundary geometry is straight (i.e. unsutured).

D1

Not expressed in this thesis investigated peridotites of the upper Seve nappe.

D2 - Foliation

Distinct in the bodies found in the upper Seve belt is the dominant orientation of the serpentine minerals. However, the S2-foliation is not pervasive enough to visibly have deformed minerals other than serpentine (figure 4.2 and 4.4).

D3 - Crenulation

The D3 deformational phase is only locally observed and exclusively in the foliated serpentine. The shape of the crenulation is open to closed, folding has not lead to the formation of an axial plane foliation cleavage. The angle of the crenulation ranges between >0° and 70°, it has a wave length of several hundreds of micrometers (figure 4.2c).

4.3.3 Lower Seve belt

Pre-D1

The protolith assemblage has a shape which displays a preferred orientation. This foliation is called the pre-D1. The large mm to cm-scale olivine minerals show an alignment due to an elongated shape. The aspect ratio ranges from 1:3 to 1:6. In addition the olivine minerals show signs of undulatory extinction.

D1 - Dynamic Recrystallization

The first generation of olivine shows signs of dynamical recrystallization (fig 4.5 d-f). The olivine porphyroclast of olivine (mm-scale) is recrystallized into smaller grains (100µm-scale). The Rheological properties of olivine put constrains on the PT-conditions for this ductile deformation event. The relation with the formation of the crenulation (D3) has not become apparent from structural analyses, but deformation must have occurred under conditions of high-T and high water fugacity. I.e. it must have pre-dated the formation of the S2 serpentine foliation as discussed in the section below. (Figure 4.5c-d-e)

D2 - Foliation

Throughout the majority of the samples a clear foliation is formed by a dominant orientation of the serpentine minerals, this foliation is called the S2/D2. Other minerals are optically un-affected by this deformational phase. (Figure 4.5a,c 4.8b)

D3 - Crenulation

The D3 deformational phase is only locally expressed. We note that D3 crenulations were not observed in the samples coming from the large peridotite lens near Marsliden. The D3 crenulation effects the foliated serpentine (S2) and, in part, (2^{nd} gen) olivine minerals. This deformation has not led to the development of a new foliation. The open angle of D3 crenulations ranges between >0° and 80°, they have a wave length of several hundreds of micrometers (figure 4.5e-f).

4.4 Metamorphism

The petrogenetic diagrams which are illustrated in the chapters below are based on the combined mineralogical and structural features found in the samples corresponding to the nappe/belts. For this research we assume the deformational and metamorphic history is identical although its expression may vary depending on location.

4.4.1 Metamorphism of the Aunere peridotite (Köli nappe)

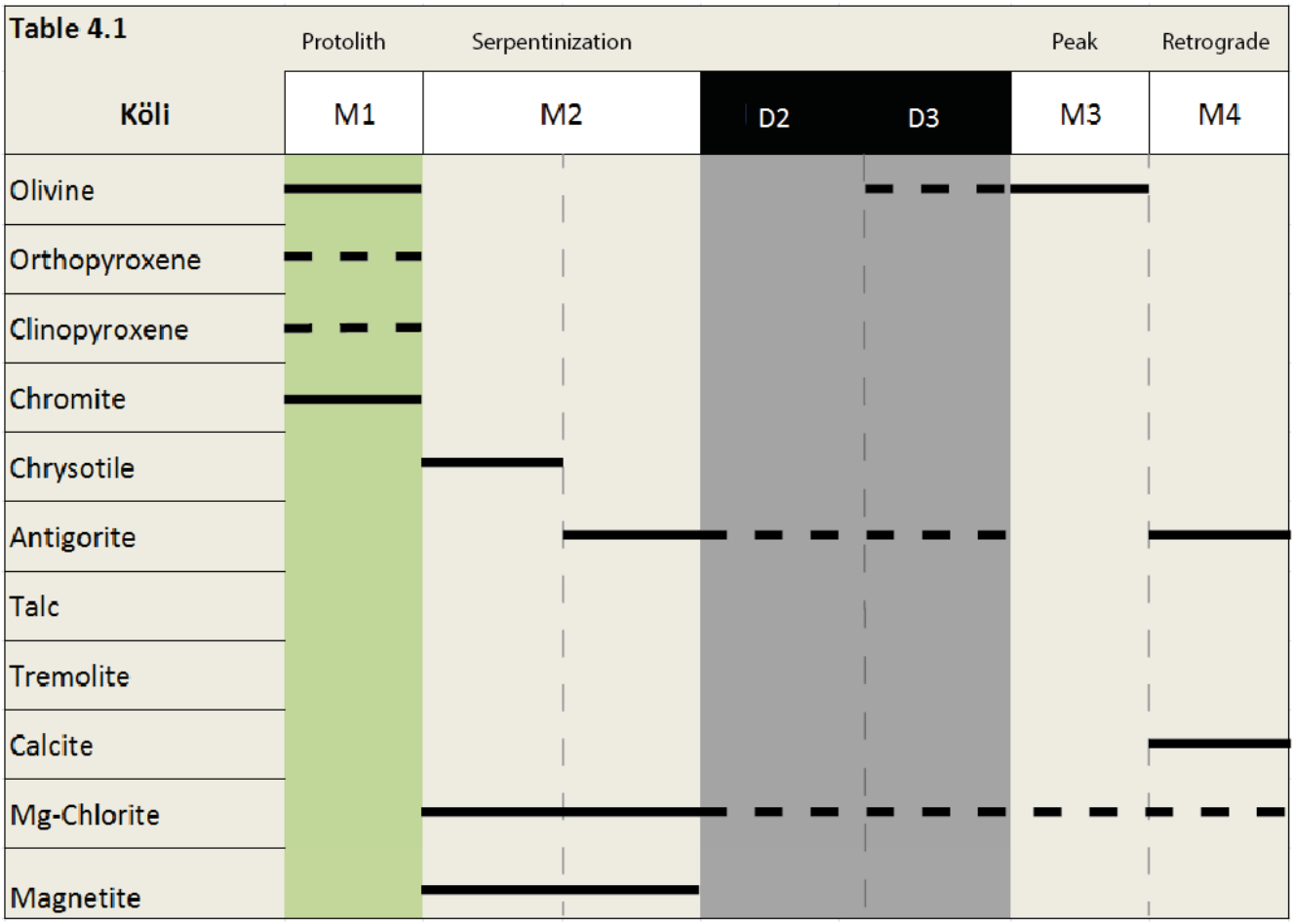

Table 4.1 Petrogenetic diagram of the Aunere peridotites Köli nappe.

M1/ Protolith assemblage (Calon, 1979)

The primary mineral assemblage (M1) of the Aunere peridotite could not be established based on the samples collected during this thesis. This is due to the intense alteration caused by the first serpentinization phase. What is presented here is based on detailed work done by Calon (1979). The sparse parts of the Aunere peridotite that are not altered by serpentinization are dominated by olivine often found in aggregates preserving the protolith assemblage. However, sporadic amounts of ortho- and clinopyroxene are found, limited due to the overall dunitic nature of the Aunere peridotite body. Chromite also forms part of the protolith assemblage and is spatially preserved in the samples in this thesis. Here chromite is present as nicely formed circular or diamond shaped minerals which reach sizes up to several mm (Figure 4.2c).

M2

The M2 mineral assemblage consists of serpentine, chlorite and magnetite. The protolith assemblage is overgrown by serpentine and related minerals. The presence of magnetite, often positioned in bands (fig 4.1b), is seen as inclusions in later phase minerals. In the case of serpentine it is not unequivocal which generation we are dealing with (i.e. M2 or M4). The fibrous nature of serpentine results in a woven structure, which can be misinterpreted as crosscutting relations. However, the inclusions found in later stage minerals (fig 4.1d) conclusively place several of these serpentine minerals to M2. In addition, the presence of this first generation serpentine is expected due to the presence of magnetite which is a by-product of the transition from olivine into serpentine, as will be discussed in more detail in chapter 4.5. The chlorite minerals are found as inclusions in M3 olivine minerals.

M3 (peak metamorphism)

The M3 mineral assemblage consists dominantly of olivine. It is marked by overstepping the olivine-in phase boundary line so olivine becomes a stabile mineral in the prograde metamorphic assemblage. Size of the olivine minerals ranges from hundred µm to several cm. This second generation of olivine (M3) grows over the magnetite minerals, which are thereafter incorporated as inclusions (fig 4.1 a-b-c-d). Similarly they overgrow the foliated and crenulated M2 serpentine deformed by D2 and D3 (fig 4.1d and 4.2d) The minerals have a slight elongated shape (aspect ratio of 1:2), suggesting minor imposed strain during formation or preferred growth in a particular direction during prograde metamorphism.

M4

The stable mineral assemblage (M4) is serpentine and calcite. This fourth metamorphic phase is marked by retrograde metamorphism and represents the second metamorphic phase in which serpentine is stable. Second generation olivine (M3) is serpentinized. In addition serpentine is found in veins crosscutting earlier foliation in samples (fig 4.2a), indicating that brittle conditions prevailed during this metamorphic event. Locally calcite overgrows serpentine (fig 4.2b).

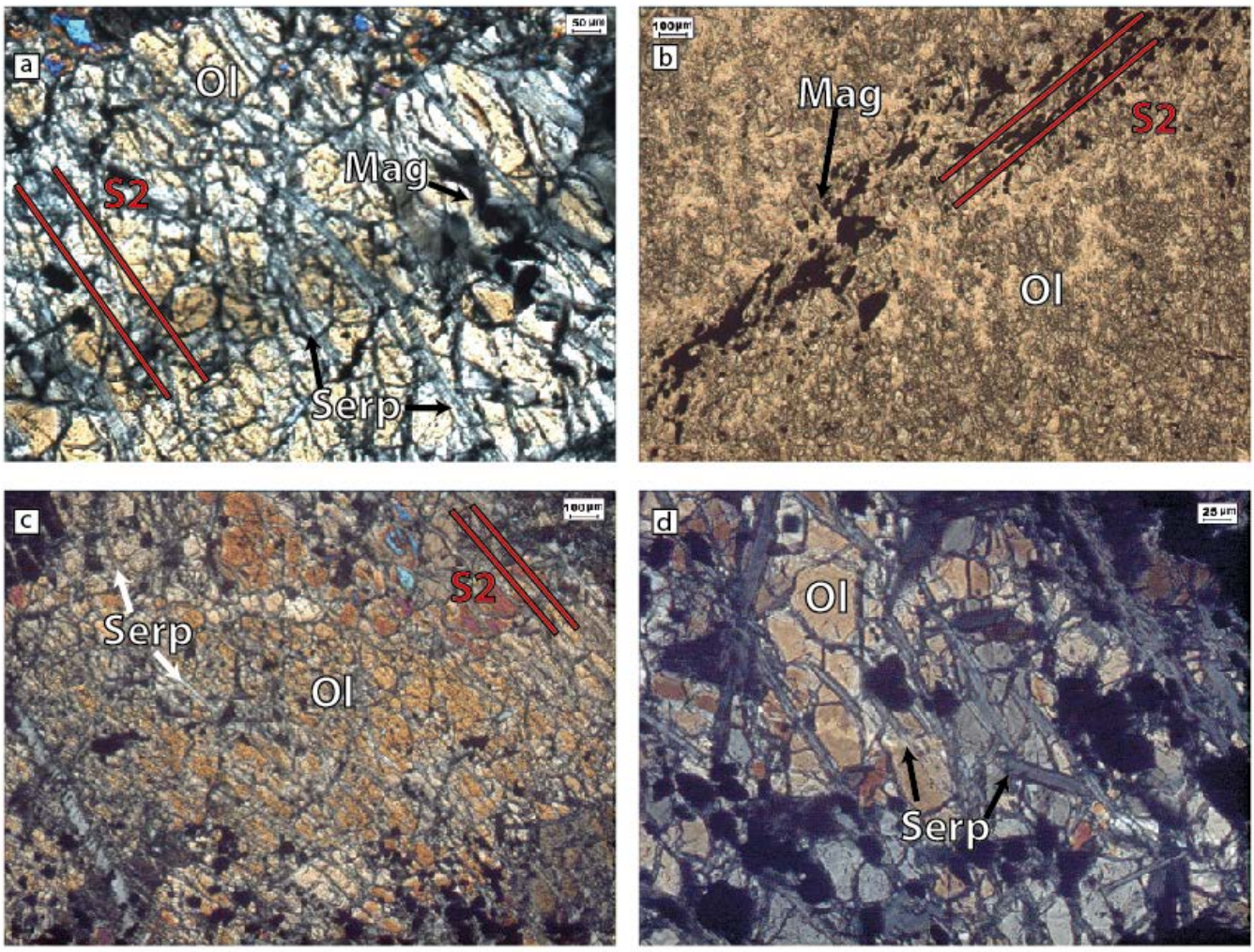

Figure 4.1 Optical microscopy photographs under PPL and XPL **a** Large olivine overgrowing foliated serpentine and magnetite. **b** Bands of magnetite run through the serpentinized and fractured olivine. **c** Large fractured olivine overgrows magnetite and serpentine **d** 2nd gen olivine overgrowing serpentine.

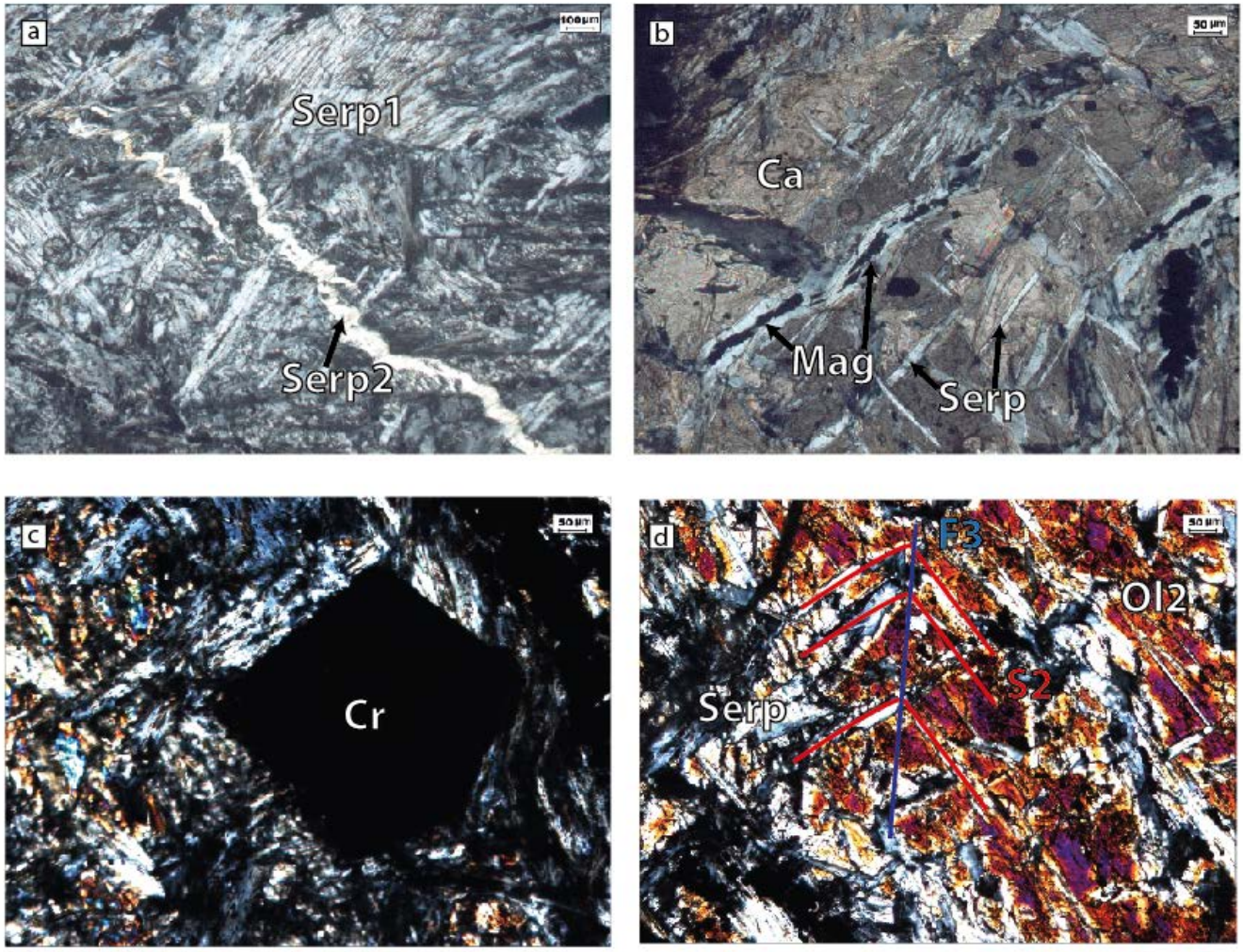

Figure 4.2 a Veins of serpentine crosscutting the earlier generation serpentine. **b** Large calcite minerals overgrowing serpentine and magnetite. **c** Well-developed chromite crystal in serpentine matrix. **d** Crenulated serpentine (D3) overgrown by second generation of olivine.

4.4.2 Metamorphism of some of the upper Seve belt peridotites

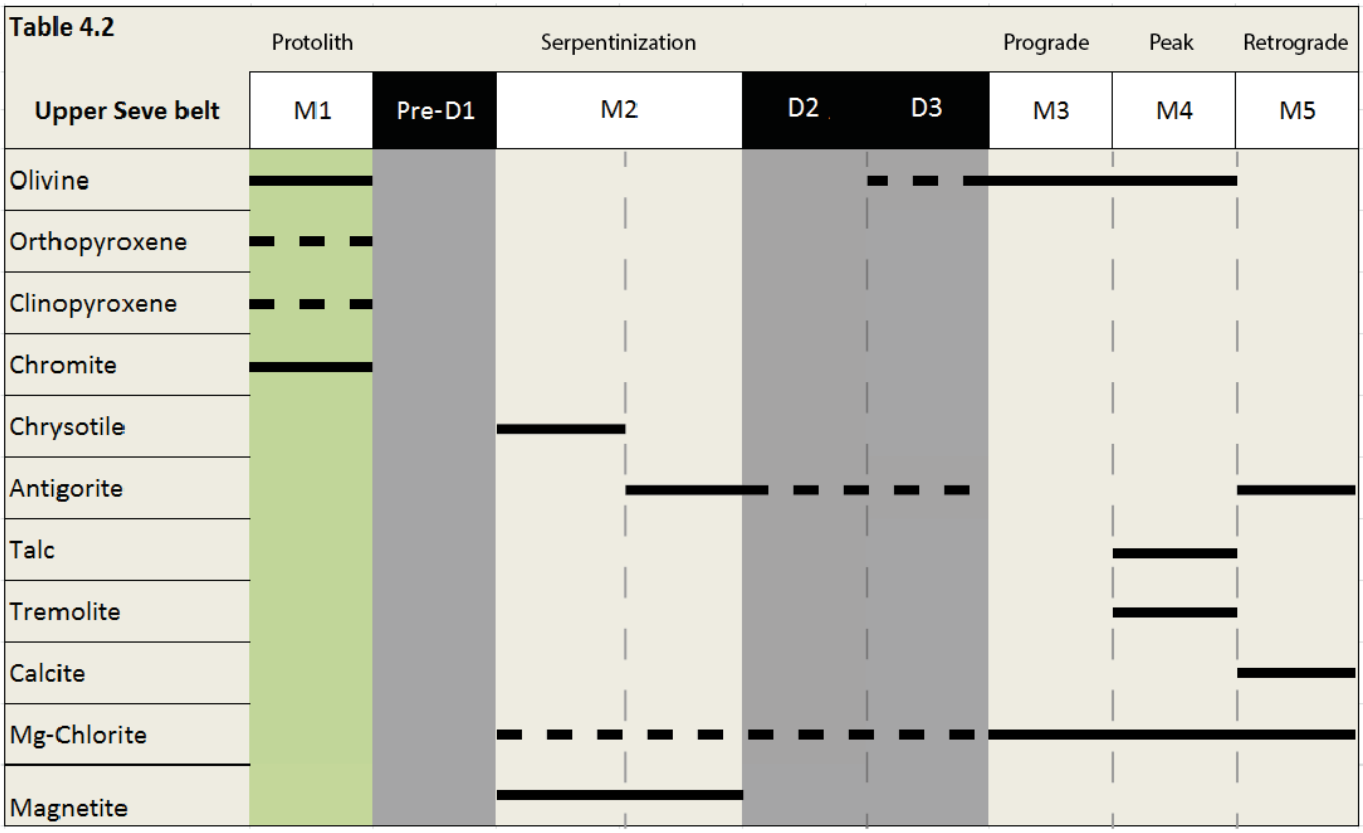

Table 4.2 petrogenetic diagram of the upper belt peridotites.

M1

The protolith mineral assemblage (M1) of the upper Seve belt peridotites consists of olivine and chromite. The size of the protolith minerals range from mm- to cm-scale. The porphyroclasts are in general intensely fractured, altered and deformed (fig 4.3 a). Olivine porphyroclasts reach up to a cm in size. They are regularly found to have undulatory extinction. Chromite minerals range from a few hundred µm to three mm. In general the chromite displays a well-developed round or diamond shaped form (fig 4.3b). However, other chromite minerals are fractured and/or have an elongated shape. Orthopyroxene and clinopyroxene are interpreted to the protolith assemblage based on work done by Calon (1979) on less depleted peridotite rocks.

M2

The M2 assemblage consists of serpentine and magnetite ± chlorite. The deformation phases (D2 and D3) are best seen in the serpentine. It forms the dominant foliation in most samples and locally, often in serpentine rich sections, the crenulation (D3) is expressed (fig 4.3 c). Serpentine growth has at the latest initiated syn-D2, but possible earlier stage growth cannot be excluded. Furthermore, throughout the upper belt samples bands of opaque minerals are found. These minerals have not organized themselves in a recognizable mineral structures, instead they form smears stretched parallel to the foliation (S2) (fig 4.3 d-e). Further analyses have indicated these minerals are magnetite.

M3

The stable mineral assemblage during this metamorphic event (M3) is olivine ± chlorite. Herein the second generation of olivine is formed, Ol2 (fig 4.3 a-d-f). The minerals usually reach a size of several hundred micrometers and are best distinguished from earlier fractured or dynamically recrystallized olivine when they form in serpentine rich parts of the rock and were not confined during growth. The timing of mineral growth is post-D3. The second generation of olivine is also positioned in the flanks of D3 crenulations this is interpreted as the overgrowth of olivine over the earlier orientated serpentine minerals. There are no cross-cutting relations found which indicate olivine growth has occurred syn- or pre-D3.

M4 (peak metamorphism)

The stable mineral assemblage is olivine, chlorite, talc and tremolite ± chlorite. During M4 amphibole entered the stabile mineral assemblage, this reflects prograde metamorphic conditions. The fairly large minerals, up to 5 mm, overgrow the foregoing M2 magnetite minerals (table 4.2 + fig 4.3 d-e). Locally the amphibole is extremely abundant, making out 40-50% of total rock volume, as seen in sample 16. At several locations chlorite and amphibole are seen overgrowing the by D3 crenulated serpentine, convincingly dating their growth as post-D3 (fig 4.4 a-b-c). The large stability field of chlorite, as can be seen from figure 4.9, suggests it was stable during other M's as well. In addition, talc is abundantly present overgrowing the D2/3 serpentine matrix (fig 4.4 d-e).

M5

The fifth mineral assemblage is marked by the re-occurrence of serpentine. In several cases amphiboles are surrounded by serpentines which curve around the large amphibole mineral (M4) (4.4 f). This is best seen in sample 15 which is heavily serpentinized. In addition, the amphibole and olivine crystals are also altered by serpentine (fig 4.3 f). This forms the final metamorphic phase (M5) related to retrogression.

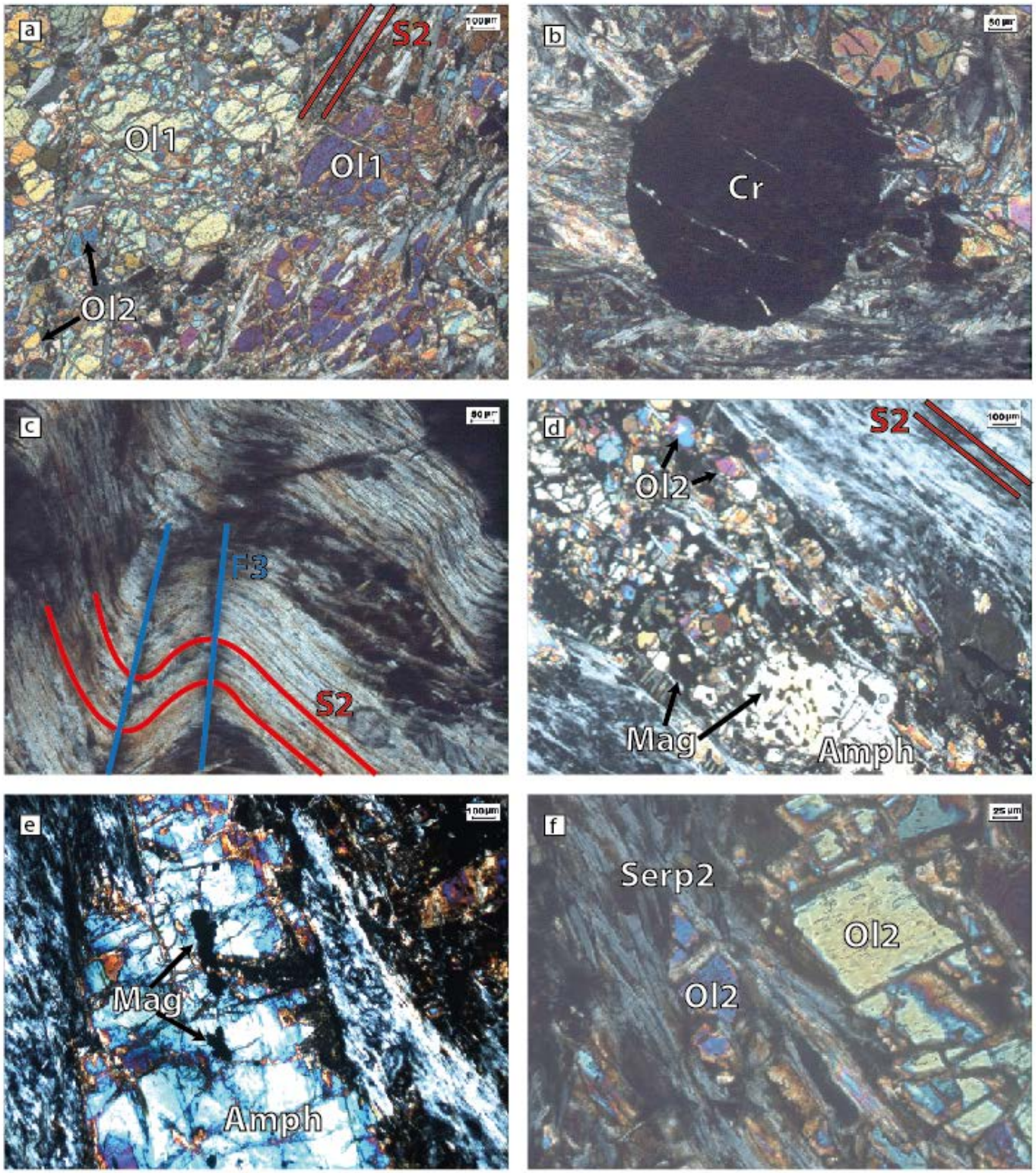

Figure 4.3 Optical microscopy photographs under XPL **a** Olivine porphyroclast fractured and serpentinized. Serpentine is overgrown by 2nd generation olivine which is also fractured. **b** Well-developed sphere-shaped chromite. Aligned inclusions due to fracturing. **c** Crenulation in serpentine. **d** Bands of magnetite and 2nd generation of olivine minerals. Magnetite occurs as inclusion in amphibole. **e** Tremolite with magnetite inclusions. **f** Late stage serpentine overgrowing 2nd generation olivine.

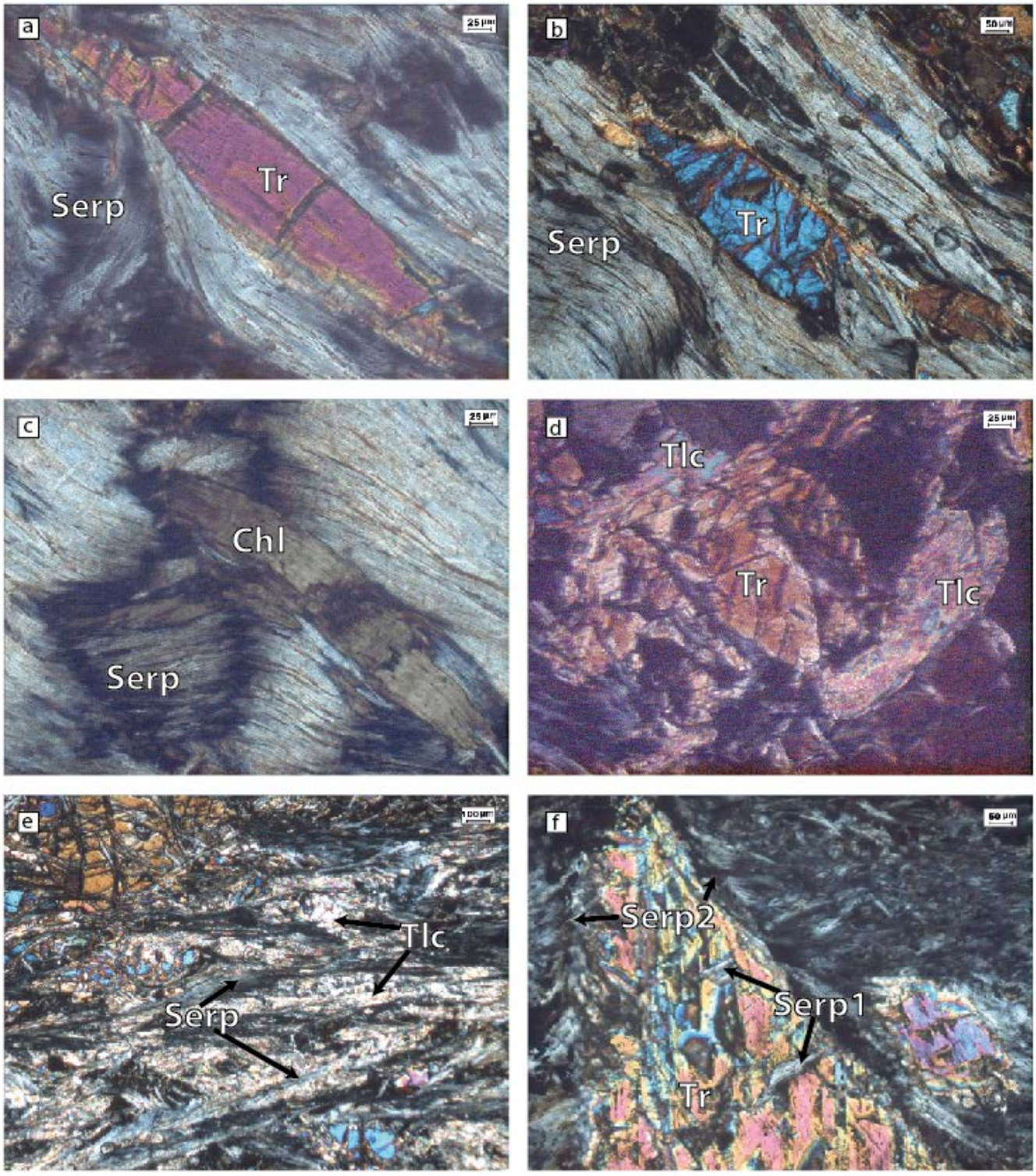

Figure 4.4 Optical microscopy photographs under XPL **a** Tremolite cross-cutting serpentine crenulation. **b** Tremolite cross-cutting serpentine crenulation. **c** Chlorite crosscutting crenulation. **d** Tremolite bounded by talc minerals. **e** Fine grained talc overgrowing serpentine. **f** Late stage serpentine curving around amphibole with earlier stage serpentine inclusions.

4.4.3 Metamorphism of some of the lower Seve belt peridotites

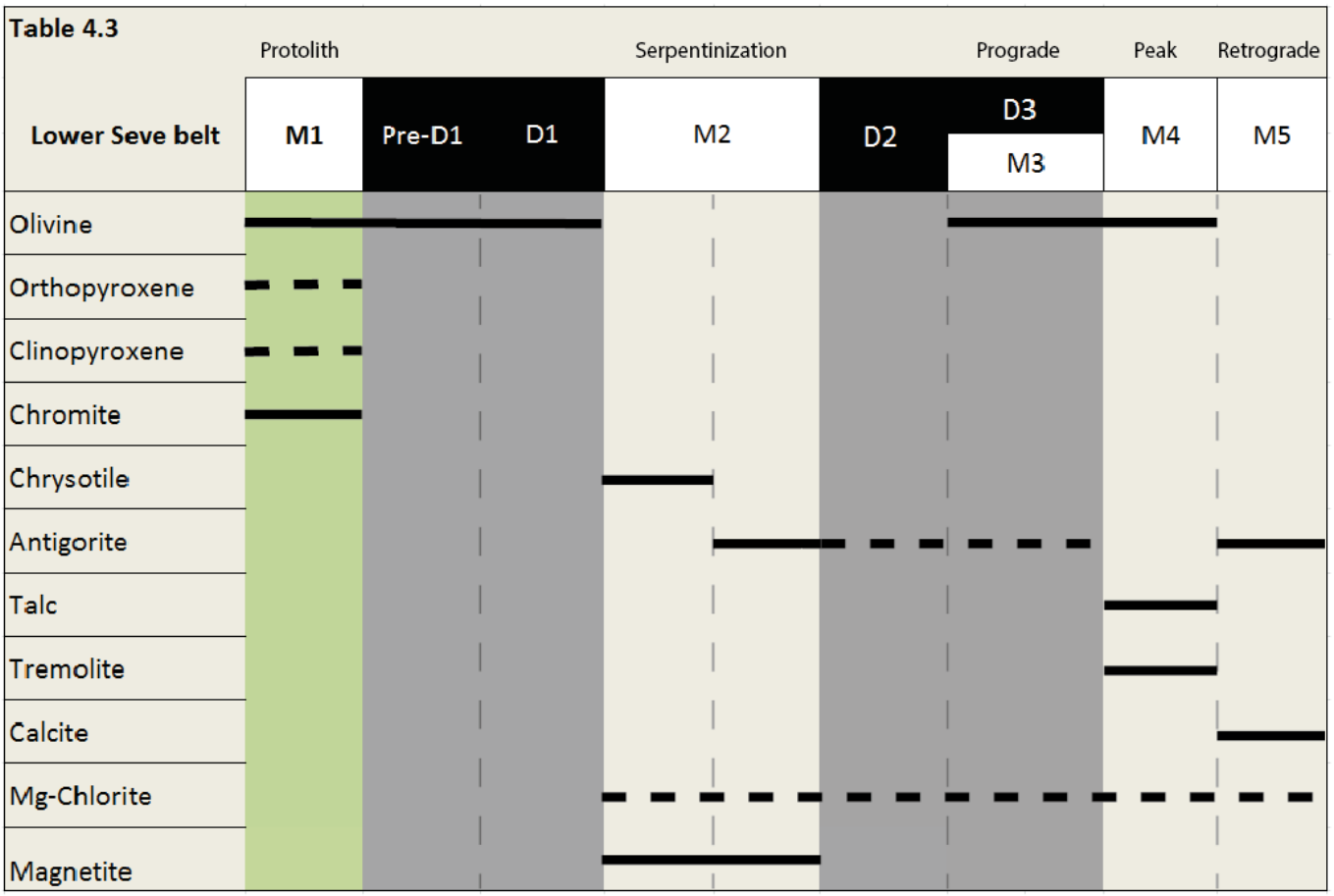

Table 4.3 petrogenetic diagram of the lower belt peridotites.

Metamorphism in the lower belt is based on the mineralogical analysis of thin sections gathered from two peridotite bodies (table 3.1 + figure 3.1). Although, both bodies are spatially separated for about 25 km, they belong to the same tectonic unit and are hence believed to have experienced a similar tectonic history. Which is indeed, reflected in the mineralogical relations. Therefore, the results are presented together as a summary of the metamorphic evolution of some of the lower Seve belt peridotites (see table 4.3).

M1

The M1 assemblage or protolith assemblage consist of olivine and chromite ± chlorite. They form mm- to cm-sized porphyroclast which are heavily fractured and deformed (fig 4.5 a-c). Olivine porphyroclast can reach up to 2 cm in size. Many show kink banding and undulatory extinction. One olivine porphyroclast shows dynamically recrystallized subgrains (fig 4.5 d-f). The chromite minerals range from a few hundred µm to three mm. In general chromite crystals are well developed and relatively unaltered when compared to Ol. However, some alterations can be seen. In several samples chromite is encircled by a rim of chlorite (fig 4.6 b). In addition, locally chromite is affected by deformational processes (fig 4.6 a). Orthopyroxene and clinopyroxene are

interpreted to the protolith assemblage based on work done by Calon (1979) and Trouw (1973) on less depleted peridotite rocks.

M2

The M2 assemblage consists of serpentine and magnetite ± chlorite.

Serpentine was present before the S2 foliation as can be seen from fig 4.6 c, where olivine and serpentine has eluded the S2 foliation imposed on the circumjacent serpentine. The timing of serpentine growth predates D2/S2. The S2 foliation is best expressed by the serpentine minerals in nearly all samples. Moreover, D3 is best expressed by crenulated serpentine, but has a local character and is not a penetrative element. Serpentine mineral growth is therefore initiated pre- or syn-D2. In addition, at several locations bands of magnetite run parallel to the S2 foliation indicating they have also been formed pre-D2 (fig 4.6 d).

M3

The stable mineral M3 assemblage is olivine, chlorite and antigorite (table 4.3). This phase is marked by the re-introduction of olivine, now as a metamorphic mineral. This second generation of olivine reaches sizes of several hundreds of micrometers in often has an elongated shape (aspect ratio of 2:1). Furthermore, the grain boundaries of olivine minerals are curved due to D3 which created the crenulations in the S1 serpentine foliation. Notwithstanding, locally the M3 olivine crystals are clearly deformed by D3 as they are bended into D3 folds, moreover other M3 olivines clearly overgrow the D3 crenulation fold axis (fig 4.6 e-f). This phase of olivine growth commenced at least as early as syn-D3 but has persisted after D3 deformation has ceased. Generally M3 olivine overgrows the serpentine matrix and forms equidimensional shaped grains (fig 4.5 c and 4.7 a). Chlorite minerals locally surround the spinel minerals of the protolith assemblage and overgrow the serpentine matrix material and are therefore interpreted to postdate the M1 retrogradation. Further pinpointing of the timing of chlorite growth is not attained by other micro-structural relations. However the petrogenetic diagram of peridotites (fig 4.9) shows that chlorite is stable throughout a large range of PT-conditions and is therefore interpreted to be stable throughout multiple metamorphic phases (table 4.3).

M4 (peak metamorphism)

The stable mineral assemblage is olivine, tremolite and talc ± chlorite. During this phase large amphibole minerals grew, reaching sizes up to one cm. Many minerals (ol, serp, chr) are incorporated into the amphiboles as inclusions (fig 4.7 b-c-d). Talc is present as fine grained minerals (micrometer scale) (fig 4.7 e) overgrowing predominantly serpentine minerals but also other minerals such as amphibole. Occasionally larger flakes (hundreds of micrometers in size) (fig 4.7 f and 4.8 a) have developed overgrowing the S2 serpentine foliation of the matrix.

M5

This metamorphic phase (M5) is marked by the stability of calcite and serpentine ± chlorite. This phase is retrograde and forms the final metamorphic event. Serpentine is re-introduced as a stabile mineral. This results in the overgrowth of serpentine over 2nd generation olivine (fig 4.8 b).

Other serpentine minerals are undeformed and form randomly orientated flakes that in certain locations are abundantly found (fig 4.8 c-d). Furthermore M5 is marked by the growth of calcite. Small minerals (tens of micrometers in size) overgrow the S2 serpentine matrix. Their relative timing can undoubtedly be placed post D3 as calcite veins crosscut crenulated serpentine (fig 4.5 a). Furthermore, this calcite postdates the formation of amphibole (fig 4.8e). In addition, the serpentine has incapsuled calcite (fig 4.8 f). This can either indicate that growth of serpentine has extended longer in time than the calcite, or serpentine growth outpaced that of calcite, at least locally.

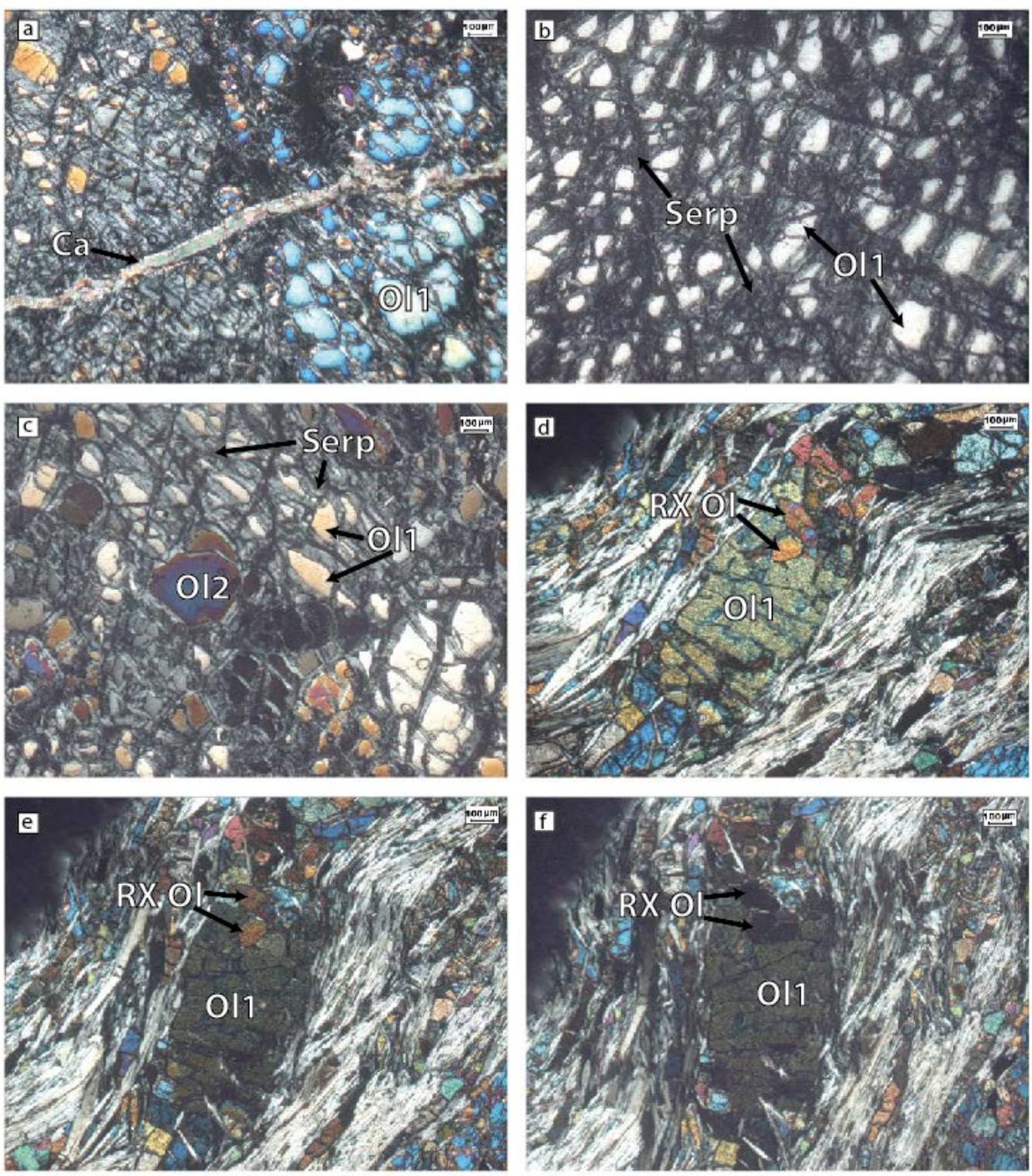

Figure 4.5 Optical microscopy photographs under XPL **a** Large olivine porphyroclast fractured and serpentinized. Late stage vein of calcite crosscuts both olivine porphyroclast as well as serpentine. **b** Large olivine porphyroclast heavily fractured and serpentinized. **c** 2nd generation equidimensional olivine growing in between the remnants of a fractured but not rotated and serpentinized olivine porphyroclast. **d-e-f** 1st generation olivine dynamically recrystallized. Gradual rotating shows extinction of the small olivine minerals slightly out of sync with the large olivine mineral below.

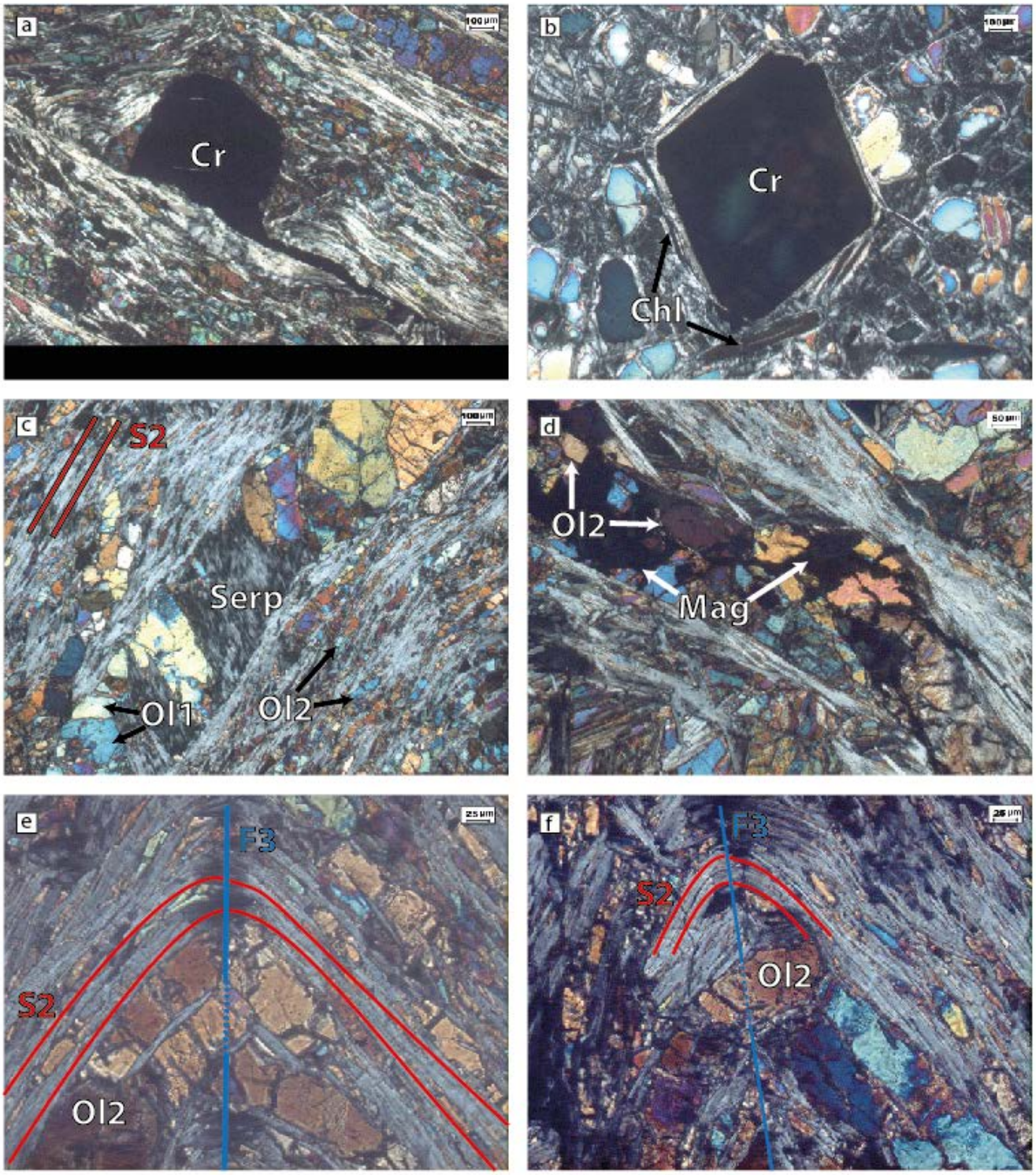

Figure 4.6 Optical microscopy photographs under XPL **a** Diamond shaped chromite of the protolith assemblage deformed and stretched out by a later stage D2 deformation. **b** Well-developed diamond shaped chromite of the protolith assemblage is bounded by a rim of chlorite. **c** Bands of serpentine overgrown by 2nd generation of olivines bound a domain of unaffected protolith minerals and M1 serpentine. They include a differently orientated serpentine patch and larger olivine minerals. **d** Band of magnetite amidst 2nd generation olivine, bounded by serpentine. **e-f** Olivine minerals overgrow the fold axis of the crenulation foliation.

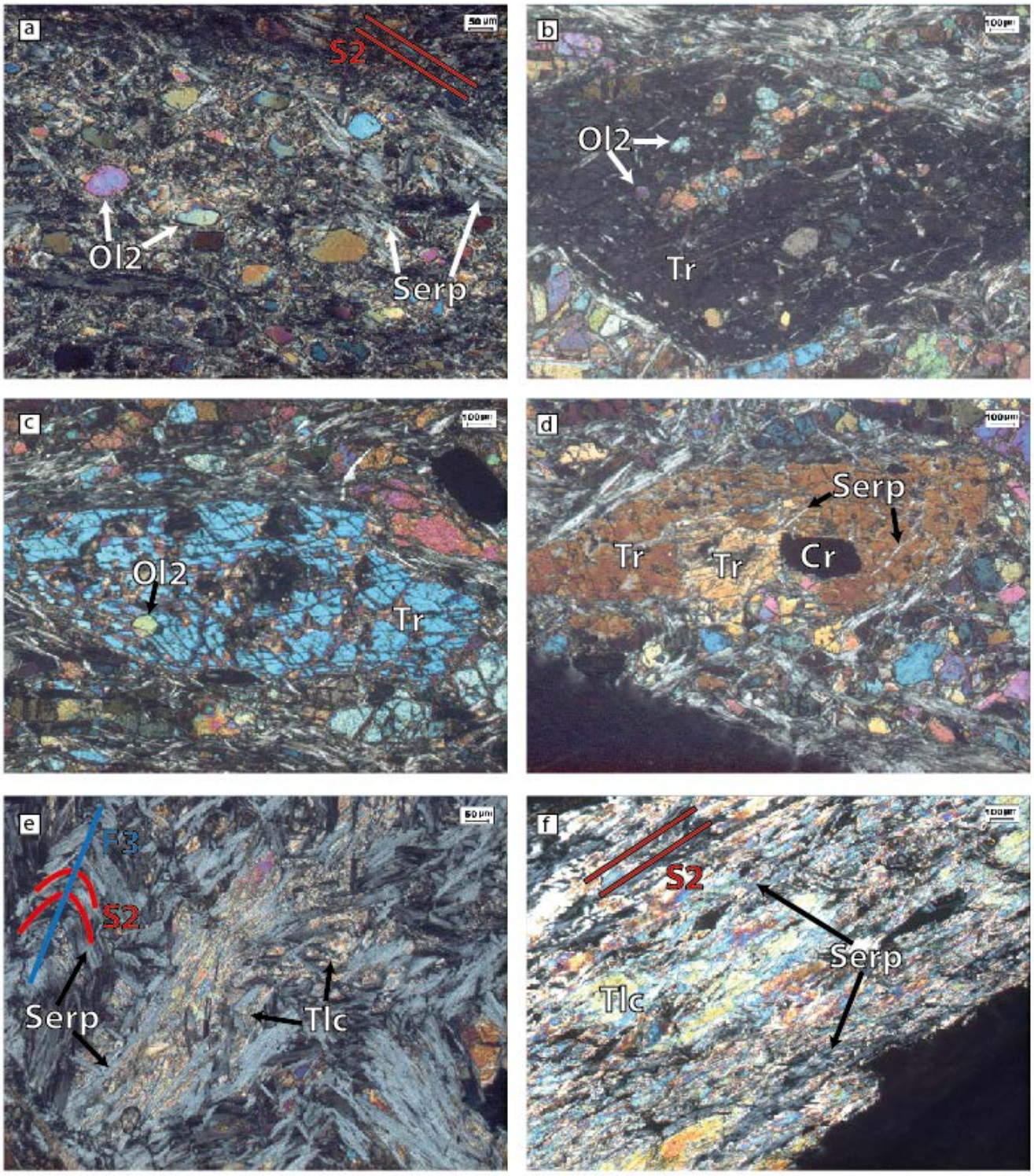

Figure 4.7 Optical microscopy photographs under XPL **a** Optically strain-free equidimensional 2nd generation olivine overgrowing the S2 foliated serpentine matrix. **b**-**c** Large tremolite overgrowing 2nd generation of olivine. **d** Large tremolite overgrows chromite, serpentine and another tremolite mineral. **e** Fine grained talc minerals overgrowing the by D3 crenulated serpentine. **f** Coarser grained talc minerals overgrowing by S2 foliated serpentine.

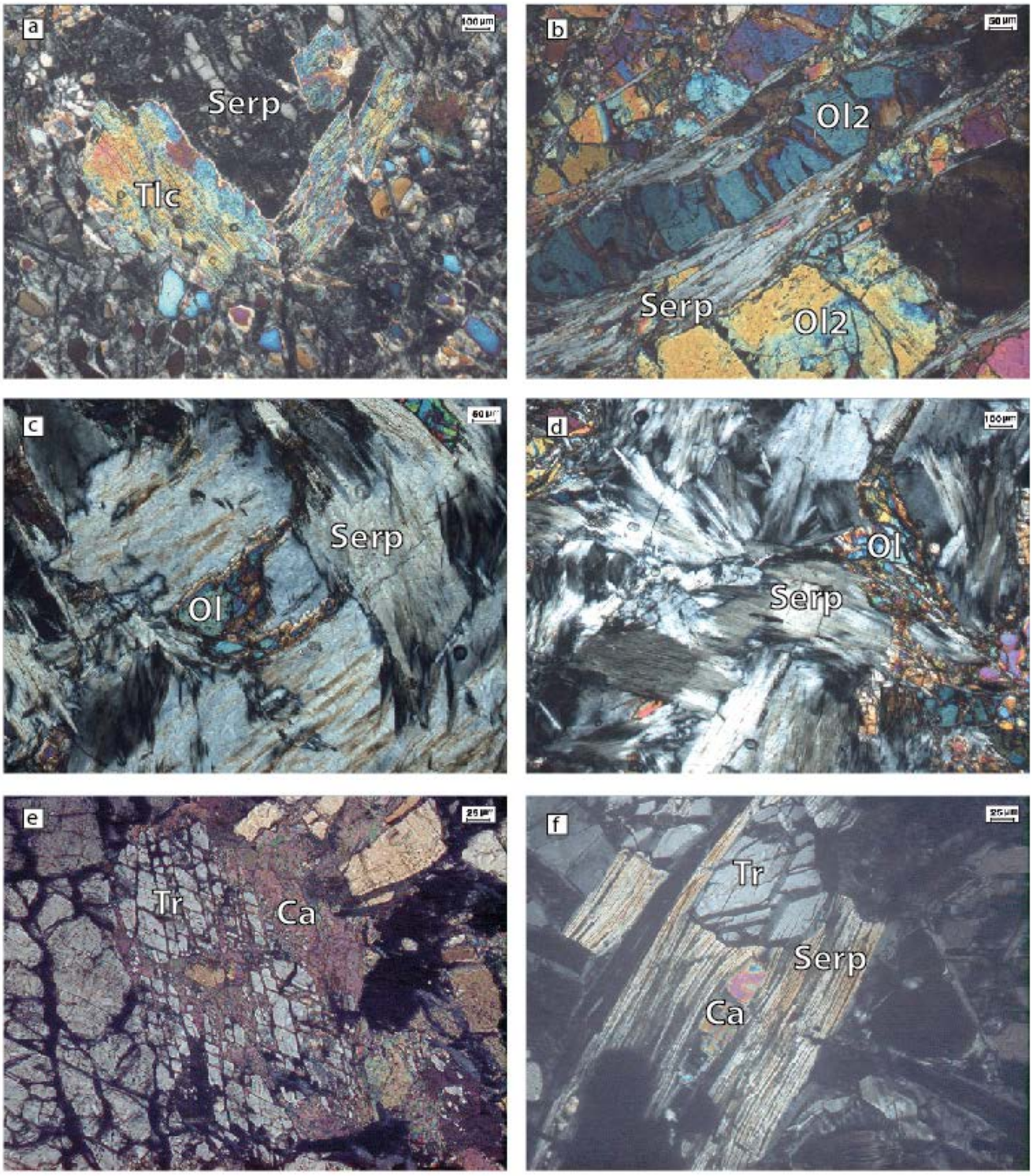

Figure 4.8 Optical microscopy photographs under XPL **a** Large talc minerals overgrowing serpentine. **b** 2nd generation serpentine overgrowing 2nd generation of olivine. **c-d** Randomly orientated flakes of serpentine overgrowing olivine. **e** Fractured tremolite mineral overgrown by calcite. **f** Calcite and tremolite inclusions in serpentine.

4.5 Discussion

In the foregoing sections (chapter 4) the occurrence of the deformational structures, the mineralogy and how they mutually relate in time were presented for the peridotites of each of the individual nappes separately. A comparison of the results between the different nappes (i.e. a comparison of the three petrogenetic grids illustrated in tables 4.1-3) will be discussed in this chapter as well as the implications this has on the physical conditions during their formation. The ensuing part of the discussion will be dedicated to a part in which the Köli nappe, the upper Seve belt and the lower Seve belt peridotite history are in correspondence with each other and secondly into a part revealing their discrepancies.

The orogenic peridotites of the Köli nappe, the upper Seve belt and the lower Seve belt have similarities in mineral and structural features, including their protolith assemblage (M1). Some samples have retained remnants of the protolith assemblage, however, in general most of the samples retrieved have been subdued to intense serpentinization which hindered determination of the protolith mineral assemblage. All the nappes contain olivine and chromite in their protolith assemblage. The presence of clinopyroxene has not been observed in this research, in contrast to comparable work done by Calon (1979) which yielded their presence in all of the nappes, albeit in minor quantities. The reasons for this can be two-fold. Firstly, the compositions of the ultramafic bodies investigated in this research are all of the harzburgite and dunite sub-types, whereas Calon (1979) may also have examined several ultramafites with a lherzolitic composition. Secondly, the clinopyroxene which was present could have been lost during serpentinization. Either options or a combination of both are plausible due to the limited outcrops from which samples were gathered. Therefore, clinopyroxene is interpreted to be present in ultramafites of all investigated nappes, albeit not recognized in this research. The protolith mineral assemblage is foliated and minerals are elongated and reveal slight undulatory microstructures with locally dynamic recrystallization textures. This indicates an environment at relatively high T-conditions that cannot be linked to the Caledonian event. Therefore this is assumed to be inherited from a foregoing deformation event not related to the Caledonian orogeny. Likely this is due to convective movement of the asthenosphere and/or lithosphere extension by the breakup of Rhodinia (i.e. Iapetus spreading stage). The first metamorphic event following the protolith assemblage (M2) is identical in all nappes. It is characterized by the growth of the serpentine minerals chrysotile and antigorite. These minerals do not form a stable mineral assemblage (fig 7.8), wherein chrysotile represents the low pressure-low temperature equivalent of antigorite which is however chemically very similar in composition. Converting olivine into serpentine can only occur when temperatures drop below 400C° (fig 7.8) and with the availability of water. Serpentine can only host the forsterite component of olivine (eq. 4.1) and magnetite, which hosts the fayalite component of olivine (eq. 4.2), is therefore an important by product produced during serpentinization. According to the following reaction:

$$3Mg_2SiO_4 + SiO_{2aq} + 2H_2O \rightarrow 2Mg_3Si_2O_5(OH)_4$$
forsterite ***chrysotile***

Equation 4.1

$$3Fe_2SiO_4 + 2H2O \rightarrow 2Fe_3O_4 + 3\ SiO2_{aq} + 2H_2$$
fayalite ***magnetite + quartz***

Equation 4.2

Both the serpentine minerals and the magnetite minerals are orientated parallel to the foliation caused by D2 and subsequently the serpentine minerals are crenulated by D3. The structural style of these two deformational phases (D2 and D3) and their relation to the M2 mineral assemblage of the Köli, upper Seve belt and the lower Seve belt are similar. In addition, the M3 phase is marked by olivine nucleation postdating crenulations of the D2 serpentine foliation. Within the lower belt there is also evidence of olivine growth occurring syn-D3. According to experimental data, temperature in excess of 400C° is required in order for olivine nucleation to occur (fig 4.9). Second generation olivine minerals in the Köli reach sizes up to several cm. Similar sizes are not observed in the upper- and lower belt, which are known to be of higher metamorphic grade. The effects of high water availability in the Köli have to be considered as the primary cause of this difference in secondary olivine grainsizes. Lastly, peridotites of all belts experienced renewed serpentinization during their final metamorphic phase, M4 in Köli and M5 in the upper- and lower belt. This phase reflects the retrograde tract of the rocks under progressively lower temperature conditions during exhumation, hereafter called M_{exh}. The M_{exh} phase is locally accompanied with calcite growth predominately located in veins thereby indicating the brittle conditions during formation. The stability of calcite means the rock is chemically altered as water percolates through the system and Ca is introduced. The absence of calcite in the peridotites of the upper belt therefore does not represent a difference in tectonic setting, but rather a local feature. In addition, no renewed growth of magnetite is recognized during this phase. Serpentinization of (remnants of) the olivine porphyroclast as well as the second generation of metamorphic olivine (M3+(M4)) which has re-incorporated their Fe-constituent could have led to the renewed formation of the Fe_3O_4 iron oxide (magnetite). In this study no evidence was found which supports the latter hypothesis and magnetite is therefore not incorporated in the retrograde metamorphic phase, M_{exh}. Discrepancies in microstructure and mineralogy between the peridotites of the various belts are limited to two points. Firstly, the lower Seve belt peridotite has one deformation phase which predates the first stage of serpentinization (M2). It is marked by the dynamic recrystallization microstructures which are recognized in M1 olivine porphyroclasts. The brittle ductile transition for upper mantle rocks, which consist predominantly of olivine, occurs at depth of roughly 40 km (Sawyer, 1985) which corresponds to a temperature of 880 C°, according to the Barrovian geothermal gradient assumed in this thesis. The mineral assemblages (M2-5) presented in this research do not support Caledonian peak metamorphic conditions to reach temperatures this level and therefore it is most likely to have developed by pre-Caledonian deformation induced during transport of lithospheric mantle into the crust. Clos et al. (2014) used similar micro-structures as indicators of the incorporation into the crustal domain. Although cross-cutting relations are missing, the temperature is constrained by the mechanical properties of the ductile behavior of olivine. This times its occurrence during the first deformational phase (D1), most likely due to the

break-up/extension of the Rhodinian plate. D1 is absent or not (yet) recognized in the upper Seve belt and Köli nappe peridotites.

The second discrepancy between the peridotites in the Köli and the two belts of the SNC is the Caledonian metamorphic grade during peak metamorphism. For the Köli peak metamorphism (M3) occurred under greenschist facies conditions (350-450 C°), whereas for the upper- and lower belt of the SNC peak metamorphism (M4) occurred under amphibolite facies conditions (500-650 C°). This is apparent from the additional metamorphic phase, M4, present within peridotite bodies of the two SNC belts. M4 is characterized by the occurrence of olivine, tremolite and talc ±chl (500-650 C°) (fig 4.9).

Abbreviations:

Chr	-Chrysotile
Atg	-Antigorite
Ol	-Olivine
Opx	-Orthopyroxene
Cpx	-Clinopyroxene
Grt	-Garnet
Spl	-Spinel
Chl	-Chlorite
Tr	-Tremolite
An	-Anorthite
Tlc	-Talc
Hbl	-Horneblende
Di	-Diopside
Brc	-Brucite

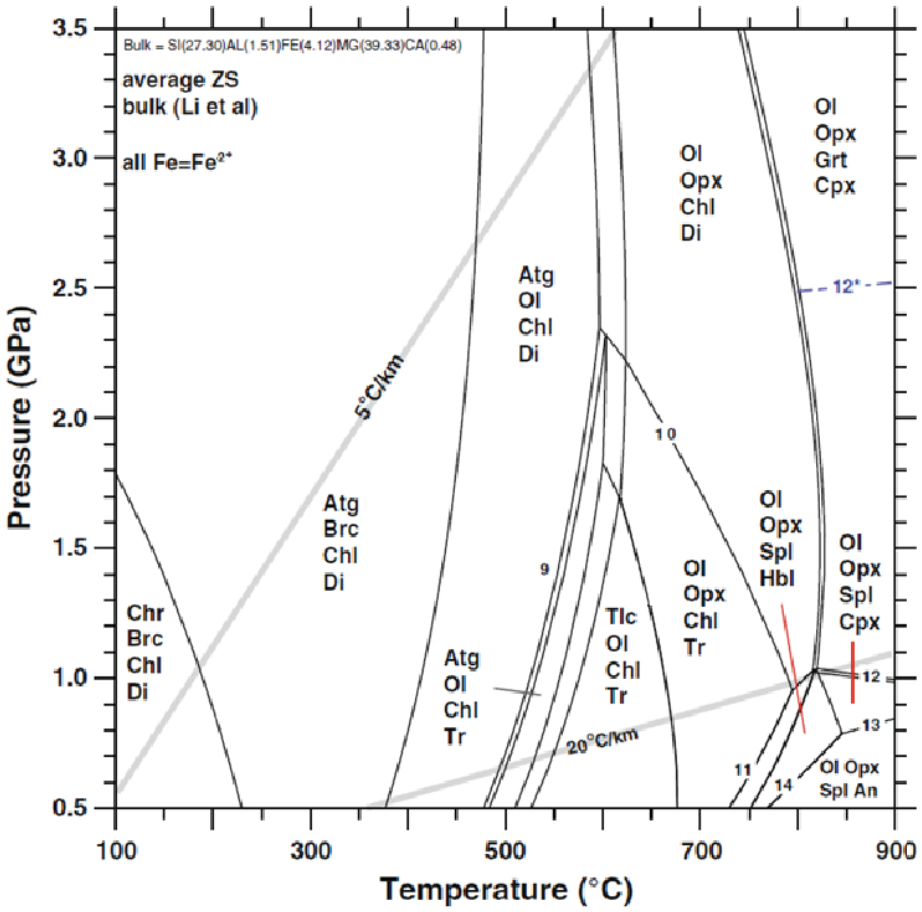

Figure 4.9 Experimentally derived petrogenetic diagram of ultramafic rocks (from Bucher & Grapes, 2011). Bulk rock composition given in the top right side of the diagram.

5) Country rock

5.1 Location

The samples are collected based on their close proximity to the ultramafic bodies as discussed in chapter 4.1. The locations are distributed over the lower Köli nappes, the upper Seve belt and the lower Seve belt. The distance between the ultramafic body and the location of the country rock outcrop has to be small in order to assume that they are part of the same tectonostratigraphic unit but distant enough not to have been profoundly affected by the chemical alterations due to fluid passage between both locations. However, due to the scarcity of outcrops some locations fulfill these criteria better than others. The exact locations of the outcrops sampled are indicated in figure 3.1 and corresponding coordinates are listed in in table 3.1.
The country rock has been investigated by several authors, Du Rietz (1935), Zachrisson (1969), Trouw (1973) and Zwart (1974) to mention a few. Their work forms the basis of the lithological and structural description in the chapters below.

5.2 Lithologies

As mentioned above the Scandinavian Caledonides are built up out of several tectonostratigraphic units (chapter 2). The lithologies as presented here will be discussed in order of the structural position within the nappe pile from high to low (e.g. Köli nappe, upper belt and lower belt).
The lower Köli nappe consists out of several layered supracrustal sequences consists of sediments of marine origin (Zachrisson, 1969) which occur predominantly as phyllites. For this reason the lower Köli belt is sometimes referred to as the phyllite belt. Other lithologies are quartz-keratophyre, amphibole-porphyroblastschist, amphibolite, mica-schist, quartzite and conglomerate (Zachrisson, 1969; Trouw; 1973; Zwart, 1974; v. Roermund & Bakker, 1983). The primary sedimentary bedding is often still recognizable and has been used to demonstrate the way-up (e.g. bedding of the Virisen Quartzite (Zachrisson, 1969)). In addition, macrofossils were discovered in the beginning of the last century (Högbom, 1920; Du Rietz, 1936) demonstrating the oceanic origin of the sediments.
The upper Seve belt consists of garnet mica schist and metabasic rock (Trouw, 1973; Zwart, 1974). The majority of the upper belt consists of schists, called the Svartsjöbäcken Schist. Metabasic rocks are present as amphibolite lenses within the Svartsjöbäcken Schist and range in size from a few meters to a few hundred meters (Zwart, 1974).
The lower Seve belt consists of various foliated rocks, namely garnet-mica schist, kyanite-staurolite schists, quartzo-feldspatic gneiss, amphibolite, quartzites and garnet-biotite rock (Trouw 1973; Zwart, 1974; v. Roermund & Bakker, 1983). Along strike the rock types are often discontinuous north- and southwards. Original bedding is generally no longer recognizable, except within carbonate-rich schist (Trouw, 1973). Compared to the upper belt the lower belt is relatively poor in garnet (Michel, 1950; Trouw, 1973).

5.3 Structures

The oldest recognizable layering in the rocks of all lithostratigraphic units is a compositional layering (S_m). It is interpreted that S_m is of tectono-metamorphic origin in contrast to a sedimentary origin (S_0) (van Roermund & Bakker, 1983). It is however not implausible that the metamorphic layering is in part due to mimic growth over the initial sedimentary bedding (i.e. $S_m//S_0$). The S_m foliation is defined by the relative volume ratio of the rock forming minerals and secondly the shape preferred orientation of individual minerals like mica and amphibole and to a lesser extent kyanite, silliminite, epidote and clinopyroxene define a foliation. However, sometimes the original shape orientation of the metamorphic minerals can be difficult to determine due to dynamic recrystallization processes creating equidimensional shaped minerals in a foam-like structure. The folding/shearing can be either syn-S_m or post-S_m folding. In general folds have been described (Zachrisson, 1969). The geometry of the folds varies between rock types from being isoclinal in incompetent rocks (phyllites) to close or open in more competent rocks (arkoses and quartzites). Due to local differences in the expression of multiple foliations the overall microstructure is called the regional foliation or S_{reg}. Therefore, S_{reg} has to be considered not as an expression of one deformation phase but as the end product of multiple deformational phases. Following Williams and Zwart (1977) and v. Roermund and Bakker (1983) the structures are subdivided into two groups. Structures which contribute to the formation of S_{reg}, are called group 1 structures, and structures which overprint S_{reg} and therefore post-date it, are called group 2 structures.

Group 1 structures

As mentioned above this group consists of different structures which together add to the formation of S_{reg}. These structures do not necessarily belong to a single deformational phase. In fact, it can be the case that group 1 structures are overprinted by structures belonging to a later group 1 deformational phase. In general such overprint relations are difficult to find and to differentiate due to the similarities in orientation and in geometry of the structures. Locally where the style is dissimilar distinguishment can be made. For further description of the type of structures recognized the reader is referred to Zachrisson (1969), Trouw (1973), Williams and Zwart (1977) and v. Roermund and Bakker (1983). The wavelength of group one folds range between cm's to several meters and their fold axes plunge slightly north-west (Zachrisson, 1969; Trouw; 1973). Moreover, the lineations (L_{reg}) which are present are best expressed in the quartzo-feldspatic rocks, as mineral aggregates or mullions. The lineation plunges, similar to the fold axis, slightly west to north-west. I.e. orientations can vary considerably due to later stage folding and/or variations in strain pattern (Zwart, 1973; Lisle, 1984).

Group 2 structures

This group is composed of structures which do not contribute to the formation of S_{reg} and occur at a slight angle to S_{reg}. Characteristic are the sub-vertical axial planes, however locally near flat-lying orientations of axial planes of post S_{reg} folds have been observed (Zachrisson, 1969). The style of the folds is usually close to open, though locally tight folds occur. In the upper- and lower belts the post S_{reg} folds axial plane can be expressed as a crenulation cleavage. The fold-axes of post S_{reg} folds plunge north-east to north-west and the wave-length of the folds range between

several meters to hundreds of meters (v. Roermund & Bakker, 1983). Furthermore, pseudotachylites, kink folding and several generations of fractures are attributed to this group.

Tectonic contacts

Classically the Seve Nappe Complex is bounded by two major tectonic contacts. The tectonic contacts at the top, separating the upper Seve belt from the overlying Köli nappe, is called the Basal Köli thrust, at the bottom, separating the lower Seve belt from the underlying nappes of the lower allochthon, is called the Seve thrust. Unfortunately, our knowledge about these contacts is limited due to lack of suitable outcrops. They are however interpreted to be present due to the steps in metamorphic grade along both contacts (Trouw, 1973; Zwart, 1974; v. Roermund & Bakker, 1983). Within the SNC discontinuous steps in metamorphic grade were also recognized between the central to lower belt (e.g. granulite and eclogite facies units are positioned directly above lower grade amphibolite facies units) (Törnebohm, 1888; v. Roermund & Bakker, 1983). Inferring a tectonic contact is therefore justified as vastly different metamorphic grades occur adjacently. Similarly, a tectonic contact can be inferred between the upper- and middle belt (e.g. lower grade amphibolite facies units directly overlying granulite and eclogite facies units). The scarcely described mylonites show a fine grained, well foliated rocks which include lineations in agreement with L_{reg} (v. Roermund & Bakker, 1983). Therefore, if the contacts separating the belts of the SNC are indeed represented by mylonites, they belong to group 1 structures.

5.4 Metamorphism

5.4.1 Metamorphism of the Köli nappe country rock

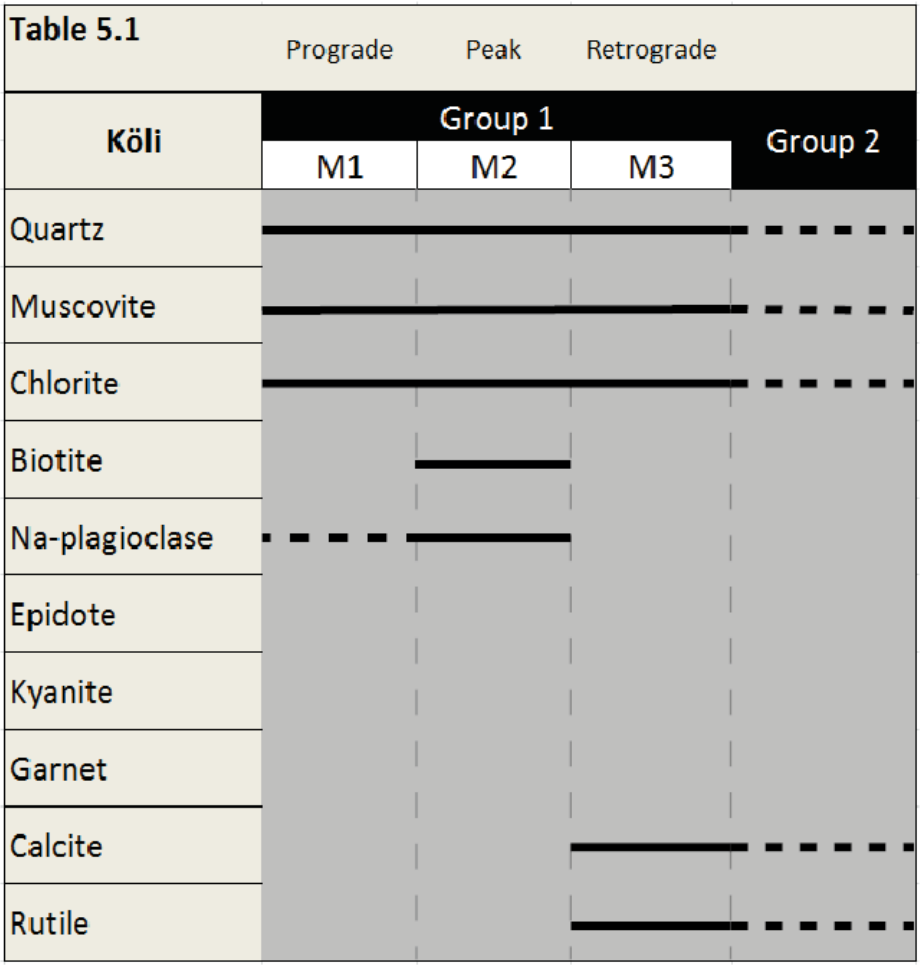

Table 5.1 Petrogenetic diagram of the Köli nappe country rock.

M1

The first metamorphic mineral assemblage (M1) is characterized by the stability of chlorite, quartz and muscovite most often nucleating or overgrowing sedimentary layering. Quartz crystals of several 100 micrometers form islands of optically undeformed minerals, occasionally bound by orientated chlorite minerals, parallel aligned to the main foliation (S_{reg}) in the rocks. Muscovite is present as small inclusions (tens of micrometers) in later stage quartz and albite/oligoclase (Na-plagioclase). The shape orientation of the latter mineral is also parallel to the main foliation (S_{reg}).

M2

This phase is marked by the stability of quartz, Na-plagioclase, muscovite, biotite and chlorite. Biotite is seen overgrowing chlorite and muscovite formed during M1 (fig 5.1a). The biotite minerals overgrow the boundaries of the chlorite reaching only micrometer scale sizes. One large biotite flake is present which deviates from this description. It is ~300µm in size and does not overgrow chlorite. It is positioned adjacent to the quartz in optically unstrained domains. The

shape preferred orientation of this biotite is sub-parallel to the main foliation (S_{reg}). Furthermore, Na-plagioclase becomes part of the stabile mineral assemblage and overgrows the minerals muscovite and chlorite (fig 5.1b). These minerals reach sizes of several hundred of micrometers, many Na-plagioclase show twinning features which are orientated with a small preference parallel to the general direction of the main foliation (S_{reg}). In addition quartz was found to overgrow muscovite and chlorite minerals.

M3

The final and third mineral assemblage consists of quartz, chlorite, muscovite, calcite and rutile. This mineral assemblage is located within mylonitic bands consisting of strongly foliated fine grained (tens of micrometer scale) minerals. Within these mylonitic bands there is a compositional layering, in which thin muscovite layers are separated by thicker chlorite rich layers (fig 5.1d). Biotite is locally overgrown by chlorite (fig 5.1c). Additionally, rectangular shaped rutile minerals are orientated parallel to the foliation and are exclusively found in the mylonitic bands (fig 5.1d). Calcite minerals tend to form in domains least effected by the D2 foliation. Other minerals in these domains reach sizes of several hundred micrometers. The calcite minerals show intense twinning in multiple directions, with a slight preference sub-parallel to the main foliation (S_{reg}). Calcite minerals locally overgrow foregoing minerals such as albite (fig 5.1e).

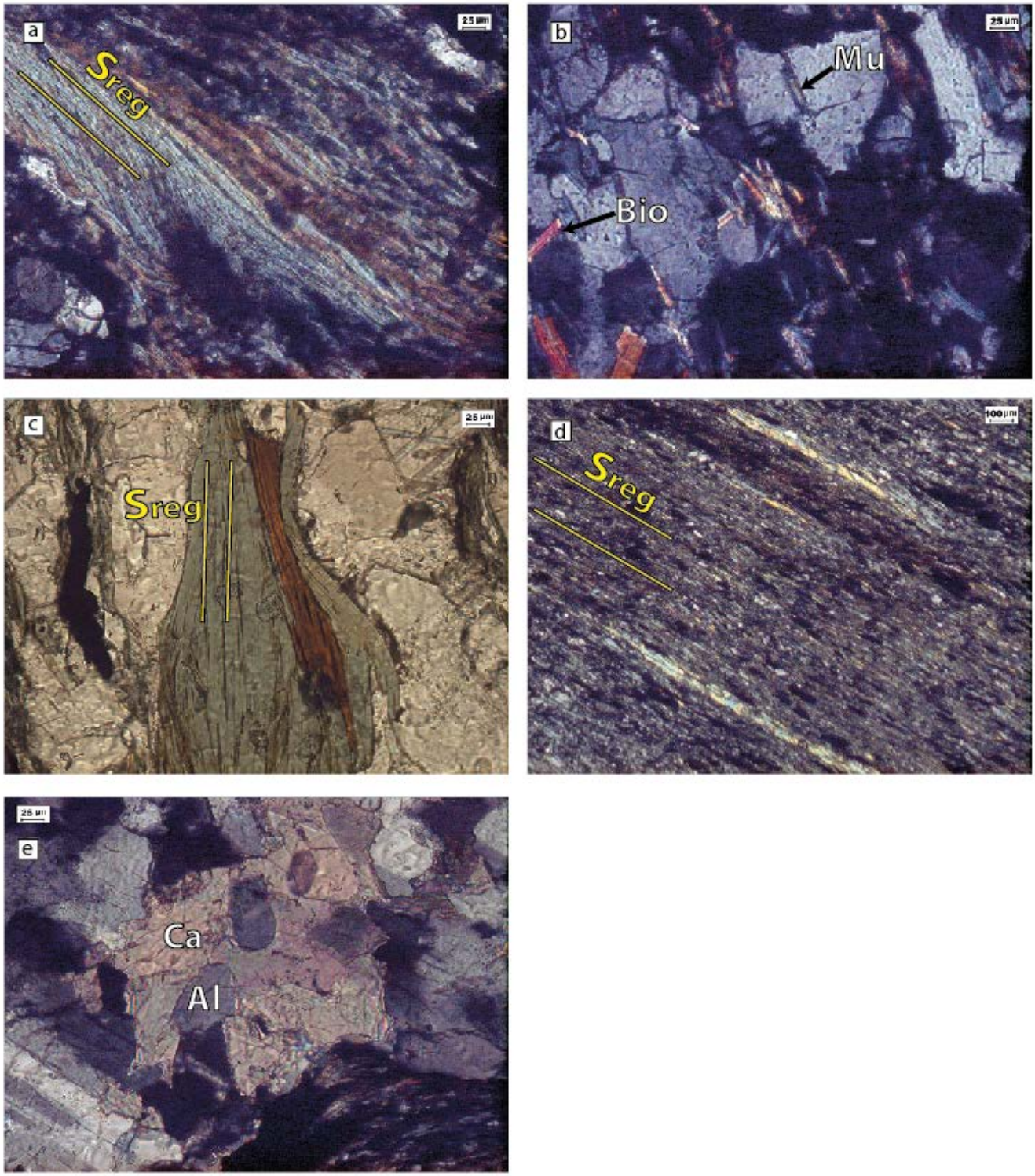

Figure 5.1 Optical microscopy photographs under PPL and XPL **a** Chlorite minerals overgrown by very fine grained biotite minerals. **b** Muscovite and chlorite inclusions in albite crystals. **c** Biotite mineral overgrown by chlorite mineral. **d** Orientated rectangular shaped opaque rutile crystals in a foliated fine grained matrix of chlorite, Na-plagioclase and quartz. Muscovite bands aligned in a similar orientation to the other elongated minerals. **e** Calcite overgrowing plagioclase.

5.4.2 Metamorphism of the upper Seve belt country rock

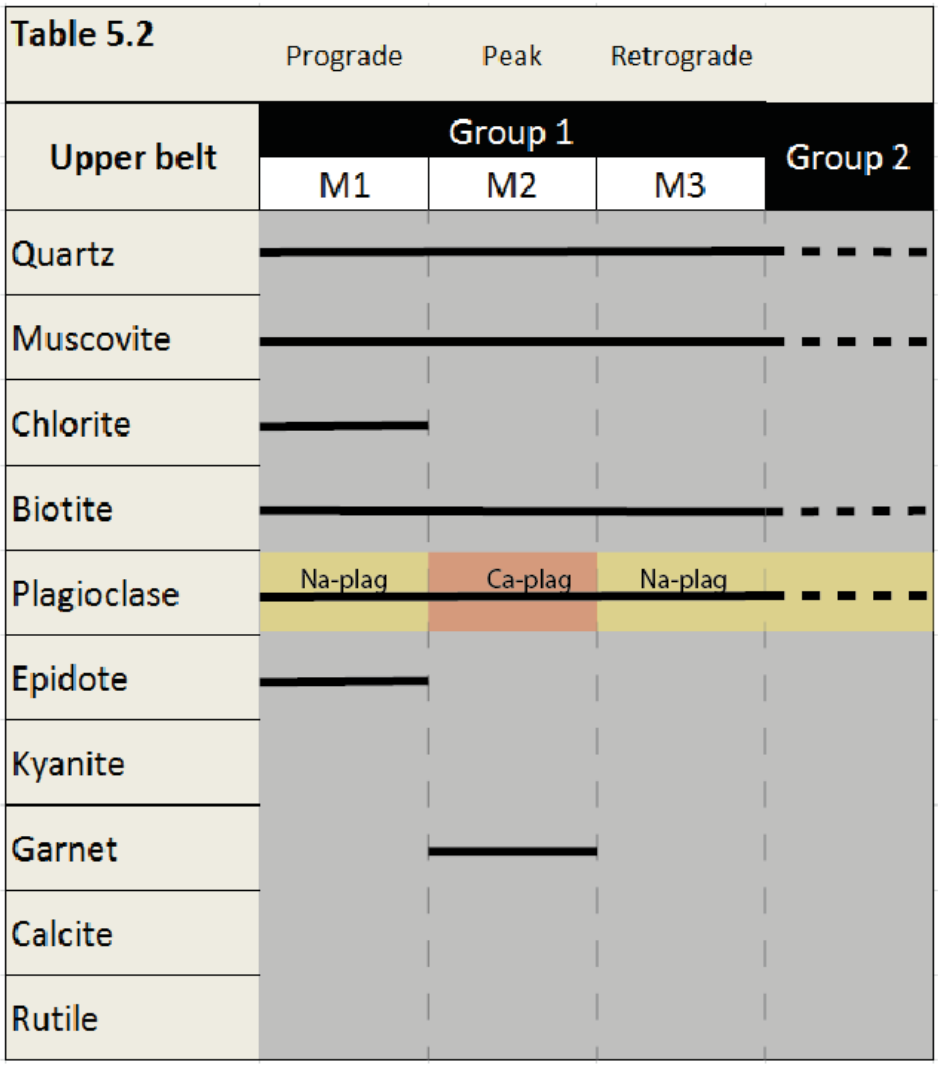

Table 5.2 Petrogenetic diagram of the upper Seve belt country rock.

M1

The first stable mineral assemblage consists of biotite, quartz, muscovite, epidote and Na-plagioclase. Multiple minerals (i.e. quartz, biotite and muscovite) are stabile throughout the entire PT-trajectory, which makes discriminating between various metamorphic phases (i.e. M1, M2, M3, M4) somewhat ambiguous. It is clear however, they form part of the first recognized metamorphic phase (M1) due to the fact that inclusions were found of these minerals in Ca-plagioclase (M2). Based on their structural relation to the deformation phases distinction cannot be made between minerals grown in M1 and minerals that might belong to later metamorphic phases. Quartz minerals are dynamically recrystallized to sizes of several tens of micrometers. Epidote minerals are widespread in the thin sections and grow up to several hundreds of micrometers, have a slight elongated shape (1:2) and are orientated subparallel to the main S_{reg} foliation (fig 5.2a-b). Inclusions of biotite and muscovite (M1) in Ca-plagioclase are orientated sub parallel, indicating that the deformation which caused the main foliation (S_{reg}) occurred syn-M1.

M2

The second mineral assemblage (M2) consists of garnet, quartz, muscovite, biotite, and Ca-plagioclase. Biotite and muscovite overgrow the epidote minerals and form bands which run parallel to the main foliation (S_{reg}). In less foliated parts of the thin sections muscovite and biotite occur as inclusion in Ca-plagioclase on a large scale. To a lesser extent also epidote is captured as inclusions (fig 5.2c-d). Ca-plagioclase minerals generally reach a size of several hundreds of micrometers, but locally they can reach a size up to two millimeter. Ca-plagioclase has a slight elongated shape (aspect ratio of 1:2-3) and is orientated sub parallel to the main foliation (S_{reg}). Large garnet minerals (up to several millimeters) overgrow the foregoing minerals biotite, muscovite, Na-plagioclase, quartz and epidote. No clear foliation has been recognized in internal pattern of the garnet inclusions.

M3

The final stabile mineral assemblage (M3) is formed by biotite, muscovite, quartz and Na-plagioclase. Bands of biotite curve around the large garnets. This microstructure indicates that the regional deformation phase (Group 1 structures) which caused the main foliation was still ongoing during formation of these biotite-rich bands (M3). In addition these bands are seen cross-cutting M2 plagioclase minerals. Furthermore, late stage cracks are filled with veins consisting of Na-plagioclase and quartz.

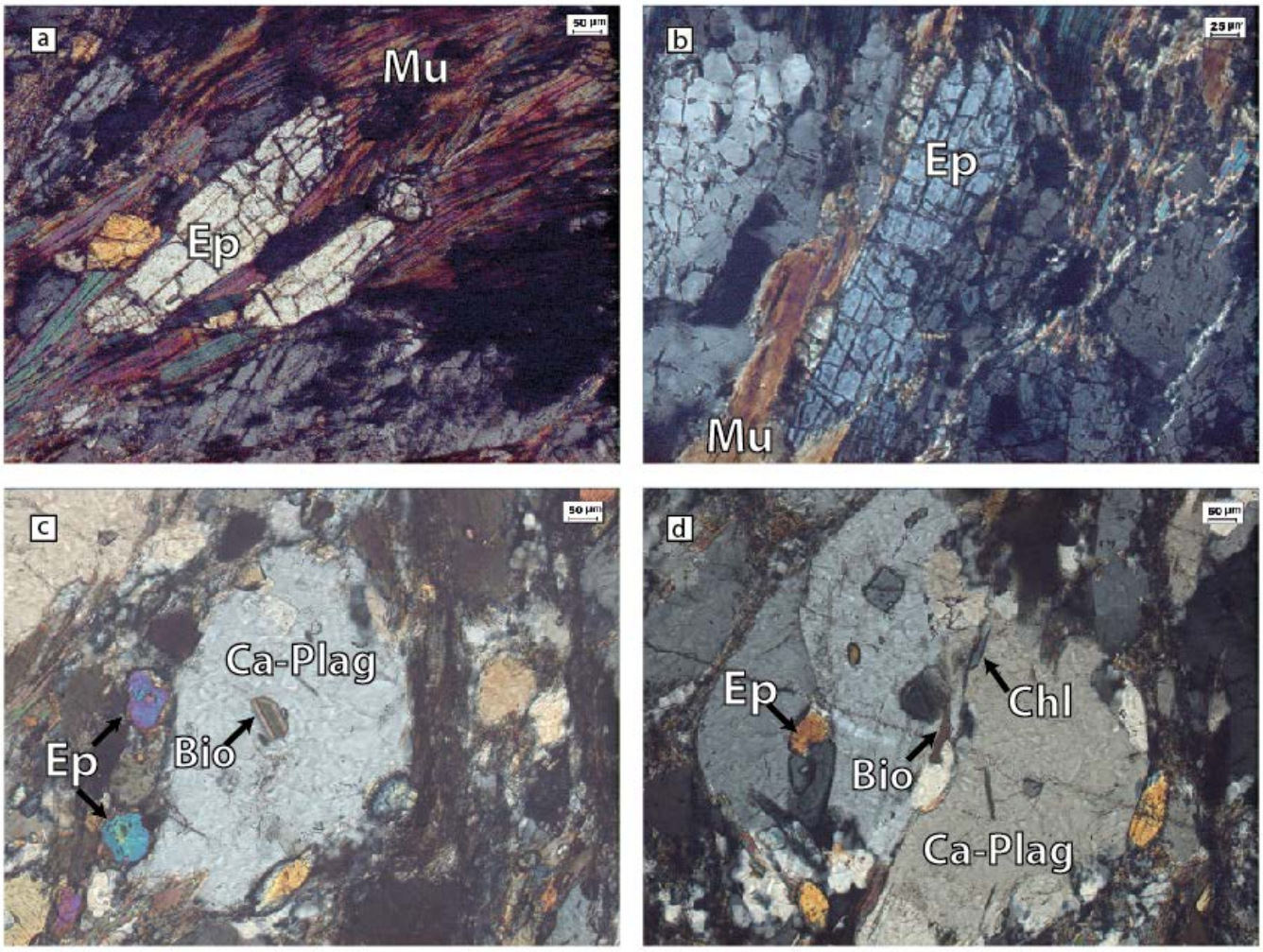

Figure 5.2 Optical microscopy photographs under XPL **a-b** Epidote bounded by a band of muscovite. **c** Ca-Plagioclase overgrowing biotite and epidote minerals. **d** Ca-Plagioclase overgrowing a biotite, chlorite and epidote minerals.

5.4.3 Metamorphism of the lower Seve belt country rock

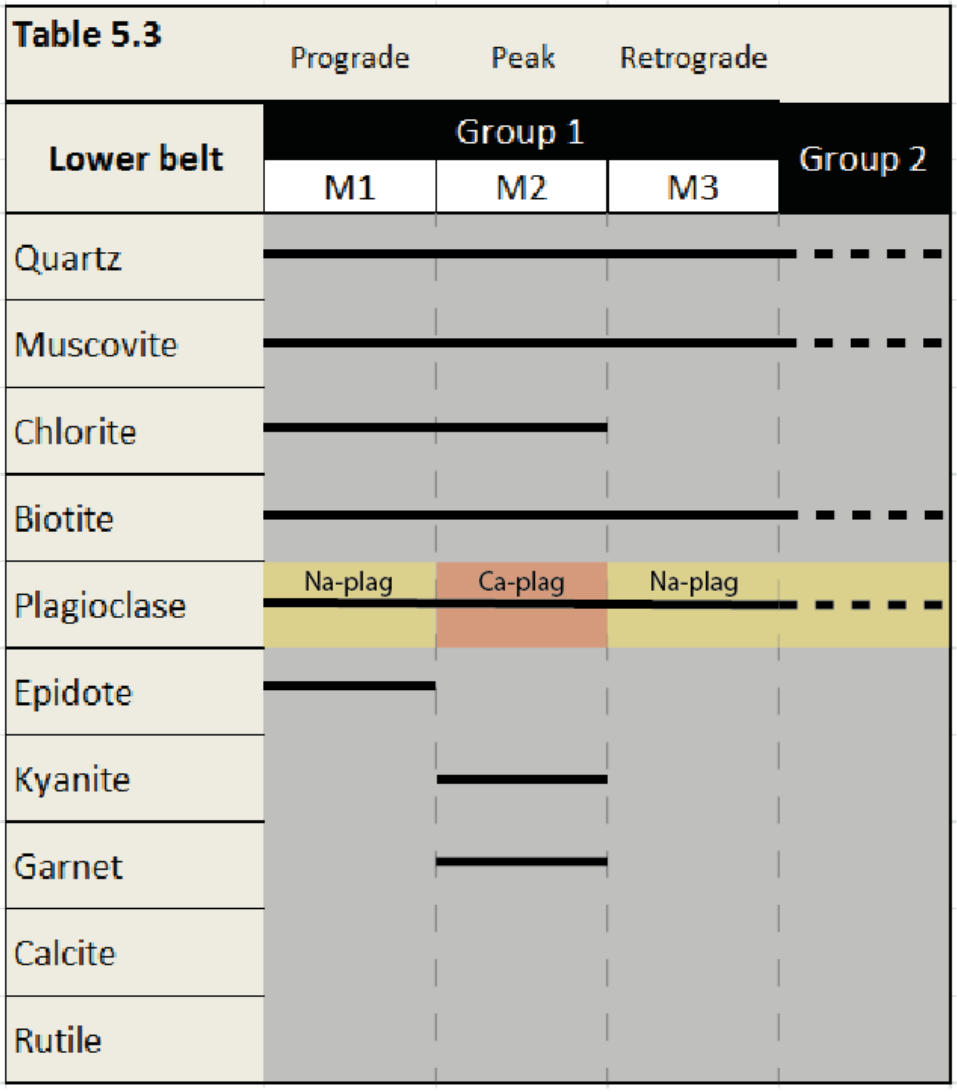

Table 5.2 Petrogenetic diagram of the lower Seve belt country rocks.

M1

The first stable mineral assemblage (M1) consists of quartz, muscovite, chlorite, Na-plagioclase and epidote. Of these minerals only epidote is still recognized in the thin sections as part of M1. The other minerals are present in the rock, but cannot be attributed to this phase based on overgrowth relations. Notwithstanding, the minerals quartz, muscovite, Na-plagioclase and chlorite are known to have been stable during M1 based on the stability diagram for pelites, as can be seen in figure 5.5. Quartz grain boundaries display intense grain boundary migration. This mechanism recrystallizes quartz into new minerals which are tens of micrometers in size. Epidote minerals are several hundreds of micrometers in size and are widespread in several thin sections occurring as inclusions in later stage Ca-plagioclase.

M2

The second stabile mineral assemblage (M2) consists of quartz, muscovite, biotite, Ca-plagioclase, garnet and kyanite. M2 muscovite and biotite are found throughout the thin sections in varying micro-structural expressions. The minerals grow largest in bands which are strongly foliated reaching sizes of almost 1 mm. In between the less foliated domains the size of the biotite is a fraction smaller, up to hundreds of micrometers. Both minerals are orientated sub parallel to the main foliation (S_{reg}). In addition, the biotite minerals overgrow M1 chlorite minerals (fig 5.3b). Ca-plagioclase is seen overgrowing muscovite, biotite and epidote minerals (fig 5.3c-d-e). They form large minerals (millimeter scale) and are positioned in bands which are aligned parallel to the main foliation (S_{reg}). The bands form a compositional banding (S_m). The garnet minerals reach sizes up to a millimeter and several have inclusions of biotite and Ca-plagioclase (fig 5.4a-b-c-d-e). These inclusions when orientated are sub parallel to the main foliation (S_{reg}). Which dates garnet growth as post- or syn-group 1 deformations. The kyanite forms a large (millimeter scale) mineral (fig 5.3a), which is indicative for the high grade (peak) metamorphism experienced during M2. It is bounded by predominately muscovite and biotite (M3) which seem to overgrown the kyanite crystal (M2) and/or kyanite growth is syngenetic with that of the mica growth and foliation (M2)

M3

The final mineral assemblage (M3) consists of quartz, biotite, Na-plagioclase and muscovite. Strongly foliated bands are built out of predominately biotite and to a lesser extent muscovite. It is seen curving around garnet minerals indicating the deformation phase which led to the main foliation was still ongoing (fig 5.4c-d-e). Furthermore, veins which are filled by Na-plagioclase (fig 5.4f) and indicate brittle conditions during formation.

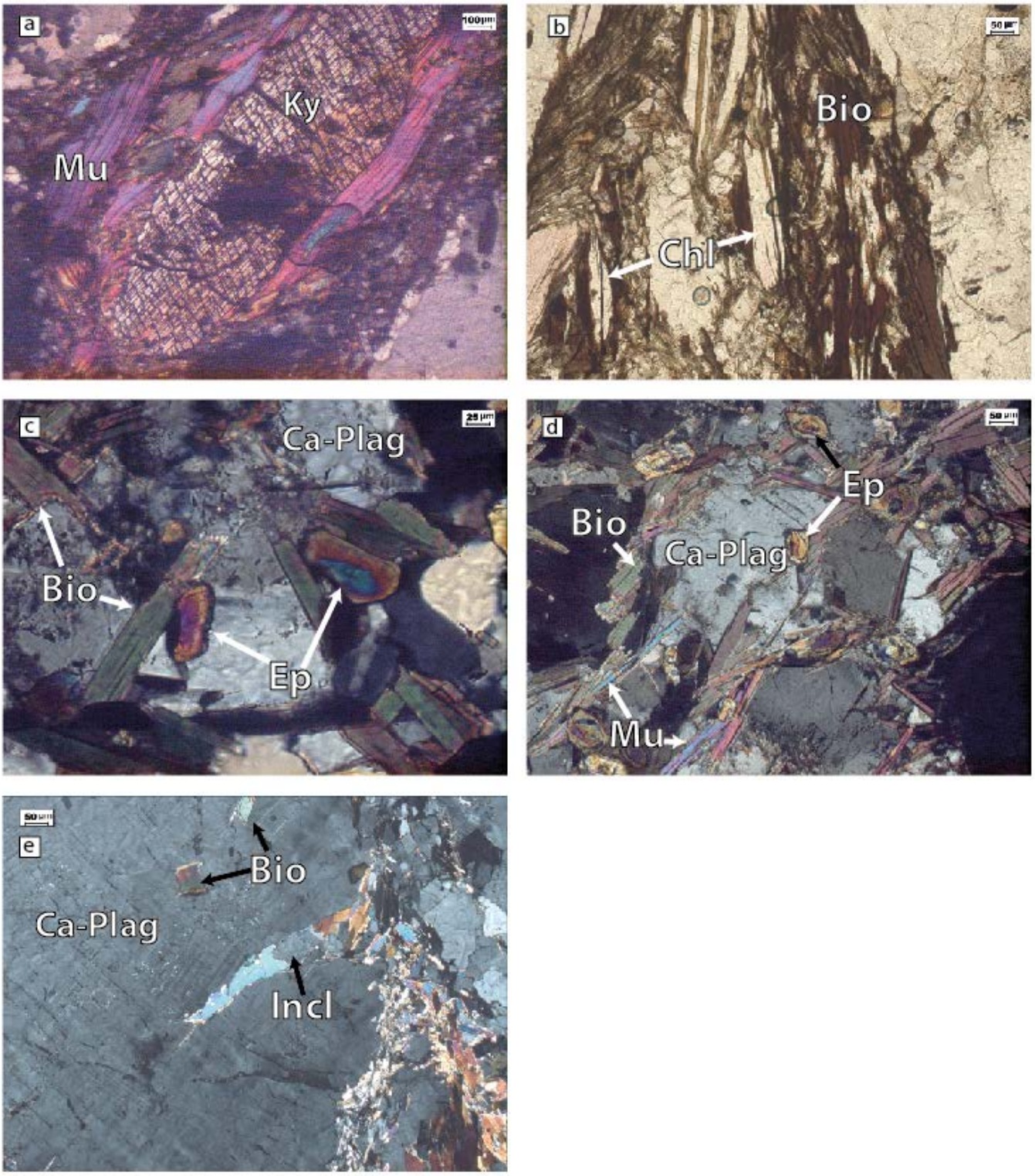

Figure 5.3 Optical microscopy photographs under XPL **a** Kyanite bounded by a band of muscovite. **b** Biotite overgrowing chlorite minerals. **c** Epidote and biotite inclusions in Ca-plagioclase. **d** Biotite, muscovite and epidote inclusions in Ca-plagioclase. **e** Ca-plagioclase with biotite inclusions. On closer inspection one of the inclusions consists out of a plagioclase fragments bounded by biotite minerals.

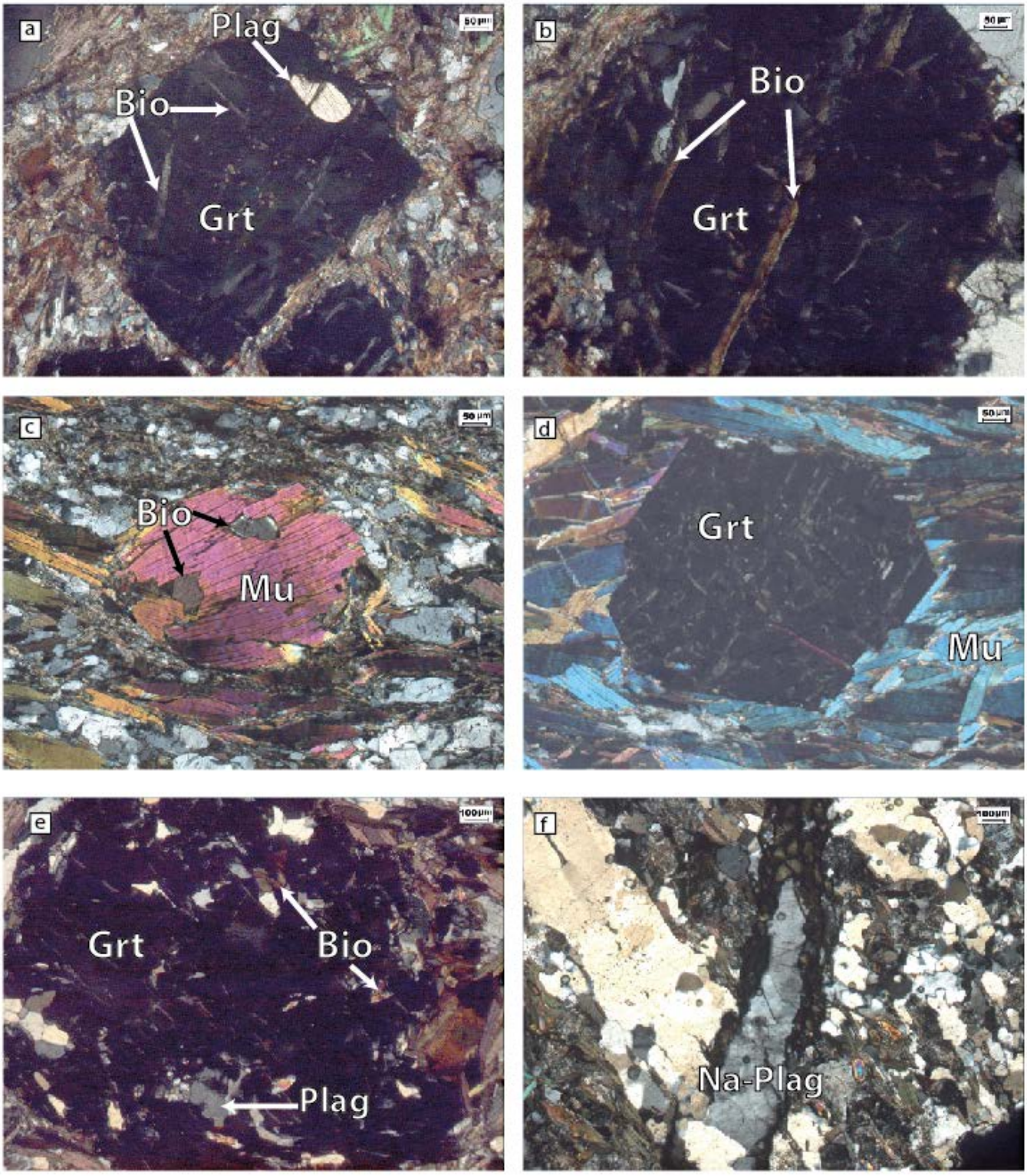

Figure 5.4 Optical microscopy photographs under XPL **a**-**b** Garnet with plagioclase and biotite inclusions. **c** A well-developed muscovite mineral overgrowing biotite and plagioclase. **d** Well-developed garnet overgrowing muscovite and biotite orientated parallel to S_{reg}. **e** Large garnet containing plagioclase and epidote inclusions and a rim of biotite. **f** Late veins of Na-plagioclase crosscutting S_{reg}.

5.5 Discussion

In the foregoing chapters some of the major characteristics like structural and metamorphic grade of the country rocks from each of the individual nappes were investigated. Subsequently by combining these characteristics for each nappe petrogenetic diagrams were constructed (table 5.1-3). The implications of the petrogenetic diagrams will be discussed here, as well as the differences and similarities between the various belts.

The determination of the metamorphic phases (M1-3) is based on the structural relations observed in the thin sections, such as overprinting. Overprinting has been interpreted as the interaction between two distinct metamorphic events. However, the possibility has to be considered that minerals can overgrow one and other during the same metamorphic phase. Different growth rates, enhanced or reduced by the availability of elements and/or fluids, could lead to the encapsulation of slow growing minerals. Specifically this could have been the case for M1 minerals of the Köli. Chlorite and muscovite inclusions (M1) are found in larger Na-plagioclase minerals (M2), which together also form a stable mineral assemblage. Hence, one could argue M1 and M2 should be the same phase. The author prefers to base the classification system solely on overgrowth relations and denote them as two distinct metamorphic phases.
In all belts we see a similar pattern: a gradual increase in metamorphic grade. With the start of the growth of low grade minerals such as quartz, muscovite, chlorite (Köli/upper Seve belt/lower Seve belt), epidote and biotite (upper belt/lower belt) occur. M1 is overgrown by higher grade minerals Na-plagioclase (Köli), Ca-plagioclase, garnet (upper and lower Seve belt) and kyanite (lower Seve belt) followed by the return to lower grade (i.e. a phase of retrogradation). The sequence of metamorphism events (M1→M3) displays a simple burial of rocks, followed by their uplift. The maximum experienced metamorphic grade differs between the 3 belts. This discrepancy is marked by the lower metamorphic peak in the Köli, greenschist facies, compared to middle amphibolite facies in the upper- and lower Seve belts. The metamorphic grade in the two Seve belts has not reached upper amphibolite facies, because this would involve migmatite formation, which is not observed in this thesis.
In fact, the upper- and lower Seve belts are very similar. The occurrence of epidote (this thesis), kyanite and staurolite (Trouw, 1973; Williams and Zwart, 1977) in both belts indicates a low to medium pressure (<650 MPa) and a medium temperature (<500 MPa) field (fig 5.5). Based on this we can exclude the high pressure/low temperature metamorphic conditions, as is characteristic for subduction zones. Further limitations are absent in the upper Seve belt, however the presence of kyanite provides an additional barometer for the upper and lower Seve belts. Kyanite is the high pressure aluminium silicate polymorph and is stable at pressures above 300-400 MPa, depending on T. The combination of epidote and kyanite in the lower belt therefore excludes low pressure/high temperature metamorphic conditions which are characteristics for a contact metamorphism event. The lower belt is thereby evidently metamorphosed under classical Barrovian type of metamorphism formed during continent-continent collisions accretionary prisms (Bucher-Nurminen, 1991).

Data of the Köli provides less constrains its exact path. However, the consecutive mineral assemblages (M1-3) lie on the same gradient as the two Seve belts. When considering the strong similarities between the nappes and our knowledge of the area it is assumed both belts have experienced the same metamorphic field gradient.

Furthermore, the deformation experienced by the nappes is marked by the pervasive foliation (S_{reg}). Note that this group 1 deformation consists of multiple deformation phases which all contribute to formation of S_{reg} (Zachrisson, 1969; Trouw, 1973; van Roermund & Bakker, 1983).

Abbreviations:

Qrz	-Quartz
Chl	-Chlorite
Grt	-Garnet
Ab	-Albite
	(Na-plagioclase)
Act	-Actinolite
Pg	-Paragonite
Clz	-Clinozoisite
Pg	-Paragonite
Ms	-Muscovite
Bt	-Biotite
Pl	-Plagioclase
Hbl	-Horneblende
St	-Staurolite
Crd	-Cordiorite
Kfs	-K-feldspar

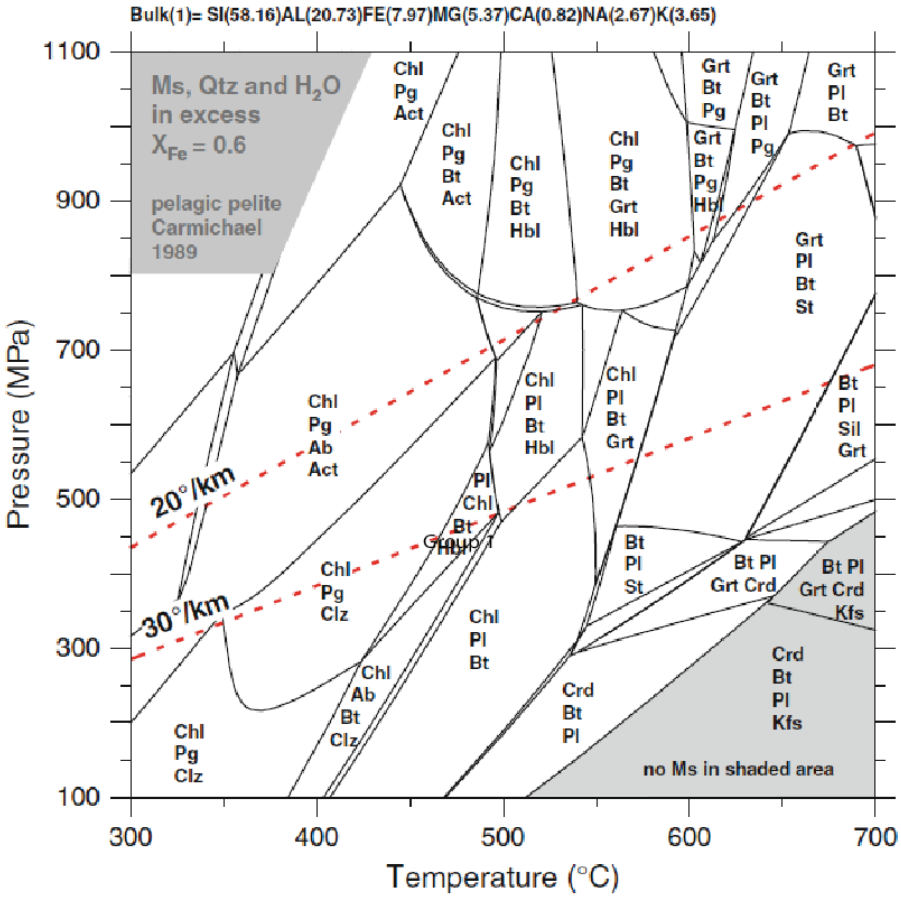

Figure 5.5 Petrogenetic diagram of pelitic rocks for the average pelagic pelite composition of Carmichael (1989) with quartz, muscovite and water added in excess. The two dashed lines represent typical geothermal gradients for continent-continent collision (from Bucher & Grapes, 2011).

6) Chemical composition of peridotite minerals

EMP mineral chemical analyses have been performed on representative mineral assemblages from rocks from the Köli, upper Seve belt and lower Seve belts. Various mineral phases were sampled corresponding to multiple metamorphic events. The results of the complete EMPA/ SEM mineral analyses (data set) are shown in appendix I. In these tables the results are given in element-oxide weight percentage (wt%) in the mineral.

6.1 Olivine

Two types of olivine are present, namely, a first generation of olivine that formed porphyroclasts (M1) is only present in the upper- and lower belt. The second generation olivine (M3) which is present in all 3 belts. The lower belt has one additional olivine micro-structure which is related to the dynamic recrystallization of olivine. All olivines are forsteritic in composition with Mg# ranging between 0.90 and 0.97 (fig 6.1). There is a strong difference between olivines of the Köli nappe on the one hand and the upper- and lower Seve belts on the other. Mg# in Aunere peridotite of the Köli belt is extremely high averaging at 0.96, whereas the Mg# in olivine in the peridotites of the upper- and lower belts average at 0.93 and 0.91 respectively. This diversity in Mg# between the belts is not seen within the individual belts. No sensible difference in Mg# composition was observed between the different olivine structures within the same belt. This holds for both the upper- and lower Seve belts as can be seen in figure 6.2 and 6.3, the Köli is excluded due to the presence of just one olivine type. The amount of NiO wt% shows a similar pattern, amongst the belts there are distinct differences however no difference in NiO wt% is observed between the various olivine types within the belts. The amount of NiO wt% is highest in the upper belt averaging at 0.47% and significantly lower in olivine of the lower belt and the Köli nappe, where it is 0.36% and 0.34% respectively.

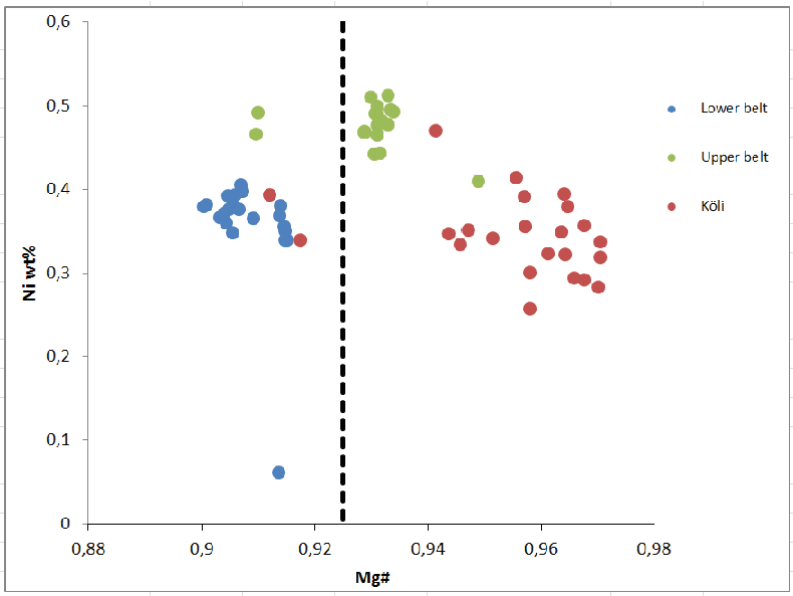

Figure 6.1 Mg# vs NiO wt% numbers in olivines from the peridotites of the 3 nappes.

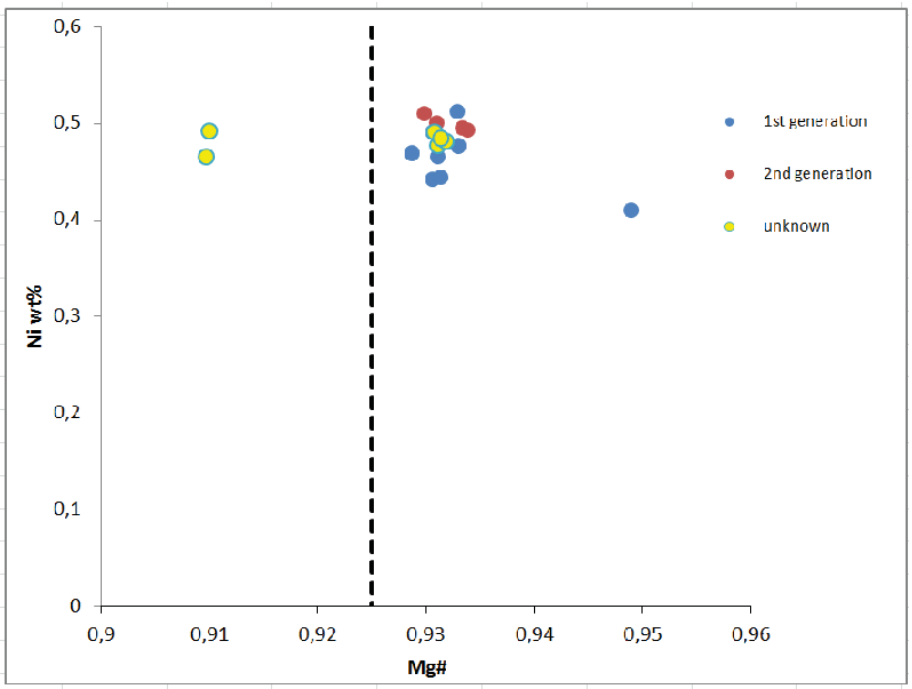

Figure 6.2 Mg# vs NiO wt% numbers in various types of olivines in peridotites of the upper belt.

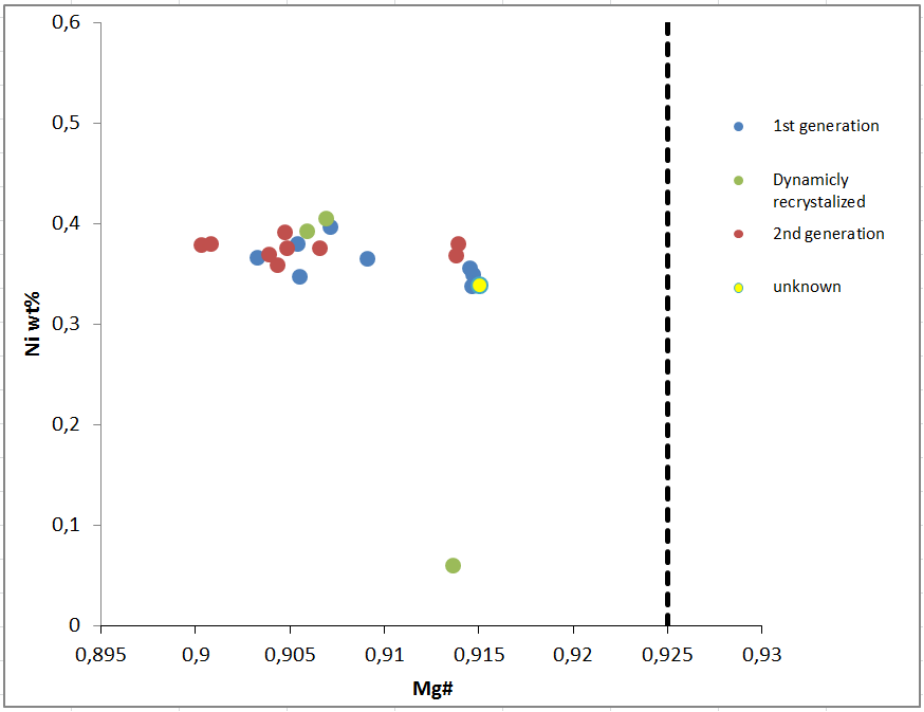

Figure 6.3 Mg# vs NiO wt% numbers in various types of olivines in peridotites of the lower belt.

6.2 Spinel

There are two types (type I and II) of spinel recognized in the peridotites of this thesis. Spinel is a solid solution with the chemical formula: AB_2X_4. The two types of spinel correspond to different metamorphic stages and have different chemical composition. Spinel I forms part of the protolith assemblage and will be discussed first. Spinel II which is often clustered in bands and forms part of the M2 assemblage, will be discussed later.

The structural formula of spinel is AB_2X_4 in which the B-position is filled by Cr^{3+}, Al^{3+} or Fe^{3+} in a solid solution. By comparing the constituents present on the B-position in spinel, it becomes apparent that spinels from the Köli and the lower Seve belt mutually overlap in composition whereas spinels from the upper belt deviates from it and contains a larger Fe^{3+} component (results are presented in figure 6.4 and table 2-appendix I). The comparison is based on EMP analyses performed in the core of the spinels, since they are least affected by secondary alteration processes. Spinel cores from peridotites of the Köli and the lower Seve belts are high in chrome (Cr) and have a minor but significant component of aluminum (Al), Cr# of 0.7-0.8 and Al# of 0.18-0.21 (Köli) and Cr# of 0.6-0.8 and Al# of 0.14-0 (lower belt). In spinels of the upper belt chrome values are significantly lower (Cr# of 0.18-0.51) and the aluminum component is nearly absent (Al# of <0.01) (fig 6.4). The A-position can be filled by Mg^{2+} and Fe^{2+}, so another comparison of spinel composition from peridotites of the belts can be made. The EMP-analyses performed on the spinels also show variable compositions on the A-position, but the Mg# values remain low never exceeding 0,5 (fig 6.5). In descending order of magnesium composition, the Köli (Mg# 0.38-0.41), the lower belt (Mg# 0.22-0.30) and the upper belt (Mg# 0.08-019) (fig 6.5).

When comparing the center of the spinels with the rims there are some clear differences. In all the belts we see a drop in Cr_2O_3 mol% towards the rims. The drop is most significant in the Köli, from 73.3 to 24.5 mol %, the lower belt drops from 77.1 to 52.4 mol % and the upper belt, which has a lower concentration Cr_2O_3 to begin with, drops from 31.7 to 15.4 mol %. Furthermore, the Al_2O_3 concentration also drops in spinel core to rim in the Köli and lower belt, from 9.5 to 3.0 and from 7.7 to 0.7 respectively. The Cr# values in the rim show a considerable spread, however the trend is unambiguously moving along the Al=0.0 line towards the Fe^{3+}-end of the diagram (fig 6.4). Once more spinel composition of the upper belt deviates from spinel composition of the other two belts. The amount of Al_2O_3 is so low in the core that no observable drop can be observed towards the rim. The drop in Cr_2O_3 (Cr^{3+}) and Al_2O_3 (Al^{3+}) is compensated by the rise in Fe_2O_3 (Fe^{3+}) which takes the place in the B-position in the structural formula (fig 6.4 and table 2-appendix I). Similarly, a change in the A-position is observed. Mg# falls form spinel core towards the rim, i.e. Fe^{2+} is replaced by Mg^{2+} (fig 6.5). In fact, the pattern corresponds to what is recognized in the B-position (fig 6.4). The most pronounced drop is present in spinels of from the Köli, closely followed by the lower belt. Spinels from the upper belt have a lower Cr# in the core compared to the other belts and the corresponding drop in Cr# towards the rim is therefore less pronounced. The Mg# and the Cr# in the data presented in this thesis together with other chemical data from spinels in the middle Seve belt (Brueckner et al. 2004; Clos et al., 2014; Gilio et al., 2015) align in figure 6.5 describing a linear depletion trend. In addition, the TiO_2 wt% vs Fe^{3+}# in spinels from this thesis also show a clear trend. There is a positive correlation between Fe^{3+} and TiO_2. This relation

was first recognized by Barnes & Roeder (2001), which attributed this due to the change in spinel composition due to crystal fractionation during formation. Notably is the clear deviation seen in several rims of the spinels from the Köli belt, at the right bottom end of the diagram (i.e. low TiO_2 per Fe^{3+}#).

The second type of spinel (spinel II) is characterized on the B-position almost exclusively by Fe^{3+} (Fe# >0.99). In addition the A-position is occupied with Fe^{2+}, resulting in very low Mg# values (0.03-0.04), results are presented in table 2-appendix I. In fact, we are dealing here with the end-member magnetite ($Fe^{2+}Fe^{3+}{}_2O_4$). Magnetite is recognized in all 3 belts, but is a product of serpentinization and therefore does not represent the protolith assemblage.

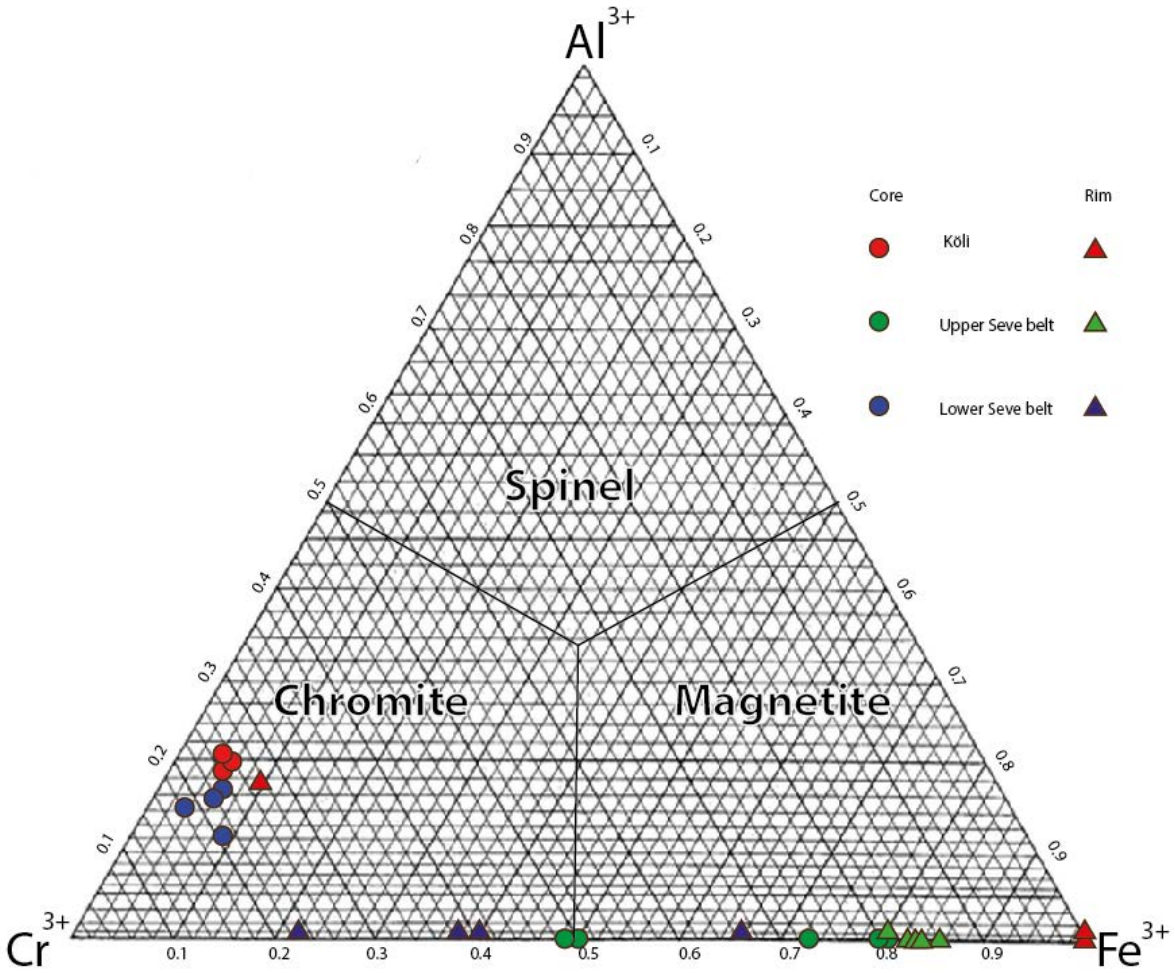

Figure 6.4 Triangular endmember-diagram for spinel compositions. This discrimination diagram is based on the elemental components in the B-position of the Spinel (occupied by Cr^{3+}, Al^{3+} or Fe^{3+}).

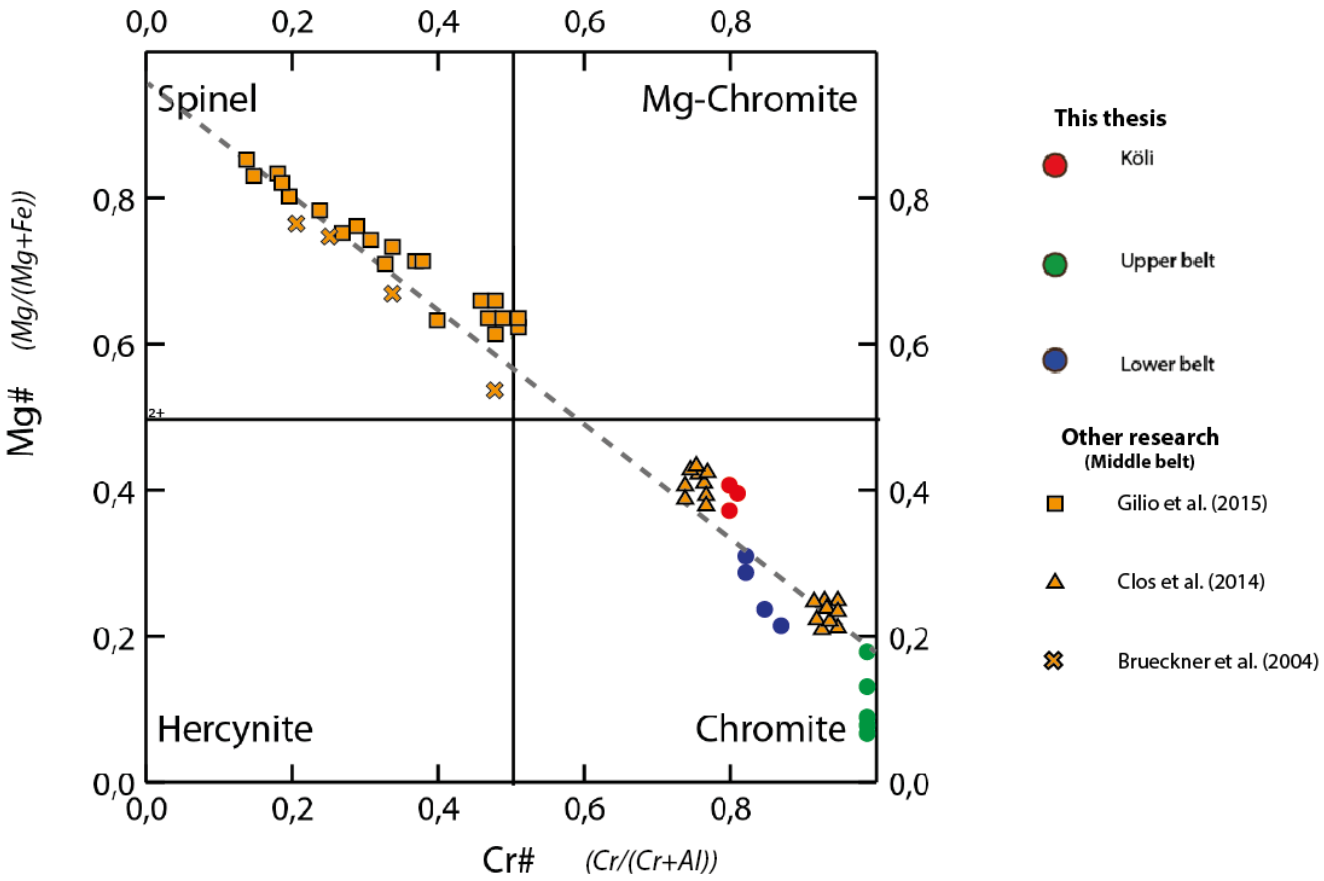

Figure 6.5 Spinel classification diagram. This classification is based on the elemental component present in the A-position vs B-position in spinel. Mg# vs Cr# data from the cores op spinel in the Köli, upper and lower Seve belt follow a linear trend when compared to data from other research performed on spinels form the middle Seve belt.

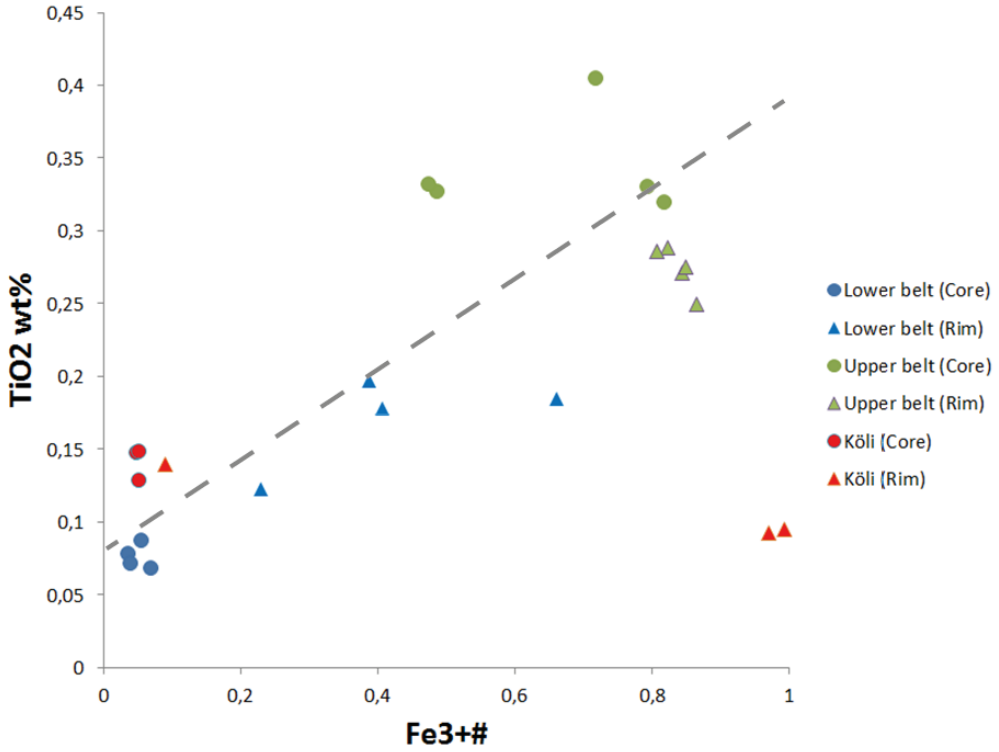

Figure 6.6 Fe^{3+}# vs TiO_2 (wt%). The Fe^{3+}# positively correlates to TiO_2. Two point from the rim of Köli spinels deviate from this trend. This trend is attributed to the change in spinel composition during fractional recrystallization (Barnes & Roeder, 2001).

6.3 Other minerals

Amphibole

The results of EMP analyses of amphibole from the western- and eastern belt peridotites are presented in table 3 of appendix I. they have high Mg and Ca contents: 22.9-23.3 wt% and 11.5-12.8 wt% respectively. Based on the classification system for Ca-bearing amphiboles (Leake et al., 1997), the amphiboles in peridotites of both belts are classified as tremolite (fig 6.7).

Chlorite

Chlorite composition in peridotites of the lower belt, the upper belt and the Köli are all characterized by their high magnesium content (table 4- appendix I). According to the classification system of Zane & Weiss (1998) they can all be classified as Mg-chlorites (fig 6.8). The composition in lower belt chlorites microstructurally positioned in rims around chromite crystals contain small quantities of chrome, ranging between 2.64 and 3.78 wt%.

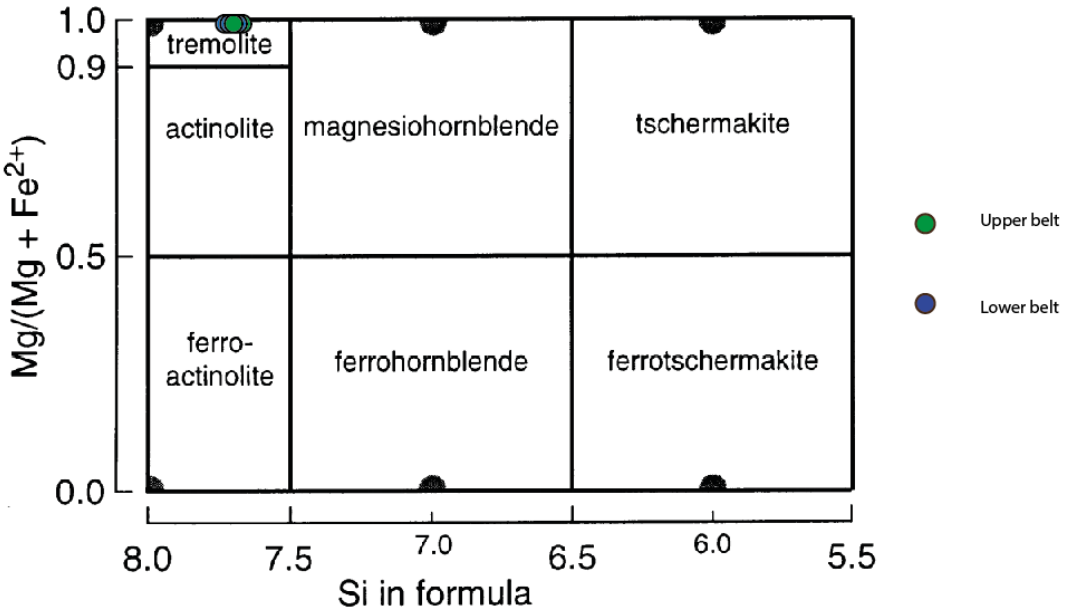

Figure 6.7 Classification diagram of Ca-bearing amphiboles (after Leake et al., 1997). Blue: amphibole in peridotites from the lower belt. Green: amphibole in peridotites from the upper belt.

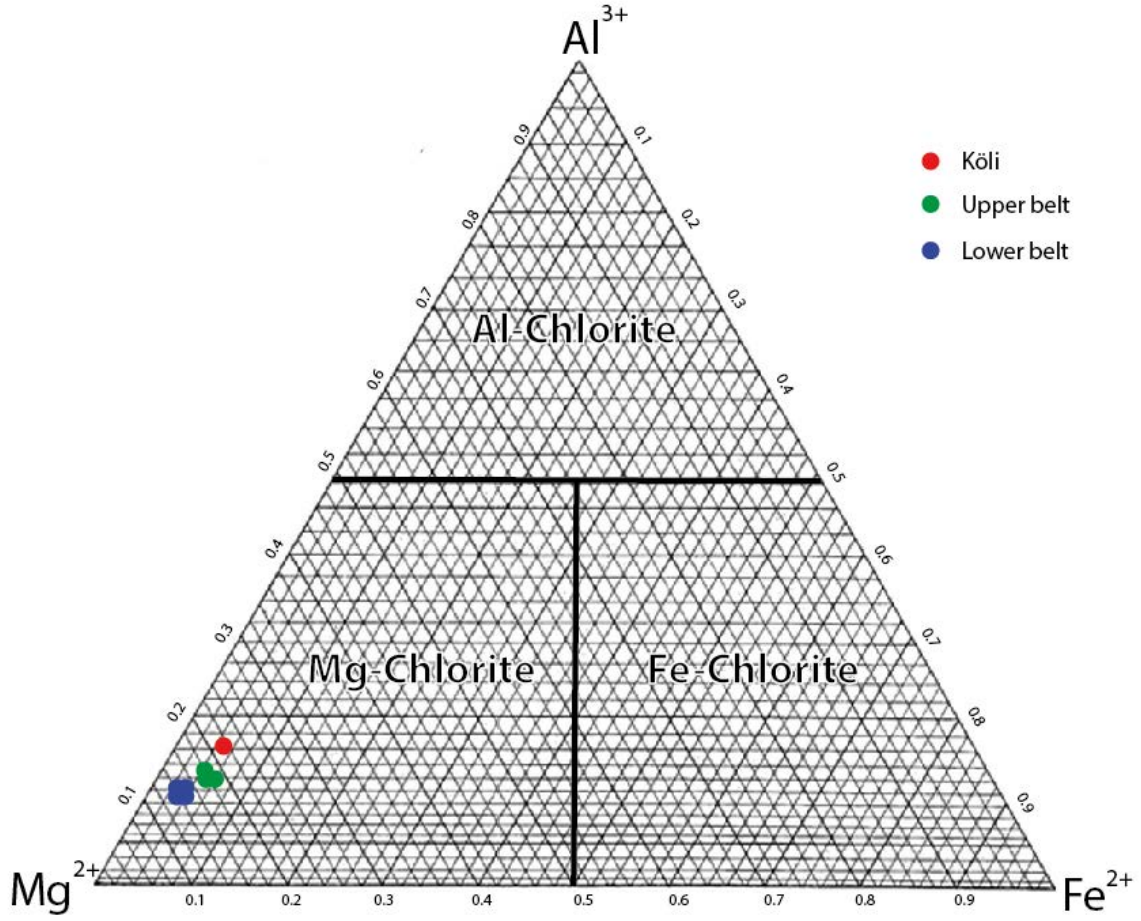

Figure 6.8 Chlorite compositional data from taken from the Köli, lower Seve and upper Seve belt peridotites plotted on the ternary endmember diagram of chlorites, modified after Zane & Weiss (1998).

6.4 Discussion

The high forsterite component (Mg# of 0.90-0.97) of the olivines found in peridotites of all 3 belts indicates that these peridotites have a depleted restite origin. The Mg# of olivines in the Köli belt is so high (0.94-0.97 Mg#) that it has to be of metamorphic origin. Kimberlitic xenoliths, i.e. highly depleted mantle restite, may yield Mg# in olivine up to 0.95 (Boyd & Nixon, 1975). The high Mg# values in olivine from the Aunere peridotite of the Köli belt are interpreted here to be due to the alteration of the olivine protolith into serpentine. The fayalite component cannot be accommodated in the Mg-rich serpentine and it becomes incorporated in magnetite minerals (Fe_3O_4). Notwithstanding, the lower- and upper belt olivines do not show any significant change in Mg# between the protolith olivine and the olivine associated with M3 and M4. This suggests a reversing of the reaction as denoted in equation 4.2 was possible in these belts. In contrast, in olivine of the Köli it was hindered. In other words: 2nd generation of olivine could therefore only be formed by conversion of Mg-rich serpentine, the reverse reaction of equation 4.1, leading to high Mg# olivine (Mg# ≥0.94). In fact, the transformation of magnetite into fayalite requires a reducing environment in order to change ferrous iron into ferric iron. Difference in such conditions is potentially dictated by sea and/or ground water availability.

Furthermore, chemical differences in primary spinel composition are revealed between the belts. Data from the core of primary spinels plot on different locations in the spinel end-member triangular diagram than their rim composition. In the investigated belts of the Marsfjället area we can distinguish three different types of spinel: 1) unaltered protolith spinel, 2) magnetite and 3) re-equilibrated ferrianchromite. The unaltered protolith spinel has a pre-Caledonian history. Data from several researches performed on peridotite in the Marsfjället area has revealed a linear trend in the Mg# vs Cr# (fig. 6.5). This trend is interpreted to be due to the PT-condition during equilibration and relative enrichment by degree in partial melting (Mellini, 2005). The cores investigated in this research all fall within in the chromite field (fig. 6.4 and 6.5). The second type of spinel is due to the low temperature serpentinization of olivine, according to the chemical reaction eq. 4.2 (chap 4). The newly formed magnetite has the tendency to accumulate on existing spinel minerals which act as a substrate to bind on (Bucher & Grapes, 2011). This process is specifically recognized in the Köli, where the spinel rim composition is the pure magnetite end-member (fig 6.4). In fact, this provides an explanation for the deviation of the points taken from the rim of the Köli spinel from the trend in the Fe^{3+}# vs TiO_2 (wt%) diagram, as indicated in figure 6.6. Throughout all belts magnetite is recognized often as belts within the foliated serpentine. The third spinel type, the re-equilibrated ferrianchromite, is recognized in the rims of spinels in the upper and lower Seve belts. Ferrianchromite is the unofficial name for indicating spinels with a composition near the magnetite-chromite border (fig 6.4) and is associated with a re-equilibration process which occurs under lower amphibolite and higher facies (Burkhard, 1993; Kapsiotis et al., 2007). This is in good agreement with the data presented in this thesis, where the upper and lower Seve belt, which are metamorphosed to amphibolite facies, exhibit ferrianchromite rims and the spinels in the Köli belt, metamorphosed to greenschist facies, do not. Chromite metasomatically reacts with antigorite to form the re-equilibrated ferrianchromite alteration rim edged by chlorite (eq. 6.1). Generally chlorite is rich in chrome, with Cr_2O_3 values around 2–6 wt%

(Merlini, 2009). This is recognized in the chlorite of all the belts (appendix I- table 4) including the Köli. High values of chrome in chlorite of the low grade Köli questions whether the statements by Burkhard (1993) and Kapsiotis et al. (2007) are correct or whether there is an alternative reaction leading to the enrichment of chrome in chlorites at lower T in the Köli. The chemical reaction which corresponds to this re-equilibration is given by the equation below (eq. 6.1). Data from this thesis deviates from the equation below by higher Fe^{3+} values. The high Fe^{3+} seen in the spinels suggest conditions during hydrothermal metamorphism were oxidizing (Kapsiotis et al., 2007).

$$2(Mg_{0.60}Fe_{0.40})(Cr_{1.30}Al_{0.70})O_4 + {}^{3}/_{2}(Mg_{2.57}Al_{0.32}Fe_{0.11})Si_2O_5(OH)_4 + H_2O + {}^{1}/_{12}O_2$$

Chromite **Antigorite**

$$\rightarrow$$

$${}^{7}/_{6}(mg_{0.40}Fe_{0.60})(Cr_{1.85}Fe_{0.08}Al_{0.07})O_4 + ½(Mg_{9.18}Fe_{0.34}Al_{1.60}Cr_{0.88})(Al_2Si_6)O_{20}(OH)_{16}$$

Ferrianchromite **Cr-chlorite**

Equation 6.1 after (Merlini, 2009)

7) Discussion

7.1 Peridotite origin

7.1.1 Chemical affinity

The chemical composition of orogenic peridotites is influenced by the tectonic setting in which it originated and/or evolved. Pressure and temperature conditions dictate the extent of depletion experienced during partial melting and fluid percolation can change the bulk rock composition by either removal or introduction of elements to the system. The later has unequivocally occurred in the peridotites from all 3 belts with the introduction of calcium. Arai (1990; 1994) has characterized peridotites from multiple tectonic settings according to the olivine-spinel mantle array, which outlines depletion trends for particular tectonic settings. A comparison of the chemical analyses (as presented in chapter 6.1 and 6.2) performed on olivine and spinel can thus be used to provide insight into the origin of the peridotites found in the Köli nappe, the upper belt and the lower belt. The indicators used by Arai (1994) are the Mg# in olivine and the Cr# in spinels ($Mg\#_{ol}$ and $Cr\#_{sp}$) (results are indicated in figure 7.1).

Spinels in the lower Seve belt peridotites are characterized by the absence of Al_2O_3 and a high average Cr# of 0.99. In addition, their average Mg# is high ≈ 0.93. Accordingly, the spinels from the lower Seve belt peridotites plot in the cratonic field (fig 7.1). Both element discrimination numbers are too high to allow for a classification in the island-arc or oceanic fields.

Compared to the lower belt peridotites spinels from the upper Seve belt peridotites are characterized by less extreme values: $Cr\#_{sp}$ averages 0.83 and the $Mg\#_{ol}$ 0.91 (chapter 6.1 and 6.2). The lower belt peridotites therefore plot on a spot where apparently the stability fields of two tectonic settings overlap (fig 7.1): the craton- and island-arc fields. Solely based on this data it is not possible to discriminate between both settings, however as all other orogenic peridotites from the Seve also plot into the cratonic field a similar origin can be assumed for the upper belt peridotites.

The Aunere peridotite of the Köli is characterized by an average $Cr\#_{sp}$ of 0.79, absence of protolith olivine inhibits determination of its provenance type solely based of the spinel-olivine array. Previous work by Bucher-Nurminnen (1991) and Zacharisson (1973) has classified the Aunere peridotite as part of an obducted ophiolite (i.e. Penrose type). Austrheim & Prestvik (2008) and Iyer et al. (2008) have performed detailed studies of the Leka ophiolite in North-central Norway. Results of the Leka ophiolite is also indicated in figure 7.1, $Cr\#_{sp}$ values are in correspondence with values found in the Aunere peridotite. The Leka ophiolite plots in the oceanic field and is in agreement with work of previous authors.

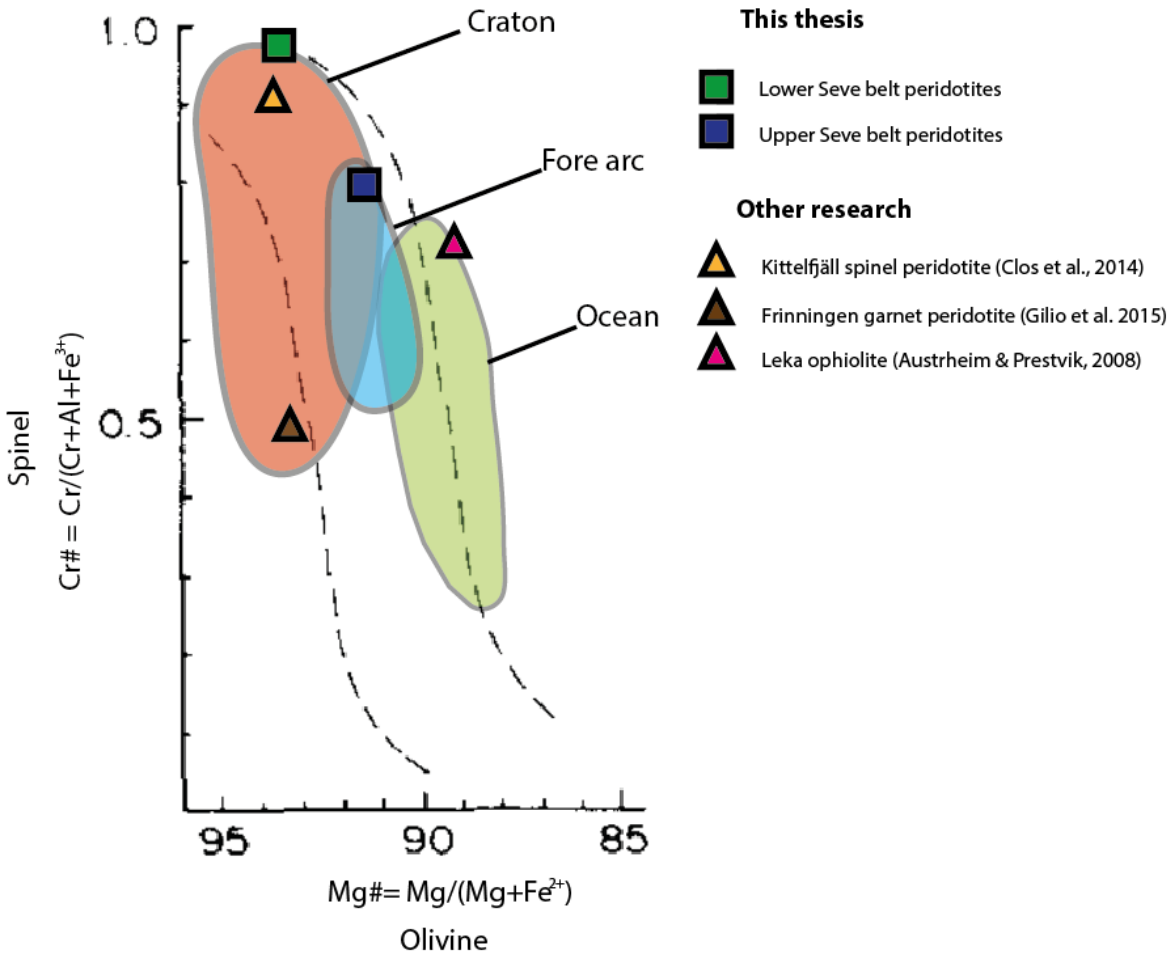

Figure 7.1 $Cr\#_{Sp}$ vs $Mg\#_{Ol}$ array, modified after Arai (1994). The elliptical colored fields outline specific tectonic settings (craton, fore-arc and ocean).

7.1.2 Age constrains

The classification of orogenic peridotites to a specific tectonic setting has implications for their formation age. The upper belt- and the lower belt peridotites are ascribed to have a cratonic provenance (section 7.1.1). The cratonic lithosphere of Baltica and Laurentia (former Rhodinia) was formed during the Archean Eon (≥2.5 Ga) (Bueckner & van Roermund, 2004; Slabunov et al., 2006). Therefore, the maximum age of peridotites of this provenance is Archean, but is potentially reworked to younger ages. In the specific case of the lower belt the origin is however ambiguous. It may potentially have formed in the tectonic setting of an island arc. Such a setting occurs in the oceanic domain during a stage of compression. Spreading of the Iapetus Ocean ceased at 560Ma (Cocks & Torsvik, 2005). This has to be considered as the maximum age for the formation of sub-island arc peridotites. According to the geodynamical model of Hacker and Gans (2005) younger SOLM was formed during a phase of extension (454-432 Ma).

The provenance of the Aunere peridotite of the Köli belt remains undetermined, however previous work classified it as an ophiolite and therefore of oceanic origin. The onset of rifting (i.e. the break-up of Rhodinia) has to be considered as the maximum formation age. The first closure of the Iapetus Ocean (~430 Ma) does not provide a minimum age, since oceanic lithosphere could have formed also under a compressional regime in a back-arc rifting setting. Age dating of the protolith

assemblage can provide conclusive evidence in determining the provenance type of the Aunere peridotite of the Köli.

7.1.3 Rock association

The depositional environment during the sedimentation of the country rock of the SNC and the lower Köli are marine. The SNC is associated with the ocean-continent transition and the Köli with the oceanic domain (Gale & Roberts, 1974; Gee, 1975; Roberts et al, 1985; Stephens & Gee, 1985). The subclassification according to the spinel-olivine array (fig 7.1), indicates a cratonic origin for all peridotites of the SNC belts. Cratonic crust needs to have been strongly depressed in order for deep marine sediments to be deposited on top of it. This can be achieved by intense extension of the margins of the continent which occurred during the break-up of Rhodinia and subsequent opening of the Iapetus Ocean resulting in so called OCT-type peridotites. This extensional event might have predated the real break up of Rhodinia and the formation of oceanic crust. The provenance of the Köli remains so far undetermined. Speculations based on the rock association are precarious. The oceanic sediments might suggest an oceanic provenance of the underlying lithosphere, however it can also be caused by a continuation of the process described above, leading to a more extreme extension and associated depression. The extent to which this process can lead, afore formation of oceanic lithosphere is not well known. An additional argument is found in the absence of the entire middle segments of the ophiolite sequence within the Köli nappe. Apart from the pelitic cover and the ultra-mafic base, the gabbros, sheeted dykes and pillow basalts are absent. This has been explained as complete dismembering of the Penrose-type ophiolite sequence (Trouw, 1971; Zacharisson, 1973; Bucher-Nurminnen, 1991; Eide & Lardeaux, 2002). The chemical affinity of the Leka ophiolite, as discussed in section 7.1.1 supports the latter idea.

7.2 PT-path

7.2.1. Köli

The Aunere peridotite of the Köli nappe

The protolith assemblage M1 (table 4.1): the original mineralogical constituent in the Köli peridotites is mainly olivine and some chromite. It is therefore highly depleted and of the dunite sub-type. This mineral assemblage falls within the entire stability field of spinel peridotites (fig 7.2), its lower boundary is defined at 0.8 GPa, depending on T (Bucher & Grapes, 2011). The upper boundary is highly dependent on the availability of Fe2+, Fe3+, Zn, and Cr. Their presence can vastly extend the spinel stability field upwards towards higher P. 3.0 GPa is considered to be the upper boundary of the spinel stability field (Bucher & Grapes, 2011). Often used geobarometric techniques applied to ultramafic rocks such as the Cr in clinopyroxene barometer (Nickel, 1989) and Al in orthopyroxene (Brey & Köhler, 1990) are not suitable for dunitic rocks. For more detailed information of these and other geobarometry techniques the reader is referred to Ravna & Paquin (2003). Temperatures during formation of the protolith assemblage are initially >1200 C° (Baker

et al., 1995), this corresponds to the minimum melting temperature for dry ultramafic rocks when hot partially molten upper mantle rocks gradually cool below the dry solidus. The spinel field extents down to sub-solidus conditions of around 750-800 C°. The formation of the M1 mineral assemblage (Ol, Sp ±Opx ±Cpx) is interpreted to have taken place at T >750-800 C°.

M2-retrograde metamorphism

The first metamorphic phase that can be ascribed to the Caledonian orogeny is the M2 (table 4.2). During this phase the Aunere peridotite became intensely serpentinized. This process resulted in the formation of the serpentine minerals chrysotile and antigorite which are stabile at temperatures <250 C° and 250-600 C° respectively (figure 7.2). The formation of serpentine requires the input of water into the system (equation 4.1 and 4.2) in order to transform the otherwise stabile protolith assemblage. The M2 mineral assemblage does not provide pressure constrains. However, the ultramafic Ro-breccia, recognized by Trouw (1973) and discussed in chapter 4.2, indicates that ultramafic bodies where elevated to surface levels and have undergone erosion prior to the pro-grade M3 metamorphism event.

M3-peak metamorphism

The third metamorphic event is marked by the renewed stability of olivine. Olivine is stable at temperatures in excess of 400 C° in upper greenschist to lower amphibolite facies fields and denotes the highest metamorphic grade experienced by the Aunere peridotite in prograde metamorphism. The stability of olivine is nearly independent of pressure (fig 7.2) and therefore no accurate depth indication can be given. The increase in temperature can be accommodated by a spreading event or a burial event. In the context of our knowledge of the area and the tectonic evolution of the Köli nappe, e.g. nappe stacking, the latter is very credible. Therefore, pressure would most likely have risen substantially to ~0.5 GPa, assuming a Barrovian regional type of metamorphism (Bucher-Nurminnen, 1991).

M4-retrograde metamorphism

The final metamorphic phase, M4, marks a second stage of retrogradation. Newly formed olivine and remnants of olivine porphyroclasts are serpentinized. Similarly this requires the addition of water into the system. Furthermore, quantities of Ca and CO_2 are added to the system in order to produce calcite. The calcite accumulates in veins which suggests it is formed under brittle conditions.

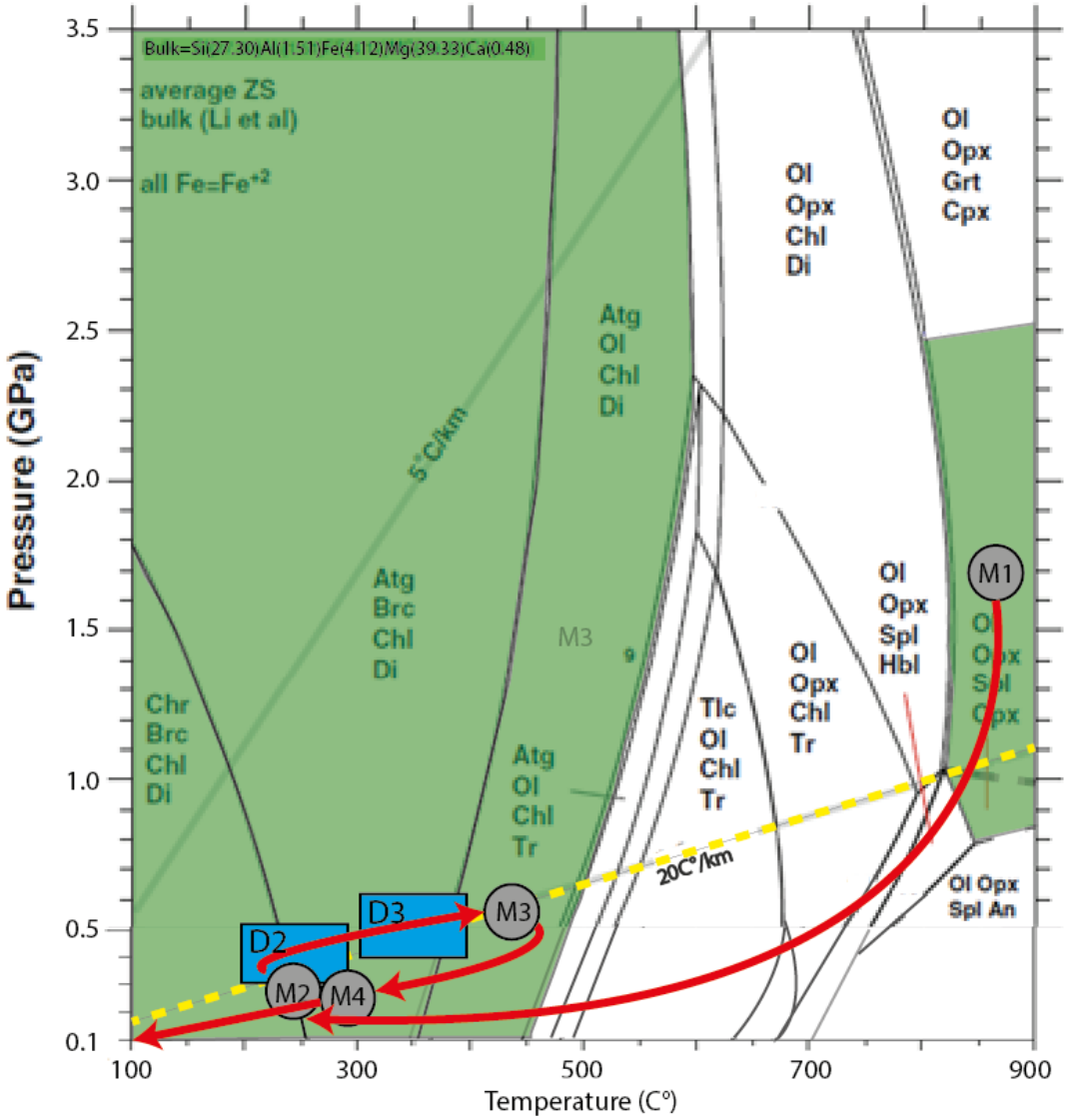

Figure 7.2 Interpreted PT-path of the Aunere peridotite of the Köli nappe. Background petrogenetic grade is modified after Bucher and Grapes (2011). BRC (upper left side) taken from Li et al. (2004).

Köli nappe country rock

M1

The prograde mineral assemblage (M1) in the country rocks of the Köli nappe consisting of quartz, muscovite and chlorite (table 5.1) is not a very fruitful mineral assemblage to determine the PT-conditions. Muscovite and quartz are the minerals which are present in excess in the used petrogenetic diagram for pelites (fig 7.3) and are stable together apart from the far right bottom corner. Furthermore, chlorite has a large stability field and does not provide any restrictions on depth. Temperature-wise the chlorite-out is positioned at approximately 600 C° (fig 7.3), following a 20 C°/km geotherm, at approximately 550 C°. The absence of albite and biotite in this assemblage marks T=<450 C°.

M2

The second minerals assemblage represents the peak metamorphosis conditions experienced by the Köli country rocks (table 5.1). It is marked by the introduction of biotite and Na-plagioclase (albite/oligoclase). The combination of these minerals in the absence of garnets is stabile in a relative small PT-field ranging between 500 and 700 MPa and 500-550 C°, assuming continent-continent collision. Under low pressure conditions the stability field can drop as far as 400 C°. The peak metamorphic grade achieved in the Köli is therefore greenschist facies, which is in agreement with previous studies (Zachrisson, 1969; Trouw, 1973; Zwart, 1974; Gee et al., 2010).

M3

The last metamorphic phase (M4) is marked by retrogradation. It is characterized by the removal of Na-plagioclase and biotite from stabile assemblage and the introduction of calcite and rutile (table 5.1). The constrains on the PT-conditions experienced during M4 are therefore identical to M1, no pressure constrains and temperature <450 C°. It is extremely likely, considering the exhumation history of the rock postdating M3 that the geothermal gradient was higher than during the burial of M1. The occurrence of rutile and calcite is interpreted to be due to the incorporation of Ca and Ti by water infiltration.

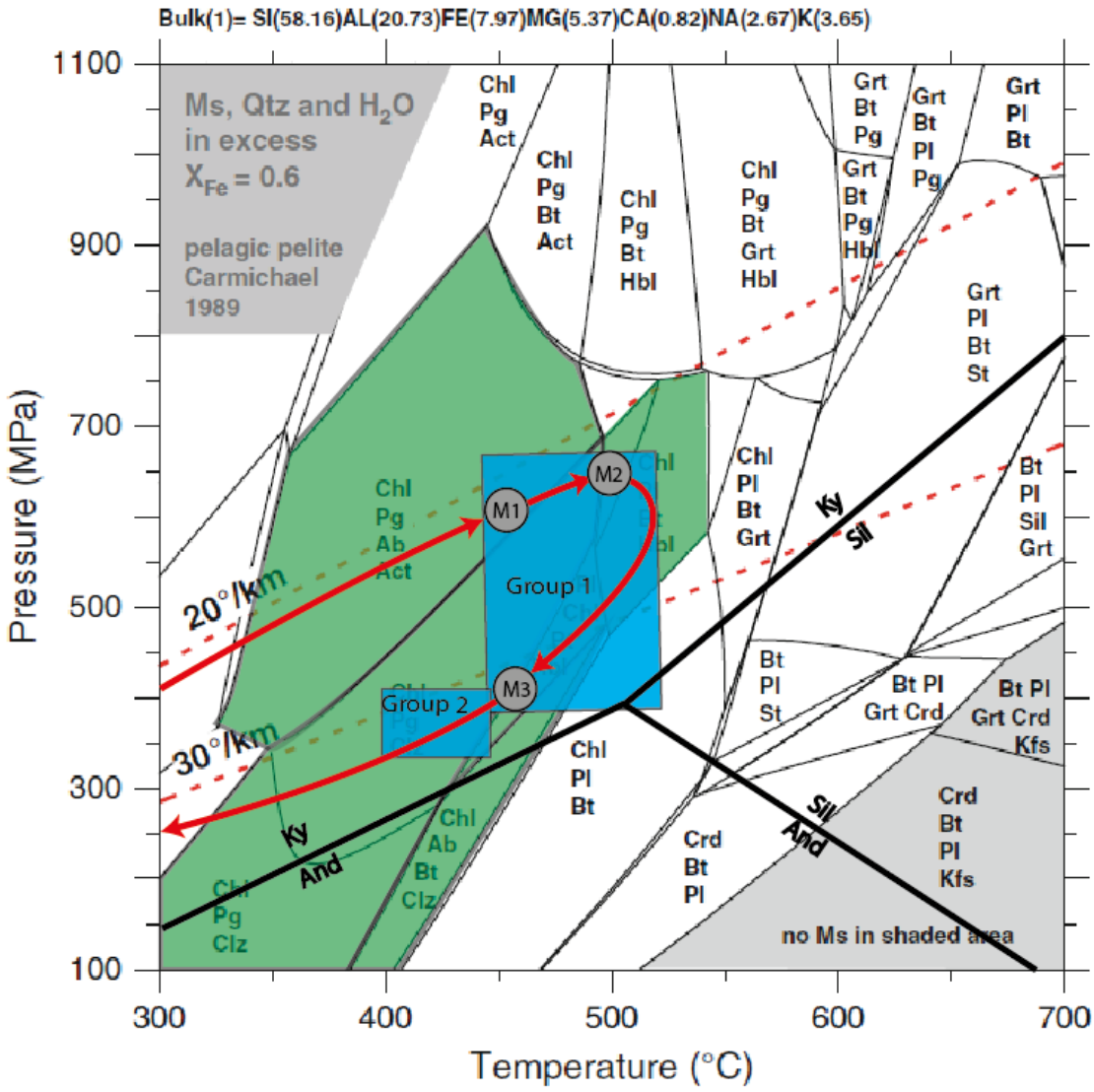

Figure 7.3 PT-path of the Köli pelites, modified after Bucher and Grapes (2011).

Köli nappe PT-paths correlation

The PT-path of the Köli country rock (fig 7.3) correlates well with the second part of the PT-path (i.e. after the first retrogradation) of the Aunere peridotite (fig 7.2). Peak metamorphism acquired for both rock types is upper greenschist facies and are of prograde nature. The mineral association in the peridotites does not provide good constrains on pressure, however the occurrence of albite in the country rocks limits peak metamorphism at <700 MPa. In addition, both rock types have calcite in their retrograde mineral assemblage (i.e. M4 in the Aunere peridotite and M3 in the country rock). Due to the similarities in PT-path and peak metamorphism the constrains on pressure for the country rock can be translated on to the peridotites. Namely, the peridotite bodies must have been incorporated into the country rock prior to their mutual burial and subsequent prograde metamorphism along a continent-continent metamorphic field gradient (of approximately 28C°/km). The peridotite bodies however also have a PT-history, marked by subsolidus equilibrium at subcrustal levels (protolith assemblage/M1), exhumation and serpentinization (M2) at

(sub)surface levels. There are discrepancies between the deformation phases experienced. D2 and D3 in the peridotite are prior to the peak metamorphic M3 phase, while group 1 deformation in the country rocks takes place during and after the peak metamorphic M2 phase. D3 is interpreted to correspond to the Group 1 deformation phases in the country rocks, as has earlier been described by Trouw (1973). From this thesis no conclusive arguments are provided to discriminate between D2 in the Aunere peridotite pre-dating or corresponding to group 1 deformation in the country rock. D2 can correspond to the emplacement of the Aunere into/onto un-metamorphosed marine sediments and therefore pre-date group 1 deformation in the country rocks or it can be related to the mutual burial and nappe stacking experienced by both rock types, and D2 in the Aunere corresponds to the group 1 deformations in the country rocks.
The Aunere peridotite has independently been exhumed to the surface prior to its incorporation in the marine sediments of the Köli. The Aunere is therefore of the obducted ophiolite type, however, a distinction cannot be made between the Penrose-type or the OCT-type ophiolite as mentioned in chapter 7.1.

7.2.2 Upper and lower Seve belt

Upper and lower Seve belt peridotites

Due to the many similarities between the upper and lower Seve belt and in order to prevent reiteration the belts are discussed together. Discrepancies between both belts will be clearly indicated.

Pre-Caledonian
Protolith assemblage, M1 (table 4.2), in both upper and lower Seve belt peridotites is chiefly olivine and chromite and the peridotites are therefore classified as belonging to the depleted dunite sub-type. In the upper Seve belt only a few M1 porphyroclast are recognized, due to the intense overprint experienced by the upper belt peridotites. However, the largest olivine crystal of the protolith assemblage is 500 µm, distinctively smaller than olivines in the Köli and lower Seve belt. The porphyroclast of olivine in peridotite of the Lower Seve belt are more abundant and reach sizes up to multiple centimeters, but are generally elongated (aspect ratio of 1:3-1:6). In addition, the M1 olivine minerals of the lower Seve belt show other signs of deformation such as undulatory extinction and dynamic recrystallization. These features could have developed during asthenosphere convectional motion or during crustal incorporation at high T. Clos et al. 2014 has presented dynamic recrystallization of olivine into a foam structure as the indicator for the incorporation into the country rock for orogenic peridotites in the central belt. However, in this thesis only one such microstructure was recognized (fig 4.5c-f). This single microstructural observation does not allow for any conclusive remarks regarding its origin. Future research is required in this field. PT-constrains are the same for both belts of the SNC. Pressure constrains are provided by the stability field of spinel (0.8-3.0 GPa). A more precise determination of PT-conditions is hindered by the absence of suitable geobarometric techniques. The protolith assemblage originated from the asthenosphere that gradually cooled down to temperatures <1200

C° (Baker et al., 1995) and equilibrated at temperatures possibly as low as 750-800 C° (i.e. the low T boundary of the Sp stability field) (fig 7.4) and becomes lithosphere.

Caledonian

M2-retrograde metamorphism

This first Caledonian metamorphic event in both belts of the SNC is the serpentinization of the protolith assemblage. Predominately M1 olivine is transformed into the serpentine sub-types chrysotile and antigorite, which are stable at conditions <250 C° and 250-600 C° respectively. The presence of both serpentine types indicate that the M2 metamorphic phase was active across the above mentioned two stability fields (fig 7.4). During M2 fluids were introduced into the system, which is requirement for the chemical transformation of olivine into serpentine (eq. 4.1). The peridotite significantly cooled between M1 and M2 and this was interpreted to be due to a reduction in depth. In order to achieve temperatures below 250 C°, the peridotites were positioned at depths at least shallower than 11 km, assuming a Barrovian regional metamorphism (Bucher-Nurminen, 1991).

M3-upper greenschist facies metamorphism.

The third metamorphic event (M3) in the upper and lower Seve belt peridotites is marked by the renewed growth of olivine. Olivine enters the stability assemblage in upper greenschist facies (>400 C°) (table 4.2). Apart from the lower limit of temperature, olivine is a very stable mineral. An upper T limit can be determined by the absence of orthopyroxene (<600 C° at P<2.0 GPa) tremolite and talc (<500 C° at P<1.0 GPa) (figure 7.4). Constrains on pressure are absent, however assuming a Barrovian regional metamorphic field gradient during the Scandian (Bucher-Nurminen, 1991) a pressure estimate of 0.5-0.6 GPa can be established.

M4-peak metamorphism

This phase is the highest grade achieved by the peridotites of the upper and lower Seve belts. The stability of talc, tremolite and olivine reveals a prograde metamorphism under middle amphibolite facies conditions (>500 C°). The absence of orthopyroxene limits the upper temperature boundary at <670 C°. The stability of talc is limited to pressures below 1.7 GPa. This is in correspondence with the assumed Barrovian field gradient (Bucher-Nurminen, 1991), which sets the upper pressure limit at ~0.7 GPa under T-conditions <650-670 C°.

M5 -retrograde metamorphism

The final metamorphic phase (M5) is renewed phase of retrogradation which occurred at the end of the Caledonian metamorphism. During M5 minerals formed during the Caledonian orogeny and remnants of the protolith assemblage are serpentinized to antigorite (between 250 C° and 600 C°). In order to achieve this serpentinization a drop in temperature and corresponding pressure to conditions comparable to M2 had to be realized plus the addition of water to the system.
Moreover, the growth of calcite, some of it located in veins, is evidence this water introduction occurred under brittle conditions.

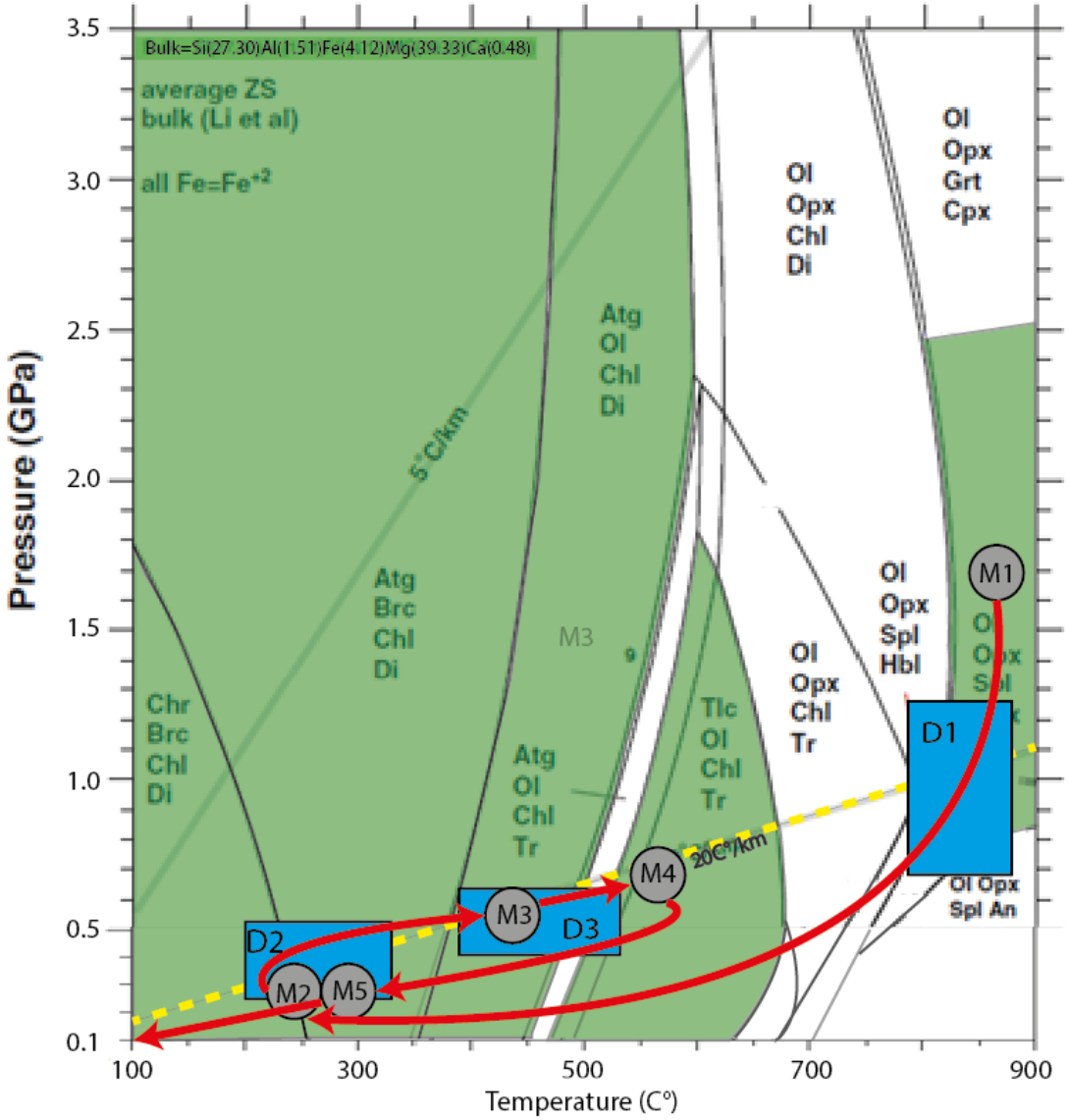

Figure 7.4 Interpreted PT-path of the upper Seve belt peridotites. Background petrogenetic grade is modified after Bucher and Grapes (2011). BRC (upper left side) taken from Li et al. (2004).

Upper and lower Seve belt country rocks

M1

The first mineral assemblage of the pelitic country rocks of the upper and lower Seve belts consists of quartz, muscovite, chlorite, biotite and epidote (table 5.2). Quartz and muscovite are available in excess and do not provide constrains on the PT-conditions. From figure 7.5 it can be seen that chlorite has a large stability field but also limits the metamorphic grade to temperatures <500-600 C°. Moreover, the occurrence of biotite requires temperatures in excess of 400 C°. Pressure constrains are provided by epidote (Clz), which is stabile until 650 MPa. Biotite and epidote, however, are not stable together apart from a very narrow band at low pressure/ medium

temperatures. According to the author the most likely metamorphic grade occurred across the epidote-out biotite-in boundary along the ~22 C°/km geotherm (Bucher-Nurminen, 1991)(fig 7.5).

M2

The second mineral assemblage is marked by the introduction of Ca-plagioclase and the removal of epidote (fig 7.5). Ca-plagioclase is stable at temperatures in excess of 450 C° and the absence of garnet in this PT-domain, restricts the temperature below 550 C°. Pressure is constrained at <700 MPa by the plagioclase-out boundary.

M3

The third mineral assemblage M3) represents the peak metamorphic grade experienced by the upper and lower Seve belt country rocks. It is marked by the introduction of garnet and thereby PT-conditions have to be in excess of 550 C° and 300 MPa (fig 7.5). Garnet puts no constrain on the upper temperature and pressure limit of the stability field. Peak metamorphism occurred at low to middle Amphibolite facies. In the lower Seve belt the presence of kyanite provides a lower pressure limit at 450 MPa, thereby excluding high geothermal contact metamorphism.

M4

The last metamorphic event (M4) is marked by a phase of retrogradation. The M4 mineral assemblage corresponds with M2 and constrains on the PT-conditions are therefore identical.

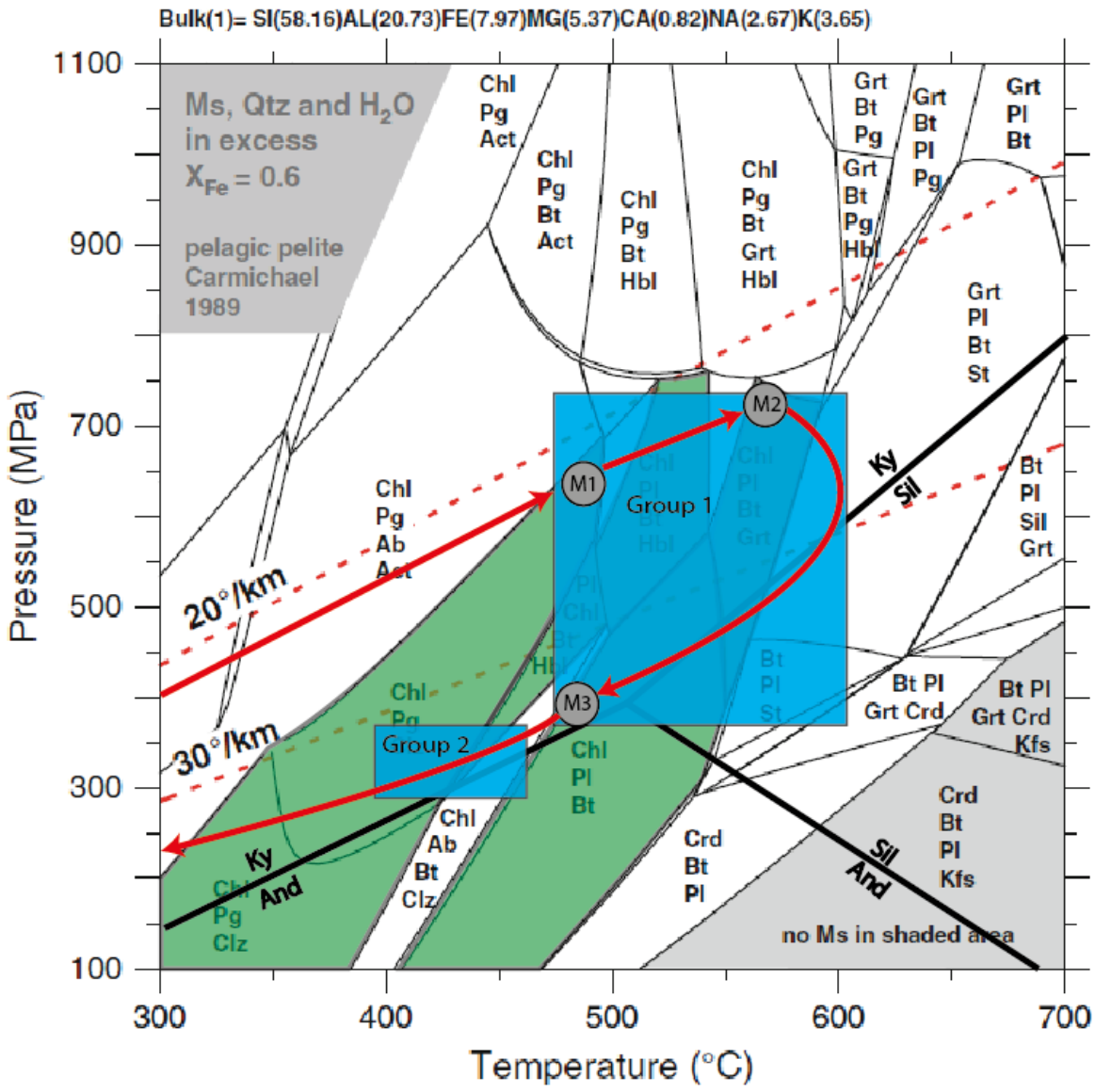

Figure 7.5 PT-path of the upper and lower Seve belt pelites, modified after Bucher and Grapes (2011).

Upper and lower Seve belts PT-paths correlation

The PT-paths of the upper and lower Seve belts country rock and associated orogenic peridotites overlap near the surface. Thereafter they follow a similar PT-trajectory and both paths achieve peak metamorphism at middle amphibolite facies conditions. These agreements argue strongly for incorporation to have occurred prior to their mutual burial. The peridotite mineral association does not provide constrains on the pressure range experienced, however the deduced metamorphic field gradient of the country rock, can be translated to the peridotites. The peridotites have experienced a protolith (M1) history which was overprinted by a retrogradational path (fig 7.4). The M1 assemblage is interpreted to sub-cratonic crust and exhumation to sub-surface levels was accompanied by serpentinization. There are discrepancies between the deformation phases experienced. D3 in the peridotites coincides with the group 1 deformation in the pelites, albeit D3

is less extensive. This is likely due to the high resistance to deformation of peridotites compared to pelites. D2 can either be a specific deformation phase related to the emplacement of the peridotites into un-metamorphosed country rock or be caused by the mutual burial experienced by both type of rocks. In the prior case the D2 in the peridotites will pre-date group 1 deformation in the country rock, whereas in the latter case D2 in the peridotites will correspond to the group 1 deformations in the country rock. This thesis does not provide arguments on which to discriminate between both hypotheses.

The incorporation of peridotites into almost un-metamorphosed marine sediments in addition to the sub-cratonic provenance of the peridotite, as discussed in chapter 7.1, requires the upper belt peridotite to be of the obducted OCT-type ophiolites.

7.3 Geodynamical interpretations

7.3.1 Geodynamical model

In this chapter we propose a geodynamical interpretation which could have led to the development of the Scandinavian Caledonides, based on data from the Marsfjällen area. Structural units (e.g. belts, nappes, allochthons and oceanic or continental plates) are indicated, however for clarity reasons the concomitant ultramafic bodies are not separately indicated after incorporation has occurred. Due to the vast size of the Scandinavian Caledonides these geodynamical interpretations are not necessarily freely translatable to other regions for lateral variations are likely to have influenced the occurrence and/or extent of an event. This interpretation should be seen as a large scale tectonic development based on the regional geology supplemented by forgoing research and the geodynamical models as presented in chapter 2.5. In our research area three distinct orogenic events have been recognized, namely the Finnmarkian event (500Ma), the Jämtlandian event (454Ma) and the Scandian event (420Ma). Orogenic phases such as the Taconian (Roberts, 2003) and Trondheimian (Roberts, 2003; Hacker & Gans, 2005) are not incorporated in the models, because there is no evidence of these phases recognized in the investigated area. It is not suggested these phases did not occur in the Scandinavian Caledonides, rather the lack of expression in the Marsfjällen area suggest it did not play any significant role in the development of the local geology. Furthermore, for comprehensibility reasons the models show a simplified east-west conversion, the anti-clockwise rotation of Baltica as described by Torsvik & Rehnström (2001) is not incorporated.

Pre-Caledonian configuration:

Before the conversion of Laurentia and Baltica began an extensive diversional event took place. Supercontinent Rhodinia broke apart and at the end of this extensional process the Iapetus Ocean was formed. This phase has had a large impact on the geometry on the Baltic lithosphere. Unaffected cratonic lithosphere has an approximate thickness of 200km, spatially removed from the epicenter of the rifting the thickness was retained, as was the case for the continents of Baltica and Laurentia. Rifting of the oceanic crust is often associated with the formation of new oceanic crust, as relative hot asthenosphere decompresses, melts and recrystallizes in the form of basic rocks and underlying oceanic lithosphere. The lithosphere below cratons is very thick and relatively cold, this holds that extension can continue for a prolonged period of time without melt derived from the asthenosphere reaching the surface (i.e. oceanic crust formation) or that melting occurs by decompression of the cold SCLM. Alternatively this led to the exhumation of the ultramafic SCLM to the surface and created windows of mantle lithosphere (Andersen et al., 2012), this process created the ocean-continent transition (OCT) c.q. passive continental margin. Progressive extension will inevitably have led to asthenosphere rise and the formation of oceanic crust (i.e. Iapetus Ocean). Notwithstanding, the extensively thinned margins of the continents and failed rift zones will retain their Archean ultramafic lithosphere at shallow or surface levels. The pre-Caledonian configuration (fig 7.8) from east to west includes: the thick Baltic craton (i.e. crust and mantle lithosphere) gradually thinning westward, followed by the OCT where the crustal lithosphere was removed by low angle extensional faults exposing the lithospheric mantle. These

windows of ultramafic lithospheric mantle are covered by pre-Caledonian marine sediments and occasional vestiges of continental crust in the form of micro-continents. Further west the extension has led to the formation of new oceanic lithosphere, the Iapetus Ocean. Proceeding even further west towards the Laurentia continent would result in the same geometry as on the Baltic side. The transition from OCT into thinned continental lithosphere gradually thickening towards unaltered cratonic lithosphere. The extensive regime transformed into a compressive regime, which initiated intra-oceanic subduction and island arc formation (fig 7.9)

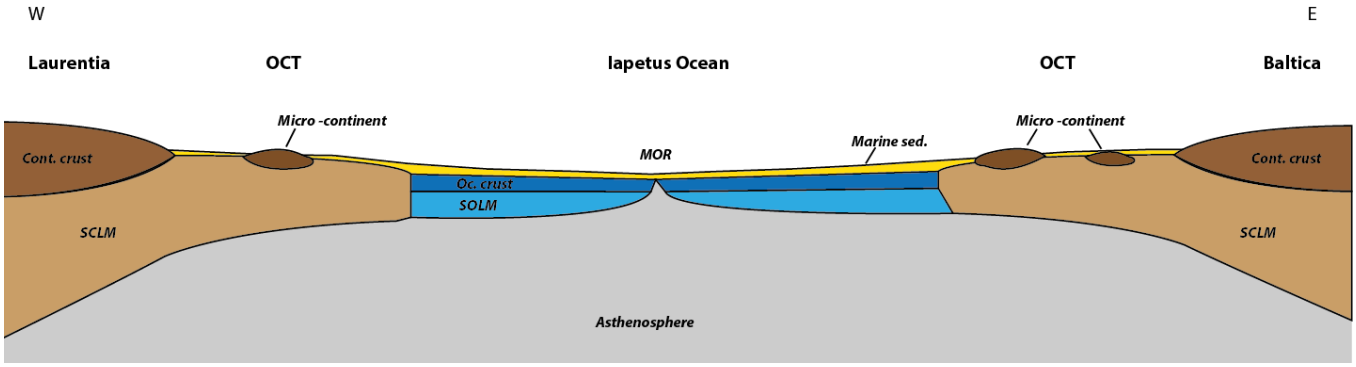

Figure 7.8 Pre-Caledonian configuration after the diversional motion of Baltica and Laurentia ceased, 560 Ma (Cocks & Torsvik). The diversional movement of Laurentia and Baltica resulted in hyperextension of the continental crust resulting in SCLM being exhumed to the surface. Locally vestiges of the continental crust are located in OCT. The OCT and oceanic crust are covered with marine sediments.

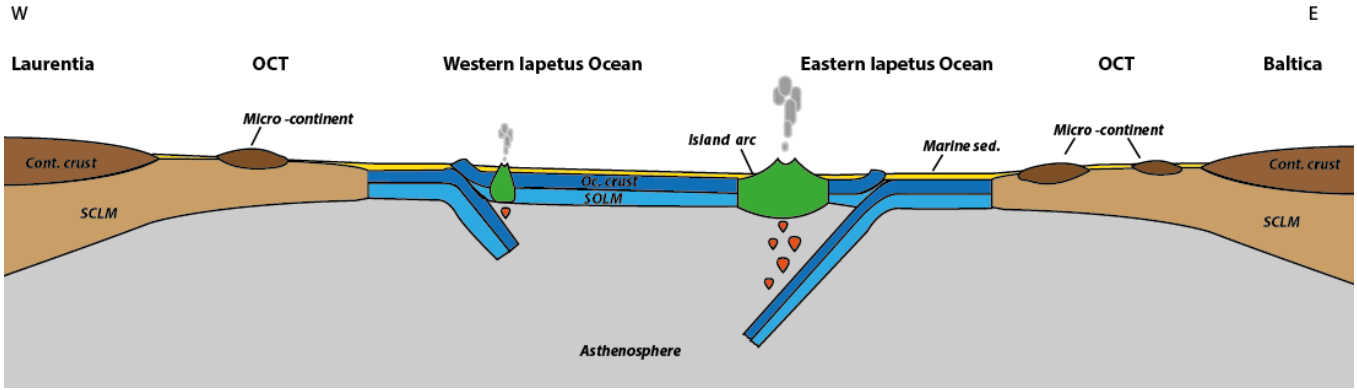

Figure 7.9 Pre-Caledonian configuration during initial closure of the Iapetus Ocean (560-500 Ma). Closure progresses along inter-oceanic subduction zones consuming oceanic crust and forming island arc.

Stage 1

The first stage of the Scandinavian Caledonides, the Finnmarkian event (500 Ma) affects the hyper-extended OCT. As the intra-oceanic subduction progresses the oceanic crust in the Eastern Iapetus becomes fully consumed. The westward dipping subduction zone will have reached the OCT which is initially pulled beneath the oceanic plate by the foregoing subducting plate. However, the OCT will have experienced extensive faulting during the divergent motion of Baltica and Laurentia, which makes them inherently structurally incoherent. As the hyper extended OCT subducts beneath the oceanic plate old rifting faults are reactivated and becomes imbricated, similar to the process described by Andréasson (1994) for the Artic Scandinavian Caledonides. The imbricated OCT will form an accretionary wedge in which the ultramafic SCLM, possible vestiges of continental crust and marine sediments are incorporated in a tectonic mélange which will later form the middle Allochthon. It is in this process in which the ultramafic bodies of OCT-type ophiolite found in the upper and lower Seve belts are incorporated in the country rock and jointly metamorphosed to amphibolite facies (upper Seve belt (491.2 Ma ± 22 Ma (Gademan, 2011)) and the lower belt (age undetermined). The ongoing convergent motion of Baltica and Laurentia has at least continued along this subduction zone below the Middle Allochthon prior to the Jämtlandian.

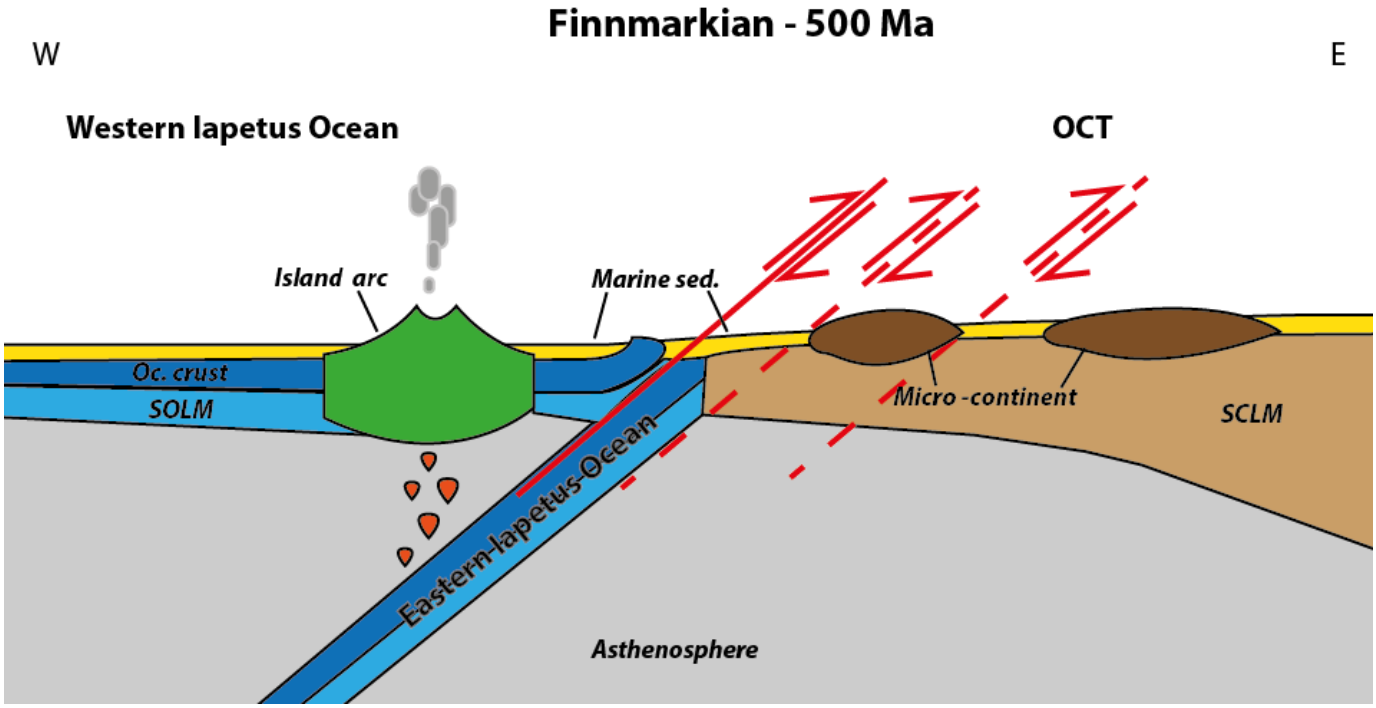

Figure 7.10 Finnmarkian event. Subduction zone translation due to fragmentation of OCT. Total consummation of oceanic crust leads to the subduction of OCT. Due to low internal integrity fragmentation occurs and the subduction zone is translated eastward.

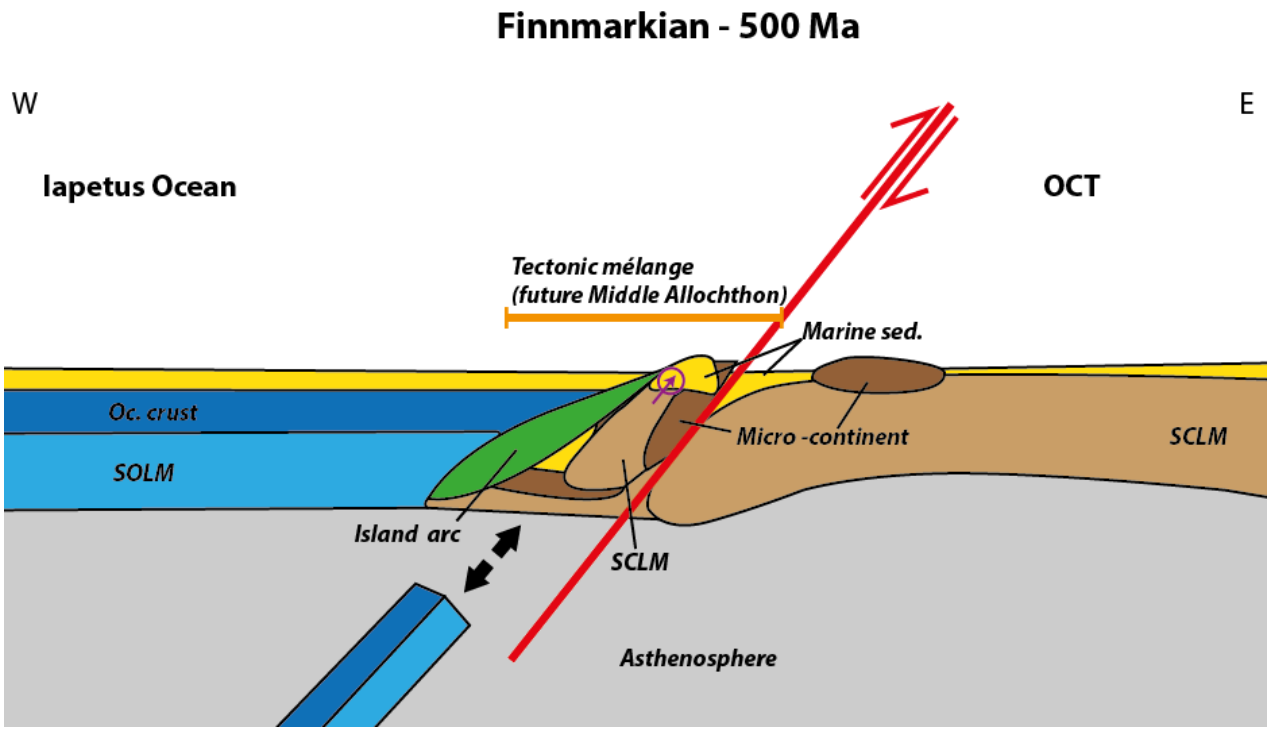

Figure 7.11 Finnmarkian event. Fragmentation of OCT related lithosphere. The fragmented OCT which includes SCLM, marine sediments and possibly vestiges of continental crust form a tectonic mélange, which will later form the Middle Allochthon (including upper and lower Seve belts). During this fragmentation the ultramafic rocks from the SCLM are incorporated in country rock, as is indicated by the purple arrow.

Stage 2

The second stage is the Jämtlandian event. Breuckner et al. (2004) determined the age of the incorporation of the Friningen Garnet Peridotite (FGP) into the middle belt to be ~455-450 Ma. The FGP is believed to be a mantle wedge peridotite and the peak metamorphism of the ultramafic body is found to be coeval with that of the surrounding country rock (Gilio et al., 2015). In addition, U-Pb age dating on zircons from the middle belt migmatites, performed by Root & Curfu (2011), has yielded a metamorphic phase aged at 445 Ma. The rocks of the middle belt are metamorphosed to granulite and eclogite facies (Zwart, 1974; Williams & Zwart, 1977; v. Roermund, 1985 and Janák et al., 2013). The Jämtlandian affect involves the subduction of a vestige of continental crust in the OCT (i.e. a micro continent). The lithosphere of the subducting slab gets increasingly thicker and is less deformed during the pre-Cambrian rifting event and therefore retained more internal integrity. The dense SCLM will subduct below the future middle allochthon and westward lying oceanic crust (fig 7.12). This process will pull along with it the micro-continent. The coherent subducting slab reached HP conditions in which mantle wedge peridotites are incorporated from the overlying SCLM into the country rock of the subducting plate. Eduction of the UHP terrane (future middle Seve belt) has positioned it in between the lower- and upper Seve belt. Eduction of the HP terrane could have occurred in multiple ways and in this model we propose two options. The first option is by slab-detachment of the foregoing negatively

buoyant crust and eduction of the positively buoyant ensuing crust, after the dunk-tectonics model of Breuckner & v. Roermund (2004). This would require a buoyancy difference which, in this geological setting, is not probable since the overriding plate is of similar composition to the underriding plate. The second option, and in view of the author most likely, is it has educted during a stage of extension, which according to Hacker & Gans (2005), occurred in the wake of the middle Seve belt peak metamorphism (454-432Ma). It is likely this extensional period inverted the subductional motion into an educational motion. In order for this to occur, however, delamination or detachment from the ensuing slab is required (fig 7.13).

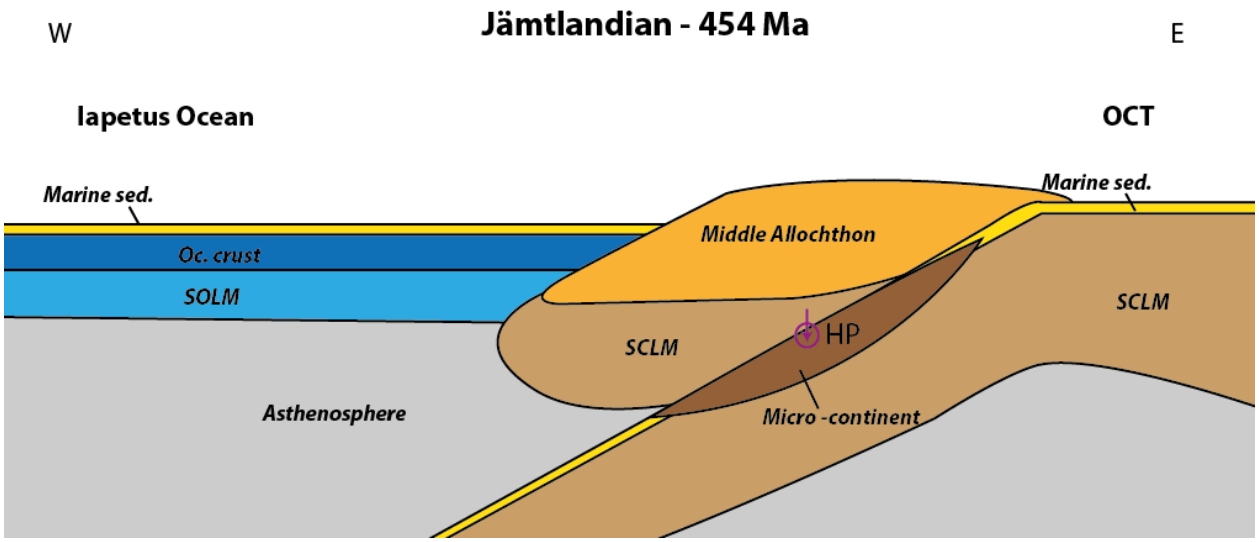

Figure 7.12 The Jämtlandian event. Ongoing conversions leads to deep subduction of the OCT and HP-metamorphism. Mantle wedge peridotites from the overriding plate become incorporated in the country subducting slab, as is indicated by the purple arrow.

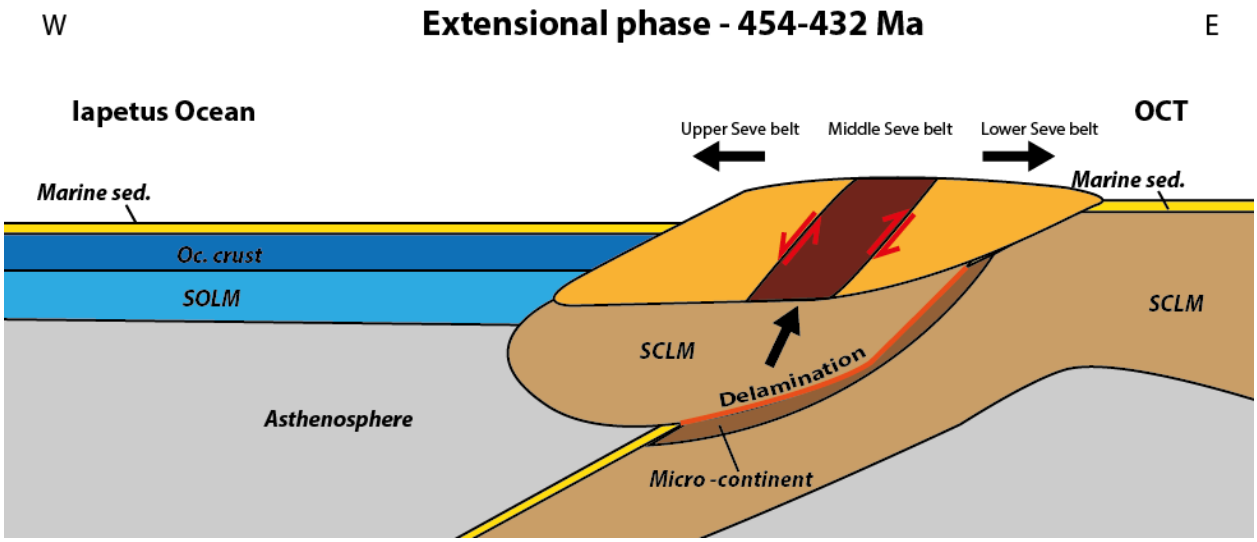

Figure 7.13 The extensional phase. During extension the part of the HP-terrane, including its ultramafic cargo, delaminates and is being wedged in between the nappes of the Middle Allochthon as it is educted.

Stage 3

The third and final stage of the Scandinavian Caledonides, the Scandian event, involves the collision of the continents Laurentia and Baltica. The Iapetus ocean west of the Middle Allochthon is fully closed leading to the obduction of oceanic crust (future Köli). This closure leads to the emplacement of ultramafic bodies as the Penrose-type ophiolites now recognized in the Köli. The continent-continent collision leads to westward dipping nappe stacking resulting in the geometry of the Scandinavian Caledonides we see today.

The uppermost allochthon is thrusted upon the upper allochthon (Köli), the latter being metamorphosed to greenschist facies at 425 ±5 Ma (Reymer, 1979). The Baltic continent continues to subduct beneath Laurentia leading to formation of UPH terranes, such as the WGR (415-397Ma (Terry et al. 2000)).

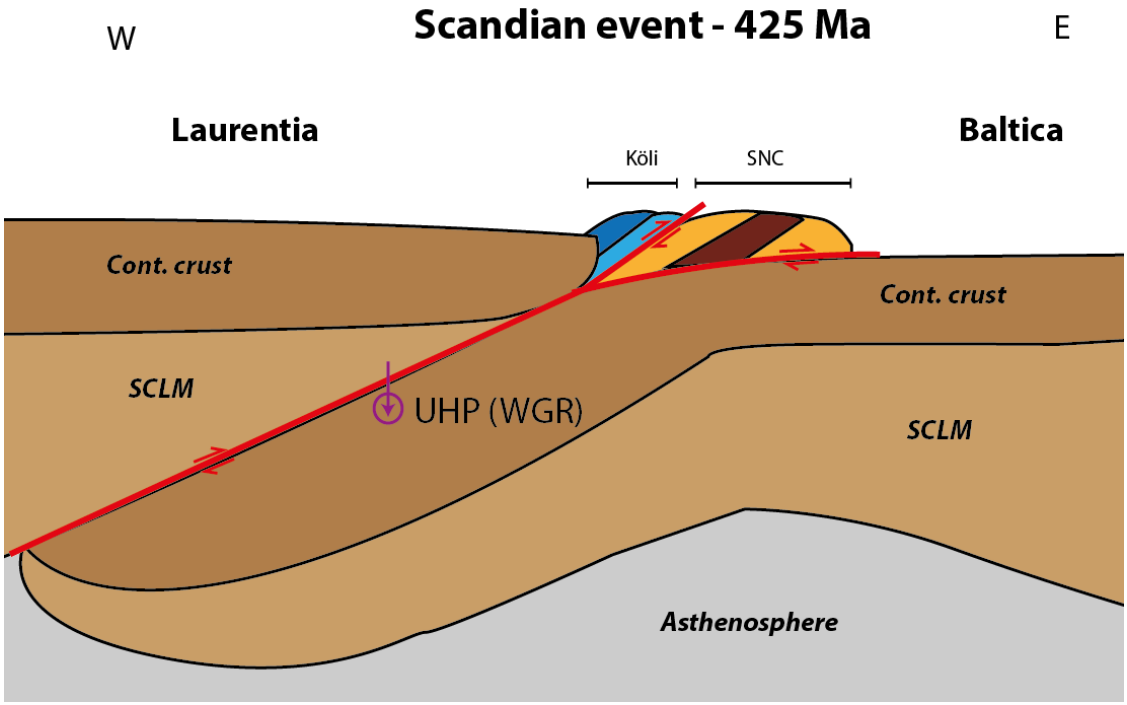

Figure 7.14 The Scandian event. The final continent-continent collision leads to the obduction of the Köli on nappe stacking of the Allochthons. The Baltic margin subducts beneath Laurentia resulting in UHP metamorphism during which MWP are incorporated, as is indicated by the purple arrow. This UHP-terrane is now recognized as the WGR.

7.3.2 Implications of the geodynamical interpretation

The geodynamical model as presented above has specific implications. This model deals with the upper and lower Seve belts as part of the Baltic OCT, which is later intruded by the delaminated crustal terranes of the middle Seve belt that has been subducted beneath the Middle Allochthon during the Jämtlandian. The age of metamorphism between the upper and lower belt should therefore correspond. Currently this is not possible to ascertain, since no geochronological study into the age of the lower belt has yet been performed. Crustal incorporation of the orogenic peridotites of the upper and lower belts is interpreted to be caused by the obduction of OCT-type ophiolites. Following Trouw (1971), Zachariassion (1973) and Bucher-Nurminnen (1991) the Köli represents dismembered obducted oceanic lithosphere, here interpreted to be accreted during the Scandian event. Hence, the ultramafic rocks which are incorporated in the Köli nappe are (dismembered) Penrose-type ophiolitic peridotites. Other studies have shown the incorporation of MWP in the middle Seve belt (Clos et al., 2014; Gilio et al., 2015), signifying there are at least three distinct types of orogenic peridotites recognized in this part of the Scandinavian Caledonides. The tectonostratigraphic sequence as formed by the nappe stacking deviates from the pre-Caledonian lateral distribution. In general the nappes from top to bottom were positioned from west to east in the pre-Caledonian configuration. However, the exception is formed by the middle belt which is currently positioned above the lower belt despite of its original position to the east. This model also requires an extensive OCT between Baltica and the Iapetus Ocean, many other studies such as the ones discussed in this thesis (Roberts, 2003; Brueckner & van Roermund, 2004; Hacker & Gans, 2005) the OCT is dealt with as oceanic crust. It is possible that the formation of oceanic crust has been successful at more than one location, meaning OCT could have alternated with oceanic crust. The author prefers the model of one mid oceanic ridge for comprehensibility reasons and the lack of evidence indicating otherwise.

8) Conclusion

I) This research endorses that the upper Seve belt and lower Seve belt country rock and peridotites are metamorphosed under low/middle amphibolite facies (Trouw 1973, Bierman 1979, Calon 1979, Zwart 1974, Williams & Zwart 1977, van Roermund & Bakker 1983). Additionally, the Köli nappe country rock and peridotites are metamorphosed under greenschist facies in accordance with foregoing studies (Zachrisson, 1969; Trouw, 1973; Zwart, 1974; Gee et al., 2010).

II) EMP geochemical analyses performed on peridotites indicate that the peridotites of the lower and the upper Seve belts have a sub-cratonic lithospheric mantle provenance. Similar results from peridotites of the Köli are missing due to the absence of the olivine protolith assemblage on which analyses can be performed.

III) The peridotites of the Köli, the upper belt and the lower belt have experienced a period of exhumation and are thereafter incorporated/emplaced in/on to the country rock at (sub)surface level.

IV) After incorporation of the peridotites into the country rocks, all units have a PT-path that overlaps and is characterized by prograde Barrovian metamorphism. The Köli, the upper and the lower Seve belts all follow the continent-continent collision metamorphic field gradient.

V) It is proposed that the upper belt and the lower belt have experienced a joint history prior to their separation due to the educting central belt. This implies that peak metamorphism in the lower Seve belt occurred around 500 Ma.

VI) The peridotites in the upper and lower Seve belt are of the OCT-type ophiolite, based on their incorporation in the country rock at the surface and their sub-cratonic provenance type mineral composition.

9) Future work

I) Geochemical analyses should be performed on the Köli peridotite protolith assemblage. In order to determine its provenance based on the spinel Cr# and olivine Mg# array (Arai, 1994).

II) Age determination in the country rock of the lower belt in order to the determine the timing of peak metamorphism. Information on this matter can either support or provide arguments against the geodynamical model as presented in this thesis.

III) An in-depth study into determining the age of potential earlier metamorphism in the country rock of the upper and lower belt. This could provide insight into whether the pre-Caledonian crystalline basement is also involved or solely the un-metamorphosed marine sediments and mantle lithosphere.

IV) A drilling program into subsurface of the Köli nappe, in order to search for the missing segments of the Penrose-type ophiolite.

V) A drilling program into subsurface of the central belt. The presence of a crystalline basement can provide insight into its provenance (i.e. continental v. oceanic).

10) Acknowledgements

I want to give my special thanks to the supervisor for this MSc thesis, Dr. H.L.M. van Roermund. His passion for the subject motivated me enormously to do my utmost best. He always made time to help when problems arose or provide additional references on his own accord and for this I am very grateful. I want to thank Mrs. M.J.C. Bouten for her technical assistance during the lab sessions on the EMP. Without her technical knowhow and willingness to do extra work, acquiring the results needed for this thesis would be very difficult if not impossible. Finally I would like to thank my mother for providing the financial support needed in order to carry out the fieldwork to the Marsfjällen area, Central Sweden, and the unconditional emotional and mental support throughout my studying career as a whole.

References

Andersen, T. B., Jamtveit, B., Dewey, J. F., & Swensson, E. (1991). Subduction and eduction of continental crust: major mechanisms during continent-continent collision and orogenic extensional collapse, a model based on the south Norwegian Caledonides. *Terra Nova*, *3*(3), 303-310.

Andersen, T. B., Corfu, F., Labrousse, L., & Osmundsen, P. T. (2012). Evidence for hyperextension along the pre-Caledonian margin of Baltica. *Journal of the Geological Society*, *169*(5), 601-612.

Andréasson, P. G. (1994). The Baltoscandian margin in Neoproterozoic-early Palaeozoic times. Some constraints on terrane derivation and accretion in the Arctic Scandinavian Caledonides. *Tectonophysics*, *231*(1), 1-32.

Andréasson, P. G., & Albrecht, L. (1995). Derivation of 500 Ma eclogites from the passive margin of Baltica and a note on the tectonometamorphic heterogeneity of eclogite-bearing crust. *Geological Magazine*, *132*(06), 729-738.

Arai, S. (1990). What kind of magmas could be equilibrated with ophiolitic peridotites. In *Symp. Trodos* (Vol. 87, pp. 557-566).

Arai, S. (1994). Characterization of spinel peridotites by olivine-spinel compositional relationships: review and interpretation. *Chemical geology*,*113*(3), 191-204.

Austrheim, H., & Prestvik, T. (2008). Rodingitization and hydration of the oceanic lithosphere as developed in the Leka ophiolite, north–central Norway.*Lithos*, *104*(1), 177-198.

Baker, M. B., Hirschmann, M. M., Ghiorso, M. S., & Stolper, E. M. (1995). Compositions of near-solidus peridotite melts from experiments and thermodynamic calculations. Nature, 375(6529), 308-311.

Barnes, S. J., & Roeder, P. L. (2001). The range of spinel compositions in terrestrial mafic and ultramafic rocks. *Journal of Petrology*, *42*(12), 2279-2302.

Biermann, C. (1979). Investigations into the development of microstructures in amphibole-bearing rocks from the Seve Köli nappe complex *(Doctoral dissertation).*

von Blanckenburg, F., & Davies, J. H. (1995). Slab breakoff: a model for syncollisional magmatism and tectonics in the Alps. *Tectonics*, *14*(1), 120-131.

Boillot, G., Recq, M., Winterer, E. L., Meyer, A. W., Applegate, J., Baltuck, M., ... & Williamson, M. (1987). Tectonic denudation of the upper mantle along passive margins: a model based on drilling results (ODP leg 103, western Galicia margin, Spain). *Tectonophysics*, *132*(4), 335-342.

Boyd, F. R., & Nixon, P. H. (1975). Origins of the ultramafic nodules from some kimberlites of northern Lesotho and the Monastery Mine, South Africa. *Physics and Chemistry of the Earth*, *9*, 431-454.
Brueckner, H. K. (1998). Sinking intrusion model for the emplacement of garnet-bearing peridotites into continent collision orogens. *Geology*, *26*(7), 631-634.

Brey, G. P., & Köhler, T. (1990). Geothermobarometry in four-phase lherzolites II. New thermobarometers, and practical assessment of existing thermobarometers. *Journal of Petrology*, *31*(6), 1353-1378.

Brueckner, H. K., & Medaris, L. G. (2000). A general model for the intrusion and evolution of 'mantle'garnet peridotites in high-pressure and ultra-high-pressure metamorphic terranes. *Journal of Metamorphic Geology*, *18*(2), 123-133.

Brueckner, H. K., & van Roermund, H. L. (2004). Dunk tectonics: a multiple subduction/eduction model for the evolution of the Scandinavian Caledonides.*Tectonics*, *23*(2).

Brueckner, H. K., & Van Roermund, H. L. (2007). Concurrent HP metamorphism on both margins of Iapetus: Ordovician ages for eclogites and garnet pyroxenites from the Seve Nappe Complex, Swedish Caledonides.*Journal of the Geological Society*, *164*(1), 117-128.

Brueckner, H. K., Van Roermund, H. L., & Pearson, N. J. (2004). An Archean (?) to Paleozoic evolution for a garnet peridotite lens with sub-Baltic Shield affinity within the Seve Nappe Complex of Jämtland, Sweden, Central Scandinavian Caledonides. *Journal of Petrology*, *45*(2), 415-437.

Brun, J. P., & Beslier, M. O. (1996). Mantle exhumation at passive margins. *Earth and Planetary Science Letters*, *142*(1), 161-173.

Bucher-Nurminen, K. (1991). Mantle fragments in the Scandinavian Caledonides. *Tectonophysics*, *190*(2), 173-192.

Bucher, K. & Grapes, R. (2011) *Petrogenisis of Metamorphic Rocks.* DOI 10.1007/978-3-540-74169-5_5

Burkhard, D. J. (1993). Accessory chromium spinels: their coexistence and alteration in serpentinites. *Geochimica et Cosmochimica Acta*, *57*(6), 1297-1306.

Calon, T. J., (1979). A study of the Alpine-type peridotites in the Seve-Köli nappe complex central Swedish caledonides with special reference to the Kittelfjäll peridotite. *(Doctoral dissertation)*

Carmichael, R. S. (1989). *Practical handbook of physical properties of rocks and minerals*. CRC press.

Chew, D. M., & van Staal, C. R. (2014). The Ocean–Continent Transition Zones Along the Appalachian–Caledonian Margin of Laurentia: Examples of Large-Scale Hyperextension During the Opening of the Iapetus Ocean. *Geoscience Canada*, *41*(2), 165-185.

Chopin, C. (1984). Coesite and pure pyrope in high-grade blueschists of the Western Alps: a first record and some consequences. *Contributions to Mineralogy and Petrology*, *86*(2), 107-118.

Clos, F., Gilio, M., & van Roermund, H. L. (2014). Fragments of deeper parts of the hanging wall mantle preserved as orogenic peridotites in the central belt of the Seve Nappe Complex, Sweden. *Lithos*, *192*, 8-20.

Cocks, L. R. M., & Torsvik, T. H. (2002). Earth geography from 500 to 400 million years ago: a faunal and palaeomagnetic review. *Journal of the Geological Society*, *159*(6), 631-644.

Cocks, L. R. M., & Torsvik, T. H. (2005). Baltica from the late Precambrian to mid-Palaeozoic times: the gain and loss of a terrane's identity. *Earth-Science Reviews*, *72*(1), 39-66.

Coleman, R. G. (1971). Plate tectonic emplacement of upper mantle peridotites along continental edges. *Journal of Geophysical Research*, *76*(5), 1212-1222.

Coleman, R. G. (1977). *Ophiolites* (p. 229). Berlin: Springer.

Corfu, F., Ravna, E. J. K., & Kullerud, K. (2003). A Late Ordovician U–Pb age for the Tromsø Nappe eclogites, uppermost allochthon of the Scandinavian Caledonides. *Contributions to Mineralogy and Petrology*, *145*(4), 502-513.

Cuthbert, S. J., & Carswell, D. A. (1990). Formation and exhumation of medium-temperature eclogites in the Scandinavian Caledonides. *Eclogite facies rocks*, 180-203.

Dewey, J. F. (1976). Ophiolite obduction. *Tectonophysics*, *31*(1), 93-120.

Dobrzhinetskaya, L. F., Eide, E. A., Larsen, R. B., Sturt, B. A., Trønnes, R. G., Smith, D. C., ... & Posukhova, T. V. (1995). Microdiamond in high-grade metamorphic rocks of the Western Gneiss region, Norway. *Geology*, *23*(7), 597-600.

Du Rietz, T. (1935). Peridotites, serpentines, and soapstones of Northern Sweden, with special reference to some occurrences in Northern Jämtland. *Geol. Fören. Stock. För. 57*, 133-260

Du Rietz, T. (1936). Något om de stratigrafiska förhållandena inom Frostvikens köli-skiffrar. *GFF*, *58*(3), 425-438.

Eide, E. A., & Lardeaux, J. M. (2002). A relict blueschist in meta-ophiolite from the central Norwegian Caledonides—discovery and consequences. *Lithos*,*60*(1), 1-19.

Ernst, W. G., Maruyama, S., & Wallis, S. (1997). Buoyancy-driven, rapid exhumation of ultrahigh-pressure metamorphosed continental crust. *Proceedings of the National Academy of Sciences*, *94*(18), 9532-9537.

Foucher, J. P., Le Pichon, X., Sibuet, J. C., Roberts, D. G., Chenet, P. Y., Bally, A. W., ... & Turcotte, D. L. (1982). The Ocean--Continent Transition in the Uniform Lithospheric Stretching Model: Role of Partial Melting in the Mantle [and Discussion]. *Philosophical Transactions of the Royal Society of London. Series A, Mathematical and Physical Sciences*, *305*(1489), 27-43.

Froitzheim, N., & Manatschal, G. (1996). Kinematics of Jurassic rifting, mantle exhumation, and passive-margin formation in the Austroalpine and Penninic nappes (eastern Switzerland). *Geological Society of America Bulletin*, *108*(9), 1120-1133.

Gademan, M. (2011) Finnmarkian Monazite EMP ages in the Central belt of the Seve Nappe, north Jämtland/south Västerbotten, Sweden. *Unpublished master's thesis*

Gale, G. H., & Roberts, D. (1974). Trace element geochemistry of Norwegian Lower Palaeozoic basic volcanics and its tectonic implications. *Earth and Planetary Science Letters*, *22*(4), 380-390.

Gayer, R. A., Rice, A. H. N., Roberts, D., Townsend, C., & Welbon, A. (1987). Restoration of the Caledonian Baltoscandian margin from balanced cross-sections: the problem of excess continental crust. *Transactions of the Royal Society of Edinburgh: Earth Sciences*, *78*(03), 197-217.

Gee, D. G. (1975). A tectonic model for the central part of the Scandinavian Caledonides. *American Journal of Science*, *275*, 468-515.

Gee, D. G. (1987). Early Caledonian tectonothermal activity in the Scandes—the Finnmarkian and Trondheimian episodes. *GFF*, *109*(4), 343-345.

Gee, D. G., Fossen, H., Henriksen, N., & Higgins, A. K. (2008). From the early Paleozoic platforms of Baltica and Laurentia to the Caledonide Orogen of Scandinavia and Greenland. *Episodes*, *31*(1), 44.

Gee, D. G., Janák, M., Majka, J., Robinson, P., & van Roermund, H. (2013). Subduction along and within the Baltoscandian margin during closing of the Iapetus Ocean and Baltica-Laurentia collision. Lithosphere, 5(2), 169-178.

Gee, D. G., Juhlin, C., Pascal, C., & Robinson, P. (2010). Collisional orogeny in the Scandinavian Caledonides (COSC). *GFF*, *132*(1), 29-44.

Gee, D. G., & Sturt, B. A. (Eds.). (1985). *The Caledonide orogen: Scandinavia and related areas* (Vol. 2). Wiley.

Gilio, M., Clos, F. & van Roermund, H.L.M. (2015). The Friningen Garnet Peridotite (Central Sweden). A good example of the characteristic PTt path of a cold mantle wedge garnet peridotite. *Manuscript submitted for publication.*

Griffin, W. L., O'Reilly, S. Y., Afonso, J. C., & Begg, G. C. (2009). The composition and evolution of lithospheric mantle: a re-evaluation and its tectonic implications. *Journal of Petrology*, *50*(7), 1185-1204.

Hacker, B. R., & Gans, P. B. (2005). Continental collisions and the creation of ultrahigh-pressure terranes: Petrology and thermochronology of nappes in the central Scandinavian Caledonides. *Geological Society of America Bulletin*,*117*(1-2), 117-134.

Herzberg, C. (2004). Geodynamic information in peridotite petrology. *Journal of Petrology*, *45*(12), 2507-2530.

Högbom, A. G. (1920). *Geologisk beskrivning över Jämtlands län*. SGU C 140.

Holtedahl, O. (1920). Paleogeography and diastrophism in the Atlantic-Arctic region during Paleozoic time. *American Journal of Science*, (289), 1-25.

Iyer, K., Austrheim, H., John, T., & Jamtveit, B. (2008). Serpentinization of the oceanic lithosphere and some geochemical consequences: constraints from the Leka Ophiolite Complex, Norway. *Chemical Geology*, *249*(1), 66-90.

Jagoutz, E., Palme, H., Baddenhausen, H., Blum, K., Cendales, M., Dreibus, G., ... & Lorenz, V. (1979). The abundances of major, minor and trace elements in the earth's mantle as derived from primitive ultramafic nodules. In *Lunar and Planetary Science Conference Proceedings* (Vol. 10, pp. 2031-2050).

Janák, M., van Roermund, H., Majka, J., & Gee, D. (2013). UHP metamorphism recorded by kyanite-bearing eclogite in the Seve Nappe Complex of northern Jämtland, Swedish Caledonides. *Gondwana Research*, *23*(3), 865-879.

Jenkins, R., (2012), *X-Ray Fluorescence Spectometry*. John Wiley & Sons, Inc.

Kapsiotis, A., Tsikouras, B., Grammatikopoulos, T. A., Karipi, Σ., & Hatzipanagiotou, K. (2007). On the metamorphic modification of Cr-spinel compositions from the ultrabasic rocks of the Pindos ophiolite copmlex (NW Greece). *Bulletin of the Geological Sociaty of Greece*, *40*(2), 781-793.

Leake, B.E., Woolley, A.R., Arps, C.E.S., et al., (1997), Nomenclature of amphiboles: report of the Subcommittee on Amphiboles of the International Mineralogical Association, Commission on New Minerals and Mineral Names*. Am. Mineral.* 82, 1019–1037

Li, X. P., Rahn, M., & Bucher, K. (2004). Serpentinites of the Zermatt-Saas ophiolite complex and their texture evolution. *Journal of Metamorphic Geology*,*22*(3), 159-177.

Lisle R.J., (1984). Strain discontinuities within the Seve-Koli Nappe Complex, Scandinavian Caledonides. *Journal Structural Geology 6;* 101-110

Majka, J., Rosén, Å., Janák, M., Froitzheim, N., Klonowska, I., Manecki, M., ... & Yoshida, K. (2014). Microdiamond discovered in the Seve Nappe (Scandinavian Caledonides) and its exhumation by the “vacuum-cleaner” mechanism. *Geology*, *42*(12), 1107-1110.

Manatschal, G. (2004). New models for evolution of magma-poor rifted margins based on a review of data and concepts from West Iberia and the Alps.*International Journal of Earth Sciences*, *93*(3), 432-466.

Mellini, M., Rumori, C., & Viti, C. (2005). Hydrothermally reset magmatic spinels in retrograde serpentinites: formation of “ferritchromit” rims and chlorite aureoles. *Contributions to Mineralogy and Petrology*, *149*(3), 266-275.

Merlini, A., Grieco, G., & Diella, V. (2009). Ferritchromite and chromian-chlorite formation in mélange-hosted Kalkan chromitite (Southern Urals, Russia).*American Mineralogist*, *94*(10), 1459-1467.

Michel, H. (1950). *Geology and petrology of the Borkafjäll region (southern Swedish Lapland)*. (Doctoral dissertation).

Nicholson, R., & Rutland, R. W. R. (1969). *A section across the Norwegian Caledonides: Bodø to Sulitjelma* (No. 260). Univ.-Forlaget.

Nickel, K. G. (1989). Garnet–pyroxene equilibria in the system SMACCR (SiO2–MgO–Al2O3–CaO–Cr2O3): the Cr-geobarometer. *Kimberlites and related rocks*, *2*, 901-912.

Penrose, C. P. (1972). Penrose field conference on ophiolites. *Geotimes*, *17*, 24-25

Péron-Pinvidic, G., & Manatschal, G. (2009). The final rifting evolution at deep magma-poor passive margins from Iberia-Newfoundland: a new point of view.*International Journal of Earth Sciences*, *98*(7), 1581-1597.

Qvale, H., & Stigh, J. (1985). Ultramafic rocks in the Scandinavian Caledonides.*The Caledonide Orogen: Scandinavia and Related Areas: Chichester, UK, Wiley*, 693-715.

Ravna, E. K., & Paquin, J. E. N. S. (2003). Thermobarometric methodologies applicable to eclogites and garnet ultrabasites. *EMU notes in mineralogy, 5(8), 229-259.*

Reymer, A. P. S. (1979). Investigations into the metamorphic nappes of the Central Scandinavian Caledonides on the basis of Rb-Sr and K-Ar age determiniations. *(Doctoral dissertation)*

van Roermund, H.L.M. (2009). Mantle-wedge garnet peridotites from the northernmost ultra-high pressure domain of the Western Gneiss Region, SW Norway. *European Journal of Mineralogy*, *21*(6), 1085-1096.

van Roermund, H. L.M., & Bakker, E. (1983). Structure and metamorphism of the Tången—Inviken area, Seve Nappes, Central Scandinavian Caledonides.*Geologiska Föreningen i Stockholm Förhandlingar*, *105*(4), 301-319.

van Roermund, H.L.M.. & Drury, M.R., (1998). Ultra-high pressure (P> 6 GPa) garnet peridotites in Western Norway: exhumation of mantle rocks from> 185 km depth. *Terra Nova*,*10*(6), 295-301.

Roberts, D. (1980). Petrochemistry and palaeogeographic setting of the Ordovician volcanic rocks of Smøla, central Norway. *Norges geologiske undersøkelse*, *359*, 43-60.

Roberts, D., & Stephens, M. B. (2000). Caledonian orogenic belt. *Description to the bedrock map of central Fennoscandia (Mid-Norden)*, *28*, 79-104.

Roberts, D., & Gee, D. G. (1985). An introduction to the structure of the Scandinavian Caledonides. *The Caledonide orogen–Scandinavia and related areas*, *1*, 55-68.

Roberts, D., Sturt, B. A., & Furnes, H. (1985). Volcanite assemblages and environments in the Scandinavian Caledonides and the sequential development history of the mountain belt. *Gee, DG & Sturt, BA (eds.), The Caledonide Orogen–Scandinavian related areas*, 919-930.

Roberts, D. (2003). The Scandinavian Caledonides: event chronology, palaeogeographic settings and likely modern analogues. *Tectonophysics*,*365*(1), 283-299.

de Roever, W. V. (1957). Sind die alpinotypen Peridotitmassen vielleicht tektonisch verfrachtete Bruchstücke der Peridotitschale?. *Geologische Rundschau*, *46*(1), 137-146.

Root, D., & Corfu, F. (2012). U–Pb geochronology of two discrete Ordovician high-pressure metamorphic events in the Seve Nappe Complex, Scandinavian Caledonides. Contributions to Mineralogy and Petrology, 163(5), 769-788.

Sawyer, D. S. (1985). Brittle failure in the upper mantle during extension of continental lithosphere. *Journal of Geophysical Research: Solid Earth (1978–2012)*, *90*(B4), 3021-3025.

Slabunov, A. I., Lobach-Zhuchenko, S. B., Bibikova, E. V., Sorjonen-Ward, P., Balangansky, V. V., Volodichev, O. I., ... & Stepanov, V. S. (2006). The Archaean nucleus of the Fennoscandian (Baltic) Shield. *Geological Society, London, Memoirs*, *32*(1), 627-644.

Smith, D. C. (1984). Coesite in clinopyroxene in the Caledonides and its implications for geodynamics. *Nature, 310*, 641-644

Sobolev, N. V., & Shatsky, V. S. (1990). Diamond inclusions in garnets from metamorphic rocks: a new environment for diamond formation. *Nature*, *343*(6260), 742-746.

Song, S., Zhang, L.F. & Niu, Y. (2004). Ultra-deep origin of garnet peridotite from the North Qaidam ultrahigh-pressure belt, Northern Tibetan Plateau, NW China. *American Mineralogist*, *89*(8-9), 1330-1336.

Spengler, D., Van Roermund, H. L., Drury, M. R., Ottolini, L., Mason, P. R., & Davies, G. R. (2006). Deep origin and hot melting of an Archaean orogenic peridotite massif in Norway. *Nature*, *440*(7086), 913-917.

Spengler, D., Brueckner, H. K., van Roermund, H. L., Drury, M. R., & Mason, P. R. (2009). Long-lived, cold burial of Baltica to 200 km depth. *Earth and Planetary Science Letters*, *281*(1), 27-35.

Stephens, M. B., & Gee, D. G. (1985). A tectonic model for the evolution of the eugeoclinal terranes in the central Scandinavian Caledonides. *The Caledonide orogen–Scandinavia and related areas*, 953-978.

Strand, R. & Kulling, O., (1972) Scandinavian Caledonides*. Interscience Publishers (Wiley), London*. 302 pp.

Sveriges Geologiska Undersokning Berggrundskartan (1991). C 689, 1-155.

Terry, M. P., Robinson, P., Hamilton, M. A., & Jercinovic, M. J. (2000). Monazite geochronology of UHP and HP metamorphism, deformation, and exhumation, Nordøyane, Western Gneiss Region, Norway. *American Mineralogist*, *85*(11-12), 1651-1664.

den Tex, E. (1969). Origin of ultramafic rocks, their tectonic setting and history: a contribution to the discussion of the paper “The origin of ultramafic and ultrabasic rocks” by PJ Wyllie. *Tectonophysics*, *7*(5), 457-488.

Törnebohm, A.E., 1872: En geognostik profil öfver den skandinaviska fjällryggen mellan Östersund och Levanger. *Sveriges Geofogiskn Undersdknitig* C 4 1 - 24.

Törnebohm, A.E., 1888: Om fjällproblemet. Geologiska Föreningens I Stockholm Förhandlingar 10, 328–336.

Torsvik, T. H. (1998). Palaeozoic palaeogeography: a North Atlantic viewpoint.*GFF*, *120*(2), 109-118.

Torsvik, T. H., & Cocks, L. R. M. (2005). Norway in space and time: a centennial cavalcade. *Norwegian Journal of Geology*, *85*(1-2), 73-86.

Torsvik, T. H., & Rehnström, E. F. (2001). Cambrian palaeomagnetic data from Baltica: implications for true polar wander and Cambrian palaeogeography. *Journal of the Geological Society*, *158*(2), 321-329.

Torsvik, T. H., Smethurst, M. A., Meert, J. G., Van der Voo, R., McKerrow, W. S., Brasier, M. D., ... & Walderhaug, H. J. (1996). Continental break-up and collision in the Neoproterozoic and Palaeozoic—a tale of Baltica and Laurentia.*Earth-Science Reviews*, *40*(3), 229-258.

Trouw, R. A. E., (1973) Structural geology of the Marsfjällen area, Caledonides of Västerbotten, Sweden, *Sveriges Geologiska Undersokning* C 689, 1-155

Tucker, R. D., Råheim, A., Krogh, T. E., & Corfu, F. (1987). Uranium-lead zircon and titanite ages from the northern portion of the Western Gneiss Region, south-central Norway. Earth and Planetary Science Letters, 81(2), 203-211.

Wakabayashi, J., & Dilek, Y. (2003). What constitutes ‘emplacement’of an ophiolite?: Mechanisms and relationship to subduction initiation and formation of metamorphic soles. *Geological Society, London, Special Publications*,*218*(1), 427-447.

Walter, M. J. (1998). Melting of garnet peridotite and the origin of komatiite and depleted lithosphere. *Journal of Petrology*, *39*(1), 29-60.

Warren, C. J. (2013). Exhumation of (ultra-) high-pressure terranes: concepts and mechanisms. *Solid Earth*, *4*(1), 75-92.

Whitmarsh, R. B., Manatschal, G., & Minshull, T. A. (2001). Evolution of magma-poor continental margins from rifting to seafloor spreading. *Nature*,*413*(6852), 150-154.

Williams, M. L., Jercinovic, M. J., & Terry, M. P. (1999). Age mapping and dating of monazite on the electron microprobe: deconvoluting multistage tectonic histories. Geology, 27(11), 1023-1026.

Williams, P. F., & Zwart, H. J. (1977). A model for the development of the Seve-Köli Caledonian nappe complex. In *Energetics of geological processes* (pp. 169-187). Springer Berlin Heidelberg.

Wilson, J. T. (1968). Theories of the origin of Hudson Bay. Part III. Comparison of the Hudson Bay arc with some other features. *Contributions from the Dominion Astrophysical Observatory in Victoria*, *4*, 31-49.

Wyllie, J. P. (1969). The origin of ultramafic and ultrabasic rocks.*Tectonophysics*, *7*(5), 437-455.

Yang, J, Godard, G., Kienast, J. R., Lu, Y., & Sun, J. (1993). Ultrahigh-pressure (60 kbar) magnesite-bearing garnet peridotites from northeastern Jiangsu, China. *The Journal of Geology*, 541-554.

Yang, J., Zhu, H., Deng, J. F., Zhou, T. Z., & Lai, S. C. (1994). Discovery of garnet-peridotite at the northern margin of the Qaidam Basin and its significance. *Acta Petrologica et Mineralogica*, *13*(2), 97-105.

Zachrisson, E. (1969). Caledonian geology of the northern Jämtland – southern Västerbotten. *Sver. Geol. Unders. Ser*. C 644, 33

Zachrisson, E. (1973). The westerly extension of Seve rocks within the Seve-Köli Nappe Complex in the Scandinavian Caledonides. *GFF*, *95*(2), 243-251.

Zachrisson, E. (1993). *Berggrundskartorna 23F Fatmomakke NV och SV, 1:50.000.* SGU Ai 75-76

Zachrisson, E. & Greiling, R.O. (1993). *Berggrundskartorna 23F Fatmomakke NO och SO*, *1:50.000*. SGU Ai 77-78

Zane, A., & Weiss, Z. (1998). A procedure for classifying rock-forming chlorites based on microprobe data. *Rendiconti Lincei*, *9*(1), 51-56.

Zhang, C., Van Roermund, H., & Zhang, L. (2010). Using garnet peridotites as tools to reconstruct paleo-geodynamic settings of fossil continental collision zones. In *EGU General Assembly Conference Abstracts*(Vol. 12, p. 5928).

Zwart, H. J. (1974). Structure and metamorphism in the Seve-Köli Nappe Complex (Scandinavian Caledonides) and its implications concerning the formation of metamorphic nappes. *Annales de la Société géologique de Belgique*.

I) Chemical data

Table 1

	Olivine		Appendix	SiO2	NiO	FeO	CaO	MgO	Cr2O3	MnO	Total	#Mg
Köli	Second generation	1	III-3-1	41,47	0,0043	0,0101	52,72	3,8	0,4132	0,318	98,7356	96,11335
		2		41,68	0,0134	0,0225	52,78	3,56	0,3303	0,3442	98,7304	96,3538
		3		41,84	0	0,0092	52,95	3,51	0,2747	0,3174	98,9013	96,41437
		4	III-4-1	41,89	0,009	0,0058	53,39	3,37	0,261	0,2906	99,2164	96,57994
		5		42,08	0,3515	5,23	0,0102	52,58	0,0233	0,1342	100,4092	94,71447
		6		40,81	0,4077	4,39	0,0156	53	0	0,1234	98,7467	95,55927
		7	III-4-2	41,15	0	0,0124	51,49	5,27	0,354	0,3288	98,6052	94,56962
		8		38,88	0,0041	0,0376	45,81	7,88	0,6531	0,3674	93,6322	91,19875
		9		40,27	0,3421	5,57	0,0154	52,31	0	0,3349	98,8424	94,36285
		10		40,59	0,3376	4,82	0,0266	52,99	0	0,2923	99,0565	95,14458
		11	III-4-3	40,36	0,3349	7,95	0,0286	49,54	0,0019	0,654	98,8694	91,74041
		12		41,46	0,315	2,94	0,0099	54,01	0	0,119	98,8539	97,0365
		13	III-4-4	42,12	0	0,0092	52,98	4,23	0,1137	0,3541	99,807	95,71276
		14		42,13	0	0,0084	53,4	3,55	0,0997	0,3925	99,5806	96,40434
		15	III-4-5	40,26	0,3729	3,54	0,02	54,17	0,0028	0,1147	98,4804	96,46329
		16		35,58	0,3381	3,74	0,0564	46,68	0	0,1348	86,5293	95,69832
		17	III-4-6	41,38	0,3512	3,21	0,0164	53,69	0,0102	0,075	98,7328	96,75455
		18		37,63	0,279	2,31	0,0165	42,49	0	0,0672	82,7927	97,04019
		19	III-4-7	41,56	0,2808	2,99	0,0064	54,35	0	0,0914	99,2786	97,00592
		20		41,3	0,2868	3,21	0,0056	53,75	0	0,0939	98,6463	96,75809
		21	III-5-1	41,61	0,034	0,011	53,11	4,15	0,1308	0,2979	99,3437	95,80024
		22		42,02	0,0014	0,0208	52,52	4,11	0,1123	0,2537	99,0382	95,79431
Upper belt	First generation	23	III-14-1	41,46	0	0,0025	50,81	6,95	0,1377	0,4668	99,827	92,87291
		24		41,99	0,0107	0,0072	50,74	6,75	0,1319	0,4417	100,0715	93,05489
		25		41,81	0	0,0056	50,13	6,86	0,1316	0,4655	99,4027	92,87004
		26		41,59	0	0,0086	50,73	6,74	0,1342	0,4888	99,6916	93,0632
		27	III-14-2	41,51	0,4398	6,64	0,0073	50,58	0,0049	0,1304	99,3124	93,14023
		28		40,86	0,4637	6,81	0,0033	51,57	0,0162	0,1444	99,8676	93,10245
		29		40,7	0,4684	6,63	0,031	50,31	0,0073	0,1168	98,2635	93,11564
		30		40,36	0,4752	6,66	0,0296	52	0,0112	0,1293	99,6653	93,29623
		31		40,71	0,5094	6,62	0,0031	51,58	0,0131	0,1271	99,5627	93,28312
		32		37,84	0,3423	3,95	0,012	41,17	0,2951	0,0511	83,6605	94,89221
		33		40,4	0,4715	6,6	0,0076	51,52	0	0,129	99,1281	93,2948
		34		40,94	0,4778	6,75	0,0004	51,3	0	0,1293	99,5975	93,12547
	Second generation	35		41,62	0,4816	6,56	0,002	49,64	0	0,1398	98,4534	93,09764
		36		39,51	0,4873	6,6	0,0273	52,22	0	0,1397	98,9843	93,37868
		37		40,56	0,4834	6,62	0,0032	52,05	0	0,139	99,8656	93,33979
		38		41,59	0,4963	6,53	0,0384	48,57	0	0,1387	97,3634	92,98631
	Unknown	39	III-14-3	41,57	0	0,0064	50,28	6,66	0,1362	0,4864	99,139	93,08269
		40		41,78	0	0,0061	50,83	6,71	0,1294	0,4756	99,9311	93,10453
		41	III-14-4	39,47	0,4736	6,73	0,0134	51,62	0,0092	0,1371	98,4533	93,18407
		42		40,1	0,4757	6,69	0,0068	50,91	0,0066	0,1235	98,3126	93,13386
		43	III-16-1a	39,13	0	0,0077	50,87	8,97	0,1876	0,4896	99,6549	90,99787
		44		41,28	0	0,0415	50,34	8,91	0,1915	0,4707	101,2337	90,96692
Lower belt	First generation	45	III-23-1	40,58	0,3391	8,37	0	50,57	0	0,1307	99,9898	91,46629
		46		40,74	0,3362	8,3	0,0107	49,91	0	0,1205	99,4174	91,46782
		47		40,73	0,3469	8,29	0,0016	49,86	0	0,1121	99,3406	91,45059
		48		40,59	0,3527	8,31	0,0075	49,87	0	0,1342	99,2644	90,53679
		49	III-9-1	39,88	0,376	9,17	0,0213	49,22	0,0115	0,1581	98,8369	90,71397
		50		39,83	0,3933	9,05	0,0049	49,6	0,0003	0,1577	99,0362	90,54981
		51		40,23	0,344	9,13	0,012	49,08	0,0039	0,1347	98,9846	90,91054
		52		39,84	0,3564	8,67	0,0306	48,65	0,0081	0,1312	97,6863	90,32868
	Dynamically recrystalized	53	III-9-2	41,88	0,3899	9,04	0,0163	48,16	0	0,1642	99,6504	90,69313
		54		40,43	0,401	8,97	0,0115	49,04	0	0,1243	98,9768	91,36144
		55		40,01	0,3892	9,14	0,0053	49,36	0	0,146	99,0505	90,58907
	Second generation	56	III-22-1	40,42	0	0,0088	50,07	8,41	0,1249	0,3777	99,4114	91,38816
		57		40,87	0	0,007	49,67	8,35	0,1168	0,3658	99,3796	91,38146
		58	III-9-3	40,71	0	0,0047	48,23	9,52	0,1498	0,375	98,9895	90,03008
		59		59,34	0,03	11,64	23,12	1,87	0,084	0,1119	96,1959	90,48361
		60		40,56	0	0,0163	49,61	9,3	0,1424	0,3759	100,0046	90,08038
		61	III-9-4	41,81	0,3595	8,96	0,0369	46,95	0,0187	0,1357	98,2708	90,65857
		62		39,94	0,3737	9,15	0,0112	49,82	0,0177	0,1337	99,4463	90,43523
		63		39,66	0,3464	8,93	0,0511	47,37	0,0045	0,1457	96,5077	90,39102
		64		40,98	0,3657	9,15	0,0167	48,29	0,0108	0,1431	98,9563	90,47236
	Unknown	65	III-9-5	41,91	0,0426	0,0836	47,33	9,29	0,125	0,3771	99,1083	91,50826

Table 2

	Spinel	Point	Appendix	SiO2	Al2O3	NiO	FeO	TiO2	MgO	Cr2O3	MnO	Total	Fe3#	Fe2#	Cr#
Köli	Centre	1	III-4-8	0,1101	8,83	0,0353	23,5	0,1294	7,75	55,61	0,4797	96,4445	0,050119	0,611954	0,808596
		2		0,0464	10,38	0,0607	23,22	0,1479	8,45	56,08	0,5547	98,9397	0,046747	0,588738	0,783741
		3	III-4-9	0,045	10,01	0,0172	24,65	0,1489	7,78	56	0,476	99,1271	0,051655	0,622054	0,789591
	Rim	4	III-4-8	0,5724	0,0788	0,9274	87,41	0,0948	2,22	0,5734	0,1077	91,9845	0,992855	0,913961	
		5		0,0999	0,0114	0,8495	89,24	0,0928	1,1851	2,94	0,1298	94,5485	0,969841	0,954475	
		6	III-4-9	0,0438	9,16	0,0408	25,5	0,1401	7,93	53,76	0,9646	97,5393	0,089717	0,612683	
	Opaques	7	III-4-10	0,0601	9,37	0,059	26,69	0,1353	7,99	52,4	0,8747	97,5791			
		8		0,0549	0	0,9977	90,54	0,0961	1,1425	0,196	0,1316	93,1588			
		9		0,0653	0	0,9292	89,88	0,0861	1,0433	0,0065	0,1172	92,1276			
Upper belt	Centre	10	III-14-3	0,0633	0,3003	0,4749	50,8	0,3278	4,23	39,42	0,7956	96,4119	0,485869	0,813973	0,98877
		11		0,1128	0,3536	0,4586	50,83	0,3326	3,34	39,14	0,7663	95,3339	0,473101	0,850969	0,986712
		12	III-14-5	0,0506	0,0993	1,0574	74,18	0,3197	2,02	15,98	0,3269	94,0339	0,816375	0,917958	0,990826
		13		0,1191	0,2145	0,8373	67,17	0,4048	2,72	23,65	0,501	95,6167	0,716271	0,888327	0,986658
		14		0,0813	0,1059	0,9663	72,23	0,3307	2,09	17,85	0,4195	94,0737	0,79186	0,914499	0,991229
	Rim	15	III-14- 3	0,0256	0,096	1,0885	74,67	0,2883	2,11	15,68	0,3095	94,2679	0,821505	0,914538	
		16		0,0275	0,0756	1,0524	73,25	0,2862	2,25	16,86	0,3296	94,1313	0,806881	0,90831	
		17	III-14-5	0,0388	0,0588	1,0944	75,99	0,2712	2,09	13,91	0,2803	93,7335	0,843466	0,915453	
		18		0,3223	0,1708	0,9553	74,17	0,2499	2,31	11,48	0,2226	89,8809	0,86419	0,904227	
		19		0,1945	0,0981	1,0564	75,98	0,2751	1,95	13,26	0,3208	93,1349	0,848264	0,921058	
	Opaques	20	III-14-6	0,0529	0,0034	0,8656	90,55	0,1405	0,6571	0,138	0,0157	92,4232			
		21		0,1165	0,0082	0,8452	88,68	0,1147	0,9064	0,2815	0,048	91,0005			
		22		0,0941	0,1923	0,7376	60,53	0,3005	2,9	26,45	0,5264	91,7309			
Lower belt	Centre	23	III-9-6	0,1855	7,32	0,0411	26,83	0,0785	4,77	56,69	0,6066	96,5217	0,035781	0,751006	0,838579
		24		0,0294	8,35	0,0712	27,73	0,088	5,44	56,33	0,6098	98,6484	0,054908	0,727149	0,819012
		25	III-9-7	0,0095	8,55	0,0233	26,22	0,072	5,92	57,97	0,5693	99,3341	0,037986	0,702359	0,819755
		26		0,0386	6,53	0,0151	29,8	0,0691	4,43	57,1	0,6352	98,618	0,069194	0,776614	0,854345
	Rim	27	III-9-6	0,1955	0,3873	0,2205	46,05	0,1775	2,62	40,68	0,6177	90,9485	0,406444	0,87502	
		28		0,0548	1,7628	0,0754	39,5	0,1222	3,26	52,58	0,6896	98,0448	0,230336	0,845051	
		29	III-9-7	0,1105	0,2354	0,5219	65,64	0,1847	1,0049	26,87	0,4154	94,9828	0,660625	0,95774	
		30		0,049	0,3433	0,1646	48,1	0,197	2,47	44,38	0,6574	96,3613	0,387403	0,887353	
	Opaques	31	III-9-8	0,1778	0,2512	0,0568	37,91	0,1227	2,56	52,99	0,7134	94,7819			
		32		0,6463	0,1738	0,0922	40,66	0,1556	3,69	49,61	0,7326	95,7605			

Table 3

Amphibole

	Point	Appendix	SiO2	Al2O3	TiO2	Cr2O3	K2O	CaO	Na2O	MgO	FeO	MnO	Total	Mg#	Si in formula
Upper belt	1	III-16-1b	58,36	0,1195	0,0095	0,0202	0,008	12,78	0,0647	23,33	0,0501	1,85	96,592	0,998781	7,6835
	2		57,84	0,0956	0,0228	0,0087	0,0041	12,55	0,048	22,88	0,055	1,83	95,3342	0,998636	7,711
Lower belt	3	III-9-5	58,02	0,0259	0	0,0108	0,0309	11,93	0,4626	23,12	0,0844	2,15	95,8346	0,997931	7,7055
	4		58,31	0,0623	0	0,0232	0,041	11,47	0,7232	23,19	0,0642	2,14	96,0239	0,998428	7,7165
	5		58,47	0,0271	0	0,0167	0,0357	11,55	0,7401	23,07	0,0858	2,33	96,3254	0,997891	7,722

Table 4

Chlorite

	Point	Appendix	O	Mg	Al	Si	Cr	Fe#	Mg#	Al#
Köli	1	III-5-2	50,72	19,64	9,70	16,16	3,78	0,055624	0,79653	0,147846
Upper belt	2	III-16-2	45,33	25,31	8,22	17,94	3,19	0,04577	0,832477	0,121752
	3	III-16-3	45,17	25,14	8,01	17,93	3,75	0,053776	0,827492	0,118731
	4		45,37	25,33	7,97	18,17	3,16	0,04542	0,836093	0,118487
Lower belt	5	III-23-2	45,13	25,61	7,05	17,73	2,93	0,023306	0,868807	0,107887
	6		44,83	25,18	6,6	17,66	3,55	0,028705	0,868799	0,102496
	7	III-23-3	44,98	25,74	7,08	17,43	2,94	0,023199	0,869104	0,107697
	8		45,1	26,17	5,84	18,36	2,64	0,021016	0,889586	0,089398

II) Thin sections

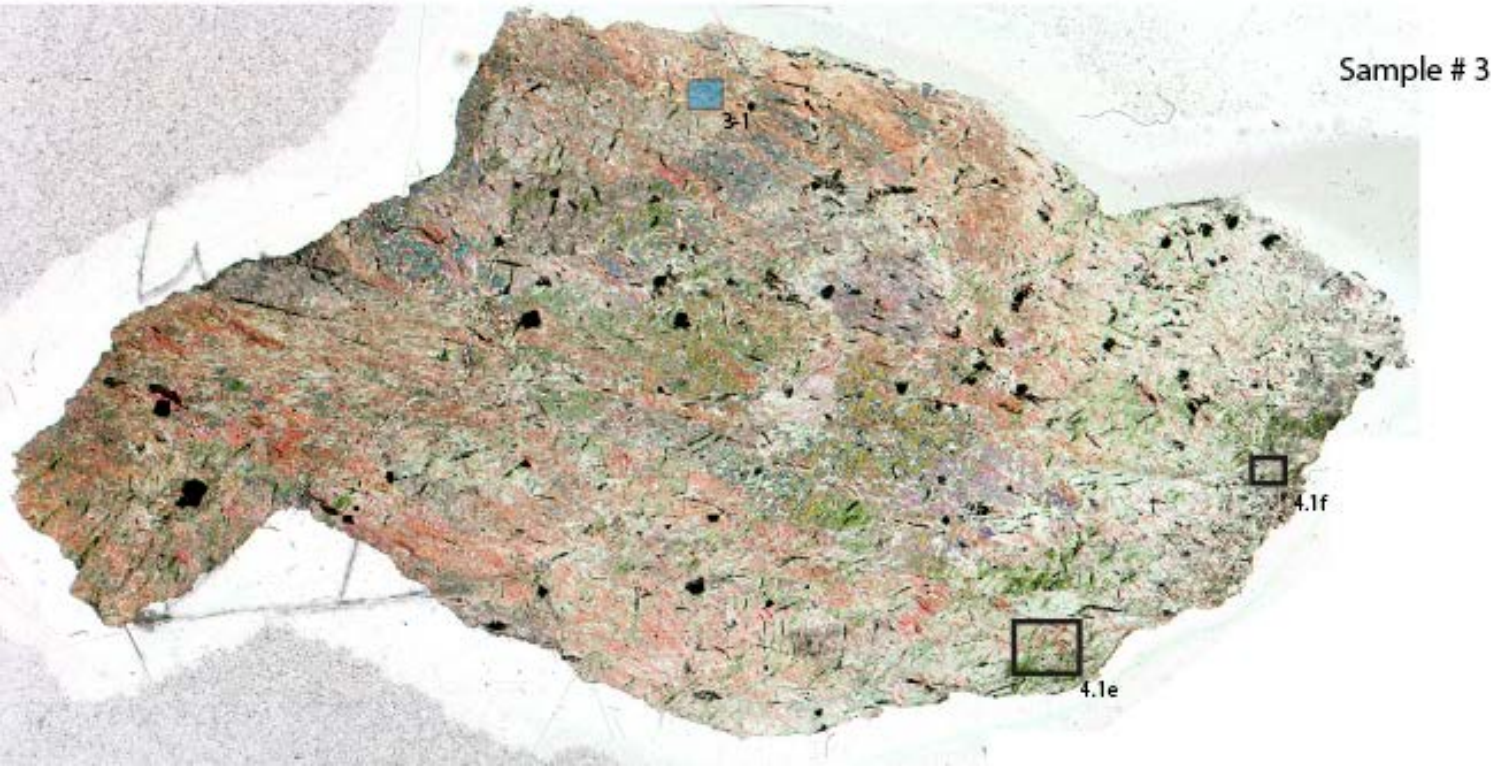

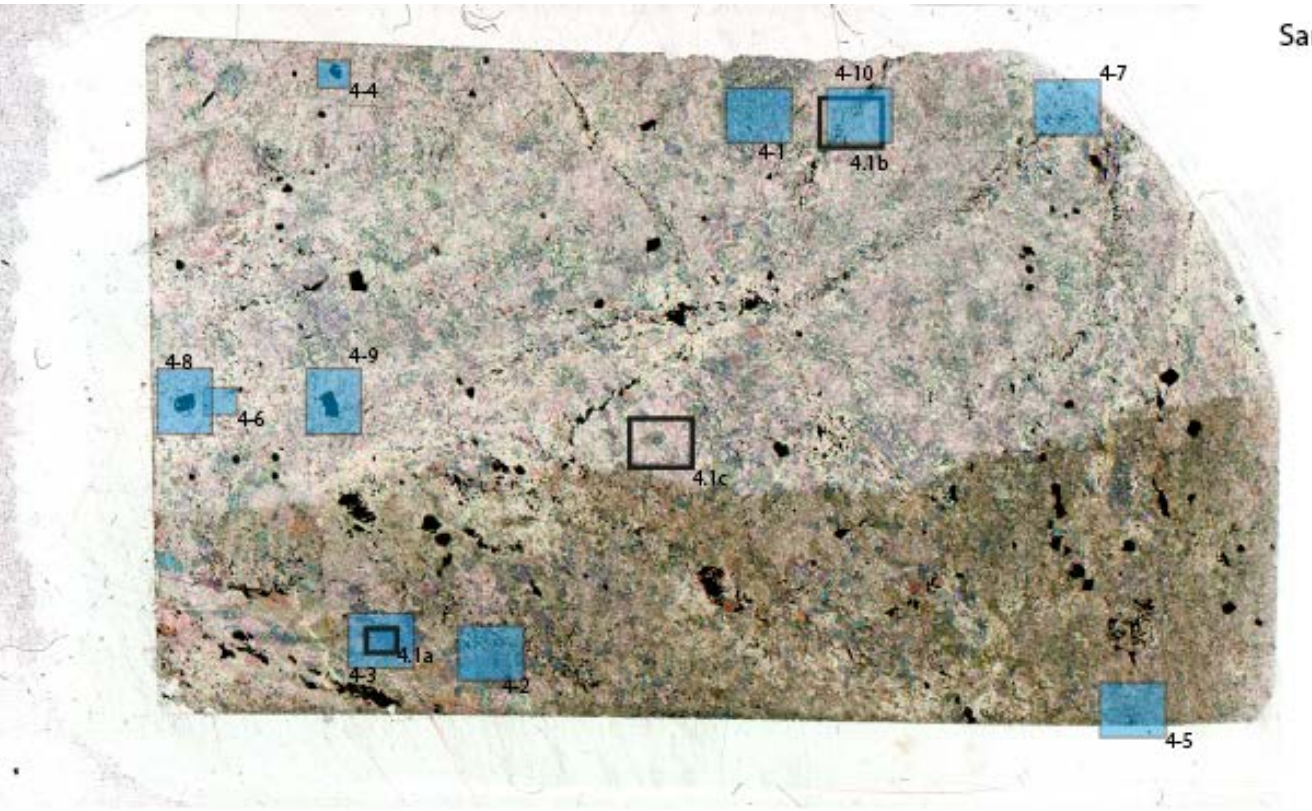

Sample #4

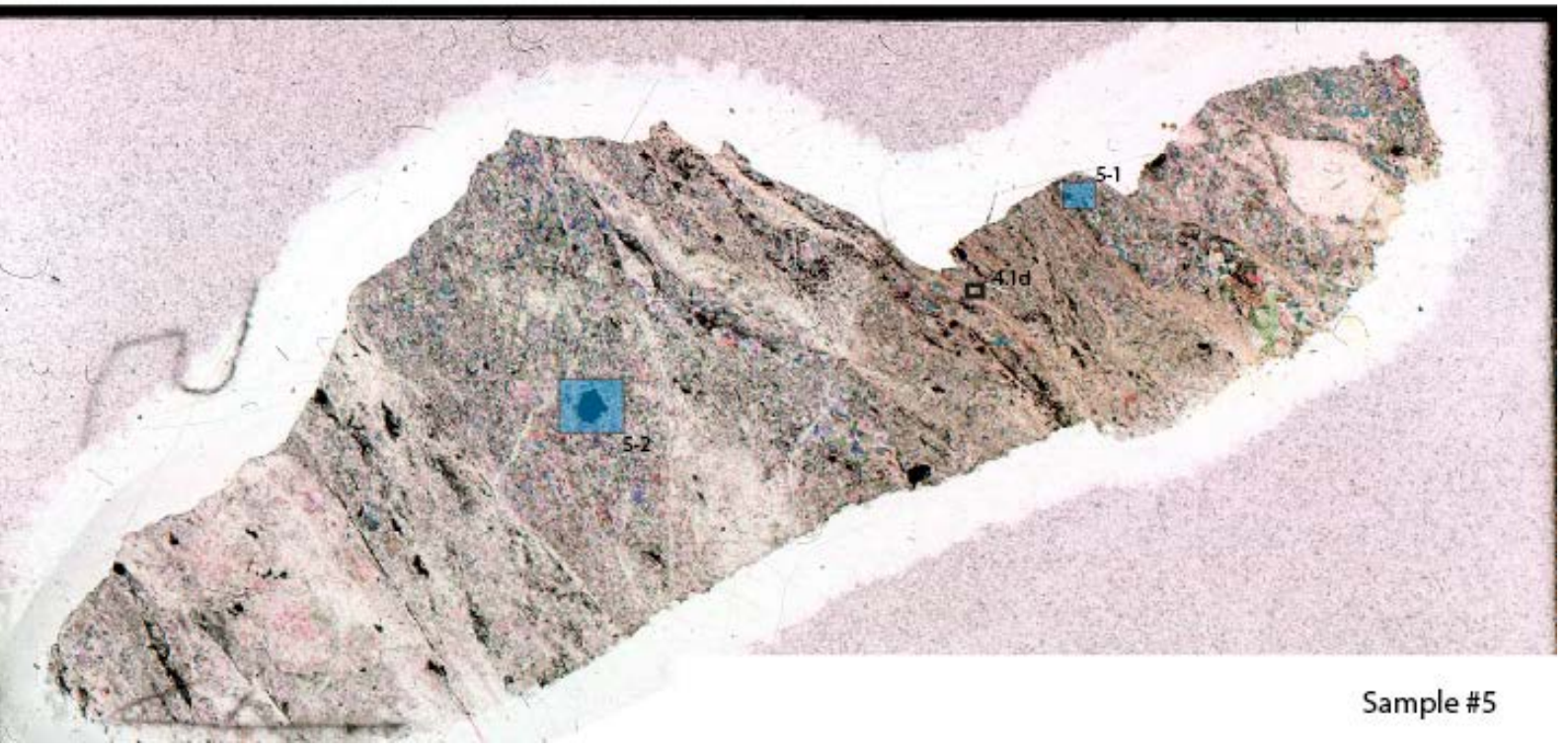

Sample #5

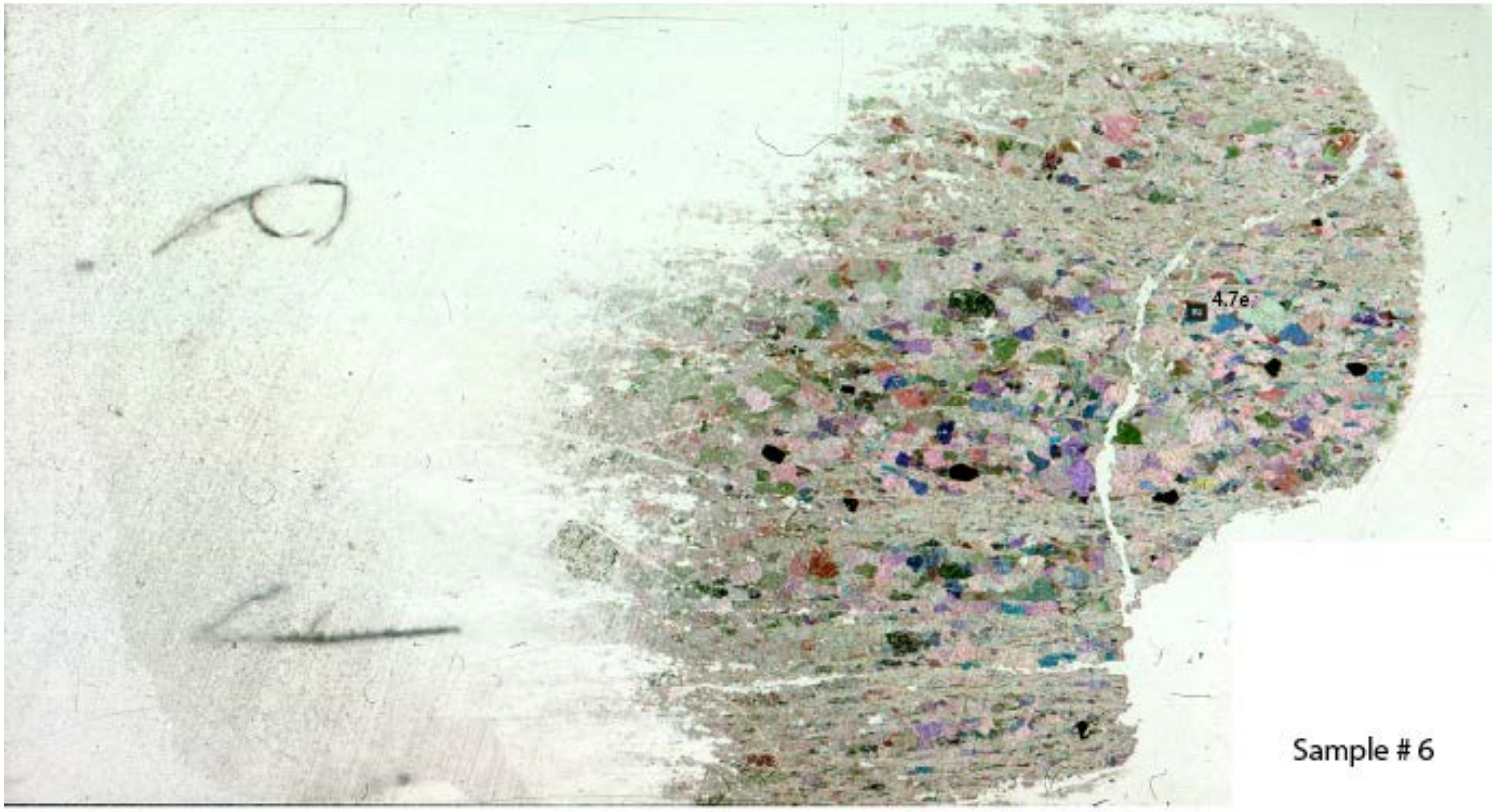

Sample # 6

Sample # 7

Sample # 8

Sample # 9

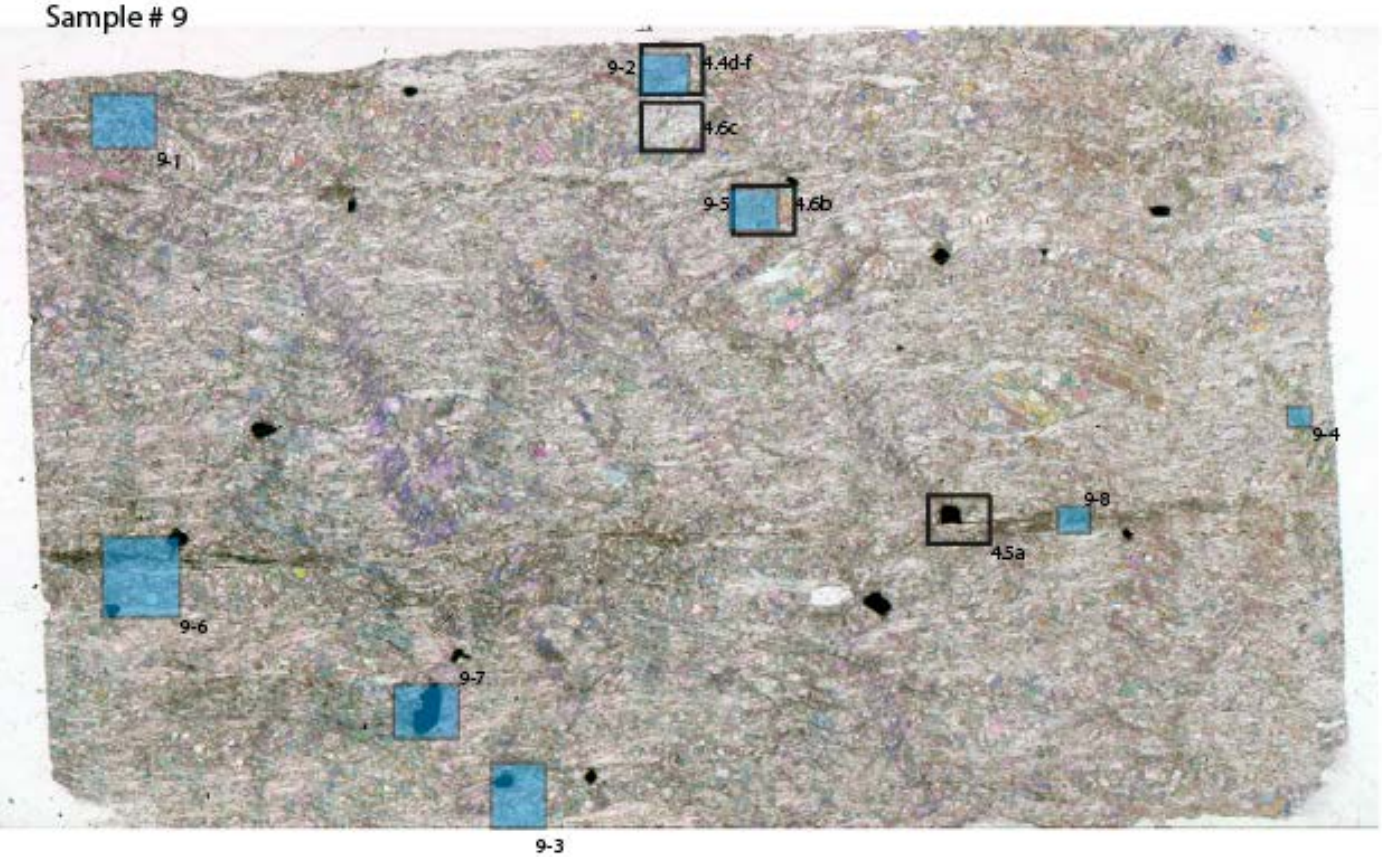

Sample # 10

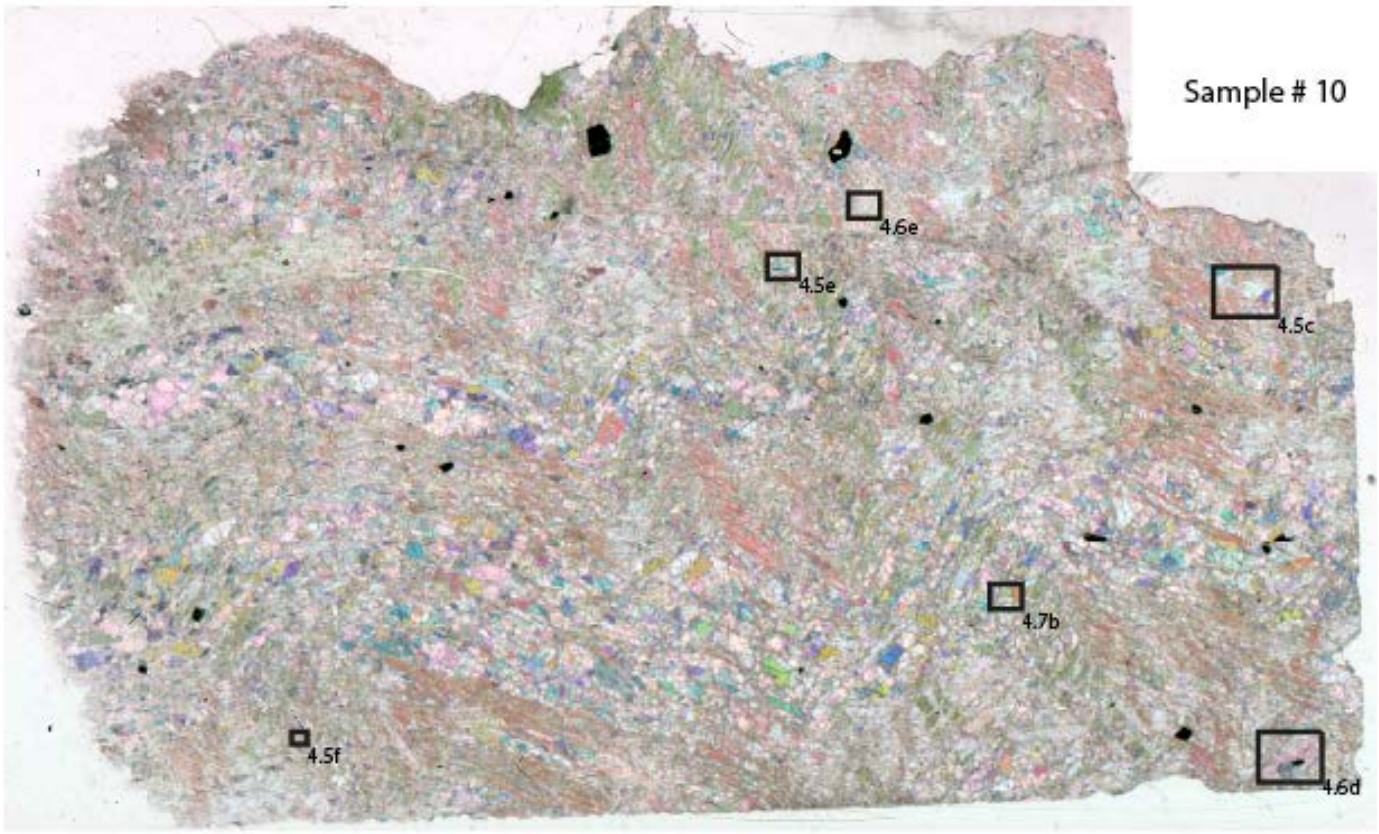

Sample # 11

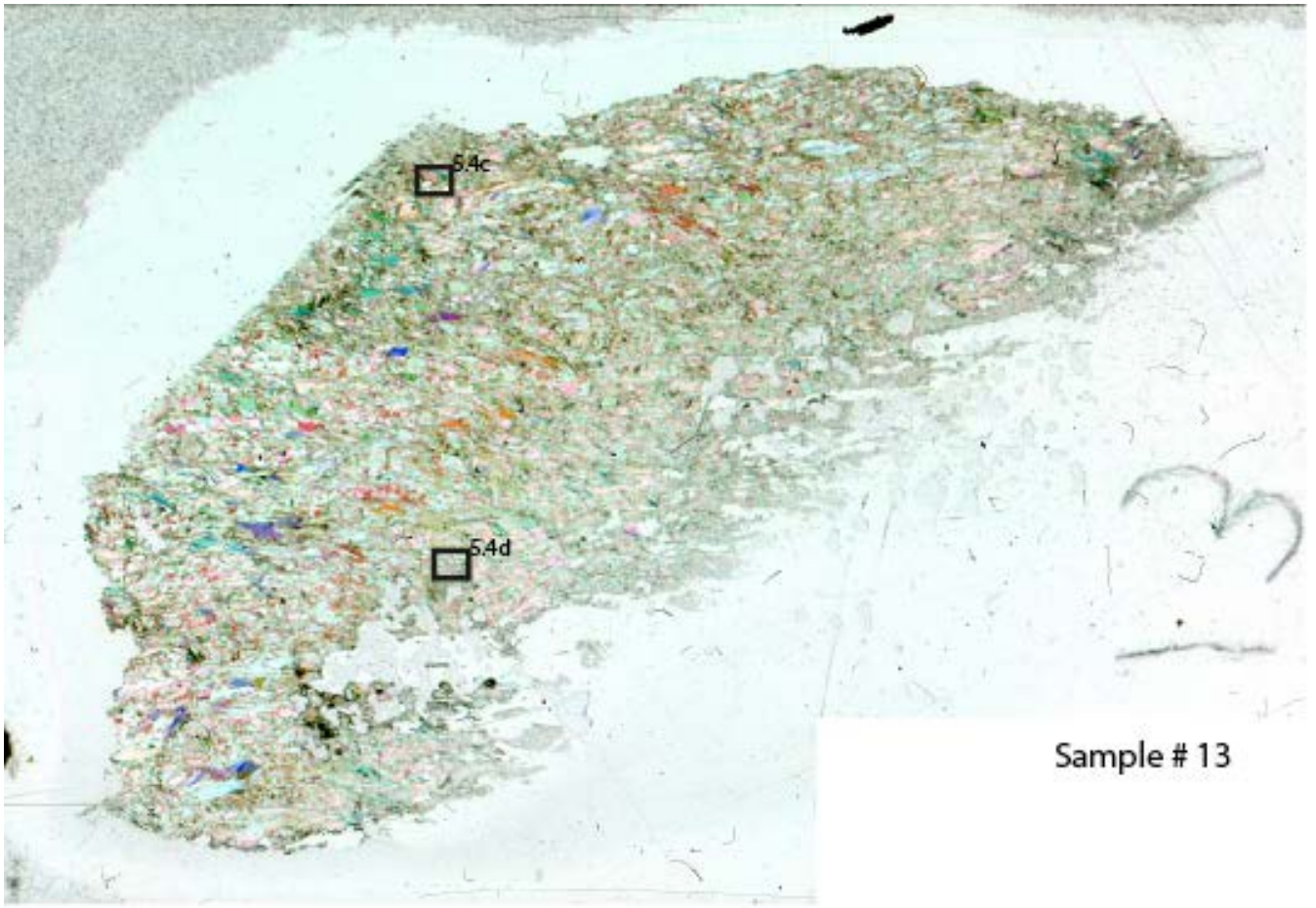

Sample # 13

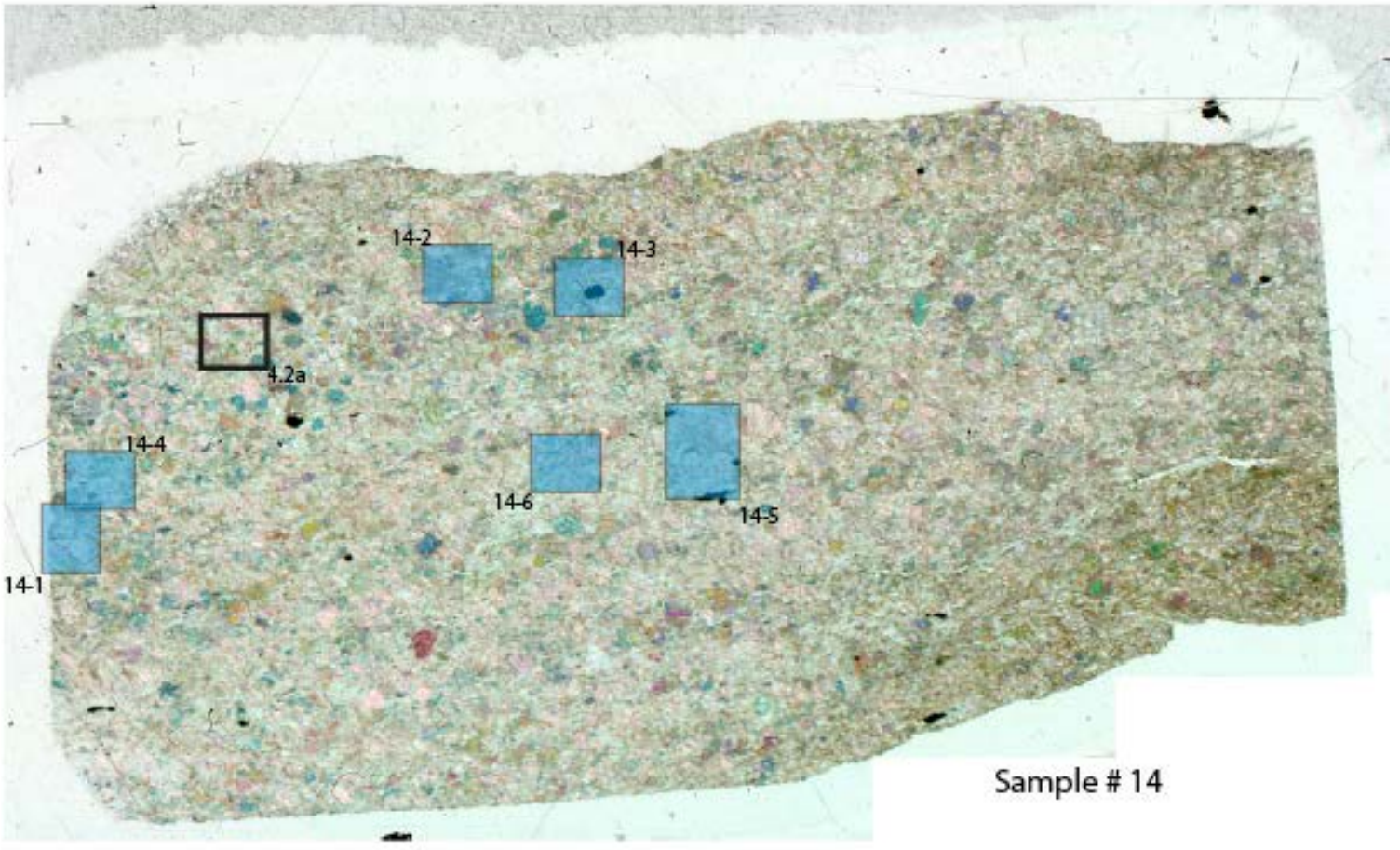

Sample # 14


4.2d
4.2e
4.3f
Sample # 15


16-1a
4.3b
4.2c
4.3c
16-1b
16-2
4.3a
16-3
4.3d
Sample # 16

Sample # 17

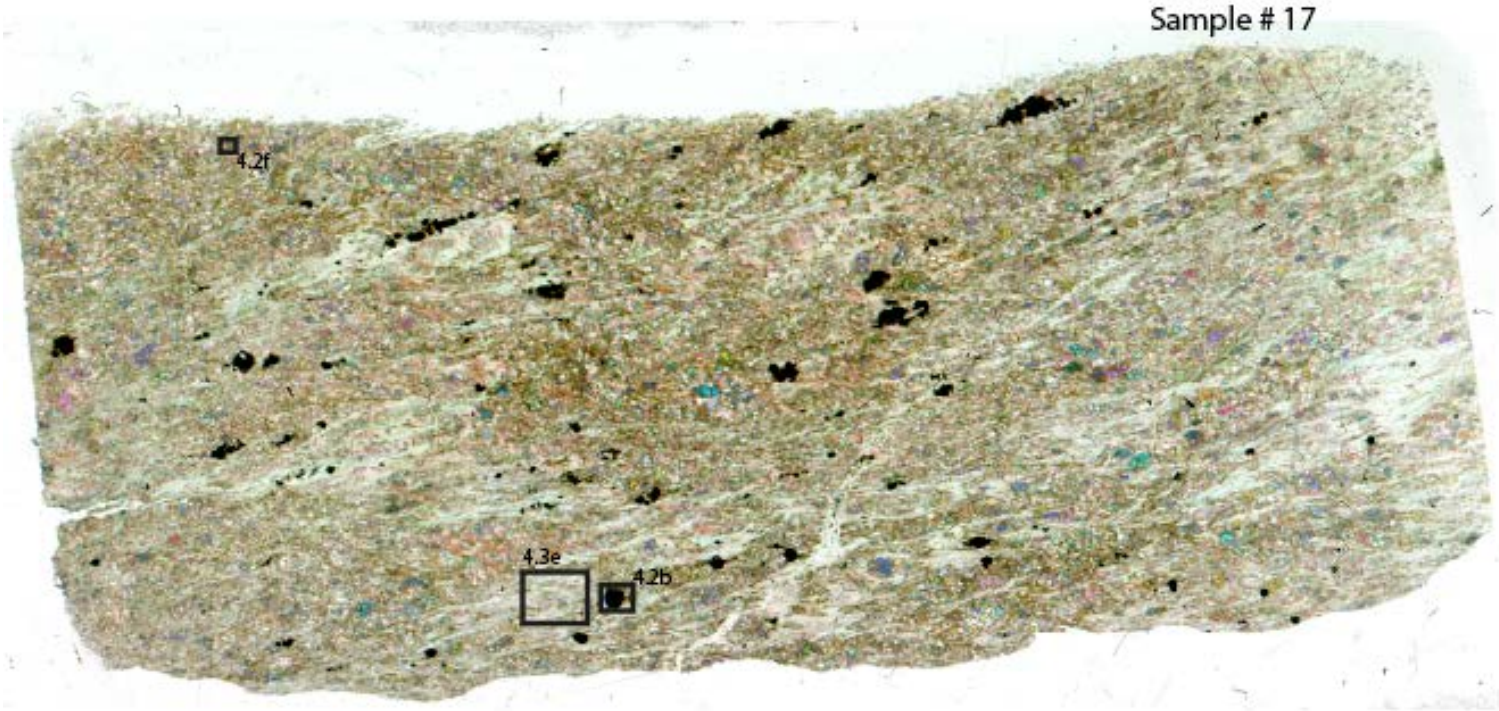

Sample # 18

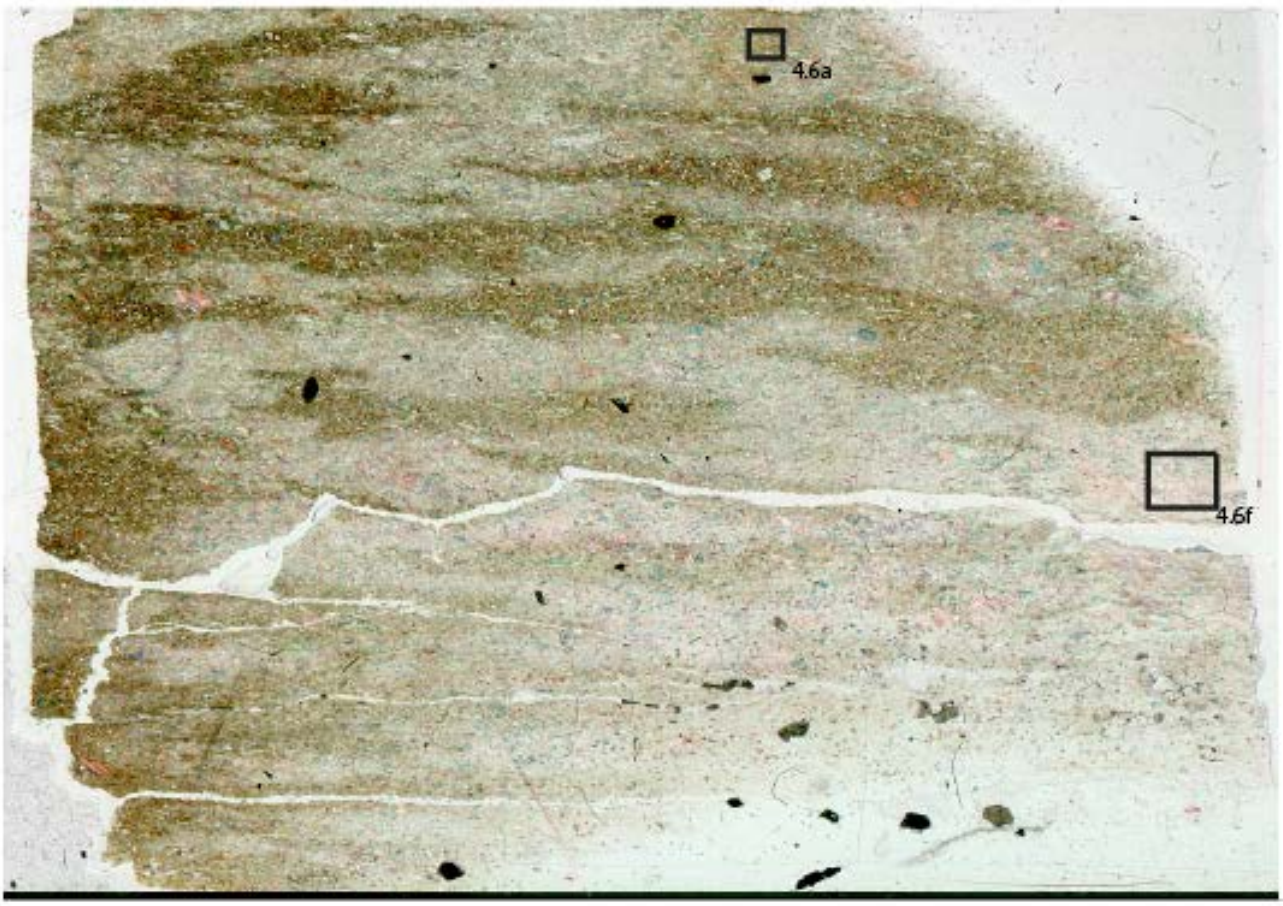

Sample # 20

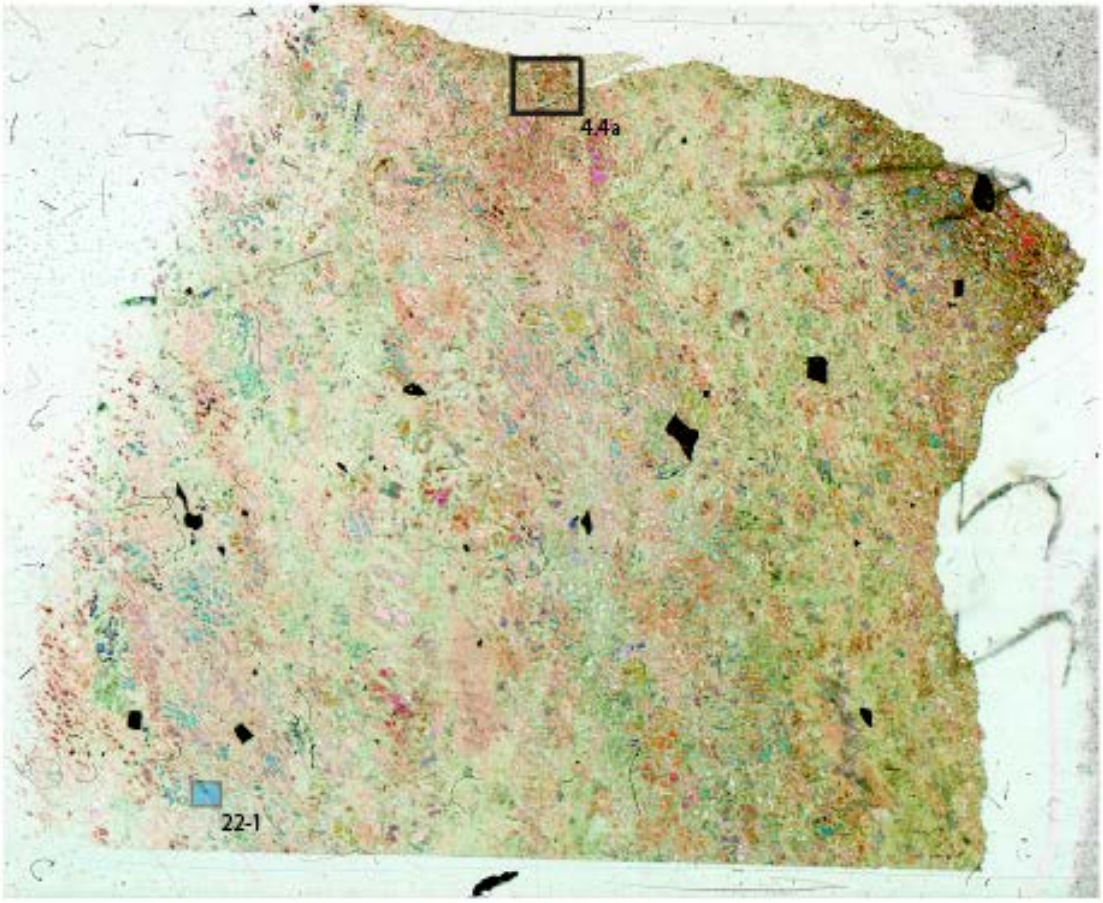

Sample # 22

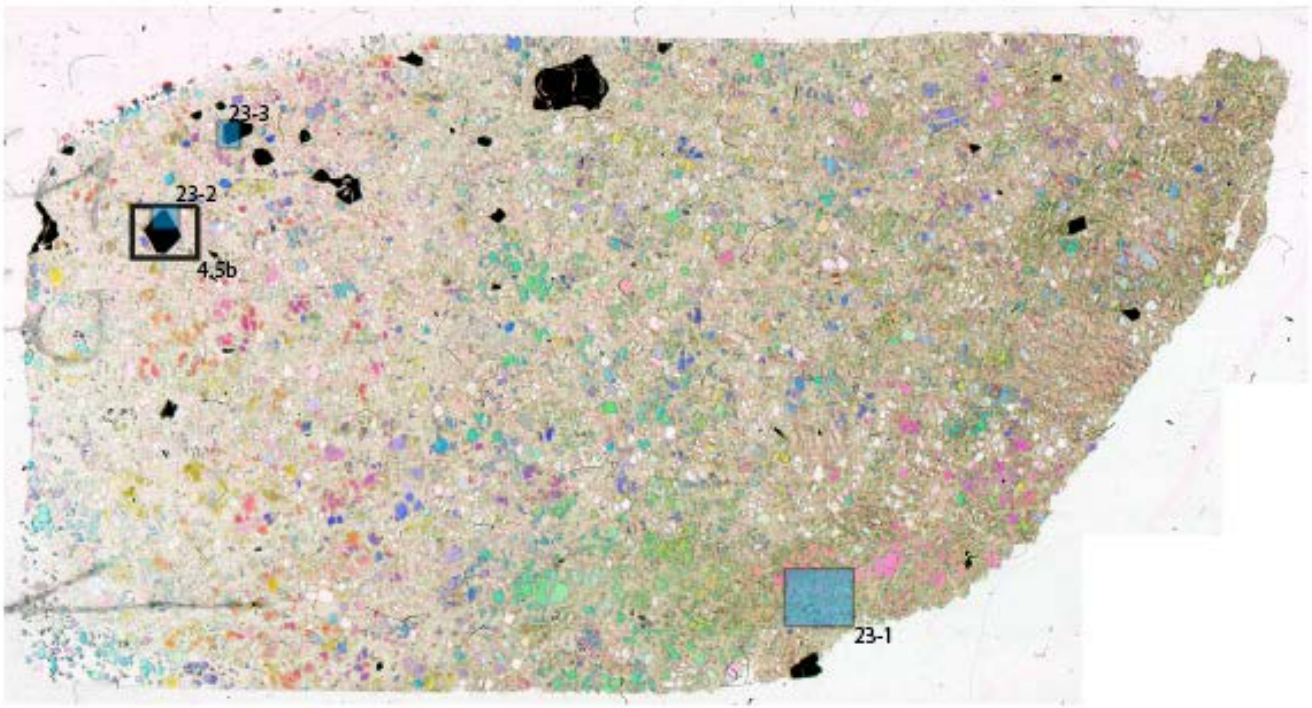

Sample # 23

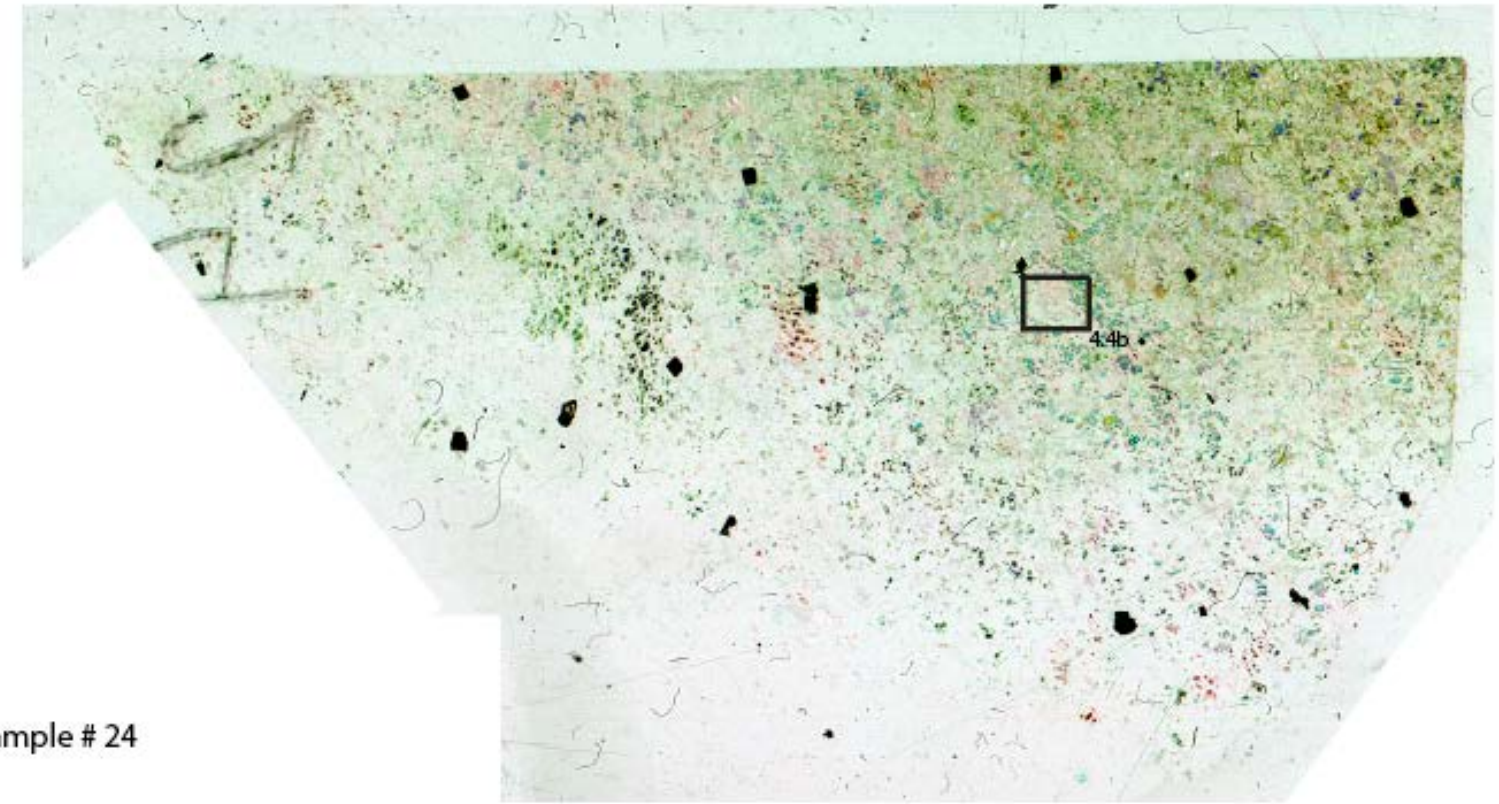

Sample # 24

Sample # 25

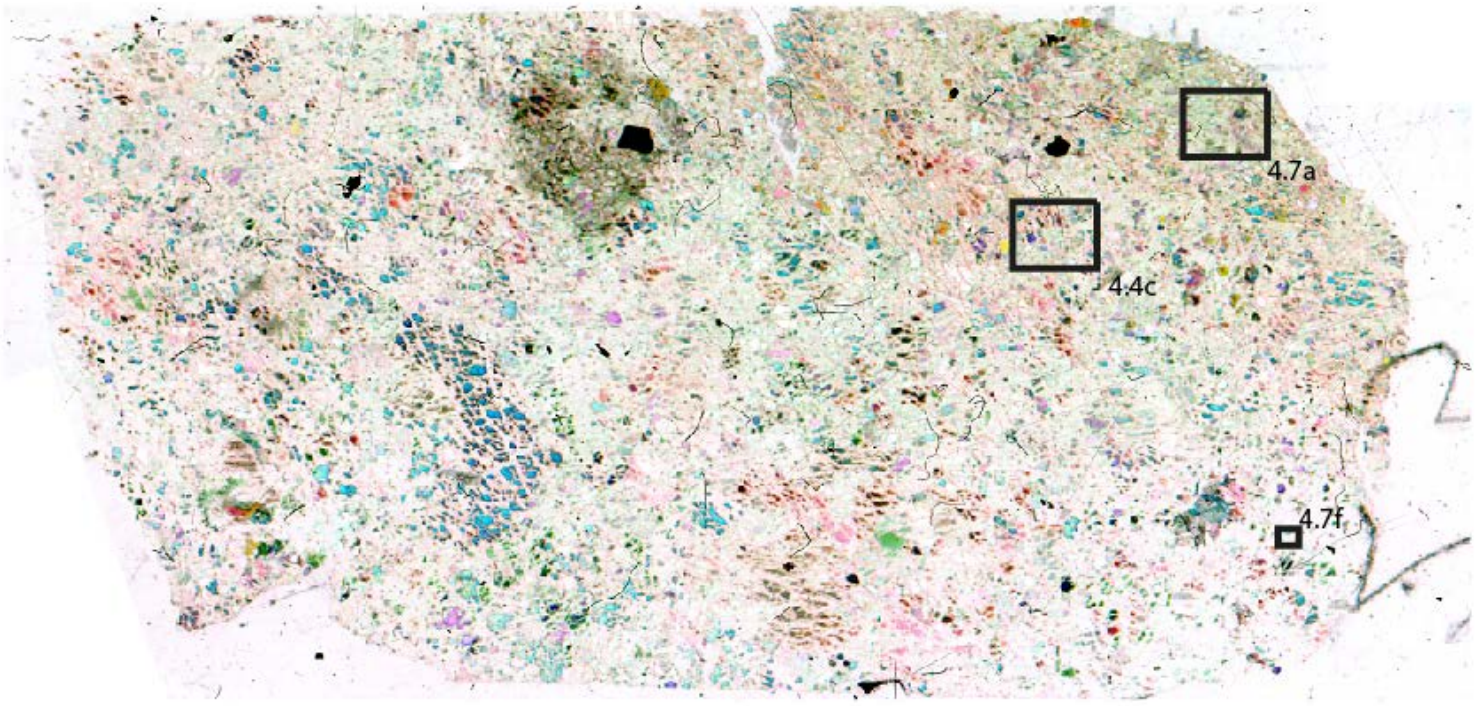

III) Enlargements

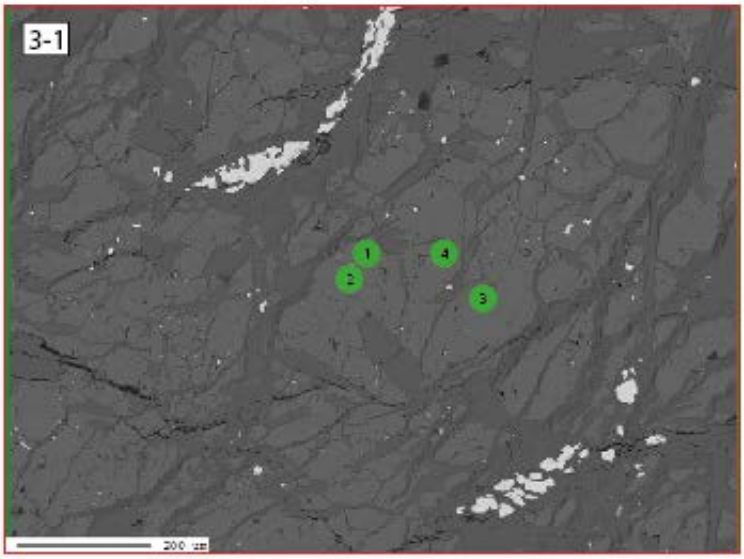

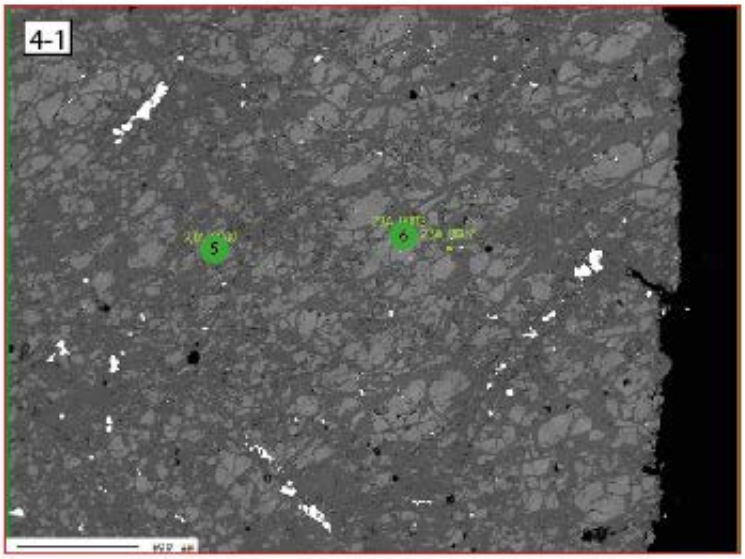

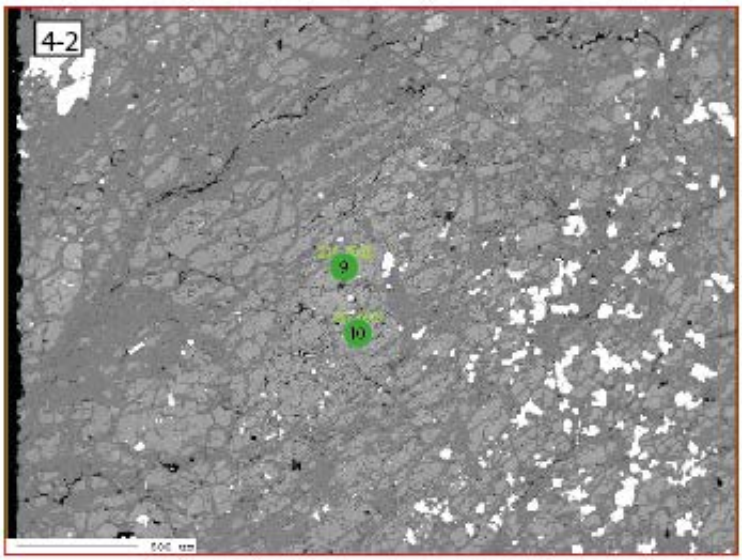

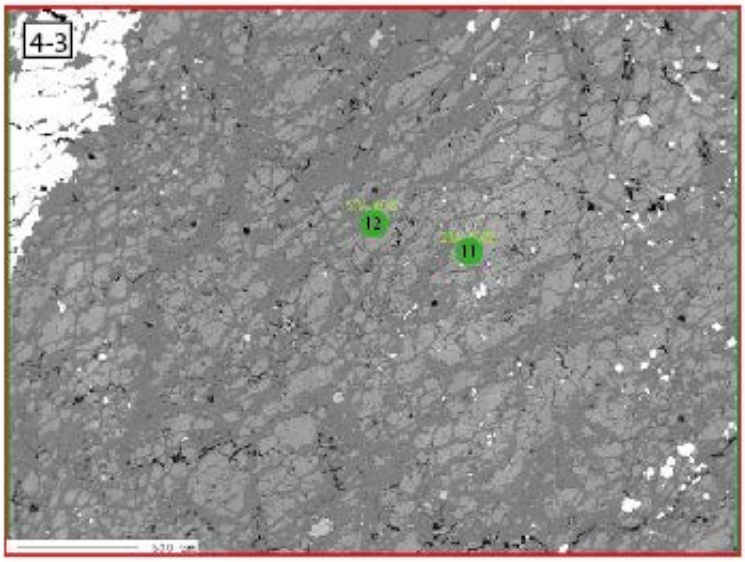

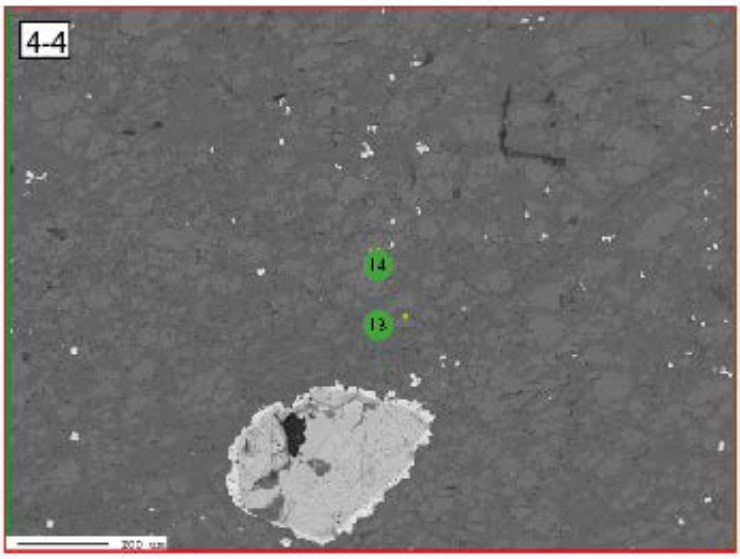

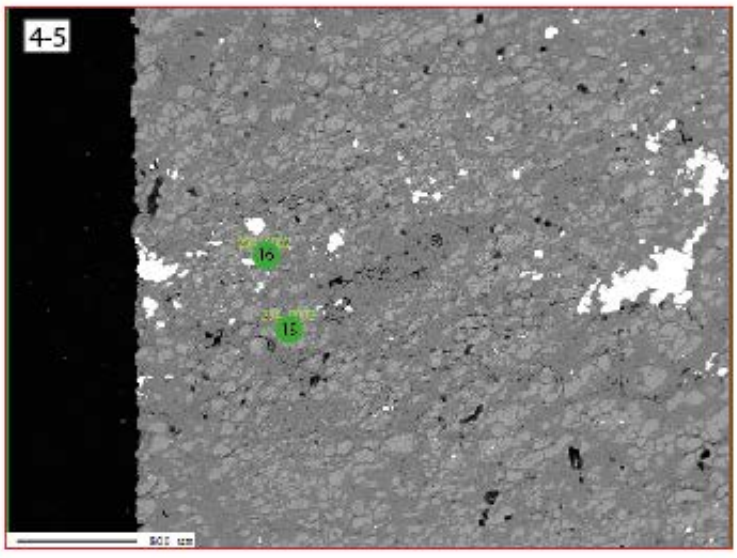

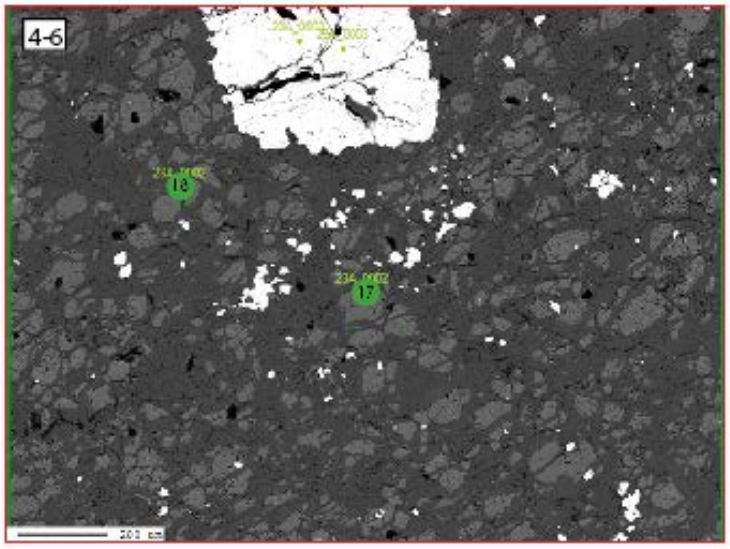
4-6
18
17

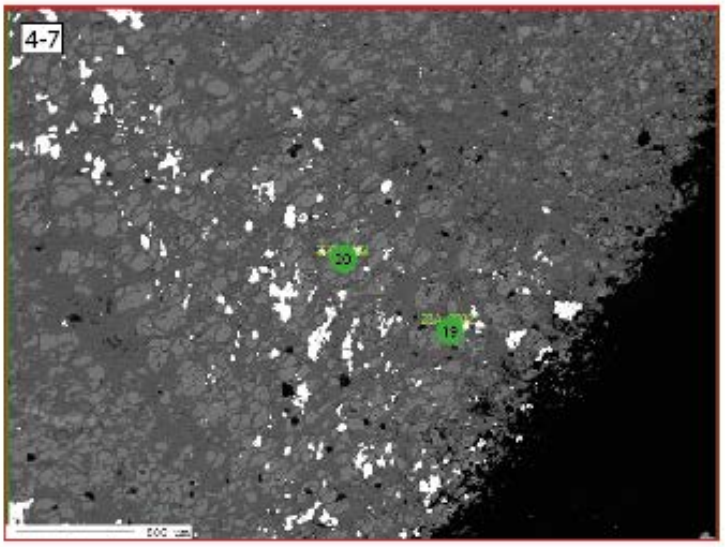
4-7
20
19

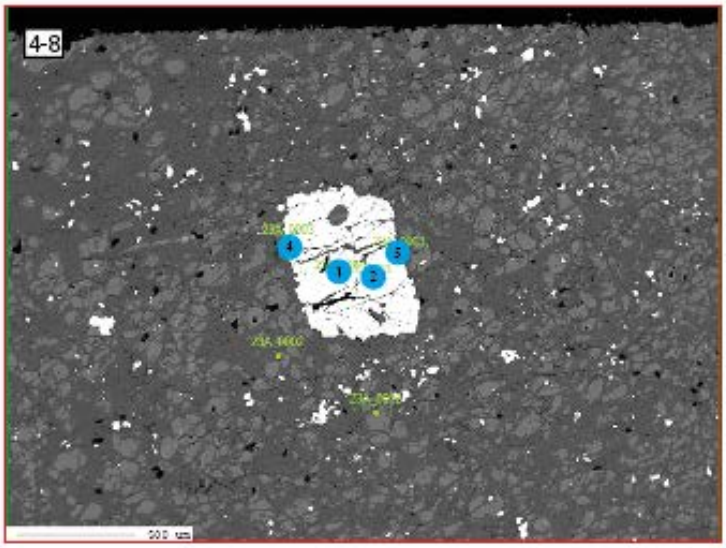
4-8
4
5
1
2

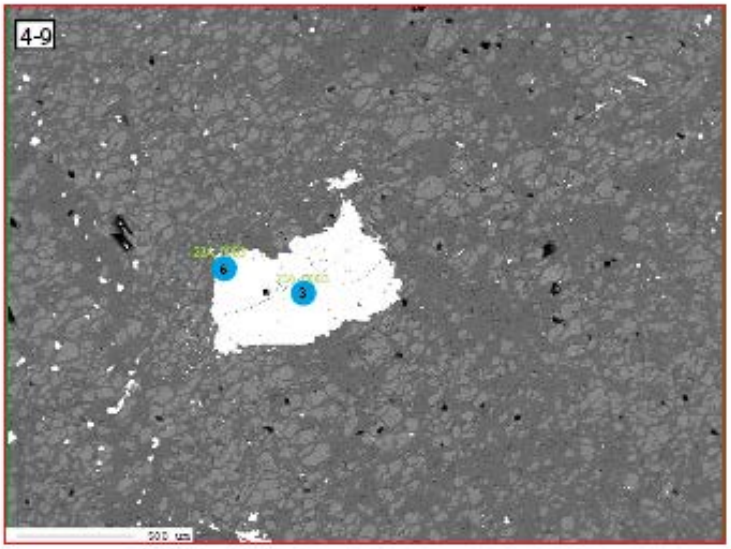
4-9
6
3

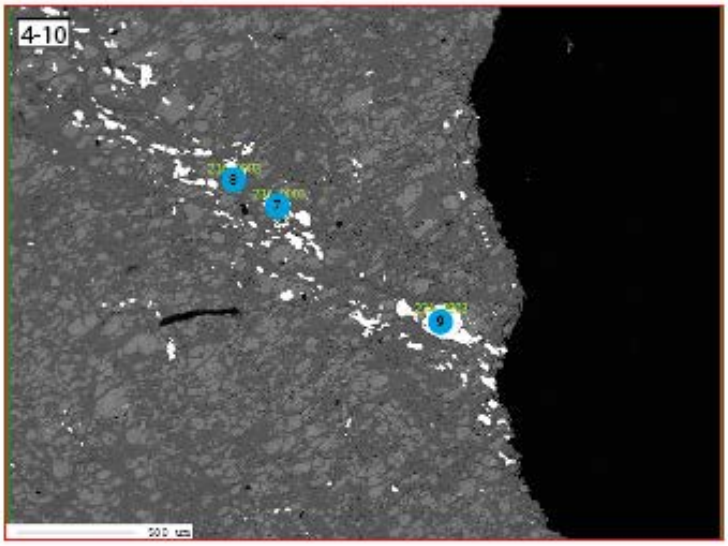
4-10
8
7
9

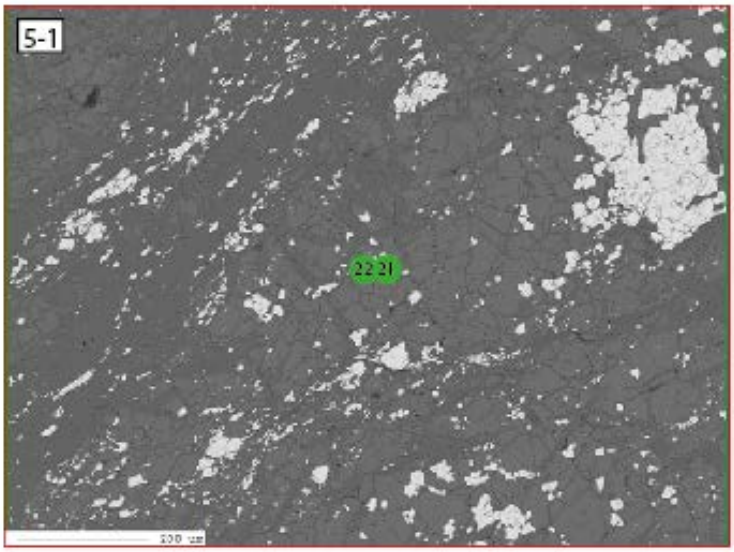
5-1
22
21

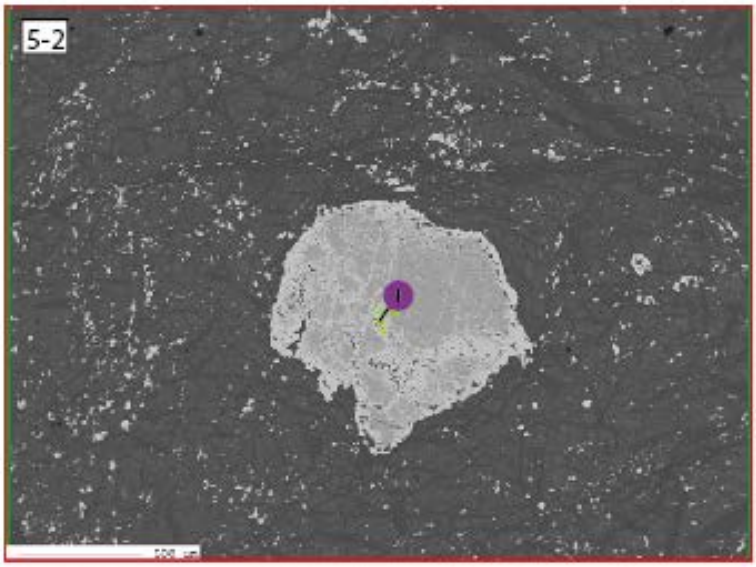
5-2
1

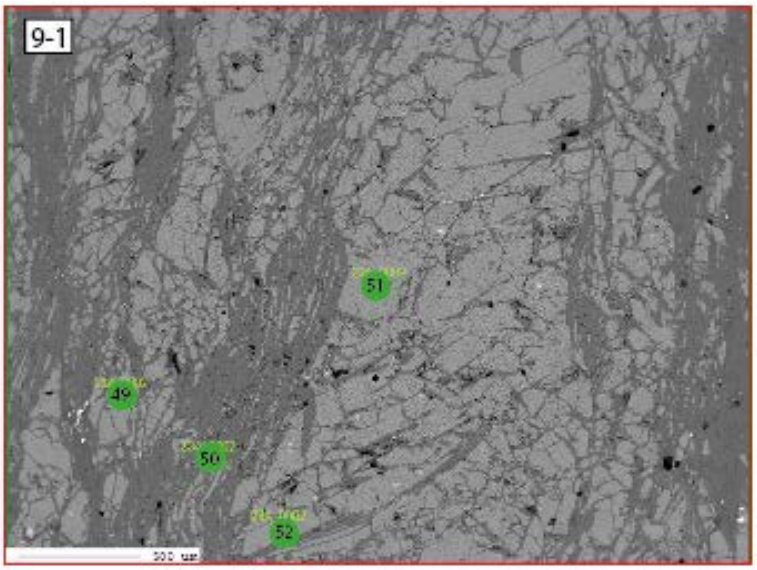
9-1
51
49
50
52

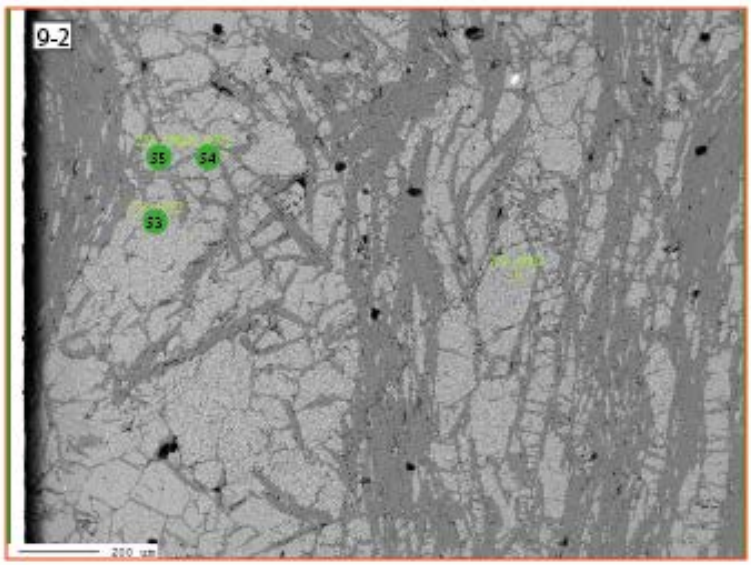
9-2
55
54
53

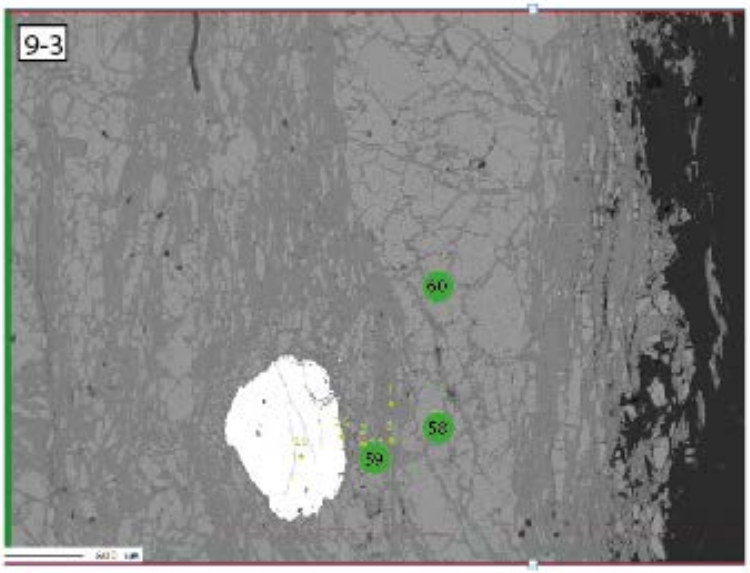
9-3
60
58
59

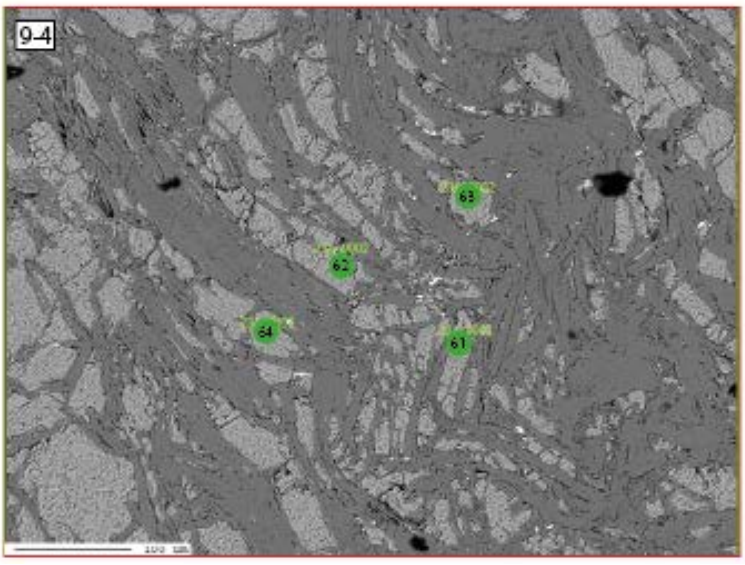
9-4
63
62
64
61

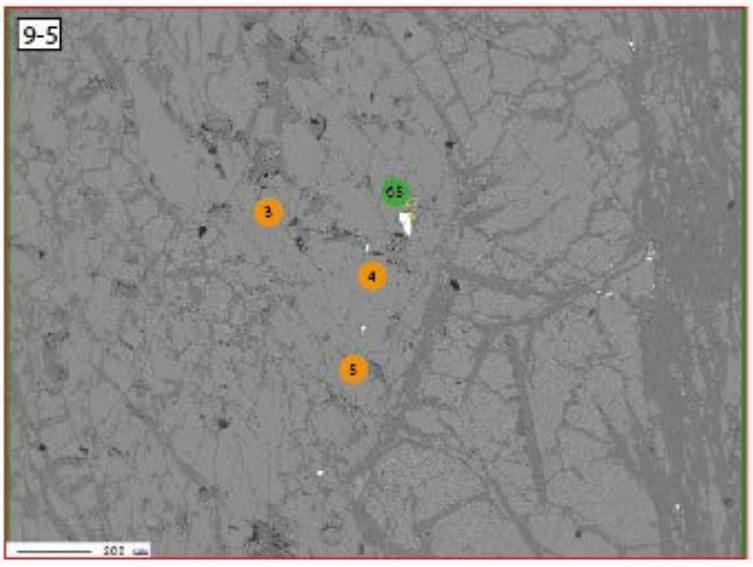
9-5
65
3
4
5

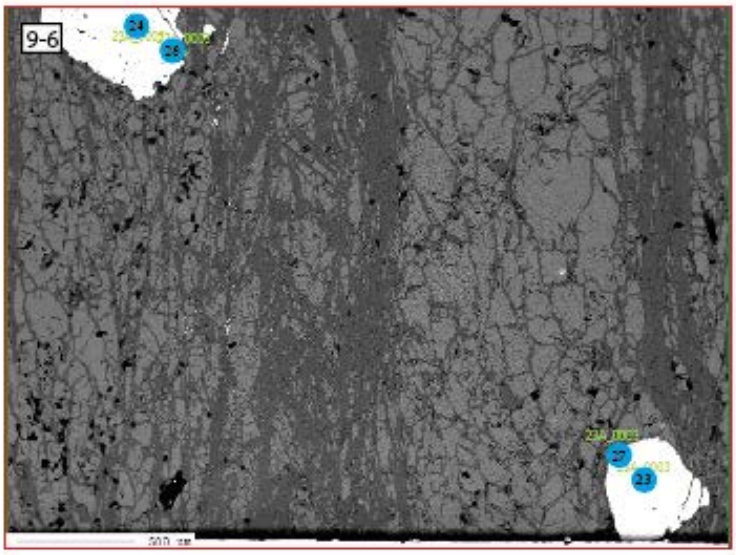
9-6
24
28
27
23

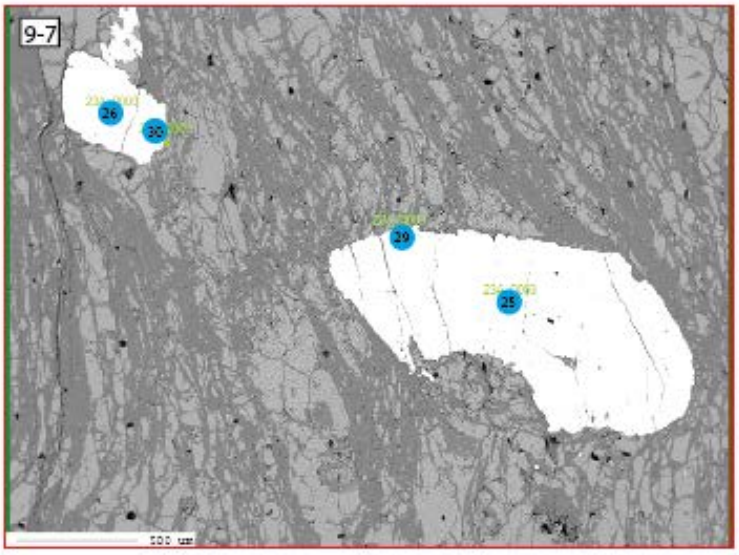
9-7
26
30
29
25

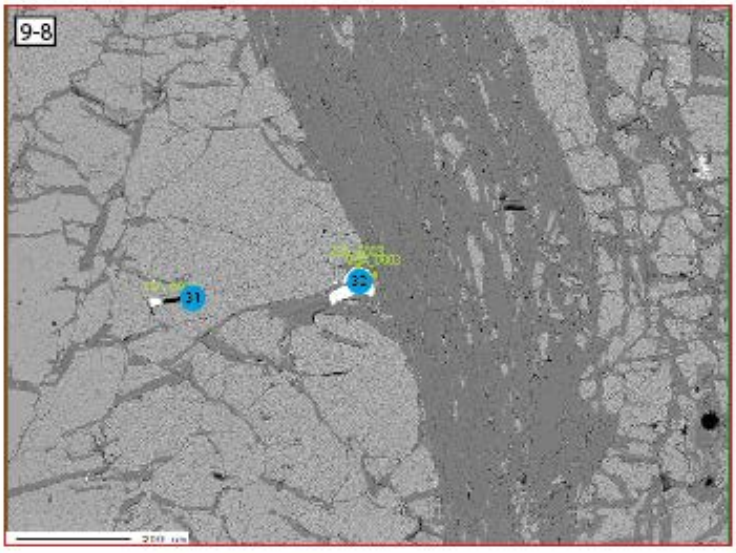
9-8
31
32

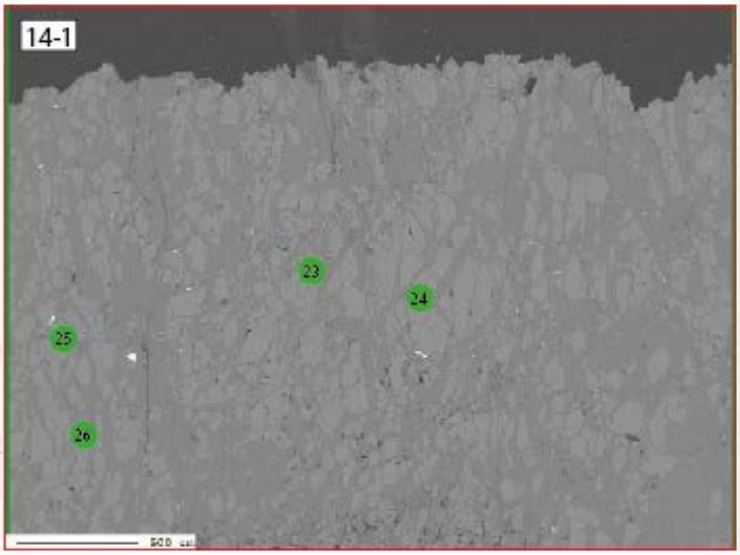
14-1
23
24
25
26

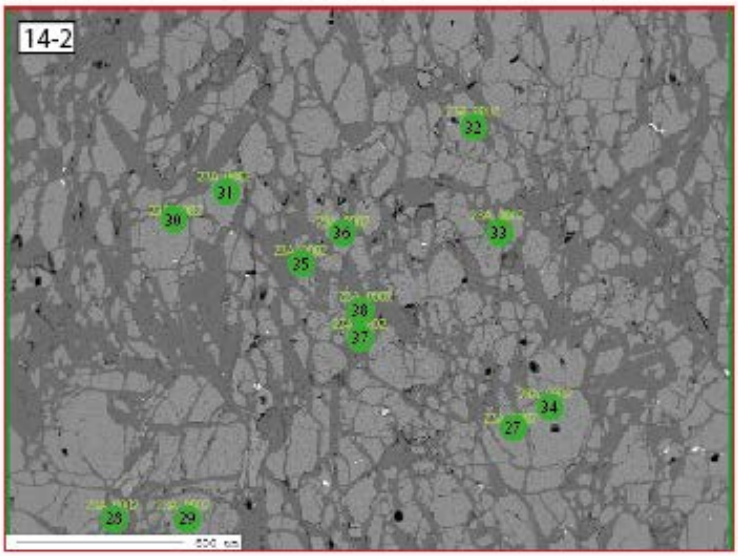
14-2
32
31
30
36
33
35
38
37
34
27
28
29

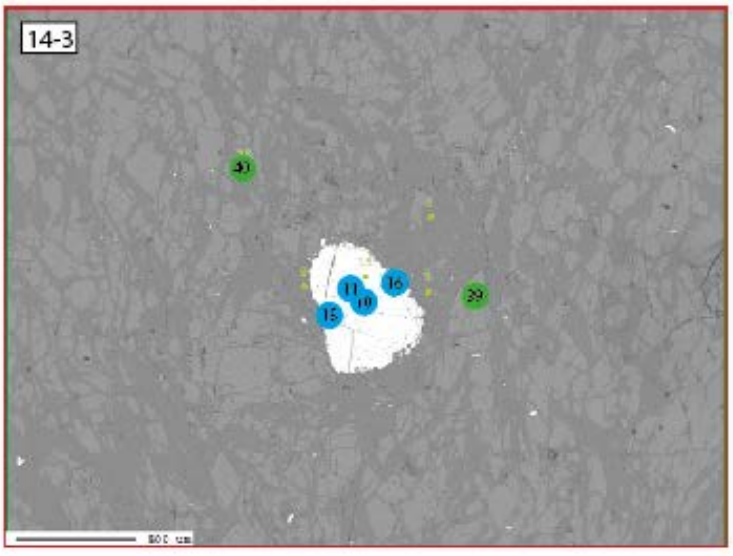
14-3
41
11
16
10
15
39

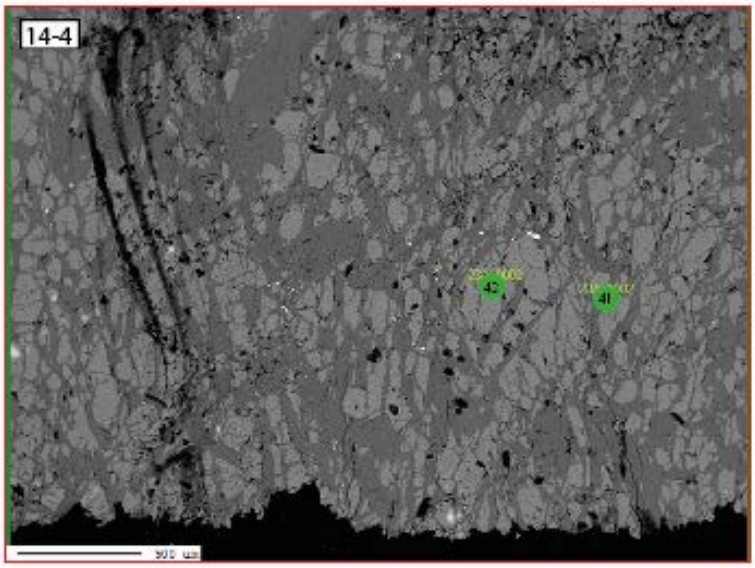
14-4
42
41

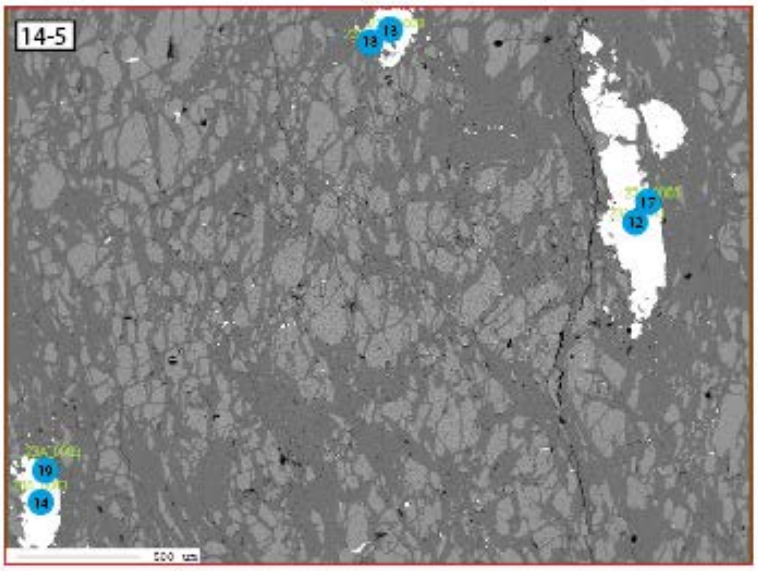
14-5
18
17
12
19
14

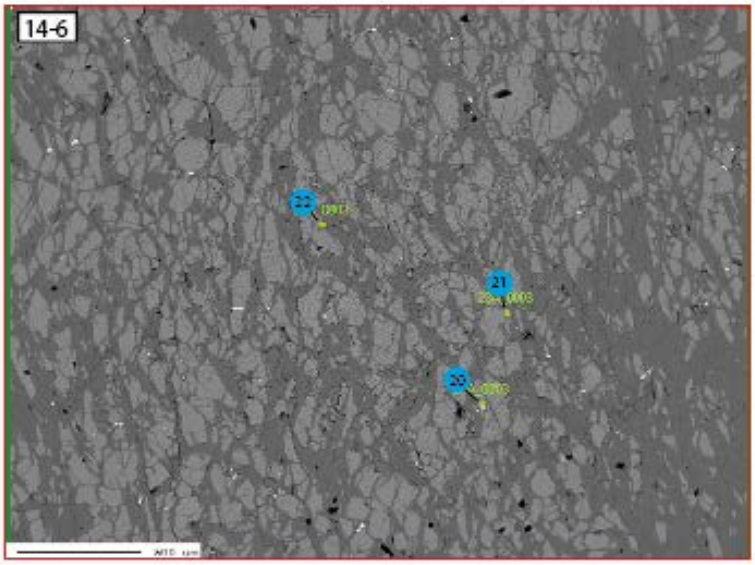
14-6
22
21
20

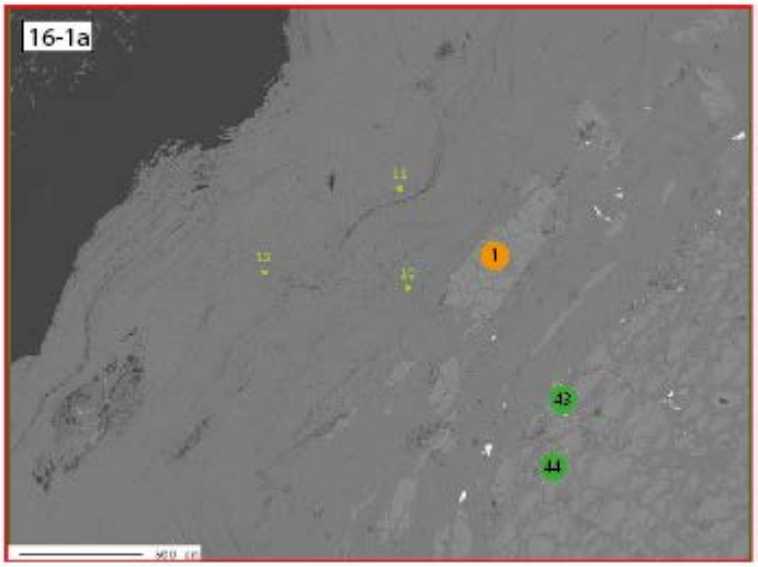
16-1a
1
43
44

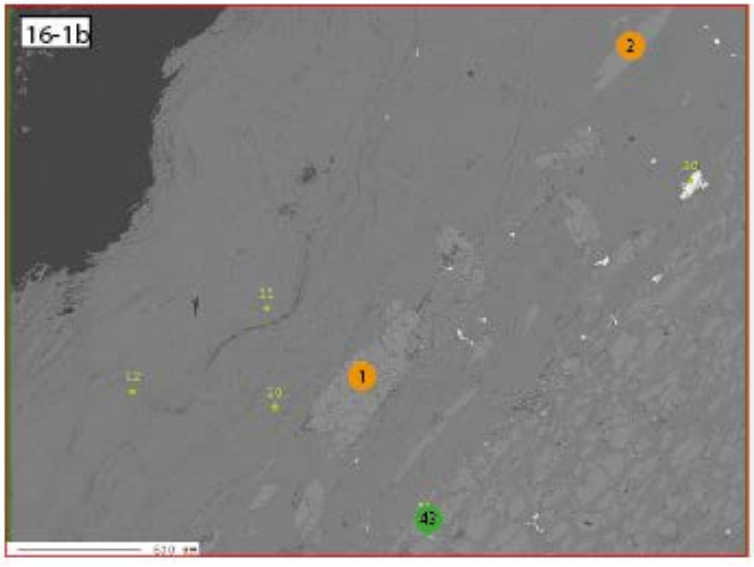
16-1b
2
1
43

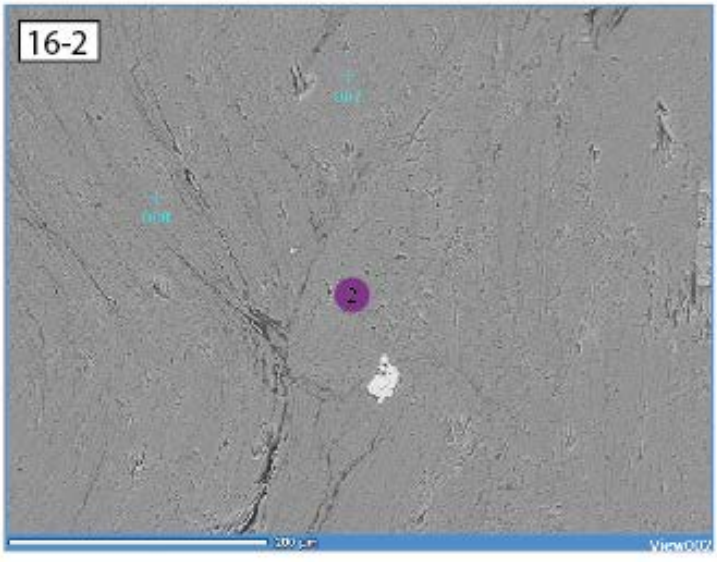
16-2
2

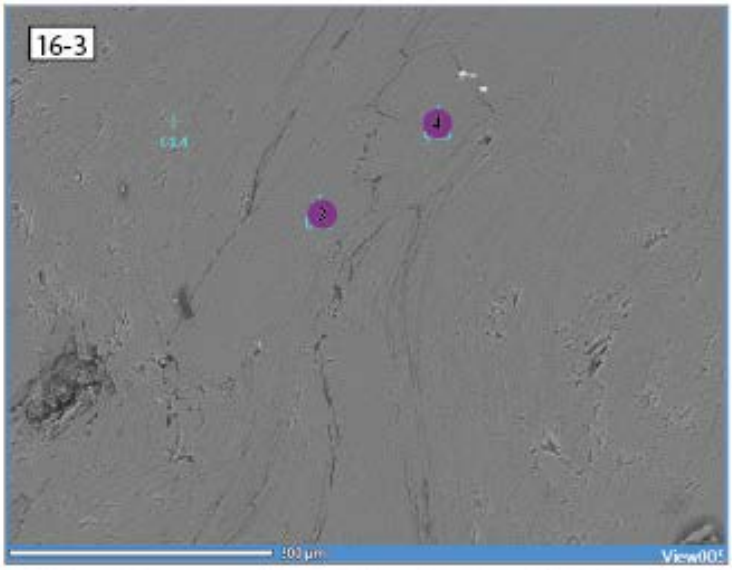
16-3

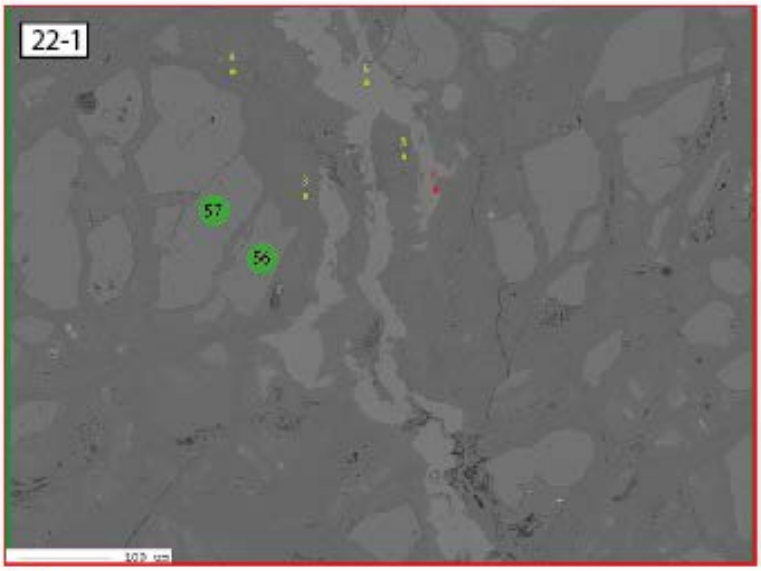
22-1
57
56

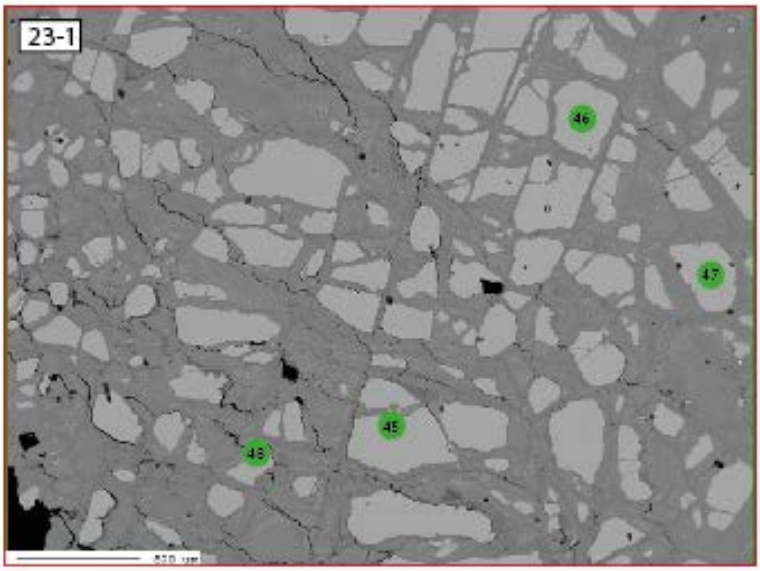
23-1
46
47
45
43

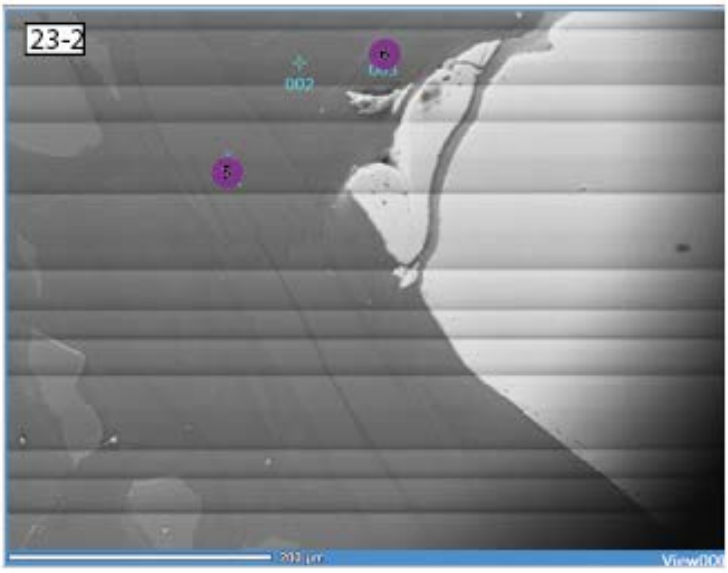
23-2

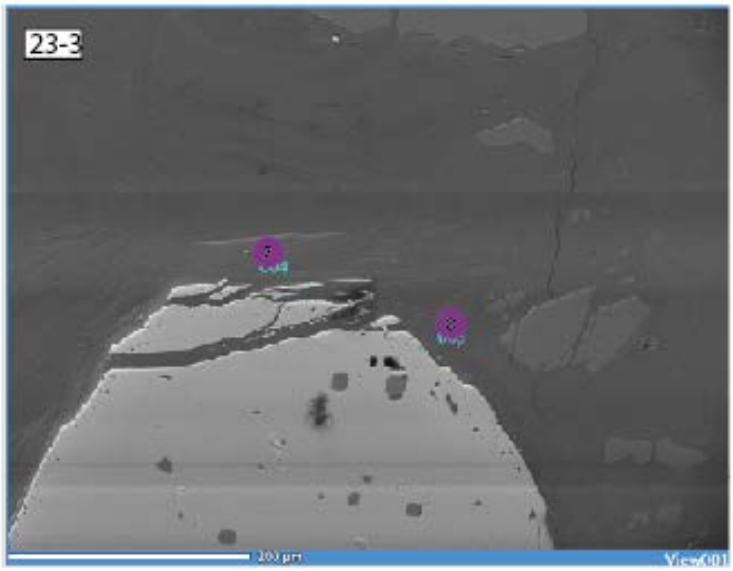
23-3